craniomaxillofacial trauma & reconstruction

Special Issue Reprint

Innovation in Oral- and Cranio-Maxillofacial Reconstruction

Edited by
Susana Heredero, Richard Yuxiong Su and Satyesh Parmar

mdpi.com/journal/cmtr

MDPI

Innovation in Oral- and Cranio-Maxillofacial Reconstruction

Innovation in Oral- and Cranio-Maxillofacial Reconstruction

Guest Editors

Susana Heredero
Richard Yuxiong Su
Satyesh Parmar

MDPI

Basel • Beijing • Wuhan • Barcelona • Belgrade • Novi Sad • Cluj • Manchester

Guest Editors

Susana Heredero
Department of Plastic and Reconstructive Surgery
Hospital de la Santa Creu i Sant Pau
Barcelona
Spain

Richard Yuxiong Su
Division of Oral and Maxillofacial Surgery
University of Hong Kong
Hong Kong
Hong Kong

Satyesh Parmar
Department of Oral and Maxillofacial Surgery
University Hospital of Birmingham
Birmingham
UK

Editorial Office
MDPI AG
Grosspeteranlage 5
4052 Basel, Switzerland

This is a reprint of the Special Issue, published open access by the journal *Craniomaxillofacial Trauma & Reconstruction* (ISSN 1943-3883), freely accessible at: https://www.mdpi.com/journal/cmtr/special_issues/L5DKD57364.

For citation purposes, cite each article independently as indicated on the article page online and as indicated below:

Lastname, A.A.; Lastname, B.B. Article Title. *Journal Name* **Year**, *Volume Number*, Page Range.

ISBN 978-3-7258-9137-5 (Hbk)
ISBN 978-3-7258-9138-2 (PDF)
https://doi.org/10.3390/books978-3-7258-9138-2

© 2026 by the authors. Articles in this reprint are Open Access and distributed under the Creative Commons Attribution (CC BY) license. The reprint as a whole is distributed by MDPI under the terms and conditions of the Creative Commons Attribution-NonCommercial-NoDerivs (CC BY-NC-ND) license (https://creativecommons.org/licenses/by-nc-nd/4.0/).

Contents

Preface . . . . . **vii**

Susana Heredero-Jung, Richard Yuxiong Su and Satyesh Parmar
Editorial for the Special Issue "Innovation in Oral- and Cranio-Maxillofacial Reconstruction"
Reprinted from: *Craniomaxillofac. Trauma Reconstr.* **2026**, *19*, 36,
https://doi.org/10.3390/cmtr19030036 . . . . . **1**

Jokin Zubizarreta Oteiza, Dominik Haenggi, Yannick Simon Krieger, Lukas Schuebel, Daniel Seiler, Florian Markus Thieringer and Neha Sharma
Surgical Performance of 3D-Printed Polyetheretherketone (PEEK) Patient-Specific Implants and Titanium Mesh in Clinically Matched Orbital Reconstruction: A Cadaveric Study
Reprinted from: *Craniomaxillofac. Trauma Reconstr.* **2026**, *19*, 13,
https://doi.org/10.3390/cmtr19010013 . . . . . **3**

Bianca Pulino, Robert Sader, Guilherme Louzada, Majeed Rana, Gabriele Millesi, Geraldo Prestes de Camargo Filho and Raphael Capelli Guerra
Finite Element Analysis of Low-Profile Reconstruction Plates for Atrophic Mandibles—Part II: A Comparison of Customized Plates with 3D Grid-Type and Conventional Designs
Reprinted from: *Craniomaxillofac. Trauma Reconstr.* **2026**, *19*, 9,
https://doi.org/10.3390/cmtr19010009 . . . . . **18**

Nicholas J. Lee, Gareth Honeybone, Mohammed Anabtawi, Mathew Thomas and Sachin M. Salvi
Over a Decade of Maxillofacial PEEK Patient-Specific Innovation: A Retrospective Review of the Evolution from In-House Craft to Virtual Design and Remote Manufacturing
Reprinted from: *Craniomaxillofac. Trauma Reconstr.* **2026**, *19*, 8,
https://doi.org/10.3390/cmtr19010008 . . . . . **27**

Jeffrey Mella, François E. Proulx and Alan W. Johnson
Minne Ties Hybrid Arch Bar System vs. Erich Arch Bars: A Cadaveric Comparison Study
Reprinted from: *Craniomaxillofac. Trauma Reconstr.* **2026**, *19*, 7,
https://doi.org/10.3390/cmtr19010007 . . . . . **50**

Alexander De Crem, Constantijn Bogaert, Frederik Piccart, Matthias Ureel, Benjamin Denoiseux, Lisa De Kock, et al.
Digital vs. Direct Anthropometry with MetiSmile® 3D Face Scanner: A Validation and Reliability Study on a Mannequin Model
Reprinted from: *Craniomaxillofac. Trauma Reconstr.* **2026**, *19*, 3,
https://doi.org/10.3390/cmtr19010003 . . . . . **60**

Ming Yan Cheung, Ankit Nayak, Xing-Na Yu, Kar Yan Li, Yu-Xiong Su and Jingya Jane Pu
Development of an Automatic Computer Program to Determine the Optimal Dental Implant Size and Position for Fibula Free Flap Surgery
Reprinted from: *Craniomaxillofac. Trauma Reconstr.* **2025**, *18*, 46,
https://doi.org/10.3390/cmtr18040046 . . . . . **73**

Bruno Nifossi Prado, Lucas Cavalieri Pereira, Bianca Pulino and Raphael Capelli Guerra
Integrative Innovation in Genioplasty: Advanced 3D Plate Design: Promoting Stability, Aesthetics, and Harmony Excellence
Reprinted from: *Craniomaxillofac. Trauma Reconstr.* **2025**, *18*, 42,
https://doi.org/10.3390/cmtr18030042 . . . . . **88**

Reinier S. A. ten Brink, Bram J. Merema, Marith E. den Otter, Willemina A. van Veldhuizen, Max J. H. Witjes and Joep Kraeima
Towards MRI-Only Mandibular Resection Planning: CT-like Bone Segmentation from Routine T1 MRI Images Using Deep Learning
Reprinted from: *Craniomaxillofac. Trauma Reconstr.* **2025**, *18*, 40,
https://doi.org/10.3390/cmtr18030040 . . . . . **96**

Enrique Vargas, Rodrigo Díaz, Juan Pablo Vargas, Andrés Campolo, Rodrigo Villanueva, Carlos Cortéz and Salvador Valladares-Pérez
Advanced Simulation System for Orbitozygomatic Fracture Reconstruction: Multicenter Validation of a Novel Training and Objective Assessment Platform
Reprinted from: *Craniomaxillofac. Trauma Reconstr.* **2025**, *18*, 34,
https://doi.org/10.3390/cmtr18030034 . . . . . **105**

Jeffrey S. Marschall
Innovations in Clinical Maxillofacial Tissue Engineering and Reconstruction: Cellular Bone Matrix Allografts, Autografts, and Growth Factors
Reprinted from: *Craniomaxillofac. Trauma Reconstr.* **2026**, *19*, 18,
https://doi.org/10.3390/cmtr19020018 . . . . . **130**

Gabriel Conceição Brito, Márcio de Moraes, Leonardo Faverani and Sergio Olate
Facial Contouring in Orthognathic Surgery: The Role of Facial Implants
Reprinted from: *Craniomaxillofac. Trauma Reconstr.* **2026**, *19*, 2,
https://doi.org/10.3390/cmtr19010002 . . . . . **150**

Yoram Fleissig, Jhonatan Elia, Nir Hirshoren, Amalia Sabato, Eleonora Ginzburg, Jawad Abu Tair, et al.
Preoperative Near-Infrared (NIR) Vein Visualization in Zygomatic Implant Perforated (ZIP) Flap †
Reprinted from: *Craniomaxillofac. Trauma Reconstr.* **2026**, *19*, 19,
https://doi.org/10.3390/cmtr19020019 . . . . . **164**

Matthias Ureel, Benjamin Denoiseux, Katrien Brijs, Pieter-Jan Boderé, Nicolas Dhooghe and Renaat Coopman
From Resection to Rehabilitation in One Day: Digital Workflow for Mandibular Reconstruction with Fibular Free Flap and Immediate Dental Rehabilitation Using CAD/CAM Guides at the Point of Care
Reprinted from: *Craniomaxillofac. Trauma Reconstr.* **2026**, *19*, 15,
https://doi.org/10.3390/cmtr19010015 . . . . . **177**

Khalid Abdel-Galil and Kemal Mustafa Tekeli
Expanding Horizons in Craniomaxillofacial Reconstruction: The Role of Exoscopic Microsurgery in Head and Neck Surgery
Reprinted from: *Craniomaxillofac. Trauma Reconstr.* **2026**, *19*, 10,
https://doi.org/10.3390/cmtr19010010 . . . . . **193**

Camilo Mosquera and Hisham Marwan
Jaw in a Day: How to Perform Your First Case—Our Workflow
Reprinted from: *Craniomaxillofac. Trauma Reconstr.* **2025**, *18*, 38,
https://doi.org/10.3390/cmtr18030038 . . . . . **206**

Preface

Reconstruction of the oral and cranio-maxillofacial region lies at the intersection of surgical expertise, technology, biology and multidisciplinary care. Rapid developments in digital planning, three-dimensional technologies, patient-specific solutions and microsurgical reconstruction are expanding the possibilities available to surgeons, while also raising new questions about how innovation can be translated into meaningful benefits for patients. This Reprint brings together a diverse collection of clinical and translational contributions illustrating this evolving landscape. We hope it will be of interest to surgeons, researchers, trainees and other professionals involved in the treatment of complex cranio-maxillofacial defects.

Susana Heredero, Richard Yuxiong Su, and Satyesh Parmar
Guest Editors

craniomaxillofacial
trauma & reconstruction

MDPI

Editorial

Editorial for the Special Issue "Innovation in Oral- and Cranio-Maxillofacial Reconstruction"

Susana Heredero [1], Richard Yuxiong Su [2,*] and Satyesh Parmar [3]

[1] Department of Plastic and Reconstructive Surgery, Hospital de la Santa Creu i Sant Pau, 08041 Barcelona, Spain
[2] Division of Oral and Maxillofacial Surgery, Faculty of Dentistry, University of Hong Kong, Hong Kong, China
[3] Department of Oral and Maxillofacial Surgery, University Hospital of Birmingham, Birmingham B15 2WB, UK
* Correspondence: richsu@hku.hk

Advancements and Future Directions in Cranio-Maxillofacial Reconstruction: Embracing Innovation to Improve Patient Outcomes

We are delighted to present this Special Issue on Innovations in Oral and Cranio-Maxillofacial Reconstruction, which collects a broad range of contemporary research and emerging technologies shaping the future of reconstructive surgery and improving patient care.

Traditional reconstructive surgery, which depends heavily on surgeons' experiences, manual templating, and off-the-shelf titanium hardware, is shifting to a patient-specific, data-driven, and biologically informed approach. This issue highlights several important advances, including the use of 3D-printed PEEK implants and the application of reconstruction plates in the management of atrophic mandibles. It also features comparative studies evaluating hybrid arch bar systems alongside the growing role of 3D facial scanning in surgical planning and assessment.

Digital innovation is a recurring theme throughout the issue, with articles describing automated computer-assisted methods for determining optimal dental implant positioning and fibular flap dimensions for jaw reconstruction. Algorithms can now analyze patients' CT data and automatically propose the ideal position for dental implants in fibula flaps, aligning prosthetic needs with available bone volume and occlusal relationships, thereby reducing the pre-operative planning burden and minimizing trial and error. Readers will also find contributions on advances in genioplasty and the development of MRI-only workflows for mandibular resection planning, reflecting the continuing evolution of image-guided surgery.

In addition, this issue includes studies addressing maxillofacial trauma, tissue engineering, facial contouring, and zygomatic implant-perforated flaps. Together, these articles demonstrate the breadth of innovation currently transforming oral and cranio-maxillofacial reconstruction, ranging from digital technologies and biomaterials to refined surgical techniques and enhanced patient pathways.

The future of oral and cranio-maxillofacial reconstruction is promising. The field is moving toward more precise and reliable surgical techniques, with the use of patient-specific computer models and 3D imaging to plan and guide surgeries, helping reduce complications, improve healing, and restore function more effectively. We can anticipate the routine integration of artificial intelligence/machine learning not only for planning but also for intraoperative navigation, where real-time AI can adjust surgical trajectories on the basis of subtle tissue shifts or unexpected anatomical variations, effectively acting as a co-pilot for surgeons. As technology continues to evolve, surgeons are becoming

better equipped with the skills and tools needed to deliver personalized care. The ultimate goal is to improve quality of life for patients by making reconstructive procedures safer, more predictable, and more effective. Additionally, advances in our understanding of the biological and regenerative aspects of healing are guiding us toward more effective, minimally invasive procedures. We are seeing a shift towards using biomaterials that respond to the body's natural conditions to improve outcomes. In parallel, innovations in 4D bioprinting, which involves creating structures with materials that change over time, are introducing new possibilities. These developments allow us to design custom scaffolds that better match a patient's anatomy and promote proper bone growth, although the clinical applications may still require further validation.

We hope this Special Issue provides valuable insights for clinicians, researchers, and trainees alike and stimulates further research and collaboration in this rapidly advancing field. We are grateful to the authors, reviewers, and editorial team, whose expertise and dedication made this collection possible, and we trust that readers will find it both informative and inspiring.

Data Availability Statement: No new data were created or analyzed in this study. Data sharing is not applicable to this article.

Conflicts of Interest: The authors declare no conflicts of interest.

Disclaimer/Publisher's Note: The statements, opinions and data contained in all publications are solely those of the individual author(s) and contributor(s) and not of MDPI and/or the editor(s). MDPI and/or the editor(s) disclaim responsibility for any injury to people or property resulting from any ideas, methods, instructions or products referred to in the content.

https://doi.org/10.3390/cmtr19030036

craniomaxillofacial
trauma & reconstruction

MDPI

Article

Surgical Performance of 3D-Printed Polyetheretherketone (PEEK) Patient-Specific Implants and Titanium Mesh in Clinically Matched Orbital Reconstruction: A Cadaveric Study

Jokin Zubizarreta Oteiza [1,2,†], Dominik Haenggi [1,2,†], Yannick Simon Krieger [3], Lukas Schuebel [3], Daniel Seiler [4], Florian Markus Thieringer [1,2] and Neha Sharma [1,2,5,*]

[1] Clinic of Oral and Cranio-Maxillofacial Surgery, University Hospital Basel, 4031 Basel, Switzerland; jokin.zubizarreta@unibas.ch (J.Z.O.); florian.thieringer@usb.ch (F.M.T.)
[2] Medical Additive Manufacturing Research Group (Swiss MAM), Department of Biomedical Engineering, University of Basel, 4123 Allschwil, Switzerland
[3] 3D Systems, 81369 Munich, Germany
[4] Institute for Medical Engineering and Medical Informatics, University of Applied Sciences and Arts Northwestern Switzerland, 4132 Muttenz, Switzerland; daniel.seiler@fhnw.ch
[5] SingHealth Duke-NUS Radiological Sciences Academic Clinical Programme (RADSC ACP), Office of Academic Medicine, Duke-NUS Medical School, Singapore 169857, Singapore
* Correspondence: neha.sharma@unibas.ch
† These authors contributed equally to this work.

Abstract

Orbital reconstruction following trauma remains challenging due to complex three-dimensional (3D) anatomy and limited surgical access. While pre-fabricated titanium mesh is standard, it requires extensive intraoperative manipulation and produces imaging artifacts. The 3D-printed polyetheretherketone (PEEK) patient-specific implants (PSIs) offer potential advantages; however, limited data exists for the acceptance of PEEK PSIs by surgeons compared to other established techniques. Fourteen surgeons performed simulated orbital reconstructions on nine cadaveric heads comparing titanium mesh and the 3D-printed PEEK PSIs. Titanium mesh was used for Class II orbital floor fractures, while the 3D-printed PEEK PSIs (native and radiopaque formulations) were used for Class IV defects. Surgeons were blinded to the PEEK formulation type. Outcomes included operative efficiency, handling characteristics, fit quality, and mechanical stability using validated 5-point Likert scales and objective timing. The 3D-printed PEEK PSIs demonstrated faster procedure times (9.5 $\pm$ 5.3 vs. 11.2 $\pm$ 5.1 min) and superior fit quality (2.00 $\pm$ 1.04 vs. 2.18 $\pm$ 0.60) and mechanical stability (1.67 $\pm$ 0.49 vs. 1.91 $\pm$ 0.54), with 100% rated stable versus 91% for the titanium mesh. Surgeons could not distinguish between the native and radiopaque PEEK formulations. Most surgeons (64.3%) preferred situation-dependent material selection. The 3D-printed PEEK PSIs demonstrated advantages in handling, fit quality, and mechanical stability for complex defects, while the titanium mesh showed a lower learning curve for simple reconstructions. Radiopaque enhancement expands PEEK's clinical utility without compromising handling.

Keywords: 3D printing; additive manufacturing; barium sulfate; craniomaxillofacial trauma; material extrusion; orbital fracture; polymers; radiopaque biomaterials; surgical simulation; virtual surgical planning

1. Introduction

Orbital reconstruction after trauma is particularly challenging because of the intricate three-dimensional (3D) structure of the orbital floor and walls, combined with restricted intraoperative visibility [1]. The current standard involves the intraoperative shaping and adaptation of pre-fabricated, stock titanium mesh implants, a process that is time-consuming, requires substantial surgical skill, and often results in suboptimal restoration [2]. Additionally, titanium mesh causes substantial imaging artefacts and beam-hardening effects that can obscure the surrounding soft tissue and complicate post-operative assessment [3], and is often associated with various complications, including implant exposure, infection, and diplopia [4]. Even when meticulously shaped, residual sharp edges can catch orbital fat or extraocular muscles during insertion or removal, increasing the risk of orbital tissue trauma [5].

The evolution toward 3D-printed patient-specific implants (PSIs) offers significant advantages over traditional approaches [6]. Point-of-care 3D printing enables streamlined workflows from computed tomography (CT) imaging to implant production, providing a precise fit and reducing operative time by eliminating manual intraoperative adaptation [7,8]. This integrated digital approach allows for pre-surgical planning and procedure rehearsal.

Polyetheretherketone (PEEK) has emerged as a promising alternative biomaterial for craniomaxillofacial (CMF) applications, offering excellent biocompatibility, chemical inertness, and imaging compatibility without artefacts that compromise diagnostic accuracy [9–11]. However, the inherent radiolucency of a native, unfilled PEEK biomaterial limits its orbital applications, where postoperative visualization and long-term monitoring are essential. This represents a prevalent challenge in polymer-based implantable biomaterials [12]. Incorporating barium sulfate ($BaSO_4$) into PEEK provides controlled radiopacity for precise implant localization while preserving excellent soft tissue contrast and avoiding the beam hardening artefacts typical of metallic implants [13].

Despite the theoretical advantages of 3D-printed PEEK PSIs for orbital reconstruction, limited data exist on their acceptance in surgery, their handling characteristics, or their comparative performance against established prefabricated titanium mesh. Transitioning from traditional materials to innovative biomaterials requires a careful evaluation of material properties and practical surgical considerations, including ease of handling, learning curve, and surgeon confidence in achieving optimal outcomes. Additionally, successfully integrating radiopaque enhancement into PEEK formulations requires validation that the material modifications do not compromise the surgical handling characteristics.

This study aimed to assess surgeons' evaluation of 3D-printed PEEK (native, unfilled, and BaSO4) PSIs and pre-fabricated, stock titanium mesh implants for orbital reconstruction through a comprehensive cadaveric study. Specifically, we aimed to compare the handling qualities, surgical workflow efficiency, confidence in implant positioning, and overall surgeon preference between the pre-bent titanium mesh and the 3D-printed PEEK orbital PSIs. Additionally, we sought to evaluate the learning curve for the 3D-printed PEEK orbital PSI implementation and to validate the successful integration of $BaSO_4$ enhancement by assessing surgeons' ability to distinguish between native (standard) and radiopaque PEEK formulations during surgical procedures.

2. Materials and Methods

2.1. Study Design and Participants

This study evaluated surgeons' assessments of the conventional pre-bent stock titanium mesh and the 3D-printed PEEK PSIs (native PEEK and radiopaque barium sulfate-enhanced PEEK ($BaSO_4$-PEEK) for orbital reconstruction. This comparative cadaveric study

https://doi.org/10.3390/cmtr19010013

was designed as a pragmatic clinical simulation that reflects real-world fracture–implant matching rather than a controlled material-property comparison. Implant selection was intentionally matched to the clinically appropriate fracture complexity to replicate routine clinical decision-making in orbital reconstruction.

This study was conducted in accordance with institutional guidelines for cadaveric research, with ethical approval obtained from the Ethics Commission of Northwestern and Central Switzerland (EKNZ). A total of 9 fresh-frozen cadaveric heads (18 orbital sites) were obtained from Rise Labs (Benit 30A, 1043BB Amsterdam, The Netherlands) with appropriate consent for research use and prepared for orbital reconstruction procedures under standardized surgical procedures. Preoperative high-resolution computed tomography (CT) images of the cadaver heads (SOMATOM go.Now, Siemens Healthineers AG, Forchheim, Germany) were obtained to enable the design of anatomically accurate PSIs based on existing orbital anatomy.

Participants with varying levels of craniomaxillofacial (CMF) surgical training were recruited from the Clinic of Oral and Cranio-Maxillofacial Surgery at University Hospital Basel and affiliated training programs through direct invitation. The participants were informed that the study aimed to compare the surgical handling characteristics of different orbital reconstruction materials and technologies. To minimize bias, the participants were blinded to the specific hypotheses regarding material superiority and were not informed which PEEK formulation (native vs. radiopaque) they were using during each procedure. Those participants without prior orbital reconstruction experience received standardized orientation on surgical approaches and implant handling principles prior to evaluation. Demographic data were collected, including sex, age, years of surgical experience, and the number of previously performed orbital reconstructions. All participants provided informed consent. Each participant performed orbital reconstruction procedures using all materials on different randomized cadaveric models, with a comprehensive evaluation completed immediately following each procedure using a structured questionnaire. The surgeons' identities were anonymized during data collection and analysis, per applicable privacy regulations and research ethics standards.

2.2. Surgical Case Complexity and Implant Assignment

This design reflects real-world clinical decision-making, where implant selection is inherently matched to fracture complexity rather than randomized across identical defect patterns. Implant evaluation was conducted using clinically appropriate fracture complexities for each material based on the Jaquiéry classification system [14]. Titanium mesh orbital reconstruction procedures were performed on simulated Class II orbital fractures (defects > 2 cm^2 of the floor and/or medial wall within zones 1–2), representing moderate defects where manual intraoperative contouring is clinically feasible. The 3D-printed PEEK PSIs were designed to simulate Class IV orbital fractures (entire orbital floor and medial wall defects extending into the posterior third/zone 3, with a missing bony ledge), representing complex multi-walled defects in which patient-specific reconstruction provides maximum clinical benefit. This design reflects real-world clinical decision-making, where implant selection is matched to fracture complexity (Table 1).

https://doi.org/10.3390/cmtr19010013

Table 1. Orbital fracture classification used in this study.

Class	Definition	Surgical Complexity	Implant Type Evaluated
Class II	Defects > 2 cm^2 of orbital floor and/or medial wall within zones 1–2	Moderate	Pre-bent titanium mesh
Class IV	Entire orbital floor and medial wall defects extending into posterior third (zone 3) with missing bony ledge	Complex multi-walled reconstruction	3D-printed PEEK PSI (native and with $BaSO_4$)

2.3. Virtual Surgical Planning and Implant Fabrication

High-resolution CT imaging data (0.8 mm slice thickness) were processed using medical image processing software (Materialise Mimics Innovation Suite v26, Materialise NV, Leuven, Belgium) to create digital anatomical models of orbital anatomy for each cadaveric specimen. Anatomical biomodels were 3D-printed using material extrusion or fused filament fabrication (FFF) technology (Bambu Lab X1 Carbon, Bambu Lab, Shenzhen, China) with polylactic acid (PLA) filament (Matte Ivory White filament Bambu Lab, Shenzhen, China) as surgical planning templates.

Pre-fabricated stock titanium meshes (Figure 1A) (Medartis Orbital Plating System OPS 1.5, M-4440, 0.3 mm, Medartis AG, Basel, Switzerland) were pre-bent using the 3D-printed anatomical models and (Figure 2B) underwent final intraoperative adjustment (if needed) according to established surgical protocols.

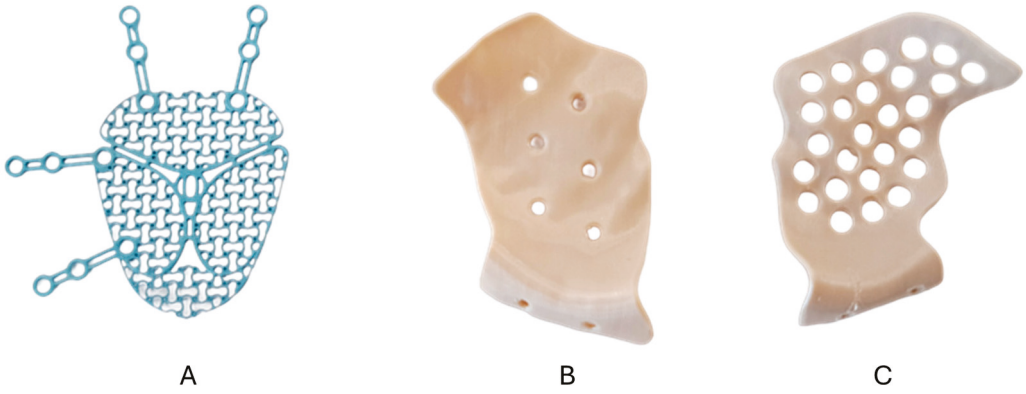

Figure 1. Orbital implants evaluated for surgical performance. (**A**) Pre-fabricated titanium mesh requiring intraoperative contouring. (**B**) 3D-printed patient-specific native (unfilled) PEEK implant. (**C**) 3D-printed patient-specific radiopaque PEEK ($BaSO_4$-enhanced) implant.

The 3D-printed PEEK PSIs were designed using computer-aided design (CAD) software (Geomagic Freeform Plus V2022.0.34, Hexagon AB, Stockholm, Sweden) with the implant geometry optimized for each cadaver specimen's unique orbital anatomy following anatomical landmarks. The 3D-printed PSIs included a native, unfilled medical-grade PEEK (Figure 1B) and a radiopaque $BaSO_4$-PEEK formulation containing 20% $BaSO_4$ by weight (Figure 1C). Prior to cadaveric surgery, the PEEK PSI fit and positioning were verified using the corresponding anatomical models (Figure 2A).

Fabrication was performed using a material extrusion 3D printer (EXT 220 MED, 3D Systems, Rock Hill, SC, USA). A layer height of 0.26 mm was applied, and implants were 3D-printed with a wall thickness of 0.8 mm. Extended support structures surrounding each implant were employed to ensure printability and to increase the nozzle travel distance between layers, thereby preventing thermal build-up and associated layer collapse.

https://doi.org/10.3390/cmtr19010013

Post-processing comprised support removal and surface refinement to facilitate surgical handling. Drainage holes were manually introduced during post-processing rather than generated in the printed geometry.



Figure 2. 3D-printed orbital biomodels for preoperative planning. (**A**) Biomodel with patient-specific PEEK implant demonstrating pre-designed fit. (**B**) Biomodel used for titanium mesh pre-contouring to match patient-specific orbital anatomy.

2.4. Surgical Technique and Implant Placement

Standardized surgical approaches were employed for all procedures to ensure consistent evaluation conditions. A transconjunctival incision with lateral canthotomy was used to access the orbital floor. For reconstructions requiring medial wall access, a transcaruncular approach was additionally utilized. Following periosteal incision and subperiosteal dissection, the orbital floor and walls were exposed to simulate appropriate fracture defect sites according to the assigned complexity classification. Physical fractures were not created in the cadaveric specimens. Instead, implants were placed on intact orbital anatomy following virtual surgical planning, using it as a reconstruction-to-native-position simulation. This approach enabled the standardized evaluation of implant handling, fit perception, and workflow efficiency across all specimens.

The pre-fabricated titanium mesh implants underwent intraoperative manual contouring and trimming to achieve an appropriate anatomical fit. Pre-bent meshes, initially shaped using 3D-printed anatomical models, required additional chairside adjustments, including cutting and bending, to achieve optimal defect coverage. The intraoperative bending time was recorded from initiation to completion of the final contouring, while the 3D-printed PEEK PSIs were oriented using anatomical landmarks established during virtual surgical planning, including the inferior orbital rim, the inferomedial orbital strut, and the transition zone between the orbital floor and the medial wall. Each PSI design incorporated reference points corresponding to these landmarks, and positioning was verified against the 3D-printed anatomical biomodels prior to and during implant placement. All implants were secured using the standardized fixation protocols appropriate for each material type. Titanium meshes and PSIs were secured using 1.5 mm diameter, 6 mm length SpeedTip surgical screws from the Medartis MODUS 2 Midface fixation system (Medartis AG, Basel, Switzerland).

2.5. Outcome Measures and Data Collection

Primary outcome measures included operative efficiency assessed through objective timing measurements: intraoperative bending time for titanium mesh and total procedure time for all implant types (measured in minutes using standardized timing protocols). Surgical performance was evaluated using a structured 10-question survey instrument administered immediately following each procedure.

https://doi.org/10.3390/cmtr19010013

The survey assessed six key performance domains using the following standardized 5-point Likert scales: (1) handling characteristics during implant manipulation (1 = easy, 5 = hard), (2) implant fit quality in the final reconstruction (1 = very good, 5 = poor), (3) position confidence regarding correct final implant placement (1 = certain, 5 = uncertain), (4) mechanical stability assessment including concerns about potential implant failure (1 = very stable, 5 = unstable), (5) learning curve requirements for mastering implant techniques (1 = easy, 5 = hard), and (6) insertion confidence reflecting ease of implant placement technique (1 = difficult, 5 = easy).

Secondary outcomes included the ability to distinguish between native (standard) and $BaSO_4$-enhanced PEEK PSIs based solely on tactile feedback (1 = clear difference, 5 = indistinguishable), the overall preference when given a free choice between implant options, and the identification of procedural challenges through open-ended responses. Fourteen CMF surgical team members utilized 18 operative sites across 9 cadaver heads. Each participant performed one or two procedures according to predefined specimen allocation and logistical availability. A material differentiation assessment was conducted immediately following each PEEK PSI procedure, with the surgeons blinded to the specific formulation throughout the evaluation. All evaluations were completed independently by each surgeon immediately post-procedure to minimize recall bias, with data collection supervised by trained research personnel using standardized protocols to ensure consistent administration across all participants.

2.6. Statistical Analysis

The sample size of 9 cadaveric heads (18 orbital sites) was determined by specimen availability within the study timeframe, consistent with established cadaveric studies in orbital reconstruction research utilizing comparable sample sizes. Given the exploratory nature of this comparative technology evaluation, a formal power analysis was not conducted.

The statistical analysis emphasized descriptive statistics and effect size estimation to assess the clinical meaningfulness of observed differences. Continuous variables were reported as mean $\pm$ standard deviation, and categorical variables were reported as frequencies and percentages. Cohen's d effect sizes were calculated to quantify the magnitude of differences between implant types, with interpretations following established conventions (small: 0.2–0.5; medium: 0.5–0.8; large: >0.8). This approach was selected as appropriate for the exploratory study objectives, emphasizing clinical significance over statistical significance testing. The learning curve assessment was based on the surgeons' perceived procedural difficulty following limited exposure (1–2 procedures). A sensitivity analysis was performed, excluding the medical student and senior surgeon, to assess the impact of experience-level outliers.

3. Results

3.1. Participant Demographics

Fourteen CMF surgical team members participated in the evaluation and provided complete datasets for analysis. The cohort included 12 male (85.7%) and 2 female (14.3%) surgeons with a mean age of 33.6 $\pm$ 7.0 years (range: 24–49 years). The experience levels comprised ten residents (71.4%), two attending physicians (14.3%), one senior physician (7.1%), and one medical student (7.1%). The number of years of surgical experience ranged from 0 to 22 years, with the majority of participants being early-career surgeons. Nine participants (64.3%) reported no prior orbital reconstruction experience. These participants received standardized orientation on surgical approaches and implant handling principles prior to evaluation. The detailed participant demographics are summarized in Table 2.

https://doi.org/10.3390/cmtr19010013

Table 2. Participant Demographics and Surgical Experience.

Parameter	Value
Number of participants	14
Sex (male/female)	12/2
Age (years)	33.6 ± 7.0 (range 24–49)
Experience level	
Residents	10 (71.4%)
Attending physicians	2 (14.3%)
Senior physician	1 (7.1%)
Medical student	1 (7.1%)
Years of surgical experience	0–22 years
Prior orbital reconstructions	
None	9 (64.3%)
1–10 cases	2 (14.3%)
>10 cases	3 (21.4%)

To evaluate the potential influence of experience-level outliers on surgeon-reported outcomes, a sensitivity analysis was performed, excluding the medical student and the senior surgeon. A comparative evaluation of operative time, handling, fit quality, positioning confidence, mechanical stability, and learning curve perception showed no meaningful change in the observed trends across the implant types. The relative performance patterns remained consistent with those observed in the full cohort.

3.2. Operative Efficiency and Time Measurements

The pre-fabricated titanium meshes' intraoperative bending time averaged 6.1 ± 5.6 min. The complete titanium mesh workflow (pre-bending and insertion) time was 11.2 ± 5.1 min compared to 9.5 ± 5.3 min for the 3D-printed PEEK PSIs, representing a 1.6-min reduction (14.7% decrease) in total procedure time (Cohen's d = −0.30, small effect).

3.3. Surgical Performance Domain Characteristics

A comparative surgeon assessment across the six performance domains (Table 3) revealed the advantages of the 3D-printed PEEK PSIs in handling, fit quality, and mechanical stability, while the titanium mesh demonstrated easier learning curve requirements (Cohen's d = 0.52, medium effect). Most differences were small in magnitude, with positioning and insertion confidence showing minimal variation between the implant types.

An analysis of the individual surgeon responses revealed varying degrees of consensus across performance domains. For handling characteristics, both implant types showed similar response ranges (Titanium: 2–4, PEEK: 1–4), with 73% of the titanium mesh assessments and 67% of PEEK assessments rated as 2–3 (easy to moderate handling). Fit quality assessments demonstrated notable variability for the PEEK PSIs (range 1–4), with 58% of responses rated as 1–2 (very good to good) compared to the titanium mesh showing more consistent ratings (range 1–3) with 64% rated as 2 (good), reflecting both fracture complexity differences and patient-specific design precision.

Mechanical stability assessments revealed the strongest consensus favoring the PEEK PSIs, with 100% of the PEEK ratings at 1–2 (very stable to stable) compared to 91% for the titanium mesh, demonstrating clear surgeon confidence in patient-specific implant structural integrity. Position confidence assessments (certainty of correct final positioning) showed similar patterns across both materials (ranging from 1–4), with 67% of the PEEK assessments and 64% of the titanium mesh assessments rated 1–2 (certain to mostly certain), indicating comparable surgeon confidence in final implant positioning regardless of technology.

https://doi.org/10.3390/cmtr19010013

Table 3. Comparative surgical performance assessment: Titanium Mesh and 3D-Printed Polyetheretherketone (PEEK) patient-specific orbital implants.

Domain	Ti Mesh	3D-Printed PEEK PSI	Cohen's d	Advantage
Handling (1 = easy, 5 = hard)	2.82 ± 0.75	2.75 ± 0.97	−0.08	PSI (PEEK)
Fit Quality (1 = very good, 5 = poor)	2.18 ± 0.60	2.00 ± 1.04	−0.21	PSI (PEEK)
Position Confidence (1 = certain, 5 = uncertain)	2.27 ± 1.01	2.25 ± 1.06	−0.02	Similar
Stability (1 = stable, 5 = unstable)	1.91 ± 0.54	1.67 ± 0.49	−0.47	PSI (PEEK)
Learning (1 = easy, 5 = hard)	3.18 ± 0.87	3.58 ± 0.67	0.52	Pre-bent (Ti)
Insertion Confidence (1 = difficult, 5 = easy)	3.36 ± 0.92	3.25 ± 1.14	−0.11	Similar

Surgeon ratings (mean ± SD) across performance domains using 5-point Likert scales. Lower scores indicate better performance except for Confidence (1 = difficult, 5 = easy). Cohen's d: effect size magnitude. Titanium (Ti), polyetheretherketone (PEEK), patient-specific implant (PSI).

Learning curve assessments confirmed the expected complexity differential, with the PEEK PSIs consistently rated as more difficult to learn (range 3–5, no ratings below 3) compared to the titanium mesh (range 2–5, with 18% rated as 2), reflecting the inherent complexity of Class IV reconstructions versus simpler fracture patterns. Insertion confidence assessments showed considerable variability for both materials, with the PEEK PSIs demonstrating the widest response distribution (range 1–5) compared to the titanium mesh (range 2–5), indicating that surgeon comfort levels with patient-specific insertion techniques varied among the participants.

3.4. Material Differentiation and Surgeon Preferences

The surgeons demonstrated limited ability to distinguish between the standard PEEK and radiopaque $BaSO_4$-PEEK PSIs during surgical procedures, with a mean differentiation score of 4.20 ± 1.40 on the 5-point scale (1 = clear difference, 5 = indistinguishable). When given a free choice among the implant options, the surgeon's preferences were notably situation-dependent. Most respondents (9/14, 64.3%) indicated that their preference would depend on the specific clinical situation, while two surgeons (14.3%) preferred the 3D-printed PEEK PSIs, one surgeon (7.1%) preferred the titanium mesh, and one surgeon (7.1%) expressed no preference.

3.5. Surgeon-Reported Technical Challenges

Open-ended responses regarding potential surgical difficulties revealed distinct challenge patterns between the implant types. For the pre-fabricated titanium mesh implants, the most frequently cited concerns included intraoperative shape instability during insertion (4/11 respondents, 36%), requirement for extensive bone exposure (3/11, 27%), and contouring difficulties (3/11, 27%). Additional titanium mesh-related challenges included sharp edges during handling (2/11, 18%) and concerns about implant positioning accuracy (2/11, 18%).

On the other hand, the 3D-printed PEEK PSI-related challenges focused primarily on implant thickness perception (3/12 respondents, 25%), planning software learning requirements (2/12, 17%), and occasional dimensional sizing concerns (2/12, 17%). Several

https://doi.org/10.3390/cmtr19010013

surgeons noted no specific technical difficulties with either implant type (Titanium: 2/11; PEEK: 4/12).

Representative surgeon comments included the following: "Mesh doesn't hold its shape during insertion" and "You have to expose a lot of bone to insert the mesh" for titanium-related concerns; while the 3D-printed PEEK PSI feedback included the following: "Feels thick compared to titanium mesh" and "Need time for planning and knowledge of using the software."

3.6. Experience-Stratified Analysis

To evaluate the potential influence of surgical experience on primary outcomes, the participants were stratified into trainees (n = 10) and attending/senior surgeons (n = 4). The experience-stratified analysis is presented in Table 4.

Table 4. Primary Outcomes Stratified by Level of Surgical Experience.

Outcome Measure	Implant	Trainees (n = 10) Mean ± SD	Attending/Senior (n = 4) Mean ± SD
Procedure Time (min)	Titanium Mesh	10.4 ± 4.9	13.5 ± 5.8
	3D-Printed PEEK PSI	9.1 ± 5.0	10.4 ± 5.9
Handling (1 = easy, 5 = hard)	Titanium Mesh	2.8 ± 0.8	2.9 ± 0.7
	3D-Printed PEEK PSI	2.7 ± 1.0	2.8 ± 0.9
Fit Quality (1 = very good, 5 = poor)	Titanium Mesh	2.2 ± 0.6	2.1 ± 0.5
	3D-Printed PEEK PSI	2.0 ± 1.1	1.9 ± 0.8
Position Confidence (1 = certain, 5 = uncertain)	Titanium Mesh	2.3 ± 1.0	2.2 ± 0.9
	3D-Printed PEEK PSI	2.3 ± 1.1	2.2 ± 1.0
Mechanical Stability (1 = stable, 5 = unstable)	Titanium Mesh	1.9 ± 0.6	1.8 ± 0.5
	3D-Printed PEEK PSI	1.7 ± 0.5	1.6 ± 0.5
Learning Curve (1 = easy, 5 = hard)	Titanium Mesh	3.2 ± 0.9	3.1 ± 0.8
	3D-Printed PEEK PSI	3.6 ± 0.7	3.4 ± 0.6

Lower scores indicate better performance except where stated.

Comparable directional trends were observed across the experience strata for operative time, handling characteristics, fit quality, positioning confidence, mechanical stability, and learning curve perception for both the titanium mesh and the 3D-printed PEEK PSIs. The trainees demonstrated slightly shorter procedure times for both the titanium mesh (10.4 ± 4.9 min) and the PEEK PSIs (9.1 ± 5.0 min) compared to the attending/senior surgeons (13.5 ± 5.8 min and 10.4 ± 5.9 min, respectively). The perceived learning curve was marginally steeper among trainees for the PEEK PSIs (3.6 ± 0.7) than among attending/senior surgeons (3.4 ± 0.6), reflecting expected differences in familiarity with virtual surgical planning workflows. Overall, experience stratification did not materially alter the relative performance trends between implant types.

4. Discussion

This cadaveric evaluation demonstrates that the 3D-printed PEEK PSIs and titanium mesh each offer distinct advantages for orbital reconstruction depending on case complexity and clinical priorities. The predominantly trainee-dominant population provides valuable insights into technology adoption patterns among future practitioners while offering a unique perspective on learning curve requirements and technology preferences among surgeons who will drive future clinical practice. Despite limited clinical experience, the finding

https://doi.org/10.3390/cmtr19010013

that 64.3% of the participants preferred a situation-dependent implant selection demonstrates the clinical reasoning and understanding of individualized treatment approaches.

The 14.7% reduction in total procedure time with the 3D-printed PEEK PSIs represents a clinically meaningful improvement in surgical efficiency, consistent with previous studies demonstrating that PSIs and computer-assisted workflows can reduce intraoperative time and streamline surgical procedures in orbital reconstruction [15]. A recent meta-analysis of 564 patients showed that pre-shaped implants on 3D-printed anatomical models reduced operative time by 23.58 min compared to manual free-hand shaping [16], while Chepurnyi et al. reported an approximately 34% reduction in surgical time with PEEK PSIs compared to pre-bent titanium plates in orbital reconstruction [17]. The elimination of intraoperative bending procedures directly addresses a primary limitation of conventional titanium mesh reconstruction. Our finding that bending titanium mesh alone required an average of 6.1 min underscores the inefficiency of intraoperative adaptation, particularly in complex cases, where PEEK PSI technology eliminates this step through precise virtual surgical planning.

The 3D-printed PEEK PSIs demonstrated advantages in handling, fit quality, and mechanical stability, with mechanical stability showing the most clinically meaningful difference (Cohen's d = -0.47). The unanimous rating of the 3D-printed PEEK PSIs as stable to very stable (100% rated 1–2), compared with the 91% rating for the titanium mesh, reflects the surgeons' confidence in the PSIs' structural integrity. These advantages reflect the precision afforded by a patient-specific design, which is crucial for multi-walled, complex orbital fractures, where reduced surgeon concern about implant failure during positioning is critical in limited-access regions [18,19]. Previous comparative studies have demonstrated superior volumetric restoration with PSIs, with mean orbital shape differences between reconstructed and intact orbits of 0.137 cm^3 for PSIs versus 1.05 cm^3 for conventional plates, particularly in complex reconstructions requiring cantilevered support [20].

The surgeon-reported technical challenges provide an important context for quantitative assessments and highlight technology-specific implementation considerations. Titanium mesh concerns are centered on intraoperative handling issues, including shape instability during insertion, extensive bone exposure requirements, and contouring difficulties. Such challenges are consistent with previous cadaveric evaluations, demonstrating the inherent limitations of manual intraoperative adaptation despite pre-bending on anatomical models [21]. By contrast, the 3D-printed PEEK PSI challenges are focused on implant thickness perception and the learning requirements for planning software. These distinct challenge patterns support the complementary nature of these technologies and inform targeted training protocols for successful implementation.

Pre-bending of the titanium mesh on 3D-printed anatomical models demonstrated easier learning curve requirements compared to the 3D-printed PEEK PSIs. However, this finding must be interpreted within the fracture complexity context rather than purely material properties. The 3D-printed PEEK PSIs were evaluated in complex Class IV orbital fracture scenarios, while the titanium mesh was assessed in simpler Class II defects with preserved anatomical landmarks. The perceived increased difficulty of the 3D-printed PEEK PSI procedures likely reflects the inherent complexity of reconstructions rather than material-handling characteristics alone, consistent with studies demonstrating rapid skill acquisition with virtual surgical planning technologies, in which novice users achieved proficiency within six planning sessions, with significant reductions in both planning time and accuracy [22]. This suggests that implant selection should be matched to both the surgeon's experience and the case's complexity.

Stratification of primary outcomes by level of surgical experience showed comparable directional trends between trainees and attending/senior surgeons for both titanium mesh

https://doi.org/10.3390/cmtr19010013

and 3D-printed PEEK PSIs. While experienced surgeons showed slightly higher procedural confidence and marginally longer procedure times, relative implant performance across handling, fit quality, positioning confidence, mechanical stability, and learning curve perception remained consistent across the experience strata. These findings suggest that the observed differences among implant technologies were not driven solely by operator experience and support the generalizability of the results across a broad range of training levels.

The successful development and validation of radiopaque PEEK formulations could represent a paradigm shift in orbital implant technology, addressing a fundamental limitation that has historically limited PEEK's use in orbital reconstruction. PEEK's traditional radiolucency has created a clinical dilemma where the postoperative visualization of implant position is essential for detecting complications such as implant migration or soft tissue entrapment. $BaSO_4$ has emerged as the preferred radiopaque filler for high-temperature polymers, like PEEK, due to its thermal stability at processing temperatures exceeding 335 °C, its excellent biocompatibility, and its ability to provide radiographic contrast without significant artefact formation. These properties distinguish it from alternative radiopaque additives, such as bismuth compounds, which degrade at lower temperatures [23]. The incorporation of $BaSO_4$ at optimal concentrations achieves controlled radiopacity and is expected to facilitate precise implant localization on standard CT images while preserving superior soft tissue contrast compared to metallic alternatives. The seamless integration of radiopaque enhancement without detectable changes in handling characteristics validates the potential for broader clinical adoption without requiring modifications to established surgical techniques.

The incorporation of barium sulfate into PEEK raises important considerations regarding cytotoxicity and long-term matrix stability. $BaSO_4$ is a chemically inert, insoluble, and thermally stable radiopaque additive that has been widely used in implantable polymeric biomaterials for decades. It has an extremely low aqueous solubility which prevents ion release and associated cellular toxicity, and preclinical testing has demonstrated that $BaSO_4$-filled PEEK exhibits cytocompatibility comparable to native PEEK, meeting ISO 10993 biocompatibility standards for implantable devices [12]. Regarding concerns of filler disintegration, $BaSO_4$ particles are homogeneously dispersed within the PEEK matrix during high-temperature compounding (>350 °C), forming a stable composite structure. At the 20% filler concentration used in this study, within the established 10–30% range for medical applications, matrix integrity is maintained under physiological loading conditions, with no evidence of particulate release reported in mechanical testing. Nevertheless, long-term clinical studies specific to orbital patient-specific implants remain warranted to confirm these favorable preclinical findings [24,25]. Table 5 summarizes the comparative advantages and limitations of each orbital reconstruction material evaluated in this study.

The situation-dependent preferences expressed by the trainee surgeons provide encouraging insights into contemporary surgical education and clinical decision-making. This pattern suggests recognition that optimal implant selection should be individualized based on defect complexity, anatomical requirements, surgeon experience, and available resources. Our findings support a nuanced approach to orbital implant selection where titanium mesh remains appropriate for simple fractures where manual contouring is feasible and cost-effectiveness is prioritized, while 3D-printed PEEK PSIs offer advantages for complex multi-walled fractures requiring precise anatomical restoration and improved imaging compatibility.

https://doi.org/10.3390/cmtr19010013

Table 5. Comparative advantages and limitations of orbital reconstruction materials.

Parameter	Ti Mesh	3D-Printed PEEK PSI (Native)	3D-Printed PEEK PSI ($BaSO_4$)
Advantages			
Radiopacity	Inherent	None	Controlled
Imaging compatibility	Limited	Excellent	Good
Intraoperative adaptability	High	Low	Low
Anatomical precision	Surgeon-dependent	High (patient-specific)	High (patient-specific)
Clinical experience	Extensive (>30 yrs)	Growing	Emerging
Limitations			
CT/MRI artifacts	Significant	None	Minimal
Sharp edge risk	Present	Absent	Absent
Planning requirements	Minimal	VSP required	VSP required
Lead time	Immediate	Days-weeks	Days-weeks

Several considerations should guide the interpretation of these findings. First, the study design intentionally matched implant types to clinically appropriate fracture complexities, reflecting real-world surgical decision-making rather than a controlled material comparison within identical defect patterns. While this approach provides realistic evaluation scenarios, it precludes a direct comparison of intrinsic material properties under identical anatomical conditions and is therefore acknowledged as a limitation of the study. Second, physical fractures were not created in the cadaveric specimens; implant placement was performed on intact orbital anatomy following reconstruction-to-native-position simulation, while these standardized evaluation conditions, fracture-specific biomechanics, and soft-tissue behavior were not replicated.

Third, the participant cohort was heterogeneous, with a predominance of trainees. The heterogeneous experience levels, including one medical student and one senior surgeon at opposite ends of the training spectrum, may introduce variability. However, the inclusion of one medical student enabled an assessment of the baseline intuitiveness of the workflow for a novice user. A sensitivity analysis excluding these experience-level outliers demonstrated no impact on the overall observed trends. The results should therefore be interpreted as reflecting perceptions of the technology across a range of training levels rather than expert consensus. The trainee-dominant cohort provides valuable insights into technology adoption patterns and learning curve requirements among future practitioners, although incorporation of additional experienced surgeon perspectives would further strengthen generalizability. Furthermore, the learning curve assessment was based on perceived difficulty following limited exposure (1–2 procedures) rather than longitudinal skill acquisition. True learning curve characterization would require prospective evaluation with repeated procedures.

Lastly, the cadaveric model offers controlled evaluation conditions while recognizing that live tissue properties, healing responses, and patient-specific factors contribute additional complexity to clinical outcomes. While volumetric and technical outcomes favor PSIs, systematic reviews have indicated that clinical outcomes remain variably reported across studies, with current evidence limited to level III, highlighting the need for prospective comparative trials with standardized outcome measures [26].

While patient-specific titanium implants represent an important emerging technology, their availability remains limited to highly specialized centers. By contrast, pre-fabricated

https://doi.org/10.3390/cmtr19010013

titanium mesh remains the global standard of care for orbital reconstruction. This study, therefore, focused on a clinically relevant decision point faced by most surgeons: whether to adopt point-of-care polymer patient-specific implants or to continue conventional titanium mesh workflows. A comparative evaluation of patient-specific titanium versus patient-specific polymer implants is an important direction for future research. Future research should focus on clinical trials that compare outcomes within matched fracture-complexity categories, incorporating experienced surgeon perspectives alongside trainee evaluations. Cost-effectiveness analyses considering case complexity factors, learning curves, and long-term outcomes would provide valuable guidance for institutional technology adoption decisions. An investigation of structured training protocols for implementing 3D-printed PEEK PSIs, along with studies of long-term clinical outcomes, would provide essential data for evidence-based practice guidelines.

5. Conclusions

This cadaveric evaluation demonstrates that the 3D-printed PEEK PSIs and pre-fabricated titanium mesh implants represent complementary technologies in orbital reconstruction, with each offering distinct advantages for specific clinical scenarios. Within clinically appropriate fracture–implant matching scenarios, the 3D-printed PEEK PSIs demonstrated advantages in handling, fit quality, and mechanical stability for complex Class IV defects, while the pre-bent titanium mesh showed a lower learning curve for Class II reconstructions. These findings support situation-dependent implant selection aligned with current clinical practice patterns. The successful development of the radiopaque PEEK formulations addresses a critical limitation in orbital applications, potentially facilitating postoperative surveillance without compromising handling characteristics. The situation-dependent preferences expressed by surgeons support personalized technology selection based on case complexity and clinical priorities, advancing orbital reconstruction toward precision medicine approaches that optimize outcomes through appropriate technology matching.

Author Contributions: Conceptualization: N.S.; methodology: J.Z.O., D.H. and N.S.; software, J.Z.O.; validation: J.Z.O., D.H. and N.S.; formal analysis: J.Z.O., D.H. and N.S.; investigation: J.Z.O., D.H., Y.S.K. and L.S.; resources: J.Z.O., Y.S.K., L.S., F.M.T. and N.S.; data curation: J.Z.O., D.H. and N.S.; writing—original draft: J.Z.O. and N.S.; writing—review and editing: J.Z.O., D.H., Y.S.K., L.S., D.S., F.M.T. and N.S.; visualization: J.Z.O. and D.H.; supervision: F.M.T. and N.S.; project administration: N.S. All authors have read and agreed to the published version of the manuscript.

Funding: This research was funded by the Werner Siemens Foundation, MIRACLE II (Minimally Invasive Robot-Assisted Computer-Guided LaserosteotomE) project and the Innovation Focus—Regenerative Surgery project, University Hospital Basel.

Institutional Review Board Statement: This study was conducted in accordance with institutional guidelines for cadaveric research, with ethical approval obtained from the Ethics Commission of Northwestern and Central Switzerland (EKNZ), BASEC-Nr. 2025-01141 (23.06.2025).

Informed Consent Statement: Informed consent was waived as the manuscript does not contain any identifiable human data or images.

Data Availability Statement: The datasets of this study are available from the corresponding author upon reasonable request.

Acknowledgments: We thank the International Bone Research Association (IBRA) for granting access to their facilities and for providing the technical resources for conducting the cadaveric experiments. Finally, we thank all the surgeons who participated in the study for their expertise and valuable contributions. During the preparation of this manuscript study, the authors used Grammarly Pro v.6.8.261 solely to improve sentence structure and language clarity. The tool did not contribute to

https://doi.org/10.3390/cmtr19010013

content generation, data interpretation, or intellectual input beyond linguistic refinement. The authors have reviewed and edited the output and take full responsibility for the content of this publication.

Conflicts of Interest: Florian M. Thieringer, who serves as the Editor-in-Chief of Craniomaxillofacial Trauma & Reconstruction (CMTR), is a coauthor of this study. In accordance with the journal's editorial policy, the submission was handled by an independent Editorial Board Member, and the manuscript was reviewed by at least two independent external reviewers. The journal staff were not involved in the peer review or editorial process of this submission. Authors Yannick Simon Krieger and Lukas Schuebel were employed by 3D Systems. The company had no role in the study design, data collection, analysis, interpretation of data, writing of the manuscript, or decision to publish the results. The remaining authors declare that the research was conducted in the absence of any commercial or financial relationships that could be construed as a potential conflict of interest.

Abbreviations

The following abbreviations are used in this manuscript:

3D	Three-Dimensional
AM	Additive Manufacturing
$BaSO_4$	Barium Sulfate
CAD	Computer-Aided Design
CMF	Craniomaxillofacial Surgery
CT	Computed Tomography
FFF	Fused Filament Fabrication
PEEK	Polyetheretherketone
PLA	Polylactic Acid
PSI	Patient-Specific Implant
SD	Standard Deviation
Ti	Titanium

References

1. Boyette, J.R.; Pemberton, J.D.; Bonilla-Velez, J. Management of orbital fractures: Challenges and solutions. *Clin. Ophthalmol.* **2015**, *9*, 2127–2137. [CrossRef] [PubMed]
2. He, Q.; Rao, P.; Wang, L.; Li, Y.; Fu, G.; Xiao, J. Reconstruction of orbital wall fractures with superior orbital fissure syndrome using individualized preformed titanium mesh: A pilot study. *Oral Surg. Oral Med. Oral Pathol. Oral Radiol.* **2023**, *135*, 24–32. [CrossRef] [PubMed]
3. Sharma, S.; Kaushal, A.; Patel, S.; Kumar, V.; Prakash, M.; Mandeep, D. Methods to address metal artifacts in post-processed CT images—A do-it-yourself guide for orthopedic surgeons. *J. Clin. Orthop. Trauma* **2021**, *20*, 101493. [CrossRef] [PubMed]
4. Shah, K.; Thakurani, S. Assessing the adequacy of orbital reconstruction with titanium mesh using clinical and radiological measures. *Cureus* **2024**, *16*, e70324. [CrossRef]
5. Strong, E.B.; Fuller, S.C.; Wiley, D.F.; Zumbansen, J.; Wilson, M.D.; Metzger, M.C. Preformed vs. intraoperative bending of titanium mesh for orbital reconstruction. *Otolaryngol. Head Neck Surg.* **2013**, *149*, 60–66. [CrossRef]
6. Huang, M.F.; Alfi, D.; Alfi, J.; Huang, A.T. The use of patient-specific implants in oral and maxillofacial surgery. *Oral Maxillofac. Surg. Clin. N. Am.* **2019**, *31*, 593–600. [CrossRef] [PubMed]
7. Kim, J.H.; Lee, C.R.; Oh, D.Y.; Jun, Y.J.; Moon, S.H. Comparison of efficacy between three-dimensional printing and manual-bending implants for inferomedial orbital fracture: A retrospective study. *Appl. Sci.* **2021**, *11*, 7971. [CrossRef]
8. Fan, B.; Chen, H.; Sun, Y.J.; Wang, B.F.; Che, L.; Liu, S.Y.; Li, G.Y. Clinical effects of 3-D printing-assisted personalized reconstructive surgery for blowout orbital fractures. *Graefes Arch. Clin. Exp. Ophthalmol.* **2017**, *255*, 2051–2057. [CrossRef]
9. Najeeb, S.; Zafar, M.S.; Khurshid, Z.; Siddiqui, F. Applications of polyetheretherketone (PEEK) in oral implantology and prosthodontics. *J. Prosthodont. Res.* **2016**, *60*, 12–19. [CrossRef]
10. Lommen, J.; Schorn, L.; Sproll, C.; Haussmann, J.; Kübler, N.R.; Budach, W.; Rana, M.; Tamaskovics, B. Reduction of CT artifacts using polyetheretherketone (PEEK), polyetherketoneketone (PEKK), polyphenylsulfone (PPSU), and polyethylene (PE) reconstruction plates in oral oncology. *J. Oral Maxillofac. Surg.* **2022**, *80*, 1272–1283. [CrossRef]
11. Saponaro, G.; Todaro, M.; Barbera, G.; Scivoletto, G.; Foresta, E.; Gasparini, G.; Moro, A. Patient-specific facial implants in polyetheretherketone and their stability: A preliminary study. *Ann. Plast. Surg.* **2023**, *90*, 564–567. [CrossRef]

https://doi.org/10.3390/cmtr19010013

12. Emonde, C.K.; Eggers, M.E.; Wichmann, M.; Hurschler, C.; Ettinger, M.; Denkena, B. Radiopacity enhancements in polymeric implant biomaterials: A comprehensive literature review. *ACS Biomater. Sci. Eng.* **2024**, *10*, 1323–1334. [CrossRef] [PubMed]
13. Green, S. Compounds and composite materials. In *PEEK Biomaterials Handbook*; Kurtz, S.M., Ed.; William Andrew Publishing: Norwich, NY, USA, 2012; pp. 23–48.
14. Jaquiéry, C.; Aeppli, C.; Cornelius, P.; Palmowsky, A.; Kunz, C.; Hammer, B. Reconstruction of orbital wall defects: Critical review of 72 patients. *Int. J. Oral Maxillofac. Surg.* **2007**, *36*, 193–199. [CrossRef] [PubMed]
15. Kotecha, S.; Ferro, A.; Harrison, P.; Fan, K. Orbital reconstruction: A systematic review and meta-analysis evaluating the role of patient-specific implants. *Oral Maxillofac. Surg.* **2023**, *27*, 213–226. [CrossRef]
16. Singh, A.K.; Khanal, N.; Chaulagain, R.; Sharma, N.; Thieringer, F.M. Is the pre-shaping of an orbital implant on a patient-specific 3D-printed model advantageous compared to conventional free-hand shaping? A systematic review and meta-analysis. *J. Clin. Med.* **2023**, *12*, 3426. [CrossRef]
17. Chepurnyi, Y.; Chernogorskyi, D.; Kopchak, A.; Petrenko, O. Clinical efficacy of peek patient-specific implants in orbital reconstruction. *J. Oral Biol. Craniofac. Res.* **2020**, *10*, 49–53. [CrossRef]
18. Sharma, N.; Welker, D.; Aghlmandi, S.; Maintz, M.; Zeilhofer, H.F.; Honigmann, P.; Seifert, T.; Thieringer, F.M. A multi-criteria assessment strategy for 3D printed porous polyetheretherketone (PEEK) patient-specific implants for orbital wall reconstruction. *J. Clin. Med.* **2021**, *10*, 3563. [CrossRef]
19. Raisian, S.; Fallahi, H.R.; Khiabani, K.S.; Heidarizadeh, M.; Azdoo, S. Customized titanium mesh based on the 3D printed model vs. manual intraoperative bending of titanium mesh for reconstructing of orbital bone fracture: A randomized clinical trial. *Rev. Recent Clin. Trials* **2017**, *12*, 154–158. [CrossRef] [PubMed]
20. Chepurnyi, Y.; Chernohorskyi, D.; Zhukovtceva, O.; Poutala, A.; Kopchak, A. Automatic evaluation of the orbital shape after application of conventional and patient-specific implants: Correlation of initial trauma patterns and outcome. *J. Oral Biol. Craniofac. Res.* **2020**, *10*, 733–737. [CrossRef]
21. Bittermann, G.; Metzger, M.C.; Schlager, S.; Lagrèze, W.A.; Gross, N.; Cornelius, C.P.; Schmelzeisen, R. Orbital reconstruction: Prefabricated implants, data transfer, and revision surgery. *Facial Plast. Surg.* **2014**, *30*, 554–560. [CrossRef]
22. Hsieh, T.Y.; Said, M.; Dedhia, R.D.; Timbang, M.R.; Steele, T.O.; Strong, E.B. Assessment of the learning curve for virtual surgical planning in orbital fractures. *Craniomaxillofac. Trauma Reconstr.* **2020**, *13*, 186–191. [CrossRef] [PubMed]
23. Panayotov, I.V.; Orti, V.; Cuisinier, F.; Yachouh, J. Polyetheretherketone (PEEK) for medical applications. *J. Mater. Sci. Mater. Med.* **2016**, *27*, 118. [CrossRef] [PubMed]
24. Kurtz, S.M. (Ed.) *PEEK Biomaterials Handbook*; William Andrew: Norwich, NY, USA, 2019.
25. Mbogori, M.; Vaish, A.; Vaishya, R.; Haleem, A.; Javaid, M. Poly-ether-ether-ketone (PEEK) in orthopaedic practice: A current concept review. *J. Orthop. Rep.* **2022**, *1*, 3–7. [CrossRef]
26. Yoon, M.K.; Aakalu, V.K.; Dagi Glass, L.R.; Grob, S.R.; McCulley, T.J.; Vagefi, M.R.; Pineles, S.L.; Wladis, E.J. Orbital patient-specific (customized) implants: A report by the American Academy of Ophthalmology. *Ophthalmology* **2025**, *132*, 945–953. [CrossRef] [PubMed]

Disclaimer/Publisher's Note: The statements, opinions and data contained in all publications are solely those of the individual author(s) and contributor(s) and not of MDPI and/or the editor(s). MDPI and/or the editor(s) disclaim responsibility for any injury to people or property resulting from any ideas, methods, instructions or products referred to in the content.

https://doi.org/10.3390/cmtr19010013

craniomaxillofacial
trauma & reconstruction

MDPI

Article

Finite Element Analysis of Low-Profile Reconstruction Plates for Atrophic Mandibles—Part II: A Comparison of Customized Plates with 3D Grid-Type and Conventional Designs

Bianca Pulino [1,2,3,*], Robert Sader [4], Guilherme Louzada [1], Majeed Rana [5], Gabriele Millesi [5], Geraldo Prestes de Camargo Filho [6] and Raphael Capelli Guerra [1,2,3,*]

1 Hospital Sírio-Libanês, Instituto de Ensino e Pesquisa, São Paulo 01308-050, Brazil
2 Faculdade Israelita de Ciências da Sáude Albert Einstein, Department of Oral and Maxillofacial Surgery, São Paulo 05652-900, Brazil
3 Hospital Israelita Albert Einstein, Department of Oral and Maxillofacial Surgery, São Paulo 05652-900, Brazil
4 Department of Craniomaxillofacial, Plastic and Reconstruction Surgery, Goëthe Universität Frankfurt, 60325 Frankfurt, Germany
5 University Hospital Vienna, Department of Oral and Maxillofacial Surgery, 1090 Vienna, Austria
6 Dental School, Nova Southeastern University, Clearwater, FL 33759, USA
* Correspondence: biancapulino@icloud.com (B.P.); dr.raphael.guerra@gmail.com (R.C.G.)

Abstract

Objectives: The aim of this study was to compare the stiffness-related mechanical response and peak von Mises stress distribution of low-profile 2.4 mm mandibular reconstruction systems (a conventional reconstruction plate, a 3D grid-type plate, and a customized plate) in a virtual atrophic mandible model with a 5 cm segmental defect. Materials and Methods: A CT-based three-dimensional mandible model was created and instrumented with three plate configurations (G1–G3). Linear static finite element analyses were performed under a 300-N masticatory load combined with literature-based muscle force vectors. Peak von Mises stresses were recorded for plates and screws, and the locations of maximum stress concentration were identified. Results: Peak plate stress was highest in the conventional reconstruction plate (G1: 695.5 MPa), followed by the 3D grid-type plate (G2: 595.6 MPa), and lowest in the customized plate (G3: 185.2 MPa). The peak screw stress was 692.9 MPa (G1), 898.0 MPa (G2), and 595.6 MPa (G3). The 3D grid-type plate increased construct stiffness but shifted stress concentration toward the mandibular angle and adjacent screws, whereas the customized plate reduced the peak plate stress and limited the extent of the high-stress region across the defect. Conclusions: Within the limitations of a linear static FEA (stiffness/stress distribution rather than failure load or fatigue resistance), the customized plate (G3) demonstrated the most favorable biomechanical performance (lowest peak plate stress). The 3D grid-type plate (G2) reduced peak plate stress compared with the conventional design (G1) but produced the highest peak screw stress. Practical considerations such as manufacturing lead time and resource requirements may favor off-the-shelf plates; however, a formal cost or operative-time analysis was not performed.

Keywords: mandible; mandibular fixation technique; edentulous mandible; finite element analysis; mandibular reconstructions

1. Introduction

Individuals with atrophic mandibles often present reduced bone volume and compromised vascularity, which can limit osteogenesis and impair healing. This condition is

frequently observed in older, edentulous patients and may be associated with nutritional limitations, impaired oral function, and reduced quality of life. Mandibular defects due to benign or malignant lesions, trauma, or infection can further result in major functional deficits (speech, mastication, swallowing, and airway support) and increase the burden of care through prolonged rehabilitation and the need for secondary interventions [1–3].

Reconstruction with load-bearing plates, with or without vascularized or non-vascularized grafts, remains an established strategy; however, postoperative complications such as screw loosening, plate fracture, and infection continue to be reported, with occurrence rates ranging from 28% to 39% [4]. Plate geometry (width, thickness, and hole/screw distribution) influences construct stiffness and how loads are transferred to screws and bone, particularly in long-span segmental defects. In current practice, plate selection is often guided by availability and surgeon experience, because direct in vivo measurement of internal stresses is not feasible and experimental testing can be limited by specimen variability and simplified loading conditions.

Conventional evaluation of fixation constructs relies on clinical case series and in vitro testing using cadaveric or synthetic models. While these approaches provide important insights, they are typically constrained in reproducing patient-specific anatomy, bone quality, and complex load transfer across plate–screw–bone interfaces. As a result, there remains a need for complementary computational methods capable of comparing construct mechanics under standardized conditions and identifying regions prone to stress concentration in anatomically realistic reconstructions.

Low-profile 2.4 mm systems may reduce hardware prominence and facilitate soft-tissue management, but their reduced cross-sectional height can decrease bending stiffness. Consequently, design-related strategies (e.g., increased plate width, 3D grid-type architectures, or patient-specific customization) may be biomechanically relevant for large defects in atrophic mandibles.

Finite element analysis (FEA) is a technique that divides a domain into smaller areas to allow for mathematical modeling of structures and the application of forces at any point [5]. In simple terms, FEA enables the estimation of internal stresses and load paths that cannot be measured easily in real patients, supporting a non-destructive comparison of fixation strategies in anatomically complex regions such as the mandible [6]. Prior FE studies have explored mandibular reconstruction plate–screw–bone mechanics and identified critical regions of stress concentration near the defect and around the first screw on the loaded side (“crucial screw”) [7–14]. Nevertheless, comparative evidence remains limited for low-profile 2.4 mm systems, particularly when contrasting conventional reconstruction plates with newer 3D grid-type and customized designs in atrophic mandibles with large segmental defects.

Therefore, the aim of this study was to compare the stiffness-related mechanical response and stress distribution of three low-profile 2.4 mm plate systems—conventional reconstruction (G1), 3D grid-type (G2), and customized (G3)—in a virtual atrophic mandible with a 5 cm segmental defect without bone grafting. We hypothesized that the customized plate (G3) would reduce peak von Mises stresses in the plate–screw assembly compared with G1 and G2, and that the 3D grid-type plate (G2) would increase construct stiffness and potentially shift peak stresses toward the mandibular angle and adjacent screws. The primary outcomes were the peak von Mises stresses on plates and screws and the locations of maximum stress concentration, with secondary assessment of stiffness-related response via displacement under the applied load.

https://doi.org/10.3390/cmtr19010009

2. Materials and Methods

2.1. Study Design and Model Generation

This in silico study compared three low-profile 2.4 mm mandibular reconstruction plate designs applied to an atrophic mandible with a 5 cm segmental defect (n = 1 virtual model per configuration: G1–G3).

A three-dimensional mandible model was generated from computed tomography (CT) images of a patient who underwent mandibular resection (axial slices, 1 mm interval). CT segmentation and surface reconstruction were performed in *Dolphin Imaging Software/32*, Chatsworth, CA 91311, USA, Dolphin Imaging. (Version: 11.9, 11.7 e 9.0), and the surface model was exported in STL format for further processing.

2.2. Ethical Approval

This study was authorized through a waiver of informed consent and approved by the Research Ethics Committee involving human subjects via Plataforma Brasil (CAAE: 80036024.4.0000.5420; approval date: 22 May 2024).

2.3. Implant Modeling

Plates were modeled in Geomagic Freeform Plus (3D Systems, Rock Hill, SC, USA) and positioned to match the external contour of the mandible, spanning the defect. Three configurations were analyzed:

- G1: Conventional low-profile 2.4 mm reconstruction plate (135 × 8 × 2.4 mm) with bicortical fixation.
- G2: A 3D grid-type low-profile 2.4 mm plate (150 × 17 × 2.4 mm) with bicortical fixation.
- G3: Customized low-profile 2.4 mm plate (140 × 22 × 2.4 mm) with bicortical fixation.

Screws were modeled with a 2.4 mm diameter; the screw closest to the defect was positioned 10 mm from the resection margin.

The Figure 1 shows the mandibular plates and the type of screw used in this study.

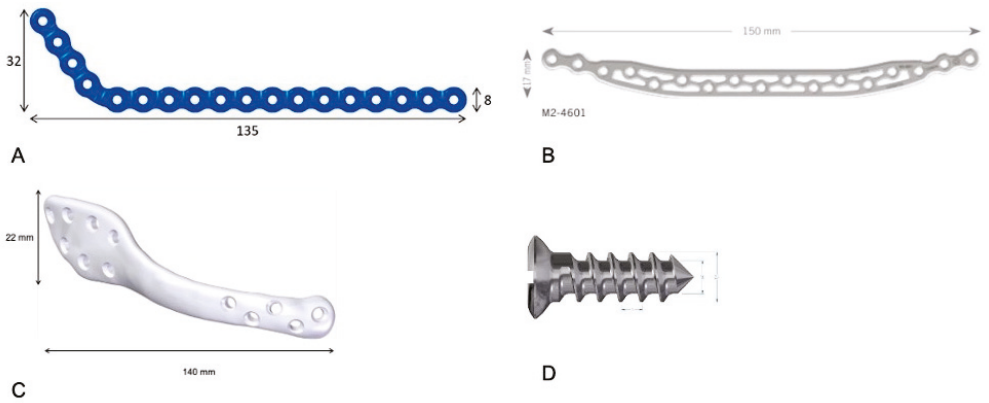

Figure 1. Plate and screw geometries used for finite element modeling. (**A**) 3D grid-type plate: 150 × 17 × 2.4 mm. (**B**) Conventional low-profile 2.4 mm reconstruction plate: 135 × 8 × 2.4 mm. (**C**) Customized low-profile 2.4 mm plate: 140 × 22 × 2.4 mm. (**D**) Bicortical screw: 2.4 mm diameter (length as modeled).

Figure 2 illustrates the plates with the correct adaptation in the atrophic mandible.

https://doi.org/10.3390/cmtr19010009

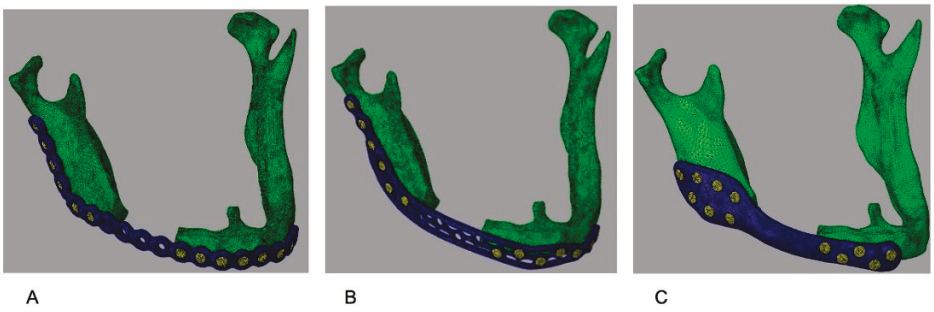

Figure 2. Virtual atrophic mandible models with a 5 cm segmental defect (no bone graft) and the three fixation configurations. (**A**) G1: conventional reconstruction plate. (**B**) G2: 3D grid-type plate. (**C**) G3: customized plate.

2.4. Material Properties

All materials were modeled as elastic, isotropic, and linearly elastic. The Young's modulus (E) and Poisson's ratio (ν) were adopted from prior finite element studies on mandibular reconstruction systems [9,11,15]. The values used in the simulations are summarized in Table 1.

Table 1. Material properties used in the simulations.

Model	Element Type	No. of Elements	No. of Nodes	Convergence Criterion
G1—Conventional reconstruction plate	Linear tetrahedral solid element	≈92,000	≈16,000	Δ peak von Mises stress < 5%
G2—3D grid-type plate	Linear tetrahedral solid element	≈92,000	≈16,000	Δ peak von Mises stress < 5%
G3—customized plate	Linear tetrahedral solid element	≈92,000	≈16,000	Δ peak von Mises stress < 5%

2.5. Bone Representation

To focus on comparative construct behavior, the mandible was modeled as a homogeneous isotropic material representing averaged properties of an atrophic mandible (Table 1). This assumption is addressed as a limitation.

2.6. Mesh Generation and Element Type

The assembly (mandible, plate, and screws) was discretized with linear tetrahedral solid elements. A mesh convergence study was conducted by refining the mesh until changes in peak von Mises stress were <5%. Final mesh characteristics for each model are reported in Table 2.

Table 2. Mesh characteristics and convergence criteria.

Material/Component	Young's Modulod, E (GPa)	Poisson's Ratio, υ	Source
Mandible (atrophic bone; homogeneous isotropic)	13.7	0.30	Adopted from previous FEA studies [9,11,15]
Titanium alloy (plates and screws)	110	0.34	Adopted from previous FEA studies [9,11,15]

2.7. Boundary Conditions and Contact Definition

To prevent rigid body motion, both condyles were constrained in all degrees of freedom. Plate–bone interaction was defined as surface-to-surface contact, and screw–bone

https://doi.org/10.3390/cmtr19010009

and screw–plate interfaces were defined as rigid coupling constraints to represent bicortical fixation (the thread geometry is not explicitly modeled).

2.8. Loading Conditions

A 300 N load was applied perpendicular to the horizontal plane of the mandible to represent masticatory loading. In addition, muscle forces from the masseter, temporalis, medial pterygoid, and anterior belly of the digastric were applied as vector loads, with directions/origins and magnitudes taken from the literature [15].

2.9. Solver and Output Measures

Linear static analyses were run in Ansys (Ansys 2024 R1 24.1) for each configuration. The prespecified outcomes were (i) maximum von Mises stress (MPa) on the plate, (ii) maximum von Mises stress (MPa) on the screws, and (iii) the anatomical/construct locations of these maxima. As a stiffness-related indicator, the displacement at the load application point was also recorded to enable standardized comparison of load transfer behavior across designs. These outputs were selected because regions of elevated plate or screw stress may represent mechanically vulnerable sites and can support preoperative construct selection when planning fixation in long-span atrophic mandibular defects.

2.10. Software Reporting

Dolphin Imaging Software/32 da Dolphin Imaging. (Versões: 11.9, 11.7 e 9.0); Geomagic Freeform Plus 3.0 (3D Systems); and Ansys (Ansys 2024 R1 24.1); Abaqus/CAE 2019 software were used.

3. Results

3.1. Peak Stress on Plates

Von Mises stress maps for all models are presented with color scale bars (MPa). The conventional reconstruction plate (G1) showed the highest peak plate stress (695.5 MPa), concentrated along the plate span over the segmental defect (Figure 3A).

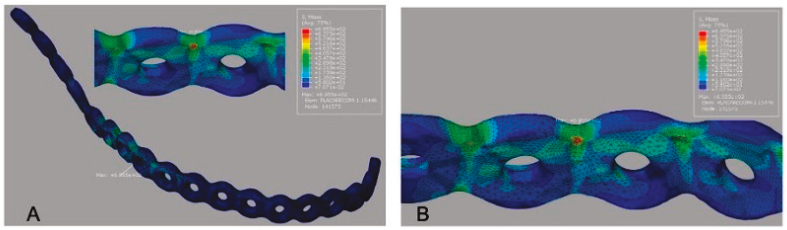

Figure 3. Von Mises stress distribution for G1 (conventional reconstruction plate). (**A**) Plate stress map (MPa; color bar shown; peak 695.5 MPa) with maximum concentration across the segmental defect span. (**B**) Screw stress map (MPa; color bar shown; peak 692.9 MPa) within the plate–screw–bone assembly, highlighting the region adjacent to the defect.

The 3D grid-type plate (G2) exhibited a lower peak plate stress (595.6 MPa) compared with G1, with the maximum concentrated in the mandibular angle region near the load application (Figure 4A).

https://doi.org/10.3390/cmtr19010009

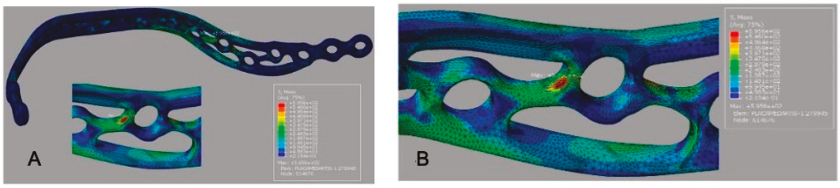

Figure 4. Von Mises stress distribution for G2 (3D grid-type plate). (**A**) Plate stress map (MPa; color bar shown; peak 595.6 MPa) with maximum concentration in the mandibular angle region. (**B**) Screw stress map (MPa; color bar shown; peak 898.0 MPa) within the assembly, indicating higher screw loading near the mandibular angle/loaded side.

The customized plate (G3) demonstrated the lowest peak plate stress (185.2 MPa) and a smaller high-stress region than the other designs (Figure 5A).

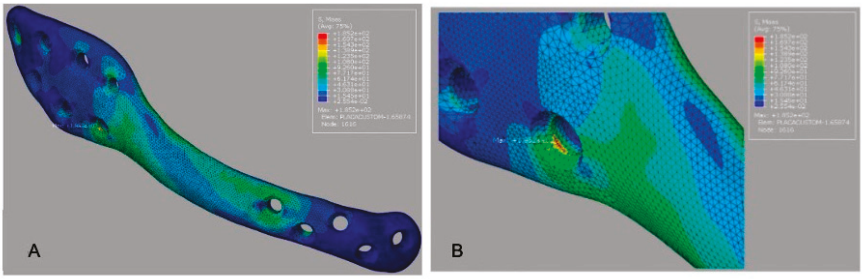

Figure 5. Von Mises stress distribution for G3 (customized plate). (**A**) Plate stress map (MPa; color bar shown; peak 185.2 MPa) demonstrating a reduced high-stress region. (**B**) Screw stress map (MPa; color bar shown; reported peak 595.6 MPa) within the assembly.

3.2. Peak Stress on Screws

Peak screw stress values are summarized in Table 3. For G1, the peak screw stress was 692.9 MPa (Figure 3B). For G2, the peak screw stress increased to 898.0 MPa (Figure 4B), indicating a transfer of load toward the screw–bone interface in the mandibular angle region. For G3, the reported peak screw stress was 595.6 MPa (Figure 5B); this value should be rechecked against the solver output because it equals the reported peak plate stress for G2.

Table 3. Peak von Mises stresses on plates and screws and locations of maximum stresses.

Model	Peak Plate Stress (MPa)	Peak Screw Stress (MPa)	Location of Peak Plate Stress	Location of Peak Screw Stress
G1—Conventional reconstruction plate	695.5	692.9	Plate span over the segmental defect	Screw adjacent to the defect on the loaded side (distal end)
G2—3D grid-type plate	595.6	898.0	Mandibular angle region near load application	Screws in the mandibular angle/loaded side region
G3—Customized plate	185.2	595.6	Localized region along the plate spanning the defect (reduced high-stress area) Peak screw stress for G3 should be verified because it matches the reported peak plate stress for G2.	Screw adjacent to the defect on the loaded side

3.3. Summary Comparison

Overall, the customized plate (G3) produced the lowest peak plate stress and a more diffuse stress distribution across the construct. The 3D grid-type plate (G2) reduced peak

https://doi.org/10.3390/cmtr19010009

plate stress relative to the conventional design (G1) but resulted in the highest peak screw stress. These patterns suggest distinct load-sharing behavior among designs, which may be clinically relevant when selecting fixation strategies for long-span atrophic mandibular defects where screw overload or plate overloading is a concern.

4. Discussion

This study used finite element analysis (FEA) to compare three low-profile fixation designs under identical boundary and loading conditions. FEA is suitable in this context because it can simulate internal stress and load transfer within plate–screw–bone assemblies that cannot be measured directly in vivo, while controlling for anatomical and loading variability. Importantly, the present analysis evaluates stiffness-related behavior and stress concentration patterns under linear static loading; it does not estimate failure load or fatigue performance.

Across configurations, the customized plate (G3) exhibited the lowest peak plate stress and a more distributed stress field, consistent with a geometry that increases effective load-bearing area and reduces local stress raisers. The 3D grid-type plate (G2) reduced peak plate stress relative to the conventional plate (G1), suggesting improved stress distribution across the defect span; however, G2 also showed higher peak screw stress, indicating a potential trade-off whereby plate stiffness and geometry shift a greater proportion of load to fixation points near the mandibular angle.

These findings align with prior biomechanical and FE studies reporting a stress concentration near the first screw adjacent to the defect and around the mandibular angle in long-span reconstructions [7–13]. The present work extends this literature by directly comparing a conventional low-profile plate with a 3D grid-type design and a customized plate in the same atrophic mandible geometry and defect length, highlighting how design-driven load paths can reduce plate stress at the expense of increased screw stress in specific regions.

From a treatment-planning perspective, the prespecified outcomes (peak plate stress, peak screw stress, and their locations) may help surgeons anticipate mechanically vulnerable regions and select fixation strategies accordingly [16,17]. For example, designs that reduce plate stress concentration (as observed for G3) may be preferable when plate overloading is a concern in long defects or poor bone stock, whereas designs associated with higher screw stress (as observed for G2) may warrant attention to screw number, position, and bone quality at the mandibular angle region. These biomechanical inferences should be interpreted cautiously and require experimental validation and clinical follow-up before being translated into definitive clinical recommendations.

Patient-specific plates may require additional steps (imaging processing, design, manufacturing, and logistics) that can influence workflow. In contrast, off-the-shelf 3D grid-type plates may offer a practical alternative when customization is not feasible. Because operative time and costs were not measured, these factors are presented as qualitative considerations rather than study outcomes [18–20]

The strengths of this study include the use of a CT-based three-dimensional mandible model, standardized comparison across three clinically relevant low-profile designs, and transparent reporting of material properties, contacts, boundary conditions, and mesh convergence to support reproducibility.

Limitations should be considered when interpreting absolute stress magnitudes. The simulations used a single CT-based mandible model and a linear elastic, static loading framework; therefore, stress values may differ in vivo due to inter-patient variation in anatomy and bone quality, non-linear contact behavior, and time-dependent effects [21]. The mandible was modeled as homogeneous bone and soft tissues were not included;

https://doi.org/10.3390/cmtr19010009

muscle forces and dynamic mastication patterns were simplified to a representative loading scenario. In addition, thread-level screw–bone mechanics and fatigue or failure behavior were not modeled. Despite these constraints, the standardized setup supports relative, between-design comparisons and helps generate hypotheses regarding load-sharing mechanisms that can be tested in future experimental and clinical studies.

5. Conclusions

This finite element study compared three low-profile 2.4 mm mandibular reconstruction constructs (conventional reconstruction plate, 3D grid-type plate, and customized plate) in an atrophic mandible with a 5 cm segmental defect, focusing on stiffness-related behavior and peak stress concentrations on plates and screws.

Biomechanically, the customized plate (G3) demonstrated the most favorable stress profile, with the lowest peak plate stress and a more distributed stress field. The 3D grid-type plate (G2) reduced peak plate stress relative to the conventional reconstruction plate (G1) but generated higher peak screw stresses, underscoring a trade-off between plate stress reduction and potential screw overloading in specific regions.

Clinically, these findings may support construct selection for long-span atrophic mandibular defects by highlighting where stress concentrations are likely to occur. In scenarios where minimizing plate stress concentration is prioritized (e.g., extensive defects, limited bone stock, or concern for plate overloading), a customized design may be considered. When customization is not feasible, a 3D grid-type plate may represent a practical alternative, with attention to screw placement and bone quality near the mandibular angle to mitigate localized screw stress. These recommendations should be interpreted as biomechanical guidance and require experimental and clinical validation.

Author Contributions: Conceptualization, B.P., R.C.G., R.S. and G.M.; methodology, B.P. and R.C.G.; software, G.L., G.P.d.C.F. and M.R.; validation, R.C.G., G.P.d.C.F. and B.P.; formal analysis, R.S.; investigation, B.P.; resources, B.P., G.P.d.C.F. and R.C.G.; data curation, G.M.; writing—original draft preparation, B.P., R.C.G., R.S. and G.L.; writing—review and editing, B.P., G.P.d.C.F. and R.C.G.; visualization, R.C.G., G.P.d.C.F. and M.R.; supervision, R.C.G., G.P.d.C.F. and R.S.; project administration, R.C.G.; funding acquisition, B.P. All authors have read and agreed to the published version of the manuscript.

Funding: The authors declare that no funding, grants, or other support were received during the preparation of this manuscript.

Institutional Review Board Statement: This study was approved by the Research Ethics Committee involving human subjects via Plataforma Brasil (CAAE: 80036024.4.0000.5420; approval date: 22 May 2024).

Informed Consent Statement: Not applicable, as this study did not involve human participants.

Data Availability Statement: The original contributions presented in this study are included in the article. Further inquiries can be directed to the corresponding author(s).

Conflicts of Interest: The authors declare no conflict interests.

References

1. Jacobson, R.; Sarver, D.M. The predictability of maxillary repositioning in LeFort I orthognathic surgery. *Am. J. Orthod. Dentofac. Orthop.* **2002**, *122*, 142–154. [CrossRef] [PubMed]
2. Madsen, M.J.; Haug, R.H.; Christensen, B.S.; Aldridge, E. Management of atrophic mandible. *Oral Maxillofac. Surg. Clin. N. Am.* **2009**, *21*, 175–183. [CrossRef] [PubMed]
3. Gutwald, R.; Jaeger, R.; Lambers, F.M. Customized mandibular reconstruction plates improve mechanical performance in a mandibular reconstruction model. *Comput. Methods Biomech. Biomed. Eng.* **2017**, *20*, 426–435. [CrossRef]

https://doi.org/10.3390/cmtr19010009

4. Kämmerer, P.W.; Klein, M.O.; Moergel, M.; Gemmel, M.; Draenert, G.F. Local and systemic risk factors influencing the long-term success of angular sta- ble alloplastic reconstruction plates of the mandible. *J. Cranio-Maxillofac. Surg.* **2014**, *42*, 271–276. [CrossRef] [PubMed]
5. Costa, F.W.G.; Bezerra, M.F.; Ribeiro, T.R.; Pouchain, E.C.; Sabóia, V.d.P.A.; Soares, E.C.S. Biomechanical analysis of titanium plate systems in mandibular condyle fractures: A systematized literature review. *Acta Cir. Bras.* **2012**, *27*, 424–429. [CrossRef]
6. Kuik, K.; De Ruiter, M.H.T.; De Lange, J.; Hoekema, A. Fixation methods in sagittal split ramus osteotomy: A systematic review on in vitro biomechanical assessments. *Int. J. Oral Maxillofac. Surg.* **2019**, *48*, 56–70. [CrossRef]
7. Kimura, A.; Nagasao, T.; Kaneko, T.; Tamaki, T.; Miyamoto, J.; Nakajima, T. Adequate fixation of plates for stability during mandibular reconstruction. *J. Cranio-Maxillofac. Surg.* **2006**, *34*, 193–200. [CrossRef]
8. De Oliveira, L.B.; Reis, J.M.N.; Spin-Neto, R.; Gabrielli, M.A.C.; Oguz, Y.; Pereira-Filho, V.A. Mechanical evaluation of six techniques for stable fixation of the sagittal split osteotomy after counterclockwise mandibular advancement. *Br. J. Oral Maxillofac. Surg.* **2016**, *54*, 573–578. [CrossRef]
9. Narra, N.; Valášek, J.; Hannula, M.; Marcián, P.; Sándor, G.K.; Hyttinen, J.; Wolff, J. Finite element analysis of customized reconstruction plates for mandibular continuity defect therapy. *J. Biomech.* **2014**, *47*, 264–268. [CrossRef]
10. Brasileiro, B.F.; Grempel, R.G.; Ambrosano, G.M.B.; Passeri, L.A.; Maurer, P.; Knoll, W.D. Comparison of stability of 2.0 mm standard and 2.0 mm locking miniplate/screws for the fixation of sagittal split ramus osteotomy on sheep mandibles. *J. Oral Maxillofac. Surg.* **2011**, *69*, 573–578.
11. Al-Ahmari, A.; Nasr, E.A.; Moiduddin, K.; Anwar, S.; Kindi, M.A.; Kamrani, A. A comparative study on the customized design of mandibular reconstruction plates using finite element method. *Adv. Mech. Eng.* **2015**, *7*, 1–11. [CrossRef]
12. Wu, C.H.; Lin, Y.S.; Liu, Y.S.; Lin, C.L. Biomechanical evaluation of a novel hybrid reconstruction plate for mandible segmental defects: A finite element analysis and fatigue testing. *J. Cranio-Maxillofac. Surg.* **2017**, *45*, 1671–1680. [CrossRef] [PubMed]
13. Bujtár, P.; Simonovics, J.; Váradi, K.; Sándor, G.K.B.; Avery, C.M.E. The biomechanical aspects of reconstruction for segmental defects of the mandible: A finite element study to assess the optimisation of plate and screw factors. *J. Cranio-Maxillofac. Surg.* **2014**, *42*, 855–862. [CrossRef] [PubMed]
14. Guimond, C.; Johnson, J.V.; Marchena, J.M. Fixation of mandibular angle fractures with a 2.0-mm 3-dimensional curved angle strut plate. *J. Oral Maxillofac. Surg.* **2005**, *63*, 209–214. [CrossRef]
15. Guerra, R.C.; de Fátima Borim Pulino, B.; Salomão Júnior, V.F.; dos Santos Pereira, R.; Thieringer, F.M.; Sacco, R.; Sader, R.; Vieira, E.H. Finite element analysis of low-profile reconstruction plates for atrophic mandibles: A comparison of novel 3D grid and conventional plate designs. *Oral Maxillofac. Surg.* **2023**, *28*, 595–603. [CrossRef]
16. Maurer, P.; Knoll, W.D.; Schubert, J. Comparative evaluation of two osteosynthesis methods on stability following sagittal split ramus osteotomy. *J. Cranio-Maxillofac. Surg.* **2003**, *31*, 284–289. [CrossRef]
17. Knoll, W.D.; Gaida, A.; Maurer, P. Analysis of mechanical stress in reconstruction plates for bridging mandibular angle defects. *J. Cranio-Maxillofac. Surg.* **2006**, *34*, 201–209. [CrossRef]
18. Bak, M.; Jacobson, A.S.; Buchbinder, D.; Urken, M.L. Contemporary reconstruction of the mandible. *Oral Oncol.* **2010**, *46*, 71–76. [CrossRef]
19. Sigua-Rodriguez, E.A.; Caldas, R.A.; Goulart, D.R.; de Moraes, P.H.; Olate, S.; Barao, V.A.R.; de Albergaria-Barbosa, J.R. Comparative evaluation of different fixation techniques for sagittal split ramus osteotomy in 10 mm advancements. Part two: Finite element analysis. *J. Cranio-Maxillofac. Surg.* **2019**, *47*, 1015–1019. [CrossRef]
20. Liang, Y.; Jiang, C.; Wu, L.; Wang, W.; Liu, Y.; Jian, X. Application of Combined Osteotomy and Reconstruction Pre-Bent Plate Position (CORPPP) Technology to Assist in the Precise Reconstruction of Segmental Mandibular Defects. *J. Oral Maxillofac. Surg.* **2017**, *75*, 2026.e1–2026.e10. [CrossRef]
21. Xue, R.; Lai, Q.; Xing, H.; Zhong, C.; Zhao, Y.; Zhu, K.; Deng, Y.; Liu, C. Finite element analysis and clinical application of 3D-printed Ti alloy implant for the reconstruction of mandibular defects. *BMC Oral Health* **2024**, *17*, 95. [CrossRef] [PubMed]

Disclaimer/Publisher's Note: The statements, opinions and data contained in all publications are solely those of the individual author(s) and contributor(s) and not of MDPI and/or the editor(s). MDPI and/or the editor(s) disclaim responsibility for any injury to people or property resulting from any ideas, methods, instructions or products referred to in the content.

https://doi.org/10.3390/cmtr19010009

craniomaxillofacial
trauma & reconstruction

MDPI

Article

Over a Decade of Maxillofacial PEEK Patient-Specific Innovation: A Retrospective Review of the Evolution from In-House Craft to Virtual Design and Remote Manufacturing

Nicholas J. Lee [1], Gareth Honeybone [1,*], Mohammed Anabtawi [2], Mathew Thomas [3] and Sachin M. Salvi [1]

[1] Sheffield Teaching Hospitals NHS Foundation Trust, Glossop Rd, Broomhall, Sheffield S10 2JF, UK; nicholas.lee@nhs.net (N.J.L.); sachin.salvi@nhs.net (S.M.S.)
[2] Leeds Hospitals NHS Trust, Great George St, Leeds LS1 3EX, UK
[3] University Hospitals of Derby and Burton NHS Foundation Trust, Uttoxeter Rd, Derby DE22 3NE, UK
* Correspondence: gareth.honeybone1@nhs.net

Abstract

Maxillofacial skeletal reconstruction presents significant challenges due to anatomical complexity, functional requirements, and aesthetic demands. Traditional materials such as titanium and autogenous bone grafts have limitations, prompting interest in Polyetheretherketone (PEEK), a versatile thermoplastic polymer with advantages like biocompatibility, radiolucency, and elasticity similar to human bone. This multi-year case series evaluates the clinical outcomes of PEEK implants used in 56 cases on 53 patients for maxillofacial reconstruction, primarily for trauma (44 patients) and deformity (9 patients). PEEK implants were applied to various facial regions including the orbit, zygoma, mandible, and maxilla. The majority of surgeries utilised virtual surgical planning. Patient-specific implants were fabricated using 3D imaging technologies, allowing customisation for optimal fit and functionality. The mean patient age was 37 years with a split of 37 to 16 females. Some complications were noted such as infection and paraesthesia. However, the majority of patients experienced positive outcomes. The findings support PEEK implants as a safe, effective, and adaptable material for maxillofacial surgery, with potential for further advancements in material properties and surgical technologies to improve long-term outcomes.

Keywords: polyetheretherketone; PEEK; facial deformity; interlocking; onlay; bespoke maxillofacial prosthesis

1. Introduction

Polyetheretherketone (PEEK) is a semi-crystalline, linear aromatic polymer recognised for its excellent biocompatibility, making it highly suitable for craniofacial reconstruction. It provides several advantages: radiolucency to X-rays, non-magnetic properties (avoiding artefacts on computed tomography [CT] and magnetic resonance [MR] imaging), non-allergenicity, low weight, resistance to fatigue and chemical degradation, and stability of mechanical properties following repeated sterilisation cycles [1].

Intraoperatively, PEEK can be readily contoured using high-speed burs and secured to bone with conventional plating systems. The integration of computer-aided design and computer-aided manufacturing (CAD/CAM) has further improved the accuracy and reproducibility of patient-specific PEEK implants [2–4].

Recent studies have identified PEEK as a promising alternative material for maxillofacial reconstruction, owing to its favourable biocompatibility, radiolucency, chemical

stability, and elastic modulus, which more closely approximates that of native bone tissue [5].

Craniofacial reconstruction remains challenging due to the intricate anatomy of the facial skeleton, its essential functional roles in mastication and speech, and the high aesthetic demands associated with restoration. Conventional reconstructive approaches have utilised titanium implants, which, while reliable, are limited by their stiffness mismatch with bone and lack of intraoperative adaptability. Similarly, autogenous bone grafts present an additional risk of donor site morbidity and infection.

This study reports on 12 years of clinical outcomes from a single maxillofacial unit, comprising 56 operations on 53 patients who underwent facial reconstruction with patient-specific PEEK implants for both trauma and deformity. In total, 69 implants were planned and 68 successfully placed as some patients required multiple implants during a single operation. The series reflects our progressive experience with PEEK technology, documenting advances in implant design, manufacturing methods, and the integration of navigational systems to optimise intraoperative placement.

2. Materials and Methods

A retrospective review of consecutive PEEK implants planned by a single surgeon and placed by the planning surgeon or the planning surgeon and a second surgeon. All implants were placed at the Royal Hallamshire Hospital, Sheffield, UK.

Preoperatively, each patient underwent imaging with either a cone beam computed tomography (CBCT) scan, or a high-resolution multislice computed tomography (CT) scan. For CBCT, a 512 $\times$ 512 matrix was used with a maximum slice thickness of 1.0 mm, following a standardised protocol with the patient positioned in natural head position (NHP). NHP provides a reproducible and standardised orientation of the head, defined as the upright posture with the eyes focused on a distant point at eye level, ensuring a horizontal visual axis [6].

We explored an analogue technique for the production of patient-specific PEEK implants, developed locally through the Sheffield Anaplastology Laboratory. The process began with acquisition of high-resolution CBCT/CT data (0.625 mm slices), which were used to generate a stereolithographic skull model. The area of the proposed reconstruction was outlined on the model, and a patient-specific wax template was sculpted directly onto the surface. This wax pattern was then converted into an acrylic implant using a two-part silicone mould and auto-polymerising polymethyl methacrylate, polymerised under pressure for dimensional stability. The resulting acrylic pattern was carefully checked for accuracy and subsequently scanned with a laser scanner to generate a stereolithographic (.stl) file. This digital file was forwarded to a manufacturing facility in Hull, where it was used to direct computer numerical control (CNC) milling of the prosthesis from implant-grade PEEK (Medipeek IM). Only minimal peripheral finishing was required before sterilisation in an autoclave and surgical implantation. We refer to this process as Digital–Analogue PEEK, a hybrid workflow combining traditional analogue modelling with digital scanning and CNC milling. Although this technique involved multiple manual steps and occasional minor adjustments for fit, it was used successfully in a series of patients, including zygomatic reconstructions, and provided a cost-effective means of delivering patient-specific PEEK implants.

The majority of our implants were planned virtually via a planning webinars performed with the surgeon and the clinical engineer to allow computer-aided design (CAD) of implants, with attention to the path of insertion and the avoidance of anatomical obstacles.

https://doi.org/10.3390/cmtr19010008

Computer-aided manufacturing (CAM) and 3D milling allowed the production of bespoke implants with complex morphology by the manufacturer (DePuy Synthes, Oberdorf, Switzerland).

Before insertion, all patients were reviewed with their 3D planning report, and informed consent for placement of their implant was obtained.

All patients were warned of risks and complications, including infection, residual asymmetry, extrusion, trigeminal nerve injuries, and, for mandibular implants, facial nerve palsy. Smokers were also signposted to further smoking cessation advice.

All surgeries were completed under general anaesthesia with one dose of intravenous antibiotics preoperatively. All zygoma implants were placed via an intra-oral approach; most orbital implants were placed via a transconjunctival approach with or without other additional surgical incision extensions such as lower eyelid swing, lateral canthotomy, or retrocaruncular incision.

A mucoperiosteal flap was designed and performed to achieve a useful subperiosteally pocket without breaching the periosteum.

All implants were soaked with Gentamicin before insertion.

To prevent rotation, implants were fixed with two, Matrix Mid-face or Mandible titanium, screws (DePuy Synthes). If the contour of the implant prevented rotation, then only one screw would suffice. For multiple segments, once interlocked together, two screws were often only required to stabilise the multiple segments now interlocked as a single implant.

Meticulous tension-free layered closure was applied to decrease the risk of wound break down, implant contamination, and exposure. Patients were discharged home with advice on oral hygiene, a soft diet, regular chlorhexidine mouthwashes, and 5 days postoperative oral antibiotics.

The following information was recorded:

- Patient details (demographics, smoking, relevant medications and medical history);
- Type of deformity;
- Side and site of implant;
- Number of segments and number of fixation screws;
- Surgical approach;
- Complications including infection, implant exposure/migration, implant removal, wound dehiscence, and implant-related facial paraesthesia;
- Follow up period.

3. Results

The total number of patients treated was 53. The total number of operations was 56 as three patients required a second surgery. The mean age of patients at the date of surgery was 37 years, with an age range from 17 to 73 years, indicating the applicability of PEEK implants across different age groups. The higher proportion of male patients (37 males vs. 16 females) may reflect a gender bias in the incidence of facial trauma or the likelihood of undergoing reconstructive surgery. The patient population was generally healthy, with 36 non-smokers vs. 17 smokers and 39 individuals without significant comorbidities. This demographic profile suggests that the outcomes reported may be more favourable than in a less healthy population, yet it provides a solid baseline for assessing the potential of PEEK implants.

Trauma was the primary indication for the use of PEEK implants, accounting for 44 out of 53 cases, compared to 9 cases due to deformities. The zygoma (15 cases) and orbital (29 cases) regions were the most frequently affected sites with 4 cases requiring both

https://doi.org/10.3390/cmtr19010008

orbital and zygoma implants, reflecting the common involvement of these areas in facial injuries. The remaining cases involved the mandible (6 cases) and maxilla (1 case).

The four cases required a two-part orbito-zygomatic implant. This was made of two segments placed at right angles to each other. The inferior segment was inserted via an intra-oral approach and the superior segment via trans-orbital incisions.

Of the five patients where the implant extended to the anterior mandible, two had direct chin augmentation with the implant and two had mandibular PSI in combination with a centralising/rotation genioplasty using a titanium patient guide and patient-specific plate [Figure 1a—Placement of titanium cutting guide. Figure 1b—Genioplasty cuts demonstrated. Figure 1c—Centralising genioplasty fixed with patient-specific titanium plate and fit with patient-specific PEEK mandibular implant. Patient 30].

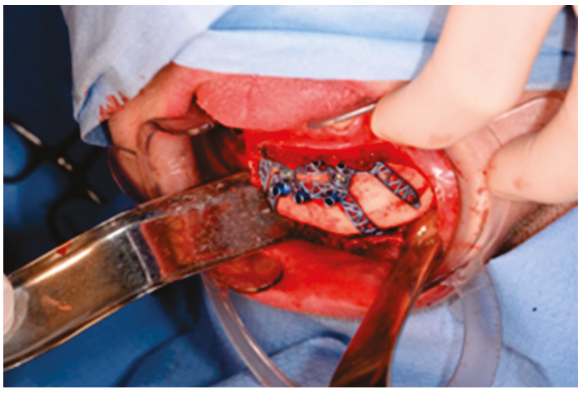

(**a**)

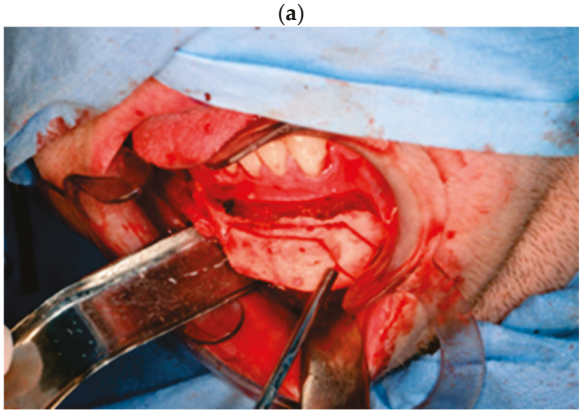

(**b**)

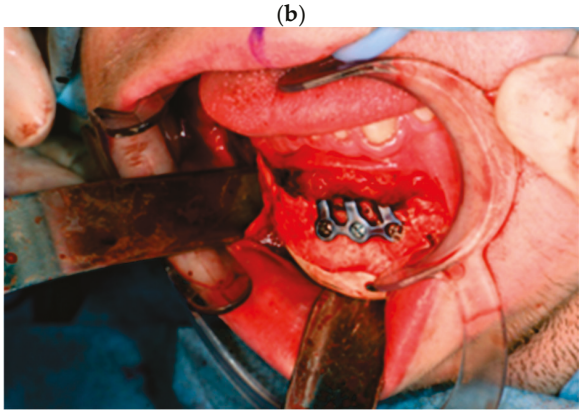

(**c**)

Figure 1. (**a**)—Placement of titanium cutting guide, (**b**)—genioplasty cuts demonstrated, (**c**)—centralising genioplasty fixed with patient-specific titanium plate and fit with patient-specific PEEK mandibular implant. Patient 30. Chin augmentation with the implant and 2 had mandibular PSI in combination with a centralising/rotation genioplasty using a titanium patient guide and patient-specific plate.

https://doi.org/10.3390/cmtr19010008

Within this hemifacial microsomia subgroup, two patients had PSI secondary to orthognathic surgery and one a PSI as a primary camouflaging procedure. One patient received a three-part mandibular implant for mandible micrognathia secondary to juvenile idiopathic arthritis. The remaining patients received implants to camouflage post-traumatic deformities.

In 23 cases, the primary surgeon operated as the sole consultant, while in 33 cases, the surgery was performed jointly with another consultant. The orbital PEEK implant surgery was performed jointly between the maxillofacial surgeon and orbital ophthalmic surgeon. This collaboration enhanced decision-making and technique, potentially improving outcomes.

The use of virtual planning was used in 52 cases vs. 4 analogue in-house which further supports the precision and success of PEEK implants, allowing for more accurate implant placement and better surgical outcomes. The first PEEK implant was placed 28 June 2012. The first two PEEK implants placed were planned with virtual. The first analogue in-house was placed 23 August 2012 and the last was 17 July 2013. A total of 14 cases were planned with interlocking joints, with the first being placed 18 March 2015.

The surgical approaches used varied significantly, highlighting the adaptability of PEEK implants to different anatomical and clinical challenges. The approaches and times they were used were: 22 intraoral approach; 9 trans-conjunctival alone; 11 transconjunctival lid swing; 5 transconjunctival with lateral canthotomy; 3 transconjunctival with lateral canthotomy and retrocaruncular; 2 transconjunctival with retrocaruncular; 2 trans conjunctival lid swing and intra-oral; 1 mid-tarsal skin incision; and 1 bicoronal. Intra-oral access was used primarily for mandibular and zygomatic reconstructions. Transconjunctival approaches, either alone or combined with lateral canthotomy or retrocaruncular techniques, were predominantly used for orbital reconstructions. The diversity of surgical techniques employed demonstrates the versatility of PEEK implants in addressing different reconstructive needs and anatomical complexities.

The data on screws and implants reveal the level of customisation and precision involved in each procedure. The number of screws used ranged from 0 to 6, with the average number of screws used being 1.8. The average screw length was 7.29 mm. Screw length selection is needed for precise fixation without penetrating critical structures.

Additionally, implants were recorded to be soaked in antibiotics in 33 cases, predominantly with Gentamicin. Dosages included 40 mg dose in 9 cases, 80 mg dose in 3 cases, and 20 cases where no dose was recorded. A Clindamycin 80 mg dose was used once. This was for the first case. In the other cases, it was not recorded that the implant was soaked, but it is our practise to soak.

Preoperative planning scans were 50:50 split with 28 cases having a Cone Beam CT (CBCT) vs. 28 CT. Postoperative CT or CBCT scans were performed in 34 cases, facilitating the assessment of implant positioning and integration.

The mean follow-up period of 672 days provides a substantial timeframe for evaluating long-term outcomes.

4. Complications

Most patients experienced no complications, highlighting the overall safety and effectiveness of PEEK implants. However, some complications were noted with 8.9% of cases resulting in swelling and/or infection. In 5.4% of cases, some paraesthesia was reported. Implants were removed in three patients. An in-house zygoma implant was replaced with a virtually planned implant as the first was too bulky [Figure 2a,b. Patient 7. The in-house planned zygoma implant that was removed was placed next to the virtually planned implant prior to insertion]. Another in-house zygoma implant had a poor fitting surface and became infected. The final one to be removed was a three-part orbital, zygoma

https://doi.org/10.3390/cmtr19010008

and lateral wall virtually planned implant that extruded over the zygoma where the skin was very thin. This developed a chronic infection, which was found to be in part due to residual exogenous implant material, which we think were the remains of a previous silicone implant [Figure 3—Patient 44. Three-part implant that extruded and was removed].



(**a**) (**b**)

Figure 2. (**a**,**b**) Patient 7. The in-house planned zygoma implant that was removed placed next to the virtually planned implant prior to insertion.

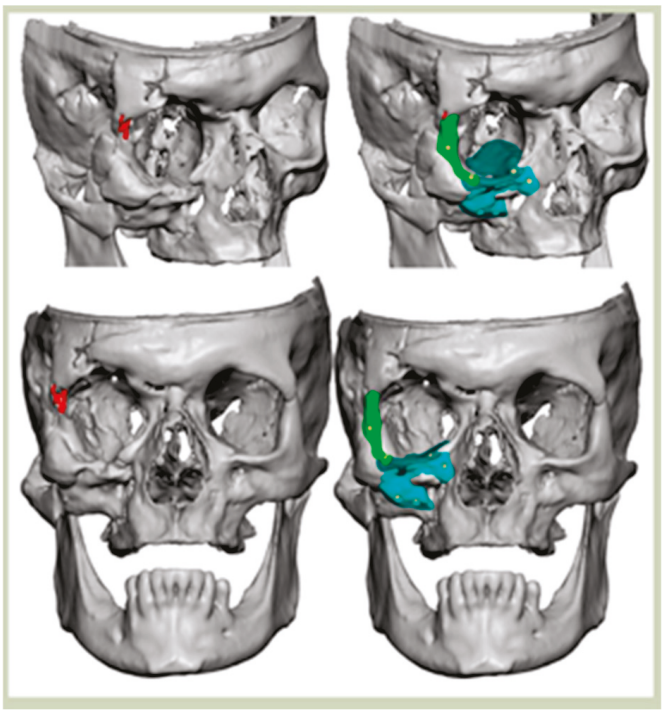

Figure 3. Patient 44. 3-part implant that extruded and was removed.

A total of 2 cases had recurrent sinusitis where screws penetrated into the sinus. A patient who received an interlocking two-part right zygomatic PEEK through an intra-oral approach, developed recurrent right maxillary sinus infection manifested by facial swelling but no signs of infection around the implant. A CT scan showed a wholly obliterated maxillary sinus and showed the fixation screw protruding into the sinus cavity. After referral to ENT, the patient was treated successfully with functional endoscopic sinus surgery (FESS), the implant still in situ and no complications three years post-FESS [Figure 4—Patient. A right sided two-piece zygomatic implant with an interlocking joint with maxillary sinus infection].

https://doi.org/10.3390/cmtr19010008



Figure 4. Patient. A right sided 2-piece zygomatic implant with an interlocking joint with maxillary sinus infection.

A patient with a three-part mandibular implant experienced bilateral altered sensation in the distribution of the mental nerve.

In 1 case, the implant was found to not have an ideal position on the posterior ledge, but there was still an improvement from preop. The patient was offered a replacement but declined [Figure 5—Patient 18. Implant not seated on posterior ledge. An improvement was still gained post-surgery. We would now plan with the implant sitting on the infra-orbital rim].

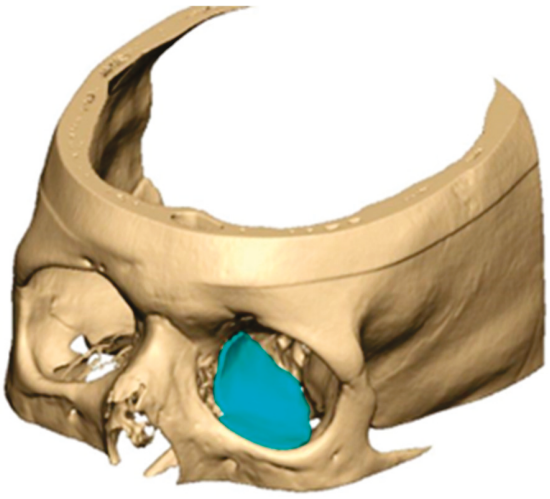

Figure 5. Patient 18. Implant not seated on posterior ledge. An improvement was still gained post-surgery. We would now plan with the implant sitting on the infra-orbital rim.

All patients had an uneventful discharge on the morning following their surgery. No interlocking implants showed signs of infection around them or required removal. The demographics, implant details, and complications for our cohort of patients are presented in Table 1.

https://doi.org/10.3390/cmtr19010008

Table 1. Cohort demographics and results.

Patient	Sex and Age at Time of Surgery (yr)	Indication	Smoking Status	Image	Side	Site	Approach	Number of Pieces	Screws	Follow-Up Since Surgery (Days)	Complications
1	39M	Trauma	No	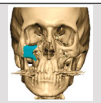	Right	Zygoma	Intra-oral	1	1	607	Right soft tissue swelling
2	41M	Trauma	No		Right	Orbital	Transconjunctival	1	2	121	None
3	42F	Trauma	Smoker		Left	Zygoma	Intra-oral	1	2	26	None
4	20M	Trauma	Smoker		Right	Zygoma	Intra-oral	1	1	489	None
5	47M	Trauma	No	In-house planning. No scan image	Left	Orbital	Transconjunctival	1	0	134	Needed squint surgery
6	33M	Trauma	Smoker	In-house planning. No scan image	Right	Orbital	Mid-tarsal skin incision	1	2	147	None
7a	31M	Trauma	Smoker	In-house planning. No scan image	Left	Zygoma	Intra-oral	1	1	881	Implant was removed as it was more prominent
8	32M	Trauma	Smoker	In-house planning. No scan image	Left	Zygoma	Intra-oral	1	1	No follow up recorded. Pt DNA	None
9	23M	Trauma	No		Right	Zygoma	Intra-oral	1	1	3614	Sinus swelling and inflammation around the screw
10	22M	Trauma	No		Right	Orbital	Transconjunctival lid swing	1	2	398	None
11	32M	Trauma	Smoker		Left	Orbital	Transconjunctival lid swing	1	2	149	None
7b	33M	Trauma	Smoker		Left	Zygoma	Intra-oral	1	2	12	None
12	44M	Trauma	Smoker		Right	Orbital	Transconjunctival lid swing	1	1	44	None

https://doi.org/10.3390/cmtr19010008

Table 1. *Cont.*

Patient	Sex and Age at Time of Surgery (yr)	Indication	Smoking Status	Image	Side	Site	Approach	Number of Pieces	Screws	Follow-Up Since Surgery (Days)	Complications
13	20M	Deformity	No	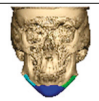	Bi lateral	Mandible	Intra-oral	3	2	1834	None
14a	17F	Deformity	No		Right	Zygoma	Intra-oral	1	2	2463	None
15	50M	Trauma	No		Right	Zygoma	Intra-oral	2	1	1886	Swelling right cheek treated with antibiotics
16	31F	Trauma	No		Right	Orbital	Transconjunctival	1	1	568	None
17	29M	Trauma	Smoker		Left	Orbital	Transconjunctival lid swing	1	1	1154	None
14b	17F	Deformity	No		Right	Mandible	Intra-oral	2	1	2253	None
18	66F	Trauma	No		Left	Orbital	Transconjunctival	1	0	421	Posterior displacement into the sinus
19	51F	Trauma	Smoker		Left	Orbital	Transconjunctival, lateral canthotomy, and transcaruncular	1	1	50	Contacted with intermittent redness around left orbit and tender lump inferior rim. Treated with antibiotics.
20	28M	Deformity	No		Left	Anterior Maxilla	Intra-oral	2	2	173	None
21a	30M	Trauma	No		Left	Orbital	Transconjunctival and lateral canthotomy	1	1	2598	Developed further enophthalmos. New onlay PEEK placed
22	72F	Trauma	Smoker		Left	Orbital	Transconjuntival	1	1	421	None
23	38M	Trauma	No		Right	Orbital	Transcaruncular and transconjunctival	1	1	330	None

https://doi.org/10.3390/cmtr19010008

Table 1. *Cont.*

Patient	Sex and Age at Time of Surgery (yr)	Indication	Smoking Status	Image	Side	Site	Approach	Number of Pieces	Screws	Follow-Up Since Surgery (Days)	Complications
24	42M	Trauma	No	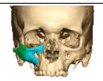	Right	Zygoma	Intra-oral	2	2	209	None
25	19M	Trauma	Smoker		Right	Orbital	Transconjunctival	1	1	1038	None
26	46F	Trauma	Smoker		Right	Zygoma	Intra-oral	2	1	265	None
27	50M	Trauma	Smoker		Left	Zygoma	Intra-oral	2	2	139	None
28	49M	Trauma	No		Right	Orbital	Transconjunctival, lateral canthotomy, and transcaruncular	1	1	1413	Screw does penetrate into the sinus. Had squint surgery and lower lid tightening procedure
29	53M	Trauma	No		Right	Orbital and Zygoma	Transconjunctival, lid swing, and intra-oral	2	1	477	None
30	20M	Deformity	No		Right	Mandible	Intra-oral	2	3	1749	None
31	30F	Trauma	No		Right	Orbital	Transconjunctival	1	2	1198	None
32	20F	Deformity	No		Right	Mandible	Intra-oral	2	2	1630	None
33	44M	Trauma	No		Right	Orbital	Transconjunctival, lateral canthotomy, and transcaruncular	1	2	754	None
34	24F	Deformity	No	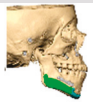	Bi lateral	Mandible	Intra-oral (Labial incision LR8-LL3)	2	3	201	Numbness lower lip

https://doi.org/10.3390/cmtr19010008

Table 1. *Cont.*

Patient	Sex and Age at Time of Surgery (yr)	Indication	Smoking Status	Image	Side	Site	Approach	Number of Pieces	Screws	Follow-Up Since Surgery (Days)	Complications
35	35M	Deformity	No		Bi lateral	Lateral Orbits (Bilateral)	Bicoronal	1	3 left 2 Right	603	None
36	18M	Trauma	No		Right	Zygoma	Intra-oral	1	2	195	None
37	23M	Trauma	No		Left	Orbital	Transconjunctival and lateral canthotomy	1	2	435	Sudden onset of pain and paraesthesia
38	45F	Trauma	No		Right	Orbital	Transconjunctival	1	3	988	Needed strabismus surgery for diplopia. Complications with inferior rectus muscle
39	27M	Trauma	Smoker		Right	Orbital	Transconjunctival and lid swing	1	2	694	None
40	60M	Trauma	No		Left	Zygoma	Intra-oral	1	2	163	Slight altered sensation
41	52F	Trauma	No		Left	Orbital	Transconjunctival and transcaruncular	1	2	162	None
42	25M	Trauma	No		Left	Orbital	Transconjunctival and lateral canthotomy	1	2	715	None
43	40M	Trauma	No		Left	Orbital and Zygoma	Transconjunctival and lid swing	2	4	792	Squint surgery
44	73M	Trauma	No		Right	Zygoma, lateral wall of orbit and orbital floor	Transconjunctival and lid swing and intra-oral	3	6	883	Needed implant removal following extrusion and then infection, which required further surgery
45	67F	Trauma	No		Right	Orbital	Transconjunctival and lateral canthotomy	1	2	491	Pain

https://doi.org/10.3390/cmtr19010008

Table 1. *Cont.*

Patient	Sex and Age at Time of Surgery (yr)	Indication	Smoking Status	Image	Side	Site	Approach	Number of Pieces	Screws	Follow-Up Since Surgery (Days)	Complications
46	61F	Trauma	No		Right	Orbital	Transconjunctival and lid swing	1	2	295	Diplopia
47	23M	Trauma	No		Left	Orbital and Zygoma	Transconjunctival and lid swing	2	4	148	None
48	20M	Trauma	Smoker		Right	Orbital	Transconjunctival and lateral canthotomy	1	2	36	None
49	29M	Deformity	No		Right	Zygoma	Intra-oral	2	2	122	None
50	38F	Trauma	Smoker		Left	Orbital	Transconjunctival and lid swing	1	2	193	Sinusitis
21b	37M	Trauma	No		Left	Orbital	Transconjunctival and lid swing	1	1	132	None
51	38M	Trauma	No		Right	Orbital	Transconjunctival	1	2	29	None
52	23F	Deformity	No		Right	Mandible	Intra-oral	2	2	48	None
53	41M	Trauma	Smoker		Right	Orbital	Transconjunctival and lid swing	1	2	15	None

https://doi.org/10.3390/cmtr19010008

5. Discussion

PEEK is a versatile material for craniofacial reconstruction, with increasing evidence supporting its use in the management of complex orbital and maxillofacial defects [7,8]. Reconstruction of the craniomaxillofacial region remains particularly challenging due to its intricate three-dimensional anatomy, characterised by variable curvatures and thicknesses [9]. Importantly, such reconstructions extend beyond aesthetic restoration, addressing functional impairment and the significant psychological consequences of craniofacial deformity.

The gold standard for bony reconstruction is autologous bone grafting. However, its widespread application is restricted by difficulties in intraoperative shaping, the risk of graft resorption, and donor site morbidity. To overcome these limitations, various alloplastic materials have been introduced, most notably, polyetheretherketone (PEEK), porous polyethylene (MEDPOR®), and titanium. Each of these materials offers specific advantages in restoring facial anatomy, with PEEK gaining prominence due to its favourable balance of strength, adaptability, and biocompatibility.

In contrast to titanium, pure PEEK exhibits one principal limitation: it is a hydrophobic material with no inherent bioactive properties and therefore does not actively bond to living tissue [10,11]. The long-term stability of PEEK implants is consequently dependent on secure screw fixation, precise three-dimensional design, and the accuracy of the implant–bone interface.

PEEK is increasingly utilised across multiple surgical disciplines, including maxillofacial surgery, orthopaedics, cardiovascular surgery, and neurosurgery. As an alloplastic material, it provides a favourable balance between structural strength and reduced rigidity, thereby lowering the risk of stress shielding when compared with more rigid alternatives such as titanium [12,13].

Our preference is to obtain a cone beam computed tomography (CBCT) scan prior to planning patient-specific implants. Brisco et al. demonstrated that CBCT delivers a significantly lower radiation dose compared with multislice CT, with the mean dose to the lens of the eye reduced by 42% (range 23–53%, SD 10; $p < 0.001$) [14]. Importantly, the effective dose—a measure of the risk of radiation-induced malignancy—was also significantly lower with CBCT than with multislice CT, making it the preferred modality for preoperative imaging in orbital reconstruction.

In our early experience, five PEEK implants were designed in-house and manufactured locally using an analogue workflow developed in Sheffield, which we term Digital–Analogue PEEK. This technique combined conventional modelling with digital scanning and CNC milling; wax patterns were fabricated on 3D-printed skull models, converted into acrylic, scanned, and then used to mill medical-grade PEEK implants. While cost-effective and reproducible, the method involved multiple manual steps and frequently required intraoperative adjustment to achieve an accurate fit. Limitations included occasional inaccuracies at the fitting surface due to cumulative errors in the pathway, the need for additional software correction of CBCT data in some cases, and a tendency for implants to be bulkier than their digitally designed counterparts.

By comparison, three-dimensional computer-assisted design and manufacturing (CAD/CAM) integrates virtual surgical planning (VSP) with direct CNC milling of PEEK, producing more precise and streamlined patient-specific implants. Thomas et al. demonstrated that CAD/CAM implants were significantly more accurate than those fabricated using in-house analogue methods [15].

During VSP the unaffected side is mirrored and used to restore damaged anatomy on the affected contralateral side. This new framework acts as a template on which a PSI is designed to onlay into sound bone. Screw holes are placed for implant fixation after checking

https://doi.org/10.3390/cmtr19010008

the bone density and the maximum bone length so that screws are encased in bone. PSIs are designed following collaboration between surgeon and clinical engineer. CAD/CAM aids a more specific implant with more complex geometric shapes and the opportunity to link multiple implants with interlocking joints. During the design phase, consideration must be given to access required for placement, avoidance of critical anatomical structures, and soft tissue coverage.

Virtual PEEK Design Considerations

Implant Thickness

For orbital reconstruction, PEEK implants were initially manufactured at 3 mm but have since been refined to 1.5 mm, providing adequate strength with reduced bulk. Cranial implants are generally supplied at 4 mm thickness, although 3 mm may be used in younger patients where clinically appropriate [Figure 6. Thickness of an orbital implant and three points of contact].

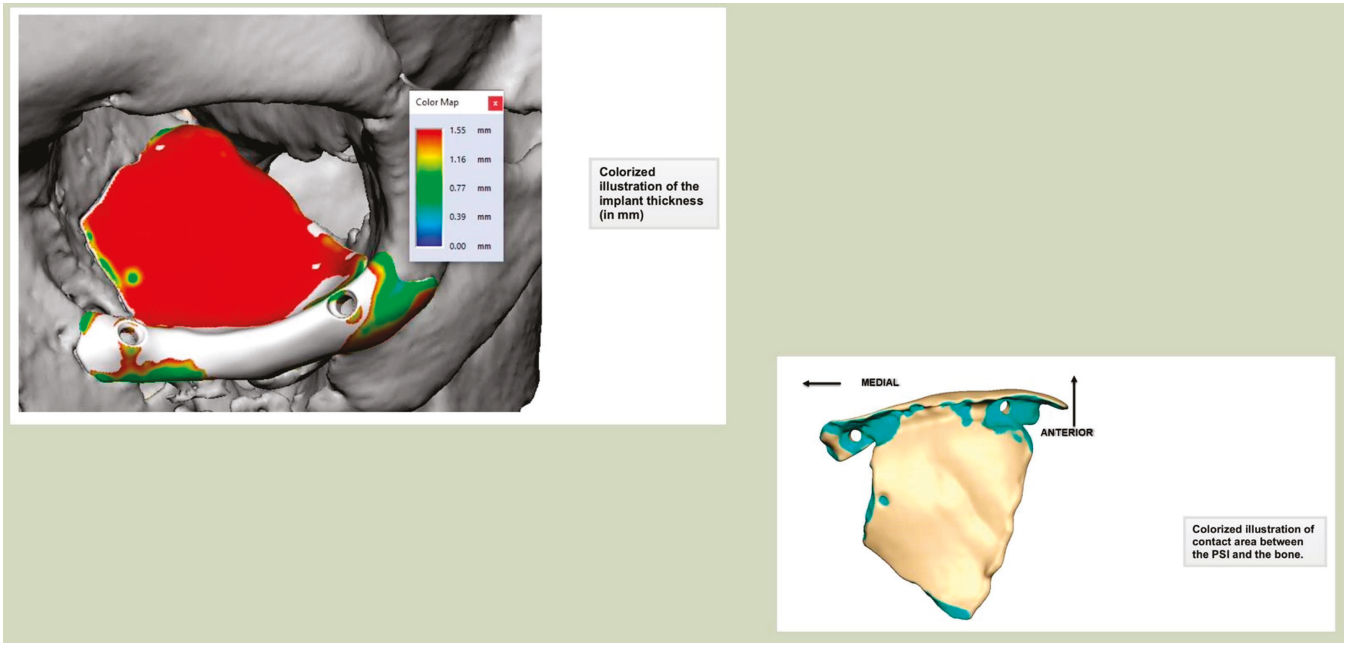

Figure 6. Thickness of an orbital implant and three points of contact.

Seating and Fixation

Secure seating of the implant is essential. In zygomatic PEEK implants, the three-dimensional morphology of the anterior maxilla and zygoma often provides a natural seat, thereby improving stability. Although two screws are generally recommended to prevent rotation, in cases of firm seating a single screw may suffice. Implants are typically designed with an implant-to-bone offset of 0.2 mm to facilitate adaptation [Figure 7—Planning to have fixation into sound bone].

Positional Features

For relatively flat surfaces, such as the lateral orbital wall and the mandible, rims can be incorporated into the design to improve positioning. In orbital reconstruction, rims may also be extended across the infra-orbital margin to enhance stability. However, exposure of the infra-orbital rim risks scarring and lid malposition due to periosteal stripping. In our series, no such complications were observed. A single case of displacement occurred in the absence of infra-orbital rim coverage, despite intraoperative confirmation of positioning.

https://doi.org/10.3390/cmtr19010008

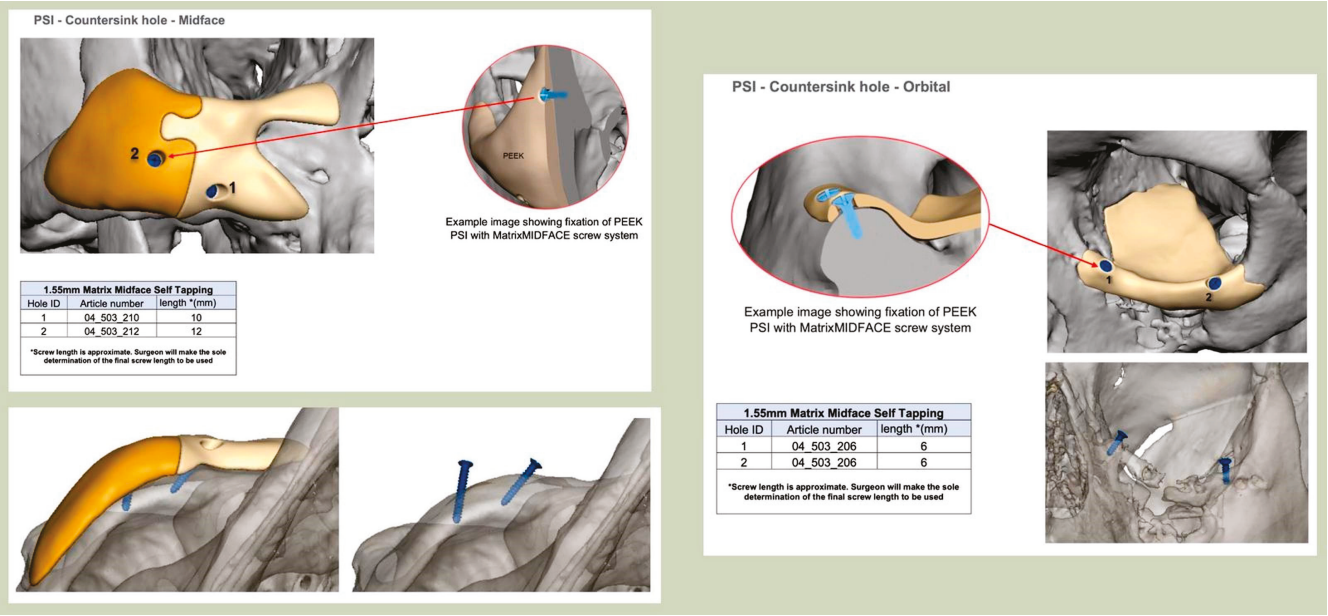

Figure 7. Planning to have fixation into sound bone.

Orbital Plate Planning

Orbital plates are optimally designed with three points of contact along the orbital floor, ideally including one posterior point of fixation. An anterior ledge provides a useful visual reference for correct positioning during surgery. Since 2018, thinner plates (1.5 mm with tapered edges) have been routinely adopted, improving intraoperative handling and reducing bulk. Planned screw holes, incorporated since April 2019, have further enhanced accuracy and ease of fixation.

In our current practice, orbital implants are always designed with an extension over the infra-orbital rim. This improves stability and provides additional support to the lower eyelid following a transconjunctival approach, which often involves a lid swing. A ledge can also be incorporated in the infra-orbital region; however, this may create an unfavourable shadow and must be weighed against the morbidity of more extensive procedures such as zygomatic osteotomy.

With the advent of patient-specific drill/cutting guides and plates, orbital reconstruction has become increasingly predictable, with improved accuracy in implant placement [Figure 8—The use of a titanium drill guide to aid placement of a PEEK orbital implant].

PEEK-on-PEEK

We have previously reported a case in which a patient underwent left orbital floor reconstruction with a patient-specific PEEK implant to correct globe dystopia. Despite the initial intervention, the patient developed progressive secondary enophthalmos and recurrent globe dystopia. To address this, a novel PEEK-on-PEEK technique was employed, whereby a second customised PEEK implant was placed directly over the original implant but within the same capsule, thereby augmenting orbital volume and improving globe position. This approach, termed PEEK-on-PEEK orbital implantation, represents a secondary augmentation strategy for the management of delayed enophthalmos [16] [Figure 9. Patient 21—Colourised illustration of PEEK-on-PEEK (max thickness 2.7 mm) showing the original PEEK implant (grey) and the additional implant (blue)].

https://doi.org/10.3390/cmtr19010008

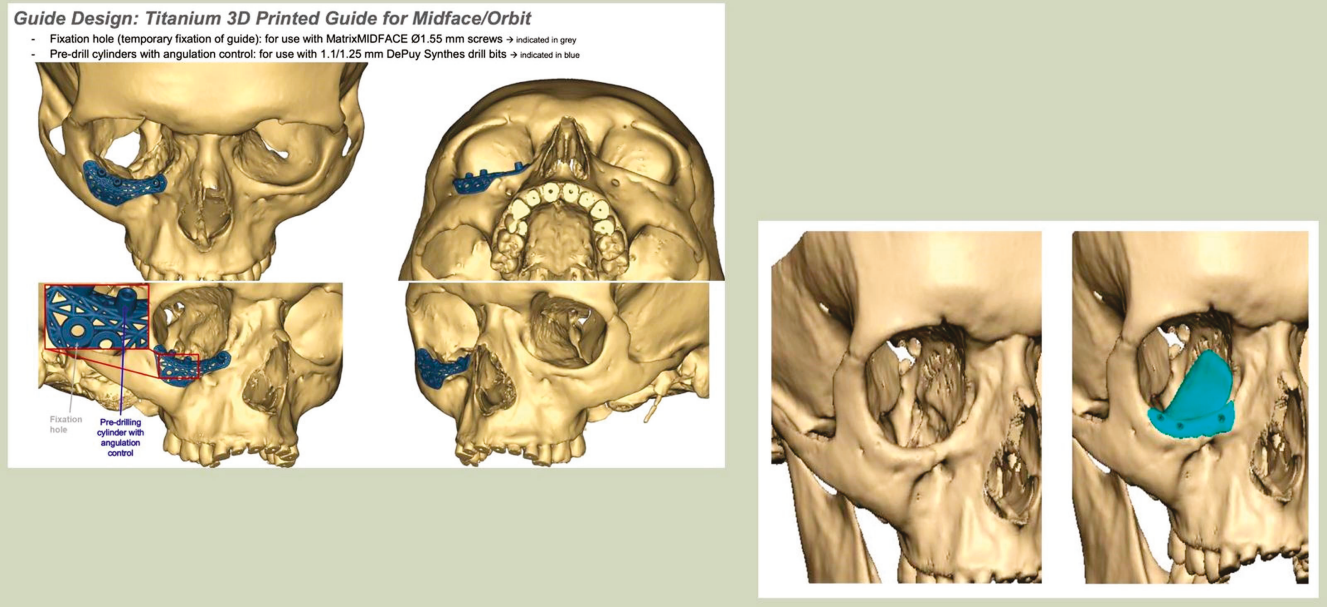

Figure 8. The use of a titanium drill guide to aid placement of a PEEK orbital implant.

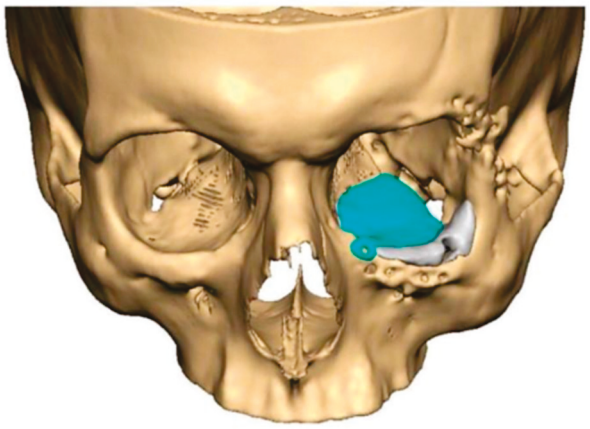

Figure 9. Patient 21—Image of patient-specific implant designed by the manufacturer. (DePuy Synthes)—Colourised illustration of PEEK-on-PEEK implant (max thickness 2.7 mm) show the original PEEK implant and the additional.

Multi-piece Designs with Interlocking Joints

In selected cases, multi-piece PEEK implants can be produced, with segments linked together by interlocking joints. These are created during the digital design process using Boolean separation, followed by refinement to ensure accurate mating surfaces and stable intraoperative assembly. Interlocking designs provide additional stability, require minimal fixation, and facilitate ease of insertion [2,4,17].

Bespoke multi-segmented implants are particularly valuable when surgical access is restricted, when reconstruction of a large surface area is required, or when implants must be placed at different planes of the facial skeleton. Conventionally, each implant requires a minimum of two screws to prevent rotation; however, the use of interlocking joints reduces the number of screws required by effectively converting multiple segments into a single integrated implant [Figure 10—Patient 29. A two-part orbito-zygomatic implant linked with an interlocking joint].

https://doi.org/10.3390/cmtr19010008

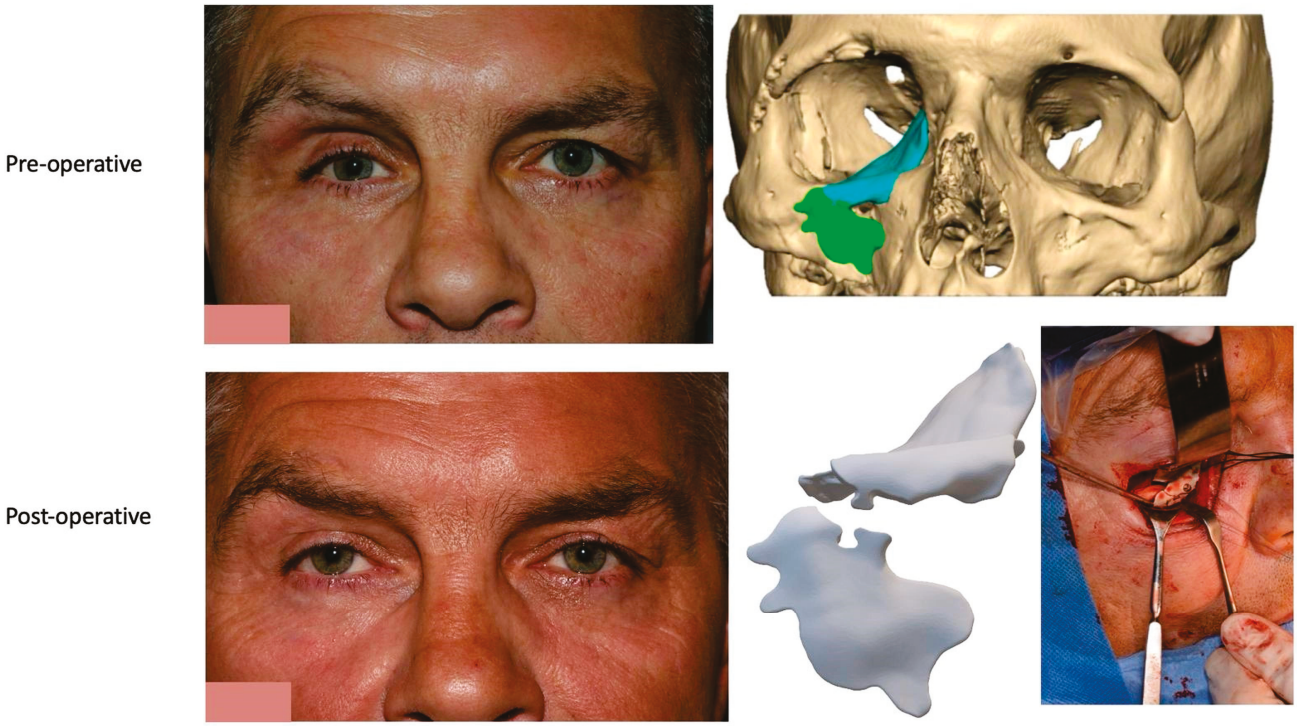

Figure 10. Patient 29. A two-part orbital-zygomatic implant linked with an interlocking joint.

Manufacturing

PEEK implants are manufactured using 5-axis computer numerical control (CNC) milling machines. Although the core milling process has remained largely unchanged, several refinements have been introduced following feasibility testing, including the addition of countersunk screw holes and plate recesses to improve handling and fixation. Earlier-generation implants were comparatively thicker and often required intraoperative trimming to achieve an accurate fit. The introduction of 1.5 mm orbital implants with tapered margins has markedly improved intraoperative adaptation, reduced the need for modification, and has been consistently associated with positive surgeon feedback.

Infection

Infection remains a key concern in cranioplasty and craniofacial reconstruction. In a two-centre cohort study of 40 patient-specific PEEK cranioplasty implants, Jonkergouw et al. reported an infection rate of 13% [18]. By comparison, Rosenthal et al. presented outcomes from 65 cases across three centres, with a lower infection rate of 7.7% [19]. A systematic review by Kwarcinski et al. compared infection rates across various implant materials, reporting an average rate of 7.9% for PEEK, which was comparable to 8.3% for titanium [20].

Biofilm formation on implant surfaces is a recognised risk factor for surgical site infection, which can lead to implant exposure, extrusion, and ultimately implant removal. Barkarmo et al. compared biofilm formation across different materials, including untreated PEEK, blasted PEEK, commercially pure titanium, and titanium alloy (Ti6Al4V) [21]. Their results demonstrated increased biofilm formation on blasted PEEK compared with the other groups. By contrast, as-prepared PEEK exhibited biofilm formation levels comparable with those of commercial titanium and titanium alloy. It is well established that surface roughness promotes bacterial adhesion and biofilm proliferation [22,23], which may account for the higher biofilm accumulation observed on blasted PEEK.

In our practice, implants are routinely soaked in Gentamicin (40–80 mg) prior to insertion, in line with local antimicrobial protocols.

https://doi.org/10.3390/cmtr19010008

Placement

PEEK also allows modification of the non-fitting surface of the implant with a bur to allow for symmetry and facial balance.

Although customised implants represent a high-cost product, the use of computer-aided design and manufacturing (CAD/CAM) has been shown to reduce both intraoperative manipulation and overall operative time [24]. CAD facilitates preoperative planning of implant position and the optimal length and orientation of fixation screws, while CAM enables the precise incorporation of screw holes directly into the implant design, thereby improving accuracy and efficiency at the time of surgery.

Prior to surgery, and if required, the implant can be placed in the planned position within the skull and imported as a segmented STL format file (Standard Tessellation Language) into our surgical navigation system (Brain Lab Navigation, Munich, Germany). Surgical navigation allows the surgeon to navigate around the craniomaxillofacial region and, once the implant has been surgically placed, navigation can be used to confirm satisfactory positioning of the implant by comparing the surgically achieved position to the planned position. Checking position can also be aided with the prior construction of a predesigned titanium patient-specific guide where fixation holes for the implant can be predrilled. For most of our PSIs, placed confirmation of planned position has been confirmed by the stability of the fitting surface of the implant with the underlying bony anatomy [Figure 11. Right sided orbital implant placed with the aid of surgical navigation].

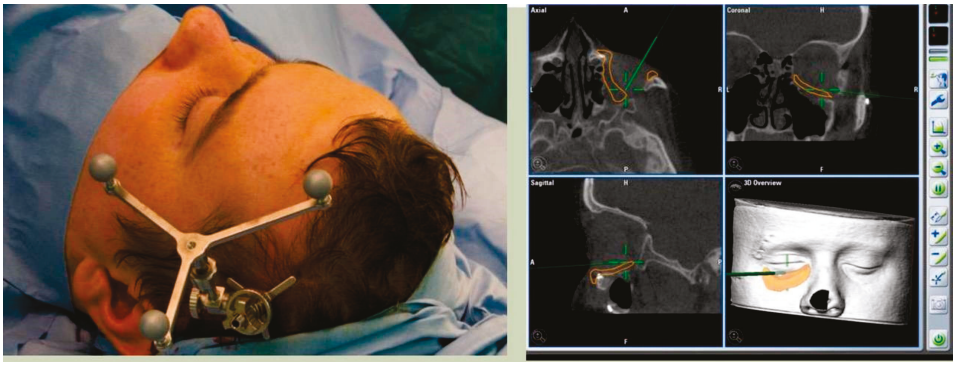

(**a**)



(**b**) (**c**)

Figure 11. (**a**) Reference array of surgical navigation attached to skull and navigation used to confirm position of implant in planned position. (**b**) Preoperative photo showing globe dystopia. (**c**) Postoperative photo showing globe dystopia corrected. Patient 10. Right sided orbital implant placed with the aid of surgical navigation.

https://doi.org/10.3390/cmtr19010008

If there are concerns on the extent of periosteal envelope achieved around the implant, especially in the region of the lower border of the mandible, including the angle of the mandible that is required to accommodate the implant, then multiple implants linked by interlocking joints can be constructed of different thicknesses at the lower border. This allows a safe thickness of the implant to be inserted within the envelope without the risk of future implant extrusion.

Over the decade of cases, our most challenging cases are post-trauma, which have had multiple attempts at reconstruction previously, often with other material used, compromising the bony framework that is used as the structure for the implant to sit on and the soft tissue envelope.

Clinical Outcomes of PEEK in Maxillofacial Surgery

Although the clinical use of PEEK in maxillofacial reconstruction has expanded considerably, there remains a limited body of high-level evidence. Current reports, however, suggest that PEEK implants are associated with favourable functional and aesthetic outcomes, combined with acceptable complication rates.

Gerbino et al. described 13 cases of post-ablative craniofacial reconstruction using patient-specific PEEK implants, of which 11 achieved satisfactory restoration of complex morphological defects with good cosmetic outcomes. Importantly, no implant-related complications were observed [1]. Järvinen et al. reported a retrospective cohort of 24 patients, in which PEEK implants fitted well without adjustment in 22 cases. Nine implants required modification of the outer contour, while two patients (8.3%) developed postoperative wound dehiscence and infection, both of which resolved without implant removal [25]. Similarly, Kim et al. presented four cases reconstructed with customised PEEK implants, all of which demonstrated excellent functional and aesthetic outcomes at 16–20 months of follow-up, without any complications such as infection or extrusion [26].

Longer-term evidence has also been published. Garg et al. reviewed 19 PEEK onlay implants placed over 11 years, primarily for orbital-zygomatic and mandibular reconstruction. Only two implants were removed—one for a design error and one due to compression neuropathy—while one case of postoperative infection was successfully managed with antibiotics [27]. Collier et al. reported on 50 consecutive cases of custom-made facial onlay implants over five years, of which 84% were manufactured from PEEK. Minor intraoperative adjustments were required in approximately one-third of cases, and a single patient required reoperation. Importantly, no implants were lost or removed during follow-up [28].

Infection remains a central concern in cranioplasty and craniofacial reconstruction. A two-centre study of 40 patient-specific PEEK cranioplasty implants reported an infection rate of 13% [18], while a multi-centre series of 65 cases demonstrated a lower rate of 7.7% [19]. A systematic review by Kwarcinski et al. found the average infection rate for PEEK to be 7.9%, comparable to titanium at 8.3% [20]. These findings suggest that PEEK carries a similar risk profile to other widely used materials. At the cellular level, Barkarmo et al. demonstrated that biofilm formation varies with implant surface preparation: blasted PEEK exhibited higher bacterial adhesion, while untreated PEEK showed levels comparable with commercial titanium and titanium alloy [21]. As surface roughness is known to promote bacterial adherence [22,23], this may partially explain variations in reported infection outcomes.

Taken together, these studies suggest that PEEK implants offer satisfactory long-term stability, with low complication and removal rates, and outcomes at least comparable to established alternatives such as titanium. However, the literature is characterised by retrospective cohorts with small sample sizes and limited follow-up, underlining the need for prospective multi-centre studies to establish the long-term safety and efficacy of PEEK in maxillofacial reconstruction.

https://doi.org/10.3390/cmtr19010008

We have previously described the use of interlocking joints to connect multiple PEEK implants, providing more controlled and predictable placement in cases where the implant lacks a straightforward path of insertion, involves multiple planes, or must be positioned around vulnerable anatomical structures such as the mental or infra-orbital nerves. Smaller implant segments that lock together within the periosteal envelope also facilitate insertion through limited surgical access with reduced periosteal stripping. However, it remains essential that the periosteal pocket is of sufficient size to accommodate the final assembled implant without creating undue soft tissue tension.

Implant stability is paramount to reducing the risks of infection, migration, and exposure. Even with an accurately fitting surface, fixation with at least two screws is recommended to prevent rotational movement. The use of a three-part interlocking PEEK patient-specific implant (PSI) allows the completed construct to be stabilised and secured with just two screws, reducing the overall fixation requirements. Looking forward, the integration of soft tissue simulation during preoperative planning may further refine implant design, enabling adjustments for the quality and thickness of overlying soft tissues to optimise both stability and aesthetic outcomes.

If required and a post-surgical CT scan is available a post-surgical planning report can be undertaken. This is of particular use in the reconstruction of orbital injuries where the correction of globe dystopia and orbital volume can be analysed. It is also possible to assess how close the achieved implant position was to the planned implant position [Figure 12—Post planning reports looking at (a) orbital volume, (b) globe position correction, and (c) the ability to check if the achieved implant position matched the planned implant position].

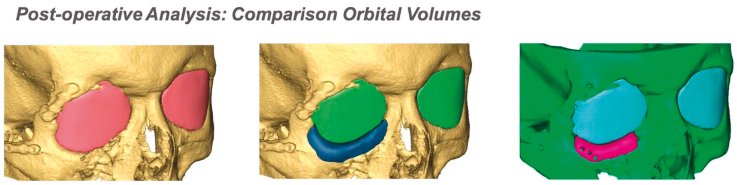

	Orbital Volume (cm³)			Post-operative Position		
	Pre-operative	Planned	Post- operative	Pre-operative vs Planned	Pre-operative vs Post- operative	Planned vs Post- operative
Left Orbit	27.3	NA	27.2	NA	-0.1	NA
Right Orbit	30.3	25.0	24.5	-5.3	-5.8	-0.5

(**a**)

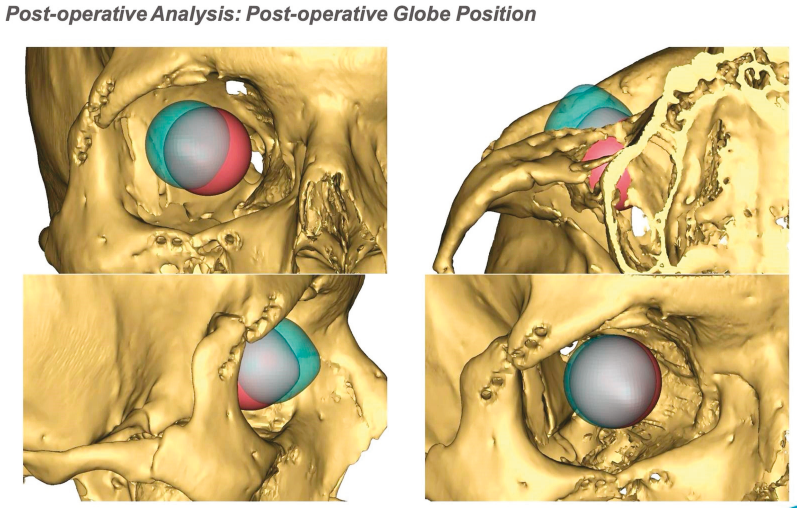

(**b**)

Figure 12. *Cont.*

https://doi.org/10.3390/cmtr19010008

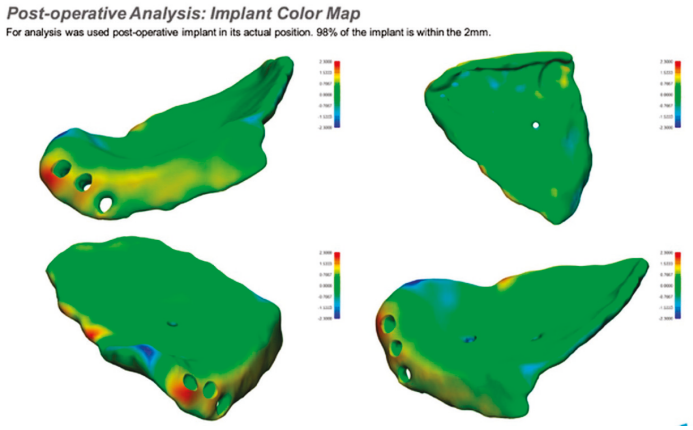

(**c**)

Figure 12. Post planning reports looking at (**a**) orbital volume, (**b**) globe position correction, and (**c**) the ability to check if the achieved implant position matched the planned implant position.

6. Conclusions

The use of patient-specific PEEK implants (PSIs) is safe, predictable, and can reduce operative time while allowing intraoperative adjustability. Virtual surgical planning enables the consistent production of customised implants, incorporating features such as reduced thickness, precisely positioned screw holes, and confirmation that fixation points engage sound bone. Unlike titanium, PEEK can be modified intraoperatively if required, although the fitting surface should not be altered. Virtually planned PEEK implants can also be integrated with other forms of personalised surgery, including patient-specific orthognathic guides and plates, to achieve comprehensive reconstruction.

The incorporation of an interlocking mechanism provides additional stability, prevents implant slippage, and reduces the need for supplementary fixation—particularly valuable in anatomically inaccessible regions or in proximity to vital structures. Multi-segmented designs also facilitate insertion through smaller surgical access incisions, without compromising functional or aesthetic outcomes. Furthermore, intraoperative navigation can be used to improve accuracy of implant placement, with post-planning reports generated to confirm that the implant has been positioned in accordance with the virtual plan.

A multi-disciplinary approach, such as dedicated joint orbital trauma clinics and joint operating by maxillofacial surgery teams and orbital ophthalmic teams. helped improve patient outcomes in complex orbital PEEK implant cases.

Author Contributions: Conceptualization—N.J.L. and S.M.S.; Methodology—N.J.L. and S.M.S.; Validation—N.J.L., G.H., M.A., M.T. and S.M.S.; Formal analysis—N.J.L., G.H., M.A., M.T. and S.M.S.; Data curation—N.J.L., G.H. and S.M.S.; Writing—original draft preparation—N.J.L. and G.H.; Writing—review and editing—N.J.L., G.H., M.A., M.T. and S.M.S.; Visualization—N.J.L., G.H., M.A., M.T. and S.M.S.; Project administration—N.J.L. and G.H. All authors have read and agreed to the published version of the manuscript.

Funding: This research received no external funding.

Institutional Review Board Statement: This study is a retrospective analysis of routinely collected clinical data. As such, it was not classified as research requiring review by an NHS Research Ethics Committee (REC) under the UK Health Research Authority (HRA) guidelines/Governance Arrangements for Research Ethics Committees (GAfREC). Therefore, no formal ethics approval was required or obtained.

Informed Consent Statement: Informed consent was obtained from all subjects involved in the study.

https://doi.org/10.3390/cmtr19010008

Data Availability Statement: The original contributions presented in this study are included in the article. Further inquiries can be directed to the corresponding author.

Acknowledgments: Clinical engineers and anaplastologists involved in planning design manufacturing and producing post planning reports. ChatGPT 5 was utilised in the preparation of this manuscript to improve and enhance readability.

Conflicts of Interest: The authors declare no conflicts of interest.

References

1. Gerbino, G.; Zavattero, E.; Zenga, F.; Bianchi, F.A.; Garzino-Demo, P.; Berrone, S. Primary and secondary reconstruction of complex craniofacial defects using polyetheretherketone custom-made implants. *J. Cranio-Maxillofac. Surg.* **2015**, *43*, 1356–1363. [CrossRef]
2. Thomas, M.; Lee, N. Interlocking polyetheretherketone implant. *Int. J. Oral Maxillofac. Surg.* **2016**, *45*, 969–970. [CrossRef]
3. Varley, I.; White, L.; Salvi, S.M.; Lee, N. Digital import of orbital implants to enhance navigation in reconstruction of the deep orbit. *Orbit* **2015**, *35*, 20–23. [CrossRef] [PubMed]
4. Anabtawi, M.; Thomas, M.; Lee, N.J. The use of interlocking polyetheretherketone (PEEK) patient-specific facial implants in the treatment of facial deformities. A retrospective review of Ten patients. *J. Oral Maxillofac. Surg.* **2021**, *79*, 1145.e1–1145.e9. [CrossRef] [PubMed]
5. Ghazal-Maghras, R.; Vilaplana-Vivo, J.; Camacho-Alonso, F.; Martínez-Beneyto, Y. Properties of polyetheretheretherketone (PEEK) implant abutments: A systematic review. *J. Clin. Exp. Dent.* **2022**, *14*, e349–e358. [CrossRef] [PubMed]
6. Bansal, N.; Singla, J.; Gera, G.; Gupta, M.; Kaur, G. Reliability of natural head position in orthodontic diagnosis: A cephalometric study. *Contemp. Clin. Dent.* **2012**, *3*, 180–183. [CrossRef]
7. Weaver, J.M.; Herford, A.S.; Thakker, J.S. Patient specific implants: Reconstruction of orbital defects with custom peek implants. *J. Oral Maxillofac. Surg.* **2015**, *73*, e16. [CrossRef]
8. Abdullakutty, A.; Madhavarajan, S.; Collyer, J.; Sneddon, K. Uses of Peek in maxillofacial reconstruction: A 6 year review of cases. *Br. J. Oral Maxillofac. Surg.* **2012**, *50*, S39–S40. [CrossRef]
9. Alonso-Rodriguez, E.; Cebrián, J.; Nieto, M.; Del Castillo, J.; Hernández-Godoy, J.; Burgueño, M. Polyetheretherketone custom-made implants for craniofacial defects: Report of 14 cases and review of the literature. *J. Cranio-Maxillofac. Surg.* **2015**, *43*, 1232–1238. [CrossRef]
10. Lethaus, B.; ter Laak, M.P.; Laeven, P.; Beerens, M.; Koper, D.; Poukens, J.; Kessler, P. A treatment algorithm for patients with large skull bone defects and first results. *J. Cranio-Maxillofac. Surg.* **2011**, *39*, 435–440. [CrossRef]
11. Awaja, F.; Bax, D.V.; Zhang, S.; James, N.; McKenzie, D.R. Cell adhesion to peek treated by plasma immersion ion implantation and deposition for active medical implants. *Plasma Process. Polym.* **2012**, *9*, 355–362. [CrossRef]
12. Thien, A.; King, N.K.; Ang, B.T.; Wang, E.; Ng, I. Comparison of polyetheretherketone and titanium cranioplasty after decompressive craniectomy. *World Neurosurg.* **2015**, *83*, 176–180. [CrossRef]
13. Scolozzi, P.; Martinez, A.; Jaques, B. Complex orbito-fronto-temporal reconstruction using computer-designed Peek Implant. *J. Craniofacial Surg.* **2007**, *18*, 224–228. [CrossRef]
14. Brisco, J.; Fuller, K.; Lee, N.; Andrew, D. Cone beam computed tomography for imaging orbital trauma—Image quality and radiation dose compared with conventional multislice computed tomography. *Br. J. Oral Maxillofac. Surg.* **2014**, *52*, 76–80. [CrossRef]
15. Thomas, M.; Frezzini, C.; Keat, R.; Lee, N. Correction of facial deformity with bespoke patient-specific polyetheretherketone implant: In-house manufacturing to Virtual Planning and navigational technology. *Int. J. Oral Maxillofac. Surg.* **2017**, *46*, 218. [CrossRef]
16. Amoura, E.B.; Evans, K.; Metherall, P.; Salvi, S.M.; Lee, N.J. PEEK-on-PEEK orbital implantation: A secondary augmentation approach for delayed Enophthalmos. *Br. J. Oral Maxillofac. Surg.* **2025**, *63*, 681–684. [CrossRef]
17. Goodson, M.; Farr, D.; Keith, D.; Banks, R. Use of two-piece polyetheretherketone (PEEK) implants in orbitozygomatic reconstruction. *Br. J. Oral Maxillofac. Surg.* **2012**, *50*, 268–269. [CrossRef]
18. Jonkergouw, J.; van de Vijfeijken, S.; Nout, E.; Theys, T.; Van de Casteele, E.; Folkersma, H.; Depauw, P.; Becking, A. Outcome in patient-specific peek cranioplasty: A two-center cohort study of 40 implants. *J. Cranio-Maxillofac. Surg.* **2016**, *44*, 1266–1272. [CrossRef]
19. Rosenthal, G.; Ng, I.; Moscovici, S.; Lee, K.K.; Lay, T.; Martin, C.; Manley, G.T. Polyetheretherketone implants for the repair of large cranial defects. *Neurosurgery* **2014**, *75*, 523–529. [CrossRef]
20. Kwarcinski, J.; Boughton, P.; Ruys, A.; Doolan, A.; Van Gelder, J. Cranioplasty and Craniofacial Reconstruction: A review of implant material, manufacturing method and Infection Risk. *Appl. Sci.* **2017**, *7*, 276. [CrossRef]

https://doi.org/10.3390/cmtr19010008

21. Barkarmo, S.; Longhorn, D.; Leer, K.; Johansson, C.B.; Stenport, V.; Franco-Tabares, S.; Kuehne, S.A.; Sammons, R. Biofilm formation on polyetheretherketone and titanium surfaces. *Clin. Exp. Dent. Res.* **2019**, *5*, 427–437. [CrossRef]
22. Katsikogianni, M.; Missirlis, Y. Concise review of mechanisms of bacterial adhesion to biomaterials and of techniques used in estimating bacteria-material interactions. *Eur. Cell Mater.* **2004**, *8*, 37–57. [CrossRef]
23. Almaguer-Flores, A.; Olivares-Navarrete, R.; Wieland, M.; Ximénez-Fyvie, L.A.; Schwartz, Z.; Boyan, B.D. Influence of topography and hydrophilicity on initial oral biofilm formation on microstructured titanium surfaces in vitro. *Clin. Oral Implant. Res.* **2011**, *23*, 301–307. [CrossRef] [PubMed]
24. Binder, W.J. Custom-designed facial implants. *Facial Plast. Surg. Clin. N. Am.* **2008**, *16*, 133–146. [CrossRef] [PubMed]
25. Järvinen, S.; Suojanen, J.; Kormi, E.; Wilkman, T.; Kiukkonen, A.; Leikola, J.; Stoor, P. The use of patient specific polyetheretherketone implants for reconstruction of maxillofacial deformities. *J. Cranio-Maxillofac. Surg.* **2019**, *47*, 1072–1076. [CrossRef]
26. Kim, M.M.; Boahene, K.D.O.; Byrne, P.J. Use of customized polyetheretherketone (PEEK) implants in the reconstruction of complex maxillofacial defects. *Arch. Facial Plast. Surg.* **2009**, *11*, 53–57. [CrossRef]
27. Garg, M.; Abdullakutty, A.; Plant, S.; Collyer, J.; Sneddon, K. Long term follow-up of patients with peek onlay implants in the maxillofacial region—The east grinstead experience and a review of literature. *Br. J. Oral Maxillofac. Surg.* **2018**, *56*, e22–e23. [CrossRef]
28. Collier, J.; Gore, S.; Dawood, A.; Kirkpatrick, N.; Eccles, S. Custom-made facial onlay implants: Our experience of 50 consecutive cases. *Br. J. Oral Maxillofac. Surg.* **2017**, *55*, e85. [CrossRef]

Disclaimer/Publisher's Note: The statements, opinions and data contained in all publications are solely those of the individual author(s) and contributor(s) and not of MDPI and/or the editor(s). MDPI and/or the editor(s) disclaim responsibility for any injury to people or property resulting from any ideas, methods, instructions or products referred to in the content.

https://doi.org/10.3390/cmtr19010008

craniomaxillofacial
trauma & reconstruction

MDPI

Article

Minne Ties Hybrid Arch Bar System vs. Erich Arch Bars: A Cadaveric Comparison Study

Jeffrey Mella [1,*], François E. Proulx [2] and Alan W. Johnson [1,3,*]

[1] Department of Otolaryngology—Head & Neck Surgery, University of Minnesota, Minneapolis, MN 55455, USA
[2] Department of Oral Maxillofacial Surgery, University of Minnesota, Minneapolis, MN 55455, USA; proul076@umn.edu
[3] Hennepin Healthcare, Minneapolis, MN 55415, USA
* Correspondence: mella043@umn.edu (J.M.); alanwellingtonjohnson@gmail.com (A.W.J.); Tel.: +801-787-2689 (J.M.)

Abstract

Jaw fracture management significantly advanced with the introduction of Erich Arch Bars (EABs) during World War II, becoming the gold standard for maxillomandibular fixation (MMF). EABs, however, are time-consuming, pose risks of sharps injuries, and hinder oral hygiene and patient comfort. This study tested the Minne Ties Hybrid Arch Bar System (MTHAB), a novel MMF technology. This cadaveric study used specimens with near-complete dentition to compare MTHAB and EABs. The technologies were applied by trained surgeons to measure occlusal forces, increasing elastic loads, and application and removal times. Surgeons completed structured usability surveys. The results indicated that MTHAB significantly reduced application time (19.8 $\pm$ 4.1 min versus 35.2 $\pm$ 5.7 min, $p = 0.0027$) and removal time (1.6 $\pm$ 0.4 min versus 5.1 $\pm$ 2.1 min, $p = 0.0465$) compared to EABs, while also being rated higher for ease of use and safety. Both technologies achieved acceptable occlusion forces, although MTHAB needed more elastics to achieve comparable forces to EABs. While MTHAB appears promising, future clinical trials are needed to evaluate long-term outcomes, fixation stability, and patient selection. MTHAB represents a potential advancement in MMF technology, balancing surgical efficiency, safety, and fixation strength.

Keywords: maxillomandibular fixation; dental occlusion; mandible fracture; maxilla fracture; hybrid arch bar; surgical efficiency

1. Introduction

Modern management of jaw fractures, including the mandible and maxilla, can be traced back to World War II. "Arch bars", as described in John B. Erich's *Traumatic Injuries of Facial Bones: An Atlas of Treatment (1944)* [1], became the standard of treatment and are commonly referred to as Erich Arch Bars (EABs) to this day. Their simplicity of design and versatility in treating the majority of types of mandible fractures have made them indispensable to facial trauma surgeons. They reliably secure the mandibular and maxillary dentition into stable occlusion, which is the definition of maxillomandibular fixation (MMF). MMF can be used as a stand-alone treatment for fractures of the upper or lower jaw (closed reduction) or it can be used in combination with internal fixation techniques, typically involving placing titanium plates and screws directly into the bone for fracture reduction and fixation.

In recent decades, numerous other techniques have emerged to establish MMF. While EABs remain the gold standard, they have multiple limitations including time-consuming application, patient discomfort, limited oral hygiene, and sharps injury risk due to the wires used to apply the bars. These newer techniques, including intermaxillary fixation (IMF) screws [2], embrasure wires [3], hybrid arch bars [4], and dental occlusion ties [5], aim to avoid the limitations of EABs. Numerous recent comparison studies have detailed the key features and limitations of different techniques [6–13]. Kalluri et al. published a systematic review and meta-analysis in 2024, further helping define the differences in technique [14]. Recognizing that the varied techniques all have strengths and weaknesses, other authors have published guides on (1) technique specifics [15], (2) how to select an ideal technique [16], and (3) comparisons of how new technologies compare to older ones [17]. Cornelius et al. have compiled the most comprehensive comparison of hybrid MMF systems to date [18].

While all the newer technologies offer specific advantages, none have fully outperformed EABs. The need remains for a technology with the versatility and strength of EABs and with the speed of application, safety, and patient comfort of newer technologies. Minne Ties Hybrid Arch Bar System™ (MTHAB) was designed with these concepts in mind. This technology utilizes Minne Ties® [5] instead of wires to secure the technology to the dentition. This cadaver study aimed to directly compare the occlusal forces as well as the speed of application and removal of EABs compared to MTHAB.

2. Materials and Methods

2.1. Study Design

This cadaver-based experiment was designed to compare and contrast traditional EABs to a novel MMF technology: MTHAB (Invisian Medical, Prairie Village, KS, USA) (Figure 1). To quantify differences in the technologies, the occlusal forces generated by standard elastics bands were assessed. Additionally, the speed of application and removal of the devices were measured. Four fresh cadavers with near complete dentition were supplied by the University of Minnesota's Anatomy Bequest Program (ABP). A team of 8 surgeons and residents from the University of Minnesota's Departments of Otolaryngology—Head & Neck Surgery and Oral Maxillofacial Surgery applied the technologies, with 2 participants per cadaver. All surgeons signed agreements to abide by ABP ethical guidelines for cadaver-based studies.

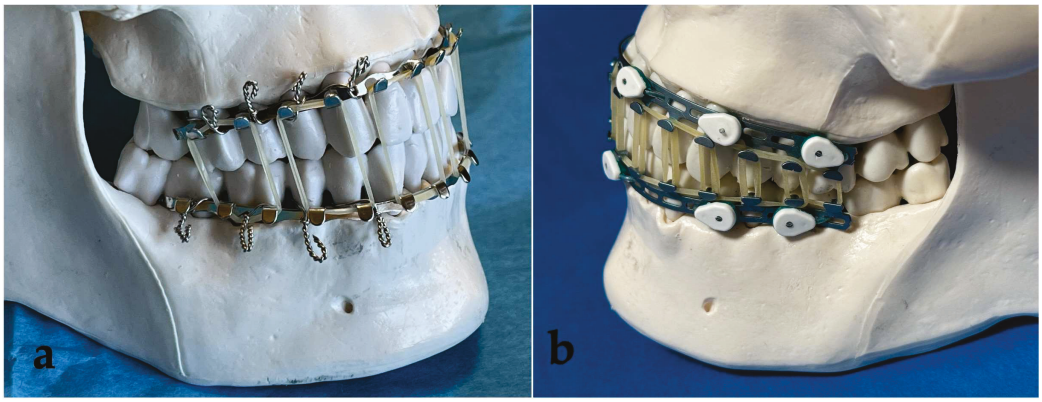

Figure 1. (**a**) Erich Arch Bars applied to a plastic model with 24 g wire with elastic bands to achieve MMF; (**b**) Minne Ties Hybrid Arch Bars applied with circumdental Minne Ties to a plastic model with elastic band MMF.

https://doi.org/10.3390/cmtr19010007

2.2. Technology Description

The Minne Ties Hybrid Arch Bar (MTHAB) System (Figure 2) is a novel maxillomandibular fixation (MMF) technology consisting of contoured titanium arch bars secured to the dentition using circumdental Minne Ties (dental occlusion ties) rather than stainless-steel wires. Each bar includes a series of apertures for passage of the Minne Ties and cleat-shaped hooks oriented toward the occlusal surfaces to permit attachment of elastics (or wire loops, if preferred) for MMF. The system is designed to provide versatile MMF optionality including short-term immobilization (up to 4 weeks), or early dynamic functional therapy with guiding elastics. The system streamlines intraoral application by eliminating wire twisting, reducing sharps exposure, and improving access in the mouth during fixation. To apply the technology, the MTHAB bars are trimmed to length, adapted closely to the gingival margins, and secured with Minne Ties placed through aligned interdental embrasures (see Figure 2). Once affixed, elastics can be applied between the superior and inferior bars to achieve maxillomandibular fixation.

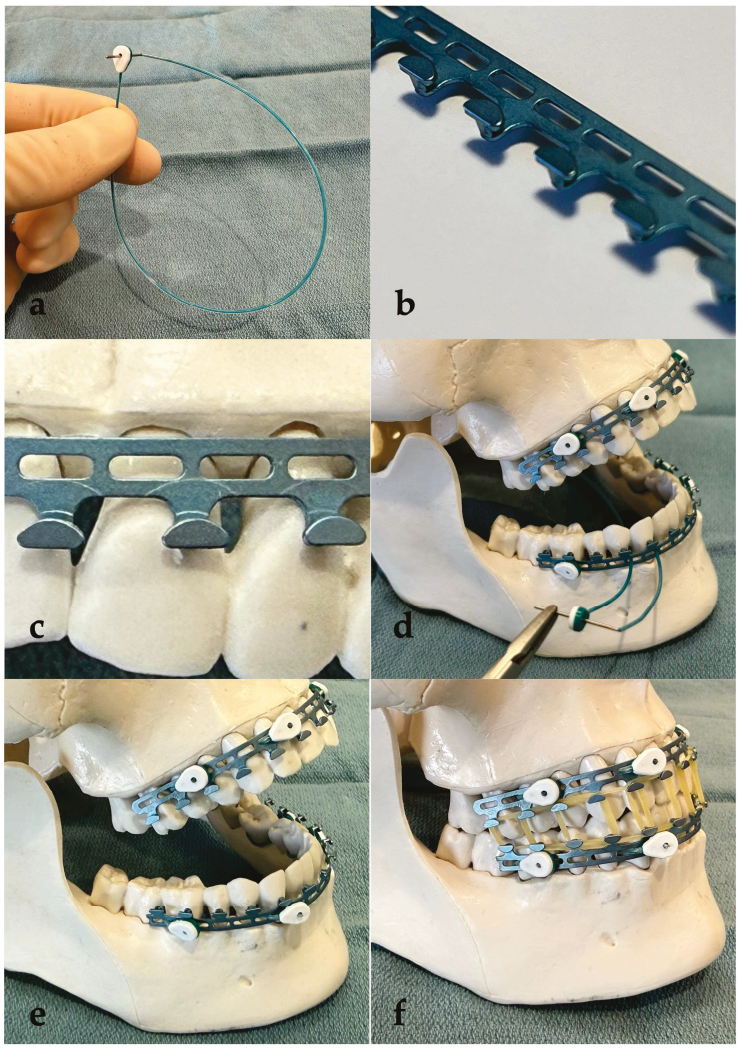

Figure 2. (**a**) Example Minne Tie (dental occlusion tie) which loops upon itself like a "zip tie"; (**b**) MTHAB bar featuring cleat-shaped hooks for elastic band application and ovoid apertures for Minne Ties passage; (**c**) MTHAB positioned along the gingival margin of the teeth; (**d**) a near-complete application of Minne Ties to secure the MTHAB to the model dentition (note the last Minne Tie being applied around the mandibular canine to secure the MTHAB); (**e**) MTHAB fully secured to the dentition (note the Minne Ties have been cut flush with the surface of the Minne Tie clasps to provide a smooth interface with the oral mucosa); (**f**) dentition placed into maxillomandibular fixation with elastic bands applied to the upper and lower MTHAB.

https://doi.org/10.3390/cmtr19010007

2.3. Interventions

Each team of 2 surgeons applied EABs and MTHAB to a single cadaver. EABs were applied with 24 g stainless steel wire. A total of 16 circumdental wires were applied. In contrast, the MTHAB was secured with a total of 8 Minne Ties according to the technology's Instructions for Use. Each application timing was recorded with a stopwatch. Application time was stopped once each technology was fully applied, but before applying any elastic bands. Pictures were obtained with digital cameras before, during, and after application. A complement of elastic bands were applied to each technology, starting with 8 elastics evenly applied to the dentition. The occlusion force was then measured by a force gauge (Mark-10 model M3-50), applied to the mandibular dentition with a single looped 24-gauge wire (Figure 3). The gauge was applied with increasing force until the force overcame the closure force of the elastics, marked by the separation of the maxillary and mandibular dentition. This measurement was then repeated with 10, 12, and finally 14 elastics. Readings were recorded in pounds of force (lb-F).



Figure 3. Mark-10 (model M3-50) force gauge applied to mandibular dentition to measure occlusal force achieved by elastic bands.

2.4. Endpoints

The primary endpoint was tensile force (lb-F) required to overcome the occlusion achieved by each MMF system. The secondary endpoints included application and removal times, recorded with stopwatches as described above. Additionally, surgeon-reported ease of use, stability, and soft tissue effects were obtained via structured questionnaires using Likert scales.

2.5. Equipment and Technology

Standard surgical instruments (retractors, needle drivers, wire cutters, headlamps) were supplied by investigators and the ABP. Erich Arch Bars, Minne Ties Hybrid Arch Bars, Minne Ties, elastics, and the tensile force gauge were provided by Invisian Medical. The experiment was a joint venture between the University of Minnesota and Invisian Medical. Minne Ties were invented at the University of Minnesota [19] and Invisian Medical licenses the intellectual property for commercialization. The Minne Ties Hybrid Arch Bar System (patent pending), is currently not commercially available, with anticipated FDA clearance in 2026.

https://doi.org/10.3390/cmtr19010007

2.6. Statistical Analysis

A linear mixed-effect model was used to compare the tensile forces achieved across the number of elastics. The team was included as a random effect for potential correlation for force measures within a team. Application and removal times were compared between systems using paired *t*-tests. *p*-values less than 0.05 were considered statistically significant. SAS V9.4 (SAS Institute Inc., Cary, NC, USA) was used for the analysis.

3. Results

3.1. Application and Removal Times

Application of the Minne Ties Hybrid Arch Bar was significantly faster than the Erich Arch Bar. The mean application time for the Minne Ties was 19.8 ± 4.1 min compared with 35.2 ± 5.7 min for the Erich Arch Bars ($p = 0.0027$). Similarly, removal was faster with the Minne Ties (1.6 ± 0.4 min) compared with the Erich Arch Bars (5.1 ± 2.1 min, $p = 0.0465$) (Table 1, Figure 4).

Table 1. Application and removal times (minutes, mean ± SD).

Erich Arch Bars	Application Time (min)	Removal Time (min)
Cadaver 1	32.53	5.18
Cadaver 2	35.92	6.03
Cadaver 3	42.85	7.15
Cadaver 4	29.63	2.20
Mean ± SD	35.23 ± 5.7	5.14 ± 2.1
Minne Ties Hybrid Arch Bars	**Application Time (min)**	**Removal Time (min)**
Cadaver 1	20.32	1.17
Cadaver 2	22.00	1.33
Cadaver 3	22.83	2.00
Cadaver 4	13.83	1.82
Mean ± SD	19.75 ± 4.1	1.58 ± 0.4

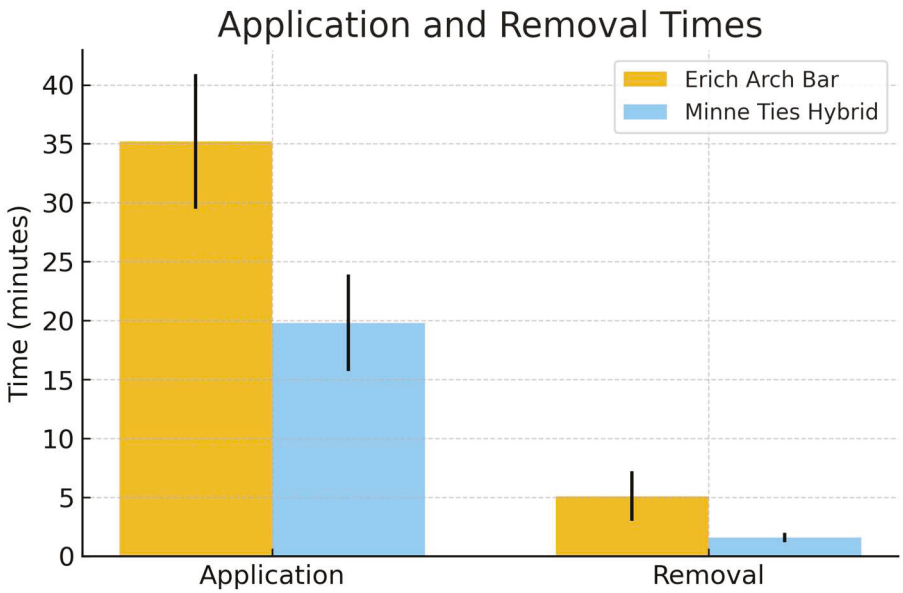

Figure 4. Application and removal times.

3.2. Occlusal Force Measurements

Across all elastic conditions, the Erich Arch Bars generated higher tensile occlusal forces compared with the Minne Ties Hybrid Arch Bars. With eight elastics, the mean force

https://doi.org/10.3390/cmtr19010007

for the Erich Arch Bars was 3.34 ± 0.96 lb-F versus 2.50 ± 1.18 lb-F for the Minne Ties. At the maximum of 14 elastics, forces increased to 6.33 ± 2.18 lb-F and 3.88 ± 1.57 lb-F, respectively. A mixed-effect model demonstrated significant main effects for the method and number of elastics ($p < 0.0001$ for both), though no interaction effect was observed ($p = 0.176$) (Figure 5).

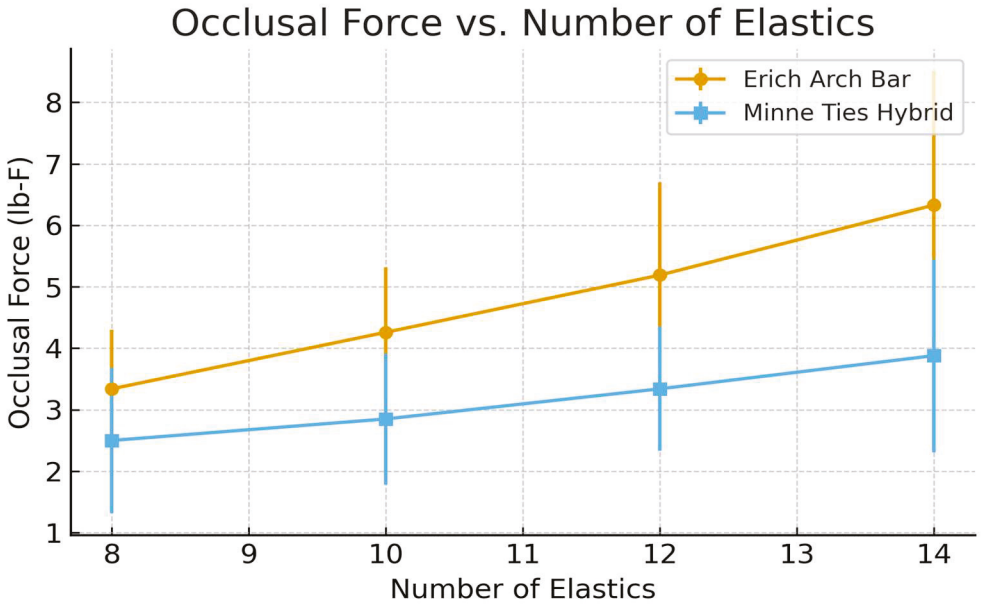

Figure 5. Mean occlusal force (lb-F) by number of elastics for Erich Arch Bar and Minne Ties Hybrid Arch Bar.

3.3. Surgeon-Reported Feedback

The results of the Surgeon-Reported Feedback survey can be found in Supplementary Table S1. The survey responses highlighted greater ease of use, improved safety, and equal to improved stability of MMF for the MTHAB system in comparison to EAR. For brevity, the most clinically meaningful survey responses were selected to be highlighted in Table 2 and reflected in Figure 6.

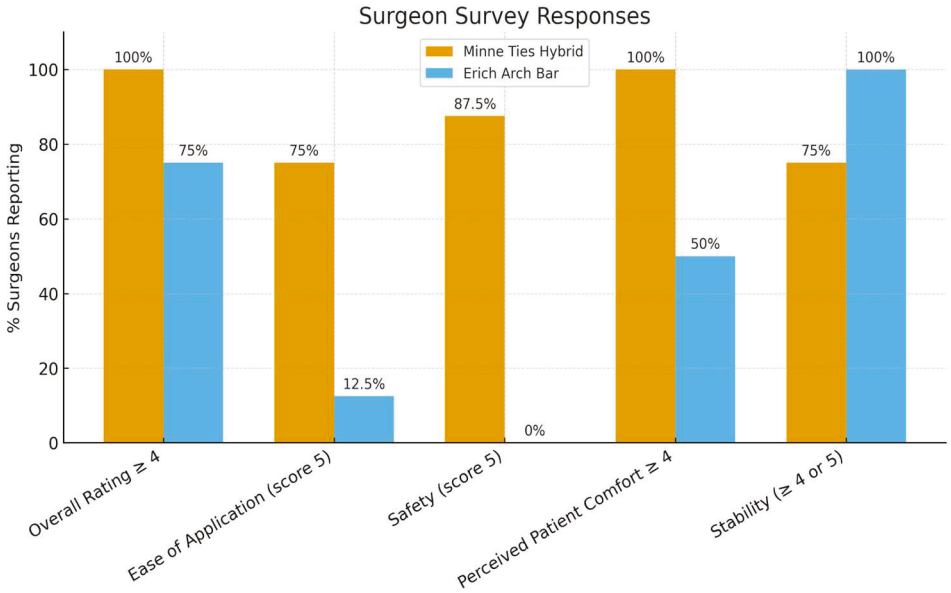

Figure 6. Surgeon survey responses (selected responses).

https://doi.org/10.3390/cmtr19010007

Table 2. Surgeon survey responses (% reporting top ratings). Responses are percentages of surgeons rating ≥ 4 or 5 on a 5-point Likert scale (Figure 6).

Category	Minne Ties Hybrid Arch Bar	Erich Arch Bar
Overall Rating ≥ 4	100%	75%
Ease of Application (score 5)	75%	12.5%
Safety (score 5)	87.5%	0%
Perceived Patient Comfort ≥ 4	100%	50%
Strength/Stability of MMF	75%	100%

Responses are percentages of surgeons rating $\geq$4 or 5 on a 5-point Likert scale.

- Overall ratings: 100% of surgeons rated Minne Ties ≥ 4 on a 5-point Likert scale, compared with only 75% for Erich Arch Bars.
- Application ease: 75% of participants rated Minne Ties as "very easy" (score of 5) for applying to dentition, compared with only 12.5% giving Erich Arch Bars the same rating.
- Safety: 87.5% of surgeons rated Minne Ties at the highest safety score (5/5), while Erich Arch Bars scored lower, with 50% rating only 2/5 on safety.
- Stability.

4. Discussion

This cadaveric comparison study demonstrates that the Minne Ties Hybrid Arch Bar provides significantly reduced application and removal times compared with traditional Erich Arch Bars, while also offering favorable surgeon-reported perceptions of ease of use and safety.

The findings align with the evolving literature on MMF techniques. EABs, first described in the mid-20th century, remain the benchmark for stability and versatility in mandibular fracture management [1,6,7]. Their primary limitations—time-consuming application, risk of sharps injury, and poor oral hygiene—have motivated the development of alternatives such as IMF screws, embrasure wires, and hybrid systems [6–8,10,11]. Studies comparing IMF screws and embrasure wires to EABs have shown improvements in application speed and surgeon ergonomics, though often at the cost of reduced stability or increased risk of complications [7–9]. Hybrid systems such as SMARTLock and MatrixWave devices have further narrowed the gap, offering reduced operative time with adequate fixation strength, yet they risk tooth root and nerve injury [9,10,16].

Our results demonstrate that the MTHAB fits into this evolving landscape, providing a pronounced improvement in application efficiency. Application times were nearly halved compared to EABs, a clinically meaningful difference in trauma settings where operative time directly impacts anesthesia exposure and patient outcomes [14,16,17]. Removal was similarly expedited, reducing intraoperative handling and potential for sharps injury. These findings are reinforced by surgeon survey data, which strongly favored MTHAB in terms of ease of application, safety, and perceived patient comfort.

We measured a notable difference between systems in the number of elastics required to generate a given occlusal force: for the same target force, the MTHAB required more elastics than EABs—roughly three elastics for MTHAB for every two with EABs. This pattern is explained by Hooke's law: the force produced by an elastic increases in proportion to how much it is stretched, and groups of elastics placed in parallel behave like a stiffer spring. Because the distance between the cleats of the superior and inferior bar is smaller for MTHAB than for EAB, each elastic is less elongated at intercuspation and therefore contributes less force per band. Adding more elastics—effectively increasing the overall

https://doi.org/10.3390/cmtr19010007

stiffness—compensates for this geometric difference. Clinically, the key point is that both systems achieved occlusal forces within ranges considered sufficient for maxillomandibular fixation in this model; the MTHAB simply reaches those targets with a higher elastic count.

We also observed meaningful variability in occlusal forces between cadavers at the same nominal elastic count. The vertical height of the dentition varied with each cadaver and influenced the same geometric factor—the distance between the cleats of the superior and inferior bar—which appeared to be the determining variable: greater inter-cleat spacing produced more elastic stretch and therefore higher force per band, regardless of the system. This effect is rarely discussed in the MMF literature but is potentially important for both study design and clinical practice when selecting the appropriate amount of elastics [18].

Several limitations warrant consideration. The study was conducted in a cadaveric model, which while anatomically accurate, cannot replicate intraoral bleeding, tissue compliance, or patient discomfort. The sample size was necessarily limited, and although the use of multiple teams improved generalizability, variability in surgical technique may have influenced the results. Furthermore, MTHAB is not yet commercially available, with anticipated FDA clearance projected for 2026, limiting immediate clinical application.

Designed as a pilot, this study provides a compelling foundation for a planned prospective human-subject randomized clinical trial comparing MTHAB with EABs in the management of mandibular fractures. The trial will evaluate clinical effectiveness—fixation stability, complication rates, oral hygiene, speed of application/removal, and patient-reported outcome measures.

5. Conclusions

In summary, the Minne Ties Hybrid Arch Bar System demonstrates substantial advantages in efficiency and surgeon safety compared to Erich Arch Bars, while generating clinically acceptable occlusal forces. The Minne Ties system offers a compelling alternative to traditional methods that may redefine the balance between surgical efficiency, safety, and guiding elastics use in maxillomandibular fixation.

Supplementary Materials: The following supporting information can be downloaded at https://www.mdpi.com/article/10.3390/cmtr19010007/s1: Table S1: Surgeon-Reported Feedback survey results.

Author Contributions: Conceptualization, A.W.J.; methodology, A.W.J. and F.E.P.; formal analysis, A.W.J., J.M. and F.E.P.; investigation, A.W.J., J.M., and F.E.P.; resources, A.W.J.; writing—original draft preparation, A.W.J. and J.M.; writing—review and editing, A.W.J., J.M. and F.E.P. All authors have read and agreed to the published version of the manuscript.

Funding: Invisian Medical provided funding for use of the anatomy lab and cadavers supplied by the University of Minnesota's Anatomy Bequest Program. Study materials including Erich Arch Bars, Minne Ties, Minne Ties Hybrid arch bars, and elastics were provided by Invisian Medical. Conference space and AV equipment were provided by the University of Minnesota's Bakken Medical Device Center at no charge.

Institutional Review Board Statement: This project was performed with the approval of the University of Minnesota Anatomy Bequest Program (ABP). The Anatomy Bequest Program Proposal Review Committee, which is similar to the University of Minnesota's Institutional Review Board that reviews research requests pertaining to living human subjects, functions to create a standardized, transparent process for evaluating education and research requests from end users for access to anatomical material. The ABP Proposal Review Committee is organized exclusively for ensuring the ethical conduct of deceased human subject research and education before access to anatomical material takes place. Committee members determine if each proposed use has scientific merit and is consistent with the disclosures published in the ABP consent documents. The authors wish to

https://doi.org/10.3390/cmtr19010007

thank the individuals who donated their bodies to the University of Minnesota's Anatomy Bequest Program for the advancement of education and research. Ethics Committee Name: UMN Anatomy Bequest Program, Approval Code: 2025010, Approval Date: 3 June 2025.

Informed Consent Statement: All surgeon participants signed agreements to abide by the University of Minnesota's Anatomy Bequest Program ethical guidelines for cadaver-based studies.

Data Availability Statement: The raw data supporting the conclusions of this article are recorded in hard copy in laboratory notebooks and will be made available by the authors on request.

Acknowledgments: The authors acknowledge Scott Lunos for providing statistical analysis of the laboratory data. We thank Jan Creiderberg and Omar Khan of Invisian Medical for supporting this study, as well as our co-surgeon participants in the cadaver lab: David Montag; Bridget Ebert; Nhut Quang Huy Tran, Nicolas Bricker; and George Sankar. Special thanks are given to the University of Minnesota Anatomy Bequest Program and those who donated their bodies to science. During the preparation of this work, the author(s) used ChatGPT 5 to aid in the editing of the manuscript. After using this tool/service, the author(s) reviewed and edited the content as needed and take(s) full responsibility for the content of the published article.

Conflicts of Interest: A.W.J. receives royalties from the University of Minnesota as an inventor of dental occlusion ties (Minne Ties). The other authors declare no conflicts of interest.

Abbreviations

The following abbreviations are used in this manuscript:

MMF	Maxillomandibular fixation
ABP	Anatomy Bequest Program
EABs	Erich Arch Bars
MTHAB	Minne Ties Hybrid Arch Bar System

References

1. Erich, J.B.; Austin, L.T. *Traumatic Injuries of Facial Bones (an Atlas of Treatment)*, 1st ed.; W.B. Saunders Co.: London, UK; Philadelphia, PA, USA, 1944; pp. 526–528.
2. Arthur, G.; Berardo, N. A simplified technique of maxillomandibular fixation. *J. Oral Maxillofac. Surg.* **1989**, *47*, 1234. [CrossRef] [PubMed]
3. Hollows, P.; Brennan, J. Temporary intermaxillary fixation: A quick reliable method. *Br. J. Oral Maxillofac. Surg.* **1999**, *37*, 422–423. [CrossRef] [PubMed]
4. Park, K.N.; Oh, S.M.; Lee, C.Y.; Kim, J.Y.; Yang, B.E. Design and application of hybrid maxillomandibular fixation for facial bone fractures. *J. Craniofac. Surg.* **2013**, *24*, 1801. [CrossRef] [PubMed]
5. Johnson, A.W. Dental occlusion ties: A rapid, safe, and non-invasive maxillo-mandibular fixation technology. *Laryngoscope Investig. Otolaryngol.* **2017**, *2*, 178–183. [CrossRef] [PubMed]
6. Qureshi, A.A.; Reddy, U.K.; Warad, N.M.; Badal, S.; Jamadar, A.A.; Qurishi, N. Intermaxillary fixation screws versus Erich arch bars in mandibular fractures: A comparative study and review of literature. *Ann. Maxillofac. Surg.* **2016**, *6*, 25–30. [CrossRef] [PubMed]
7. Rastogi, S.; Ahmed, T.; Giri, K.; Dandriyal, R.; Indra, B.N.P.; Joshi, A.; Choudhury, S.; Mall, S. Comparative Evaluation of the Embrasure Wire versus Arch Bar Maxillomandibular Fixation in the Management of Mandibular Fractures: Are Arch Bars Replaceable? *Craniomaxillofac. Trauma Reconstr.* **2018**, *11*, 118–123. [CrossRef] [PubMed]
8. Satpute, A.S.; Mohiuddin, S.A.; Doiphode, A.M.; Kulkarni, S.S.; Qureshi, A.A.; Jadhav, S.B. Comparison of Erich arch bar versus embrasure wires for intraoperative intermaxillary fixation in mandibular fractures. *Oral Maxillofac. Surg.* **2018**, *22*, 419–428. [CrossRef] [PubMed]
9. Pathak, P.; Thomas, S.; Bhargava, D.; Beena, S. A prospective comparative clinical study on modified screw retained arch bar (SRAB) and conventional Erich's arch bar (CEAB). *Oral Maxillofac. Surg.* **2019**, *23*, 285–289. [CrossRef]
10. Aslam-Pervez, N.; Caccamese, J.F., Jr.; Warburton, G. A randomized prospective comparison of maxillomandibular fixation (MMF) techniques: "SMARTLock" hybrid MMF versus MMF screws. *Oral Surg. Oral Med. Oral Pathol. Oral Radiol.* **2020**, *130*, 640–644. [CrossRef]
11. Kaur, T.; Dhawan, A.; Bhullar, R.S.; Kapila, S.; Gupta, S.; Resham, R. Are Embrasure Wires Effective and Reliable Method for Intraoperative Maxillomandibular Fixation in Mandibular Fractures? *J. Maxillofac. Oral Surg.* **2022**, *21*, 433–441. [CrossRef]

https://doi.org/10.3390/cmtr19010007

12. Burman, S.; Rao, S.; Ankush, A.; Uppal, N. Comparison of hybrid arch bar versus conventional arch bar for temporary maxillomandibular fixation during treatment of jaw fractures: A prospective comparative study. *J. Korean Assoc. Oral Maxillofac. Surg.* **2023**, *49*, 332–338. [CrossRef] [PubMed]
13. Salavadi, R.K.; Sowmya, J.; Mani Kumari, B.; Kamath, K.P.; Anand, P.S.; Kumar, N.M.R.; Jadhav, P. Comparison of the efficacy of Erich arch bars, IMF screws and SMART Lock Hybrid arch bars in the management of mandibular fractures—A Randomized clinical study. *J. Stomatol. Oral Maxillofac. Surg.* **2025**, *126*, 102217. [CrossRef] [PubMed]
14. Kalluri, M.H.; Edalatpour, A.; Thadikonda, K.M.; Blum, J.D.; Garland, C.B.; Cho, D.Y. Patient outcomes and complications following various maxillomandibular fixation techniques: A systematic review and meta-analysis. *J. Plast. Reconstr. Aesthet. Surg.* **2024**, *92*, 151–176. [CrossRef] [PubMed]
15. McGinn, J.D.; Fedok, F.G. Techniques of maxillary-mandibular fixation. *Oper. Tech. Otolaryngol.* **2008**, *19*, 117–122. [CrossRef]
16. Johnson, A.W.; Akkina, S.R.; Bevans, S.E. Maxillomandibular Fixation: Understanding the Risks and Benefits of Contemporary Techniques in Adults. *Facial. Plast. Surg. Aesthet. Med.* **2025**, *27*, 98–105. [CrossRef] [PubMed]
17. Akkina, S.R.; Bevans, S.E.; Johnson, A.W. Techniques for maxillomandibular fixation: Old and new. *Curr. Opin. Otolaryngol. Head Neck Surg.* **2025**, *33*, 216–221. [CrossRef] [PubMed]
18. Cornelius, C.P.; Liokatis, P.G.; Doerr, T.; Matic, D.; Fusetti, S.; Rasse, M.; Gellrich, N.C.; Heiland, M.; Schubert, W.; Buchbinder, D. Matrix Wave^{TM} System for Mandibulo-Maxillary Fixation-Just Another Variation on the MMF Theme? Part II: In Context to Self-Made Hybrid Erich Arch Bars and Commercial Hybrid MMF Systems-Literature Review and Analysis of Design Features. *Craniomaxillofac. Trauma Reconstr.* **2025**, *18*, 33. [CrossRef] [PubMed] [PubMed Central]
19. Johnson, A.W.; Brown, L.F.; Levine, S.C.; Rolfes, C. Dental Occlusion Tension Band Ties Systems Methods. U.S. Patent No. 11045235B2, 29 June 2021. U.S. Patent and Trademark Office.

Disclaimer/Publisher's Note: The statements, opinions and data contained in all publications are solely those of the individual author(s) and contributor(s) and not of MDPI and/or the editor(s). MDPI and/or the editor(s) disclaim responsibility for any injury to people or property resulting from any ideas, methods, instructions or products referred to in the content.

https://doi.org/10.3390/cmtr19010007

craniomaxillofacial trauma & reconstruction

MDPI

Article

Digital vs. Direct Anthropometry with MetiSmile® 3D Face Scanner: A Validation and Reliability Study on a Mannequin Model

Alexander De Crem [1,†], Constantijn Bogaert [2,†], Frederik Piccart [3], Matthias Ureel [1,4], Benjamin Denoiseux [1,4], Lisa De Kock [1,5], Marieke Brands [2,6,7,8], Olivier Lenssen [2] and Renaat Coopman [1,4,*]

1 Department of Oral and Maxillofacial Surgery and Head and Neck Surgery, Vrije Universiteit Brussel (VUB), 1090 Brussels, Belgium; alexander.decrem@uzbrussel.be (A.D.C.); matthias.ureel@uzgent.be (M.U.); benjamin.denoiseux@uzgent.be (B.D.); lisa.dekock@uzgent.be (L.D.K.)
2 Department of Oral and Craniomaxillofacial (OCMF) Surgery, University Hospital Ghent, 9000 Ghent, Belgium; constantijn.bogaert@ugent.be (C.B.); marieke.brands@uzbrussel.be (M.B.); olivier.lenssen@uzbrussel.be (O.L.)
3 Ziekenhuis Heusden-Zolder, 3550 Heusden-Zolder, Belgium; frederik.piccart@sfz.be
4 Cancer Research Institute Ghent (CRIG), 9000 Ghent, Belgium
5 Sint-Blasius Hospital, 9200 Dendermonde, Belgium
6 Department of Oral and Craniomaxillofacial (OCMF) Surgery, University Hospital Brussels (UZ Brussel), 1090 Brussels, Belgium
7 Department of Oral and Craniomaxillofacial (OCMF) Surgery, Ziekenhuis Netwerk Antwerpen (ZNA), Middelheim Hospital, 2020 Antwerp, Belgium
8 Integraal Kankercentrum Nederland (IKNL), 3511 LC Utrecht, The Netherlands
* Correspondence: renaat.coopman@ugent.be; Tel.: +32-9-332-32-05
† These authors contributed equally to this work.

Abstract

Background: Three-dimensional facial anthropometry is increasingly used in orthodontics and orthognathic surgery. Conventional face scanning systems such as Vectra® and 3dMD® are well validated but remain costly and technically demanding. The MetiSmile® 3D face scanner provides a more affordable and portable alternative, yet its accuracy and reproducibility have not been rigorously evaluated. Methods: Validation was performed on a standardized mannequin head in two phases. Phase 1 assessed mesh reproducibility under artificial lighting (AL), natural lighting (n-AL), and after mesh-refinement (AL-F). Landmark-based pre-registration with Iterative Closest Point refinement was applied; root-mean-square error (RMS) and distance maps were calculated. In phase 2, three observers (student, resident, consultant) performed 14 predefined linear measurements by direct anthropometry (DA) and digital anthropometry (DiA). Intra- and inter-observer reliability was evaluated using intraclass correlation coefficients. Results: Phase 1 yielded mean RMS values of 0.041 mm (AL), 0.043 mm (n-AL), and 0.030 mm (AL-F), with largest deviations near eyes, alar regions, and lip commissures. Phase 2 showed excellent ICCs ($\geq$0.997) and mean absolute DA–DiA differences of 0.25–0.33 mm, with only few differences > 2 mm. Conclusion: The MetiSmile® scanner generates highly reproducible meshes and clinically acceptable linear measurements on mannequin models. Further validation on live subjects is warranted before routine clinical application.

Keywords: facial scan; facial anthropometry; orthognathic surgery; digitalization; facial analysis

1. Introduction

In the diagnostic work-up for orthognathic procedures, facial anthropometry plays a central role. The quantitative assessment of facial dimensions and proportions was traditionally performed using direct anthropometry which involved the manual use of calipers and rulers. This has long been considered the gold standard due to its simplicity and direct applicability [1–4].

As in many other disciplines, digitization is transforming OCMF diagnostics and treatment planning. A key advantage lies in the acquisition and analysis of complete 3D datasets, which provide more comprehensive and reproducible measurements. In contrast to 2D photography, 3D imaging enables realistic simulation, longitudinal monitoring, and seamless integration with other digital modalities (e.g., intraoral scans, CBCT) [5]. This has led to a shift towards digital anthropometry, which leverages 3D imaging and computational analysis to measure and evaluate facial structures.

A variety of 3D imaging methods and commercial systems are currently available for digital facial anthropometry. These include stereophotogrammetry, structured light scanning, photogrammetry, laser surface scanning, and time-of-flight (ToF) systems. Each technology offers clinically acceptable results and carries its own set of strengths and limitations [6].

The MetiSmile® scanner (Shining3D, Hangzhou, China) represents a compact and portable stereophotogrammetric system designed for soft tissue analysis in dentistry and OCMF surgery. It combines four calibrated cameras with an infrared proximity sensor, facilitating rapid acquisition of facial geometry without the use of visible flash. While the MetiSmile® system shows promising potential for clinical integration, formal validation studies are still required to establish its accuracy, reliability, and clinical usability.

This study therefore aims to validate the MetiSmile® 3D facial scanner as a stepping stone toward establishing a validated, fully digital and clinically acceptable 3D anthropometric workflow for orthognathic surgery consultations.

2. Materials and Methods

2.1. Study Design

The validation of the MetiSmile® 3D facial scanner was conducted in two phases. Phase I focused on reproducibility and precision by analyzing the consistency of repeated scans under varying lighting conditions and across different operators. Phase II addressed accuracy by comparing digital anthropometric measurements obtained with the MetiSmile® system (Digital Anthropometry, DiA) against traditional direct anthropometry (DA) using calipers on the same reference model.

Across both phases, three fundamental quality parameters were assessed: accuracy, precision, and reproducibility. Together, these metrics determine the clinical applicability of the scanning system [7–9].

Accuracy (Trueness) describes how closely measurements correspond to a reference or "gold standard." It is typically assessed by comparing 3D models from the test device with high-resolution reference scans or certified phantoms (e.g., plaster casts, 3D-printed replicas, anthropometric models). Deviations are quantified with metrics such as Root Mean Square (RMS) Error or Mean Absolute Error (MAE).

Precision (Repeatability) reflects the consistency of repeated measurements under identical conditions. This is evaluated by performing multiple scans of the same object without altering settings, followed by inter-comparison of models. Variability is expressed using the Intraclass Correlation Coefficient (ICC), Coefficient of Variation (CV), or standard deviation of differences.

https://doi.org/10.3390/cmtr19010003

Reproducibility (Inter-Observer Reliability) indicates robustness under varying conditions or operators. It is tested by repeating scans across different users or settings, with agreement assessed through ICC values and Bland–Altman plots. High reproducibility confirms the system's reliability in clinical workflows.

2.2. Reference Model and Anatomical Landmarks

A standardized mannequin head (bald male, soft PVC, head circumference 55.90 cm) served as the surrogate model throughout the study (Figure 1). Nineteen anatomical landmarks were marked on the facial surface using a fine black marker (Artline 200 Fine 0.4) by the primary author and verified by the senior author [10]. These landmarks were selected to represent the vertical upper, middle, and lower thirds of the face, ensuring appropriate coverage of key facial regions for linear measurement. From these landmarks, 14 linear measurements were defined (Table 1).

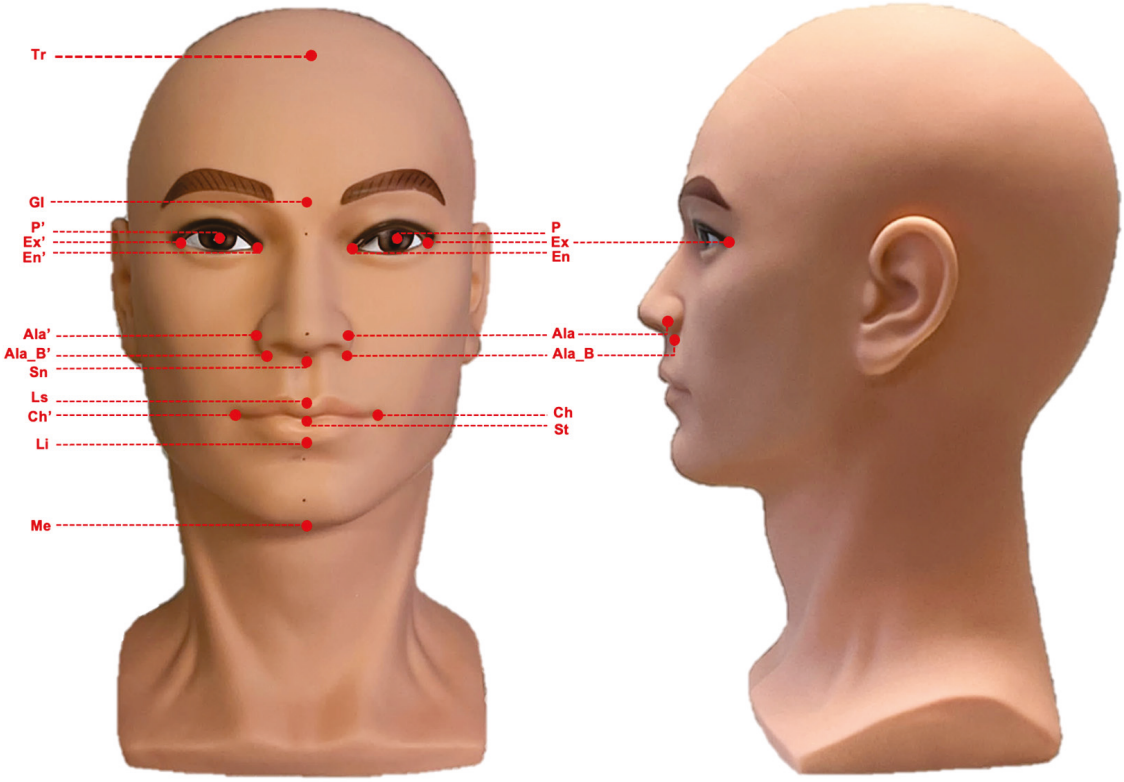

Figure 1. Standardized mannequin head used for three-dimensional facial imaging and measurement analyses. The image shows the frontal (**left**) and lateral (**right**) views. Abbreviations: Trichion (Tr), Glabella (Gl), Subnasale (Sn), Labiale Superior (Ls), Stomion (St), Labiale inferior (Li), Menton (Me), Cheilon (Ch/Ch'), Ala (Ala/Ala'), Alar base (Ala_B/Ala_B'), Exocanthion (Ex/Ex'), Endocanthion (En/En'), Center of pupil (P/P').

Direct anthropometric measurements were obtained with a digital caliper (Fiber Composite Digital Caliper—resolution: 0.100 mm; accuracy: 0.200 mm) served as the gold standard for accuracy analyses. Digital scans were acquired using the MetiSmile® scanner and analyzed with the Shining3D software packages version 2.2.5.7 (FScan, Shining3D, Hangzhou, China; Facial Analyzer, Shining3D, Hangzhou, China). All processing was performed on a Dell Precision 7680 workstation (Intel 13th generation i7-13850HX processor, 2 × 16 GB RAM, Windows 11).

https://doi.org/10.3390/cmtr19010003

Table 1. Linear measurements.

Vertical Distances	Landmarks
Upper facial $^{1}/_{3}$ *	Trichion, Glabella
Middle $^{1}/_{3}$ *	Glabella, Subnasale
Lower $^{1}/_{3}$	Subnasale, Menton
Upper lip height *	Subnasale, Stomion
Chin height	Stomion, Menton
Philtrum Length	Subnasale, Labiale Superior
Upper vermilion	Labiale Superior, Stomion
Lower vermilion	Stomion, Labiale Inferior
Horizontal Distances	**Landmarks**
Interpupillary distance	Center of Pupil Left and Right
Ca-Ca medial	Endocanthion Left and Right
Ca-Ca lateral	Exocanthion Left and Right
Alar width	Ala Left and Right
Alar base width *	Alar base Left and Right
Mouth Width (Ch-Ch)	Cheilon Left and Right

*: these measurements were not automatically generated in the FScan software version 2.2.5.7.

2.2.1. Phase I: Mesh Reproducibility and Precision Analysis

To evaluate the reproducibility of mesh acquisition, the mannequin was scanned 20 times by the main researcher under two different lighting conditions. Ten scans were performed with ambient artificial lighting combined with daylight from a window (AL scans), while the remaining ten were carried out in the evening under overcast conditions without artificial light (n-AL scans). In both settings, the brightness of the scanner was automatically optimized by the software. The resulting meshes were cropped to include the face, ears and part of the neck. (Figure 2) One mesh (n°3) was randomly selected as the reference mesh, to which all other meshes were aligned using three common anatomical landmarks (exocanthion left, exocanthion right and pronasale) followed by fine registration with Iterative Closest Point (ICP) alignment.

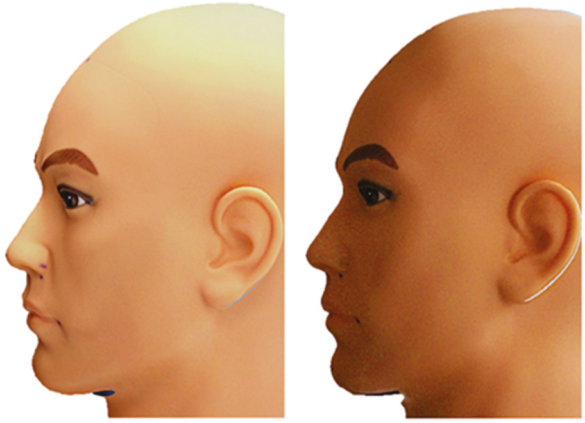

Figure 2. Left: AL Scan n°3; Right: AL-F Scan n°3.

For clinical evaluation, the artificially lit meshes were subsequently trimmed to include the facial regions of highest relevance. The trimming was performed in a circular fashion as to include all facial landmarks anterior of the trichion, tragal point and cervical point.

https://doi.org/10.3390/cmtr19010003

2.2.2. Phase II: Accuracy—Direct Anthropometry vs. Digital Anthropometry

For the assessment of accuracy, both DA and DiA were performed on the mannequin, that consisted of a fixed head component mounted on an integrated stand. For each measurement, the entire assembly was placed on the same flat table surface at eye level of the primary investigator to ensure a consistent baseline position. On this stable platform, the head was visually aligned to the Frankfort horizontal plane by checking the tragion–orbitale line in the frontal and lateral views. Because the head remained in the same fixed position throughout all scans, a consistent orientation across consecutive acquisitions was guaranteed.

During scanning, the mannequin remained completely static while the examiner moved the handheld MetiSmile® scanner (FScan, Shining3D, Hangzhou, China; Facial Analyzer, Shining3D, Hangzhou, China). around the facial surface in accordance with the manufacturer's recommended workflow. This involved a continuous sweep along the frontal, lateral, and inferior facial regions. The average time required to complete a full scan was approximately 15–20 s, depending on operator experience.

The measurements were carried out by three observers with different levels of experience: a dental student (DS) with no prior experience in anthropometry, a maxillofacial surgery trainee (MT) with eight years of experience, and a maxillofacial surgery consultant (MC) with more than ten years of experience. Each observer performed three repeated measurements per DA and DiA session, yielding a total of six measurements for both methods. To further reduce the influence of memory, a second series of sessions was repeated after two weeks.

DA measurements were performed with a 150 mm digital caliper (Carbon Fiber Composite Digital Caliper, resolution: 0.100 mm, accuracy: ±0.200 mm). DiA measurements were obtained from 3D scans generated with the MetiSmile® system. Semi-automated landmark detection was provided by the Shining3D Face Analyzer software 2.2.5.7., although manual repositioning was required to ensure alignment with the predefined 19 landmarks. For four linear distances were not automatically generated (see table) and had to be measured manually through the "Free Measure" tool which allows measuring distances between two (freely) chosen points.

2.3. Statistical Analysis

In Phase I, reproducibility was evaluated by comparing meshes through the calculation using CloudCompare v2.13 beta of RMS error, mean deviations, and 95% confidence intervals to quantify intra-device variability under different lighting conditions (Table 2) [11].

Table 2. Average distances compared with the reference mesh.

	Final RMS	Mean	95% C.I.	Minimal	Maximum
AL scans	0.041	−0.002	−0.097; 0.093	−0.414	0.345
n-AL scans	0.043	−0.004	−0.099; 0.091	−0.339	0.351
AL-F scans	0.030	0.003	−0.130; 0.136	−0.191	0.252

In Phase II, which focused on accuracy and inter-observer reliability, descriptive statistics including range, interquartile range (IQR), mean, and difference in means were generated in IBM SPSS Statistics 26 after collecting both DA and DiA measurements. Because of the limited sample size and non-normally distributed data, we opted to use the median and IQR as robust, non-parametric measures of variability instead of the standard deviation. Negative deviation values indicate that the DiA measurement exceeded the corresponding DA measurement. To assess intra- and inter-observer reliability, a two-way mixed-effects model with absolute agreement was used, and single-measure ICC values

https://doi.org/10.3390/cmtr19010003

were reported. For inter-observer reliability specifically, ICCs (two-way mixed, average measures) were calculated for both the direct and digital measurements between each pair of observers [8]. Separate ICC values were obtained for DA and DiA, as well as for the combined dataset. In addition, Bland–Altman plots were generated to provide a visual assessment of agreement and bias between observers and across measurement methods [7,9]. RMS values (mean, minimum, and maximum) are reported as positive values, reflecting the absolute magnitude of measurement error.

3. Results

3.1. Mesh Reproducibility

The AL-scans showed a maximal and minimal deviation of, respectively, 0.345 and −0.414 mm (range: 0.759 mm) when aligned with the reference scan. The n-AL scans showed a smaller range with a maximal and minimal distance of, respectively, 0.351 and −0.339 mm (range: 0.690 mm). The scans edited to contain the clinical region of interest only (AL-F scans) had maximal and minimal deviations of, respectively, 0.252 and −0.191 mm (range: 0.443). The highest distances between meshes were seen in the inferior and inferiolateral nasal region, auricle, Glogau-Klein points (upper cupid's bow), cheilon, endo- and exocanthion, submental point, medial half of the supraorbital margin, upper and lower eyelid margins and submental region (see Figure 3 distance color map). The final RMS for the AL, n-AL and AL-F scans was 0.041, 0.043 and 0.030 with the mean distances, respectively, being −0.002 mm, −0.004 mm and 0.003 mm and submillimeter confidence intervals (Figure 4: narrow distribution of distances).

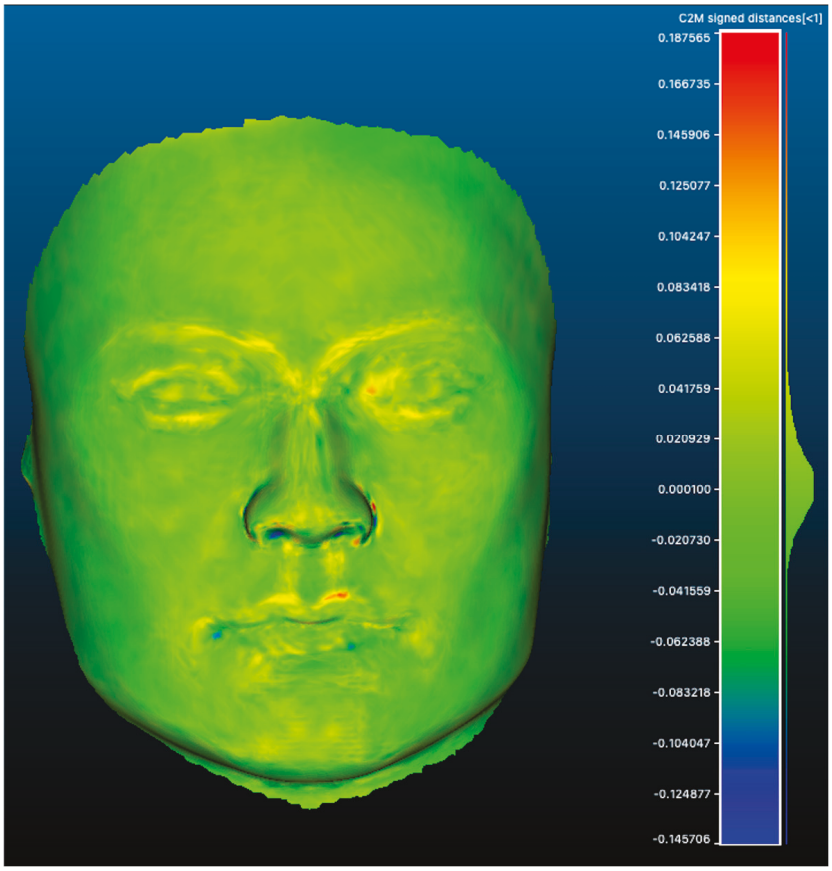

Figure 3. Colormap of distances between meshes (scan AL-F n°5 vs reference mesh) showing a narrow distribution with largest distances seen as a red (+) or blue (−) color (highest distance).

https://doi.org/10.3390/cmtr19010003

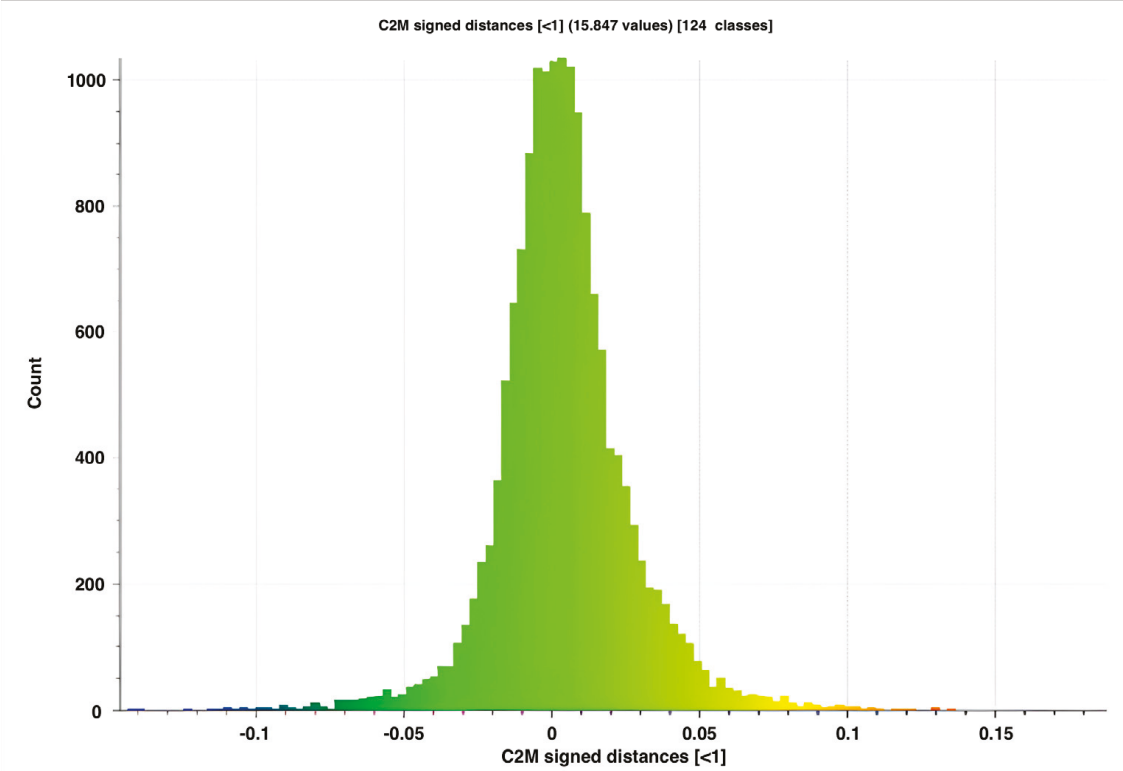

Figure 4. Distribution of distances for AL-F scan n°5 compared to the reference mesh.

3.2. Inter- and Intra-Observer Reliability

The descriptive analyses show a range for direct and digital measurements of, respectively, 1.610 and 1.900 mm for the MC, 0.940 and 1.090 mm for the MT, and 0.670 and 1.430 mm for the DS. The difference in means between the direct and digital measurements were 0.250 mm for the consultant, 0.330 mm for the trainee and 0.320 mm for the student (Table 3).

Table 3. Summary of the comparison between direct anthropometry (DA) and digital anthropometry (DiA) across three observers: maxillofacial surgery consultant (MC), maxillofacial surgery trainee (MT), and dental student (DS).

Group	Region	N	Range_DA	IQR_DA	Mean_DA	Mean_DiA	IQR_DiA	Range_DiA	Mean_DA-DiA
MC	**Upper3**	6vs6	2.000	0.800	58.933	58.983	0.830	1.200	−0.050
	Middle3	6vs6	1.000	0.470	54.216	54.733	0.600	0.900	−0.517
	Lower3	6vs6	3.700 *	1.750	60.400	58.557	1.580	2.640 *	1.843 *
	InterPupil	6vs6	0.500	0.280	62.350	63.218	0.660	1.900	−0.868
	EndoCanth	6vs6	2.200 *	1.220	33.567	32.888	3.630 *	4.750 *	0.678
	ExoCanth	6vs6	0.700	0.400	86.567	88.523	1.580	2.340 *	−1.957 *
	AlarBase	6vs6	0.800	0.730	25.583	25.250	0.320	0.400	0.333
	AlarWidth	6vs6	0.300	0.150	32.967	32.408	0.680	1.100	0.558
	Cheilon	6vs6	0.900	0.520	49.117	48.688	2.600 *	3.620 *	0.428
	UpLipHeight	6vs6	1.000	0.920	20.033	19.367	0.300	0.600	0.667
	Philtrum	6vs6	1.900	0.700	14.817	13.220	1.320	1.940	1.597 *
	ChinHeight	6vs6	3.600 *	1.950	40.767	40.433	0.630	1.000	0.333
	UpVermillion	6vs6	1.300	0.700	6.717	6.890	1.150	1.650	−0.173
	LowVermillion	6vs6	2.700 *	1.280	8.100	7.507	2.340 *	2.620 *	0.593
	Mean:		1.610					1.900	0.250

https://doi.org/10.3390/cmtr19010003

Table 3. *Cont.*

Group	Region	N	Range_DA	IQR_DA	Mean_DA	Mean_DiA	IQR_DiA	Range_DiA	Mean_DA-DiA
MT	**Upper3**	6vs6	1.000	0.770	59.717	59.283	0.220	0.300	0.433
	Middle3	6vs6	0.500	0.350	54.733	54.650	0.450	0.600	0.083
	Lower3	6vs6	1.800	1.130	59.950	57.935	1.150	2.720 *	2.015 *
	InterPupil	6vs6	0.800	0.350	62.833	63.752	0.700	0.950	−0.918
	EndoCanth	6vs6	0.900	0.380	34.083	32.862	0.930	1.610	1.222 *
	ExoCanth	6vs6	0.600	0.380	86.783	87.720	0.950	1.710	−0.937
	AlarBase	6vs6	0.400	0.180	25.750	25.500	0.580	1.100	0.250
	AlarWidth	6vs6	0.500	0.270	32.800	32.572	0.410	0.580	0.228
	Cheilon	6vs6	1.200	0.820	49.367	49.157	0.450	0.970	0.210
	UpLipHeight	6vs6	1.500	1.420	19.783	19.433	0.380	0.600	0.350
	Philtrum	6vs6	1.100	0.500	14.467	13.810	0.400	0.490	0.657
	ChinHeight	6vs6	0.700	0.550	40.900	40.967	0.380	0.900	−0.067
	UpVermillion	6vs6	0.500	0.200	7.033	6.382	0.790	1.580	0.652
	LowVermillion	6vs6	1.700	1.320	7.350	6.973	1.040	1.080	0.377
	Mean:		0.940					1.090	0.330
DS	**Upper3**	6vs6	1.000	0.630	59.412	58.917	0.630	0.700	0.500
	Middle3	6vs6	0.600	0.450	54.683	54.683	0.270	0.500	0.000
	Lower3	6vs6	0.900	0.600	60.150	58.142	1.130	1.970	2.008 *
	InterPupil	6vs6	0.600	0.300	62.633	63.052	0.900	3.110 *	−0.418
	EndoCanth	6vs6	0.800	0.650	33.867	31.847	1.270	3.140 *	2.020 *
	ExoCanth	6vs6	0.300	0.300	86.650	88.348	1.320	3.820 *	−1.698 *
	AlarBase	6vs6	0.600	0.520	25.650	25.617	0.120	0.200	0.033
	AlarWidth	6vs6	0.500	0.200	32.750	32.597	0.280	0.320	0.153
	Cheilon	6vs6	0.600	0.370	49.183	49.183	0.560	1.450	0.000
	UpLipHeight	6vs6	1.500	0.680	19.550	19.517	0.250	0.400	0.033
	Philtrum	6vs6	0.700	0.330	14.317	13.868	0.840	1.570	0.448
	ChinHeight	6vs6	0.400	0.330	41.000	40.533	0.520	0.600	0.467
	UpVermillion	6vs6	0.600	0.530	7.517	7.382	1.090	1.280	0.135
	LowVermillion	6vs6	0.300	0.150	7.250	6.620	0.930	0.980	0.630
	Mean:		0.670					1.430	0.310

Footnote: Each measurement was performed six times under both DA and DiA ("6 vs. 6"). Values marked with an asterisk (*) indicate increased variability or a larger difference between DA and DiA, signifying reduced agreement between the two measurement conditions.

When analyzing the ICC, excellent intra-observer reliability (ICC > 0.900) is noted for all observers independent for both the direct and the digital anthropometry methods for each observer. Excellent inter-observer reliability is noted as well between each pair of observers for both the direct as well as the digital measuring method. (Tables 4 and 5) The same results were seen for the inter-observer reliability between all three observers for both direct and digital anthropometry.

Bland–Altman plots (Figure 5) demonstrated strong agreement between DA and DiA across all observers. The consultant group showed a mean difference of 0.25 mm (95% LoA −1.630 to +2.130 mm), the trainee 0.330 mm (−1.140 to +1.790 mm), and the student 0.310 mm (−1.490 to +2.110 mm). The combined dataset confirmed a consistent submillimeter bias with narrow limits of agreement (LoA). Individual anatomical landmarks were evenly distributed without evidence of systematic measurement bias.

https://doi.org/10.3390/cmtr19010003

Table 4. IntraClass Correlation Coefficient Single measures for Intra-observer reliability.

Group	ICC	CI Lower	CI Upper	*p*
DA Consultant	0.999	0.998	1.000	<0.001
DiA Consultant	0.999	0.997	1.000	<0.001
DA + DiA Consultant	0.999	0.997	0.999	<0.001
DA resident	1.000	0.999	1.000	<0.001
DiA resident	1.000	0.999	1.000	<0.001
DA + DiA resident	0.999	0.999	1.000	<0.001
DA student	1.000	1.000	1.000	<0.001
DiA student	0.999	0.998	1.000	<0.001
DA + DiA student	0.999	0.998	1.000	<0.001

Table 5. Intraclass Correlation Coefficients Average measures for inter-observer reliability.

Direct Measurements	ICC	CI Lower	CI Upper	*p*
Consultant vs. resident	1.000	1.000	1.000	<0.001
Consultant vs. student	1.000	1.000	1.000	<0.001
Resident vs. student	1.000	1.000	1.000	<0.001
Digital measurements	**ICC**	**CI lower**	**CI upper**	*p*
Consultant vs. resident	1.000	1.000	1.000	<0.001
Consultant vs. student	1.000	1.000	1.000	<0.001
Resident vs. student	1.000	1.000	1.000	<0.001

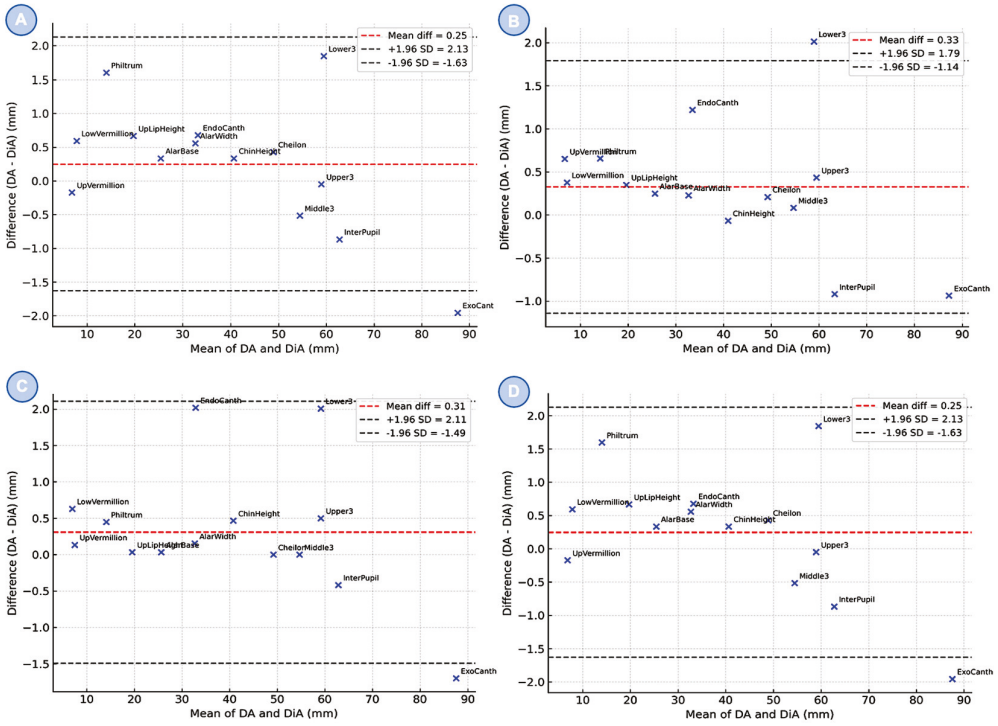

Figure 5. Bland–Altman plots comparing direct anthropometry (DA) and digital anthropometry (DiA) across three groups: (**A**) maxillofacial surgery consultant (MC), (**B**) maxillofacial surgery trainee (MT), (**C**) dental student (DS) and combined results (**D**). The red dashed line indicates the mean difference between methods, while the gray dashed lines represent the 95% limits of agreement (±1.96 SD). Each dot corresponds to a specific anatomical landmark.

4. Discussion

Stereophotogrammetry remains one of the most reliable and established modalities for 3D facial imaging [1,2]. Systems such as Vectra (Canfield Scientific), 3dMDface (3dMD), and

https://doi.org/10.3390/cmtr19010003

Di3D (Dimensional Imaging) acquire simultaneous images from multiple fixed cameras and reconstruct facial geometry through triangulation, offering high surface accuracy and suitability for a wide range of clinical applications [12,13]. Structured light scanning represents an alternative approach in which a projected pattern is distorted across the facial surface and captured by cameras to compute depth. Examples include the Artec Eva (Artec 3D), Bellus3D Face Camera Pro, and HP Structured Light Scanner. These systems are valued for their high resolution and are used in prosthodontics, surgical planning, and digital smile design.

The choice of imaging modality should be guided by clinical requirements, including resolution, workflow integration, patient comfort, and cost. Regardless of the system selected, rigorous validation is essential before clinical implementation.

The MetiSmile® handheld structured light scanner is a recent addition to this field. Several groups have investigated its performance. Bor et al. and Nuytens et al. demonstrated in vitro that MetiSmile® outperformed desktop and mobile scanners in both trueness (0.18 ± 0.15 mm) and precision (0.22 ± 0.04 mm), even surpassing repeated anthropometric caliper measurements [14,15]. A subsequent study by the same group confirmed that MetiSmile® achieved the highest mesh density and regional accuracy, particularly in perioral regions, although acquisition required longer than with stationary systems [16]. Kumar et al. validated the scanner in vivo, showing the lowest mean deviation compared with CBCT (0.35 ± 0.33 mm) and superior accuracy relative to Carestream and Medit scanners [17]. Together with the present study, these reports provide converging evidence that MetiSmile® consistently produces clinically acceptable—and often superior—results across diverse settings.

In the first phase of our study, reproducibility of meshes was confirmed across different lighting conditions. RMS values for artificial and natural light scans were almost identical (0.041 vs. 0.043 mm), indicating robustness to environmental variation. Restricting analysis to clinically relevant facial regions (AL-F meshes) further improved RMS values (0.030 mm) and reduced the deviation range by 41.6%. As in previous work, the largest errors occurred in anatomically complex regions such as the nasal base, eyelid margins, commissures, and periorbital areas (Figure 3) [18]. Compared with validated stereophotogrammetric and structured light systems, the MetiSmile® results were equal or better [4,19–24]. However, mannequin-based RMS values cannot be directly extrapolated to live patients, where skin texture, soft tissue elasticity, and movement introduce additional complexity.

The second phase compared DA and DiA. While most landmarks were generated automatically, several clinically relevant distances (e.g., alar base width, lip height) required manual placement, reducing efficiency and reproducibility. Landmarks were sometimes difficult to visualize on the mesh, and no strict protocol was used for their annotation. Establishing standardized protocols and implementing customizable measurement sets in the software would improve consistency and clinical utility. Despite these limitations, intra- and inter-observer ICCs were excellent ($\geq$0.997). Mean DA–DiA differences remained well below 1 mm, confirming clinical acceptability [1,25]. Only a few landmarks exceeded $\pm$2 mm, mainly at anatomically complex sites such as the exocanthion, cheilon, and philtrum height. These discrepancies are likely related to anatomy and landmark placement rather than scanner limitations, but they highlight the need for improved protocols and automated landmark detection.

The time efficiency of digital measurements remains unclear. Unlike caliper-based methods, digital analysis involves scanner calibration, acquisition, and annotation. Future studies should directly compare workflow efficiency, particularly since some dental parameters (e.g., overjet, incisor display) still require direct measurement. Importantly, ICCs in this study were likely strengthened by the use of pre-marked landmarks on the

https://doi.org/10.3390/cmtr19010003

mannequin, which may not fully extrapolate to clinical settings. Inter-observer variability in live patients should therefore be quantified in follow-up studies.

This study has several limitations that should be acknowledged. First, the use of a single standardized mannequin head inherently restricts the generalizability of the findings. This choice was deliberate, as working with one surrogate model allowed us to isolate measurement variability without introducing confounding morphological differences between specimens. Second, the anatomical landmarks were pre-marked on the mannequin head to ensure consistency across repeated measurements and to reduce landmark localization ambiguity. While we recognize that performing measurements on unmarked landmarks may better reflect real-world clinical practice, the controlled setup of this exploratory study enabled a focused and reliable comparison between direct and digital anthropometry. Future research should expand on this work by including multiple surrogate models and evaluating measurements based on unmarked anatomical landmarks to improve clinical applicability and external validity.

A strength of this work was the inclusion of multiple operators with varying expertise, yet excellent ICCs were maintained. This indicates robustness to user variation. However, a notable limitation is the exclusive use of a male mannequin head, which does not reflect sex-related differences in facial curvature and soft tissue distribution. Although current evidence suggests that scanner accuracy is unlikely to differ substantially between sexes, this limitation should be acknowledged. Furthermore, mannequin-based validation cannot account for patient-related factors such as motion, skin reflectivity, and heterogeneity in facial morphology.

Taken together, these considerations highlight the need for broader and more clinically oriented research. Several important avenues for future research arise from this work. Further studies are needed to evaluate newer 3D-scanning technologies, including stereophotogrammetry systems. In vivo validation on living subjects is also essential to account for soft-tissue dynamics, patient movement, and varying environmental conditions. Additionally, the role of proper calibration requires investigation, as inadequate calibration may introduce systematic errors. Research into inter- and intra-observer variability is equally important to quantify observer-dependent measurement differences. Such studies will provide crucial insight into potential sources of error. Together, these efforts will help improve the accuracy, precision, and reproducibility of facial measurements in orthognathic surgery.

5. Conclusions

In summary, this study adds to growing evidence that the MetiSmile® scanner is accurate, reproducible, and clinically acceptable. While mannequin studies cannot replace patient validation, our findings—combined with recent reports—support MetiSmile® as a reliable, cost-effective tool for orthodontic and orthognathic workflows. Future research should prioritize in vivo validation across diverse populations, both male and female, and explore integration with intraoral and CBCT data to move towards a validated and fully digital workflow. The development of automated landmark detection, standardized measurement protocols, and systematic evaluation of workflow efficiency will be essential for translating this technology into routine clinical practice.

Author Contributions: Conceptualization, A.D.C., C.B. and R.C.; methodology, A.D.C., C.B. and R.C.; software, A.D.C.; validation, A.D.C., C.B. and R.C.; formal analysis, A.D.C., C.B. and R.C.; investigation, A.D.C., C.B., F.P. and R.C.; resources, A.D.C., C.B. and R.C.; data curation, A.D.C., C.B. and R.C.; writing—original draft preparation, A.D.C., C.B. and R.C.; writing—review and editing, A.D.C., C.B., M.B. and R.C.; visualization, A.D.C., C.B., F.P., M.U., L.D.K., B.D., M.B., O.L. and R.C.;

https://doi.org/10.3390/cmtr19010003

supervision, M.B. and R.C.; project administration, C.B. and R.C. All authors have read and agreed to the published version of the manuscript.

Funding: This research received no external funding.

Institutional Review Board Statement: Ethical review and approval were waived for this study because it did not fall under the scope of medical research involving human subjects. The study involved non-invasive facial imaging and anthropometric measurements only, with no intervention or treatment, and all data were anonymized prior to analysis, and therefore did not require formal ethical approval under institutional and national regulations.

Informed Consent Statement: Informed consent was waived due to the use of fully anonymized data and the non-interventional nature of the study.

Data Availability Statement: The data presented in this study are available from the corresponding author upon reasonable request.

Conflicts of Interest: The authors declare no conflict of interest.

References

1. Liu, J.; Zhang, C.; Cai, R.; Yao, Y.; Zhao, Z.; Liao, W. Accuracy of 3-dimensional stereophotogrammetry: Comparison of the 3dMD and Bellus3D facial scanning systems with one another and with direct anthropometry. *Am. J. Orthod. Dentofac. Orthop.* **2021**, *160*, 862–871. [CrossRef] [PubMed]
2. Heike, C.; Upson, K.; Stuhaug, E.; Weinberg, S.; Heike, C.L.; Upson, K.; Stuhaug, E.; Weinberg, S.M. 3D digital stereophotogrammetry: A practical guide to facial image acquisition. *Head Face Med.* **2010**, *6*, 18. [CrossRef] [PubMed]
3. Naini, F.B.; Akram, S.; Kepinska, J.; Garagiola, U.; McDonald, F.; Wertheim, D. Validation of a new three-dimensional imaging system using comparative craniofacial anthropometry. *Maxillofac. Plast. Reconstr. Surg.* **2017**, *39*, 23. [CrossRef] [PubMed]
4. Gibelli, D.; Pucciarelli, V.; Cappella, A.; Dolci, C.; Sforza, C. Are Portable Stereophotogrammetric Devices Reliable in Facial Imaging? A Validation Study of VECTRA H1 Device. *J. Oral Maxillofac. Surg.* **2018**, *76*, 1772–1784. [CrossRef]
5. Dindaroğlu, F.; Kutlu, P.; Duran, G.S.; Görgülü, S.; Aslan, E. Accuracy and reliability of 3D stereophotogrammetry: A comparison to direct anthropometry and 2D photogrammetry. *Angle Orthod.* **2016**, *86*, 487–494. [CrossRef]
6. Piedra-Cascón, W.; Meyer, M.J.; Methani, M.M.; Revilla-León, M. Accuracy (trueness and precision) of a dual-structured light facial scanner and interexaminer reliability. *J. Prosthet. Dent.* **2020**, *124*, 567–574. [CrossRef]
7. Gerke, O. Reporting Standards for a Bland-Altman Agreement Analysis: A Review of Methodological Reviews. *Diagnostics* **2020**, *10*, 334. [CrossRef]
8. Koo, T.K.; Li, M.Y. A Guideline of Selecting and Reporting Intraclass Correlation Coefficients for Reliability Research. *J. Chiropr. Med.* **2016**, *15*, 155–163. [CrossRef]
9. Giavarina, D. Understanding Bland Altman analysis. *Biochem. Med.* **2015**, *25*, 141–151. [CrossRef]
10. Gwen, R.J.; Swennen, F.S.; Hausamen, J.-E. *Three-Dimensional Cephalometry—A Color Atlas and Manual*; Springer: Berlin/Heidelberg, Germany, 2006.
11. Girardeau-Montaut, D.; Raphaël Marc, M.R.; Thibault, G. *Change Detection on Point Cloud Data Acquired with a Ground Laser Scanner*; Thesis Telecom Paris; ISPRS: Enschede, The Netherlands, 2005.
12. Wong, J.Y.; Oh, A.K.; Ohta, E.; Hunt, A.T.; Rogers, G.F.; Mulliken, J.B.; Deutsch, C.K. Validity and reliability of craniofacial anthropometric measurement of 3D digital photogrammetric images. *Cleft Palate Craniofac. J.* **2008**, *45*, 232–239. [CrossRef]
13. Khambay, B.; Nairn, N.; Bell, A.; Miller, J.; Bowman, A.; Ayoub, A.F. Validation and reproducibility of a high-resolution three-dimensional facial imaging system. *Br. J. Oral Maxillofac. Surg.* **2008**, *46*, 27–32. [CrossRef] [PubMed]
14. Nuytens, P.; Vandeweghe, S.; D'Haese, R.; Ruggiero, G. Comparative evaluation of mesh density and 3D accuracy in stationary, handheld, and mobile facial scanning systems: An in vitro study. *J. Dent.* **2025**, *162*, 106029. [CrossRef] [PubMed]
15. Bor, S.; Oğuz, F.; Özdemir, D. Evaluation of trueness and precision of 3 face-scanning devices. *Am. J. Orthod. Dentofac. Orthop.* **2025**, *168*, 358–366.e1. [CrossRef] [PubMed]
16. Nuytens, P.; Ruggiero, G.; Vandeweghe, S.; D'Haese, R. Trueness and precision of a handheld, a desktop and a mobile 3D face scanning system: An in vitro study. *J. Dent.* **2025**, *155*, 105639. [CrossRef]
17. Kumar, L.; Maiti, S. Comparative evaluation of the accuracy of three different three-dimensional facial scanning systems: An observational crossover study. *J. Indian Prosthodont. Soc.* **2025**, *25*, 220–228. [CrossRef]
18. Secher, J.J.; Darvann, T.A.; Pinholt, E.M. Accuracy and reproducibility of the DAVID SLS−2 scanner in three-dimensional facial imaging. *J. Cranio-Maxillofac. Surg.* **2017**, *45*, 1662–1670. [CrossRef]

https://doi.org/10.3390/cmtr19010003

19. Wang, X.W.; Liu, Z.J.; Diao, J.; Zhao, Y.J.; Jiang, J.H. Morphologic reproducibility in 6 regions of the 3-dimensional facial models acquired by a standardized procedure: An in vivo study. *Am. J. Orthod. Dentofac. Orthop.* **2022**, *161*, e287–e295. [CrossRef]
20. Koban, K.C.; Perko, P.; Etzel, L.; Li, Z.; Schenck, T.L.; Giunta, R.E. Validation of two handheld devices against a non-portable three-dimensional surface scanner and assessment of potential use for intraoperative facial imaging. *J. Plast Reconstr. Aesthet. Surg.* **2020**, *73*, 141–148. [CrossRef]
21. Akan, B.; Akan, E.; Şahan, A.O.; Kalak, M. Evaluation of 3D Face-Scan images obtained by stereophotogrammetry and smartphone camera. *Int. Orthod.* **2021**, *19*, 669–678. [CrossRef]
22. Schipper, J.A.; Merema, B.J.; Hollander, M.H.; Spijkervet, F.K.; Dijkstra, P.U.; Jansma, J.; Schepers, R.H.; Kraeima, J. Reliability and validity of handheld structured light scanners and a static stereophotogrammetry system in facial three-dimensional surface imaging. *Sci. Rep.* **2024**, *14*, 8172. [CrossRef]
23. Andrews, J.; Alwafi, A.; Bichu, Y.; Pliska, B.; Mostafa, N.; Zou, B. Validation of three-dimensional facial imaging captured with smartphone-based photogrammetry application in comparison to stereophotogrammetry system. *Heliyon* **2023**, *9*, e15834. [CrossRef]
24. Barone, S.; Antonelli, A.; Salviati, M.; Greco, V.; Bennardo, F.; Becker, K.; Giudice, A.; Simeone, M. Accuracy Assessment of EM3D App-Based 3D Facial Scanning Compared to Cone Beam Computed Tomography. *Dent. J.* **2024**, *12*, 342. [CrossRef]
25. Knoops, P.G.; Beaumont, C.A.; Borghi, A.; Rodriguez-Florez, N.; Breakey, R.W.; Rodgers, W.; Angullia, F.; Jeelani, N.O.; Schievano, S.; Dunaway, D.J. Comparison of three-dimensional scanner systems for craniomaxillofacial imaging. *J. Plast Reconstr. Aesthet. Surg.* **2017**, *70*, 441–449. [CrossRef]

Disclaimer/Publisher's Note: The statements, opinions and data contained in all publications are solely those of the individual author(s) and contributor(s) and not of MDPI and/or the editor(s). MDPI and/or the editor(s) disclaim responsibility for any injury to people or property resulting from any ideas, methods, instructions or products referred to in the content.

https://doi.org/10.3390/cmtr19010003

craniomaxillofacial
trauma & reconstruction

MDPI

Article

Development of an Automatic Computer Program to Determine the Optimal Dental Implant Size and Position for Fibula Free Flap Surgery

Ming Yan Cheung [1], Ankit Nayak [1,2], Xing-Na Yu [1], Kar Yan Li [3], Yu-Xiong Su [1,*] and Jingya Jane Pu [1,*]

[1] Division of Oral and Maxillofacial Surgery, Faculty of Dentistry, The University of Hong Kong, 34 Hospital Road, Sai Ying Pun, Hong Kong, China; ccmy8@connect.hku.hk (M.Y.C.); ankitnayak42@gmail.com (A.N.); rinayu812@gmail.com (X.-N.Y.)
[2] School of Advance Engineering, UPES, Dehradun 248007, India
[3] Clinical Research Centre, Faculty of Dentistry, The University of Hong Kong, Hong Kong, China; skyli@hku.hk
* Correspondence: richsu@hku.hk (Y.-X.S.); drjanepu@hku.hk (J.J.P.); Tel.: +(852)-2859-0363 (J.J.P.)

Abstract: Computer-assisted surgery (CAS) and virtual surgical planning (VSP) have transformed jaw reconstruction, allowing immediate insertion of dental implants during surgery for better rehabilitation of occlusal function. However, traditional planning for optimal location and angulation of dental implants and fibula relies on experience and can be time-consuming. This study aimed to propose a function-driven workflow and develop an automatic computer program for optimal positioning of simultaneous dental implants and fibula segments. A customized computer program was developed using MATLAB. Computed tomography (CT) of the lower limbs of ninety-one Southern Chinese individuals was retrieved and cross-sections of three-dimensional (3D) fibula models were comprehensively investigated for implant installation. Our research proves that the accuracy of the program in identifying the anatomical orientation of the fibula was 92%. The ideal location, angulation and length of implant could be automatically generated based on any selected implant diameter, with a surgical feasibility of 94%. To the best of our knowledge, this is the first study to develop and validate a customized automatic computer program for osseointegrated implant design in fibula flap surgery. This program can be incorporated into the current workflow of CAS to further the development of reliable and efficient surgical planning for function-driven jaw reconstruction.

Keywords: computer-assisted surgery; Jaw reconstruction; fibula free flap; simultaneous dental implant; oral oncology; head and neck cancer; dental rehabilitation

1. Introduction

Defects of the maxilla and mandible as a result of tumor resection, trauma, bony necrosis after radiation, or anti-resorptive drugs often lead to significant aesthetic and functional deficits [1]. Hidalgo first described the use of a fibula free flap (FFF) in the maxillofacial region for mandibular reconstruction in 1989 [2]. FFF reconstruction with simultaneous dental implant placement has become a pivotal approach for the functional reconstruction of jaw defects following resection of benign or malignant tumors, allowing the functional rehabilitation of chewing, swallowing, speech, and aesthetics [3]. Conventional freehand mandibular reconstruction could be challenging and time-consuming as it greatly relies on the surgeon's experiences with 'trial and error' during the operation [4–6]. Positioning of fibula segments using the conventional approach could make dental implant placement

technically challenging or impossible. Computer-assisted surgery (CAS) and Virtual Surgical Planning (VSP) have transformed jaw reconstruction, enabling the immediate insertion of dental implants during surgery for improved rehabilitation of occlusal function [7–11]. Our center has previously proposed and adopted the novel "surgeon-dominated" approach to the design of 3D-printed patient-specific surgical plates [12]. Figure 1 demonstrates the current digital workflow at our center. The size of the selected implant depends on the height and width of available bone [13]. Although the fibula looks like a uniformly shaped long bone, determining the ideal implant position and angulation at the fibula segments during VSP could be time-consuming as its cross-sectional shape and dimension vary along its length [11,14]. 'Trial and error' and frequent switching between the planning software and CT scan were often needed to ensure that there would be enough bone surrounding the implant to optimize its stability and survival.

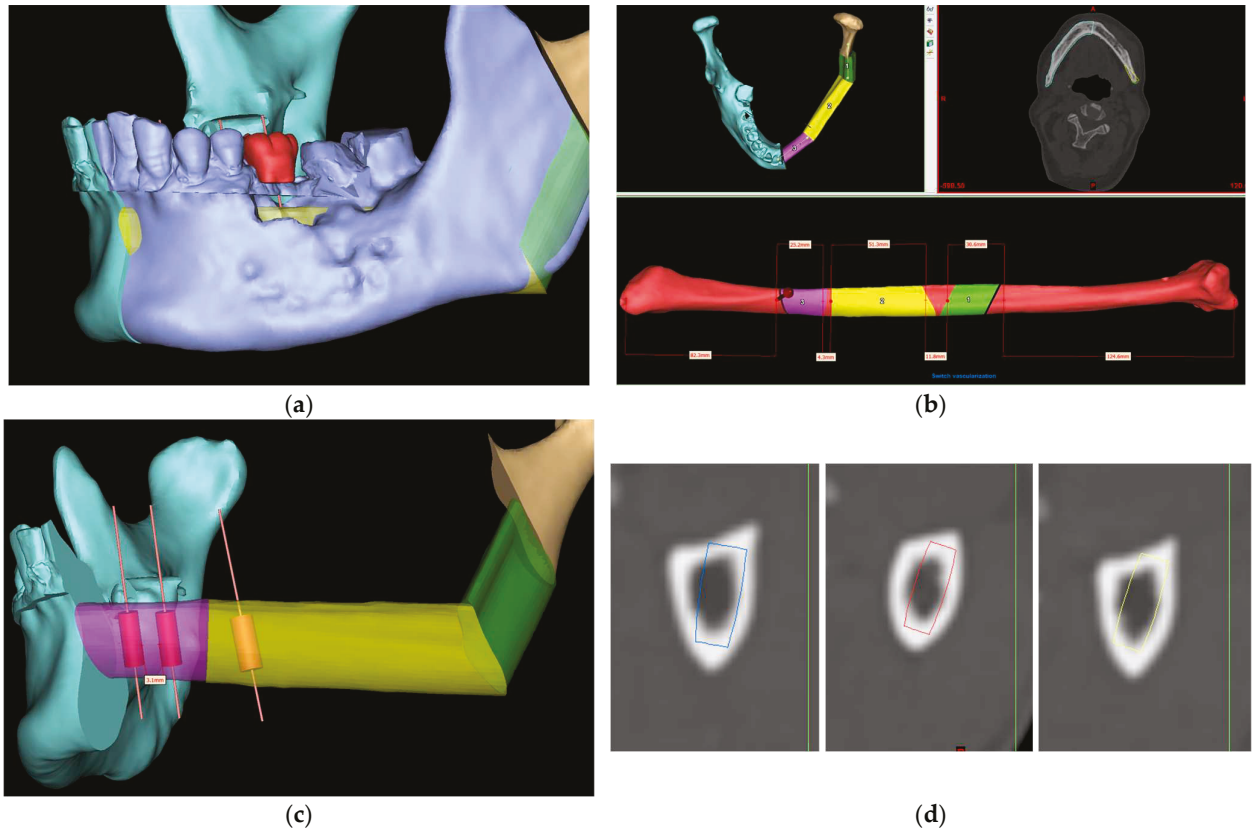

Figure 1. Computer-aided virtual surgical planning workflow: (**a**) CT data of the recipient jaw and donor fibula were segmented to construct the 3D models; (**b**) virtual reconstructive surgeries were conducted using ProPlan CMF 3.0 and the positions of fibula segments were optimized to provide an excellent contouring of defects; (**c**) implants were planned digitally on ideal positions based on the pre-existing dentition; and (**d**) implant positions were checked in the CT lower limbs to ensure bi-cortical engagement and no threads exposure.

Fibula free flap surgery with simultaneous dental implant placement is now routinely performed for functional jaw reconstruction in our center. However, additional time was needed for preoperative planning, especially in determining the orientation of dental implants and fibula segments to restore aesthetics and function after ablative surgery. To address this issue, a precise evaluation of bone dimensions and morphology is essential [15]. Previous cadaveric anatomical studies of the fibula have shown that the length of the harvested fibula and the bone available for implant placement vary between ethnicities [4,14,16–18]. And more recently, a CT scan-based analysis of fibula anatomy was carried out to find out the optimal site for implant installation in the fibula; however,

the sample size of 20 patients was small [19]. Another limitation of previous studies was that only a linear measurement was recorded from the anterior surface to the posterior aspect of the fibula cross-section, with little attention paid to the anatomical orientation, surgical feasibility, or width of the dental implant within the cross-section.

Although CAS showed increased intraoperative efficiency with a reduced total operative time, pre-operative computer planning could be time-consuming [4]. In the case of fibula implant planning, the process of choosing the appropriate implant dimension could be tedious as it often requires 'trial and error' to ensure good angulation of dental implants, bi-cortical engagement, and enough bony collar over the entire implant without any thread exposure, thereby improving its stability and survival. Existing commercial planning software (for example, Materialise ProPlan CMF 3.0 and Materialise Mimics Enlight CMF 7.0) is mainly designed for virtual surgical planning for jaw reconstruction rather than dental implant planning. Therefore, a fully automatic program is required to determine the optimal size and location of dental implants and fibula segments while respecting the anatomical considerations of a fibula free flap harvest. This will pave the way towards automatic placement of dental implants during VSP to provide a reliable and efficient solution for functional jaw reconstruction with a fibula free flap.

The aim of the current study is to describe the development and verification of an automatic program to determine the optimal size and angulation of simultaneous dental implants in functional jaw reconstruction of jaw defects with a fibula free flap.

2. Materials and Methods

2.1. Study Population

This study was approved by the Institutional Review Board of the University of Hong Kong/Hospital Authority of Hong Kong West Cluster (IRB: UW 24-121). Patients planned for fibula free flap jaw reconstruction in the Department of Oral and Maxillofacial Surgery, Queen Mary Hospital, Hong Kong, from January 2018 to February 2023 were retrospectively recruited. Ninety-one CT scans of the lower limbs were available and retrieved for analysis. CT angiography (CTA) of the lower extremity was taken on a General Electric Revolution System (GE Healthcare, Chicago, IL, USA) with a 1.25 mm thickness with bolus tracking at the popliteal artery at the arterial phase. The patients' demographic and clinical information were obtained from medical records.

Inclusion criteria included the following: (a) Chinese patients aged 18 years or above at the time of diagnosis; (b) patients diagnosed with oral and maxillofacial pathology from January 2018 to February 2023 and indicated for fibula free flap reconstruction with or without simultaneous implant rehabilitation; and (c) a CT scan of the lower limbs was performed and available for analysis.

Exclusion criteria included the following: (a) patients younger than 18 years old at the time of diagnosis; (b) ethnicity that was not Chinese; (c) fibula free flap was not required for the reconstruction of the defect after tumor resection; and (d) patients who were unable to undergo a preoperative CT scan of the lower limbs.

2.2. Image Processing for Measurements

The CTA of lower limbs were exported as Digital Imaging and Communications in Medicine (DICOM) file format, which were then imported into ProPlan CMF 3.0 software (Materialize, Leuven, Belgium). Images were segmented by radiodensity to rebuild the 3D virtual models of the fibula bone (CT threshold values: Min. 226; Max. 3071). The models were exported as stereolithography (STL) data and analyzed using a customized computer program created by our team, as described in detail below.

2.3. Customized Computer Program

2.3.1. Identifying the Anterior Aspect of the Fibula

MATLAB platform R2024a was used to develop and run the customized computer program. The computer program began by calculating the central axis of the bone. The bone was repositioned so that its lowest point was at the origin (0, 0, 0). The bone point cloud was aligned with the *z*-axis, maintaining the vertical orientation during slicing. The algorithm identified the anterior direction of the fibula using the most protruded part, which involved calculating the distance of each point from the central axis, identifying the furthest group of points, and computing their average vector to represent the anterior direction of the bone.

The anterior aspect of the 3D fibula model was indicated by a green arrow in Figure 2. Once the anterior vector was calculated, the bone point cloud was rotated to align the anterior vector along the *y*-axis (0, 1, 0), ensuring a consistent orientation of the anterior direction relative to the coordinate system. The threshold for defining the protrusion and the averaging method were determined after iterative testing on multiple fibula models to ensure consistent identification of the anterior vector.

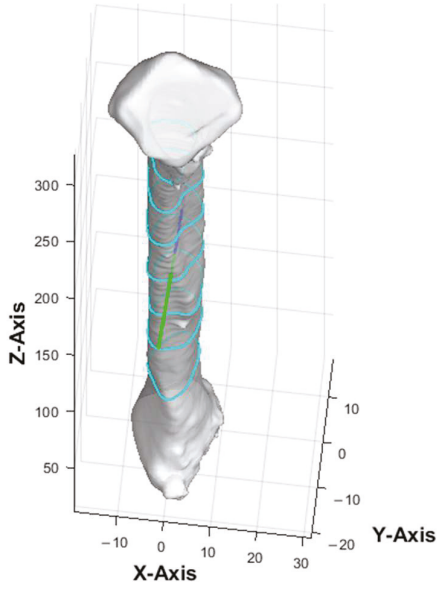

Figure 2. Three-dimensional model of fibula. The contour, as illustrated by the light blue lines, represented the cross-section of the fibula model at different slice heights. Green arrow represented the anterior aspect of fibula model.

2.3.2. Cross-Section of Fibula at Different Heights

The apex of the fibula head was denoted as point A, and that of the lateral malleolus was point I (Figure 3). The bone was then sliced at seven different heights. The 8 cm distances measured from the apex of the fibula head and that of the lateral malleolus were not generally used for harvesting to maintain the integrity of the knee and ankle [13,16]. These areas each correspond to approximately 20% at the top and bottom of the fibula length and were excluded from the analysis. The remaining 60% of the fibula length was divided into six equal segments to obtain the cross-section geometry along the fibula. Each of the dividing points from the apex of the fibula head was denoted B, C, D, E, F, G, and H as illustrated in Figure 3. This provided a detailed representation of the bone's structure at various heights, enabling a comprehensive understanding of its geometry and features. The number of segments and the distance between each layer were user-defined parameters.

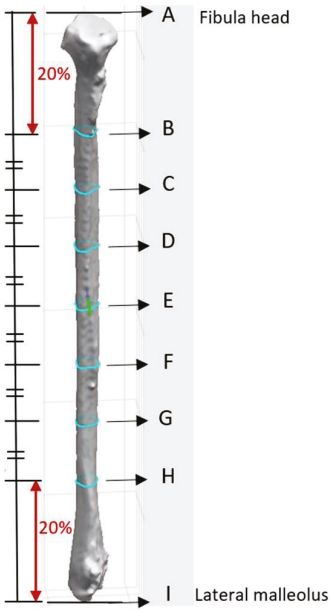

Figure 3. Position of the cross-section of the fibula bone model.

Four different-colored reference lines represented the outputs of four distinct algorithms, which helped differentiate their outputs and facilitate comparison and analysis of the results. Each algorithm and its contribution to the overall analysis of the bone geometry are detailed in the following sections:

Red line: A set of 100 equidistant gridlines was drawn parallel to the *y*-axis (anterior direction), as illustrated in Figure 4a. Among these gridlines, the one with the maximum length was identified as the central axis of the red rectangle.

Green line: The algorithm calculated the geometric center point of the contour and drew a vertical line through this center point, parallel to the *y*-axis, as illustrated in Figure 4b. Since the anterior direction is aligned to the *y*-axis (as described in Section 2.3.1), the vertical line that is parallel to the *y*-axis represents the thickness of the bone in the anterior direction.

Blue line: It computed the average position of all vertices in the contour and drew lines from each point situated on the contour's boundary that pass through the contour's average position (geometric center) and end on the opposite side of the average point, as illustrated in Figure 4c.

Black line: In this algorithm, the blue line served as a reference line and was continuously rotated around its midpoint, which referred to the middle of the line itself rather than the center of the entire contour. The rotation was performed in 1° increments, and each orientation was analyzed to determine the configuration that generated the largest possible rectangle of a predetermined fixed width within the polygon. The 1° step size was selected following pilot testing with increments ranging from 0.5° to 5°, where it offered the best balance between accuracy and computational efficiency. This parameter remains user-adjustable, allowing flexibility in defining the rotation resolution. The line with the optimal orientation was then used to construct the final rectangle, as illustrated in Figure 4d.

Cross-sections at the potential harvesting sites (points B to H) were then analyzed, alongside the generation of red, green, blue, and black reference lines (Figure 5).

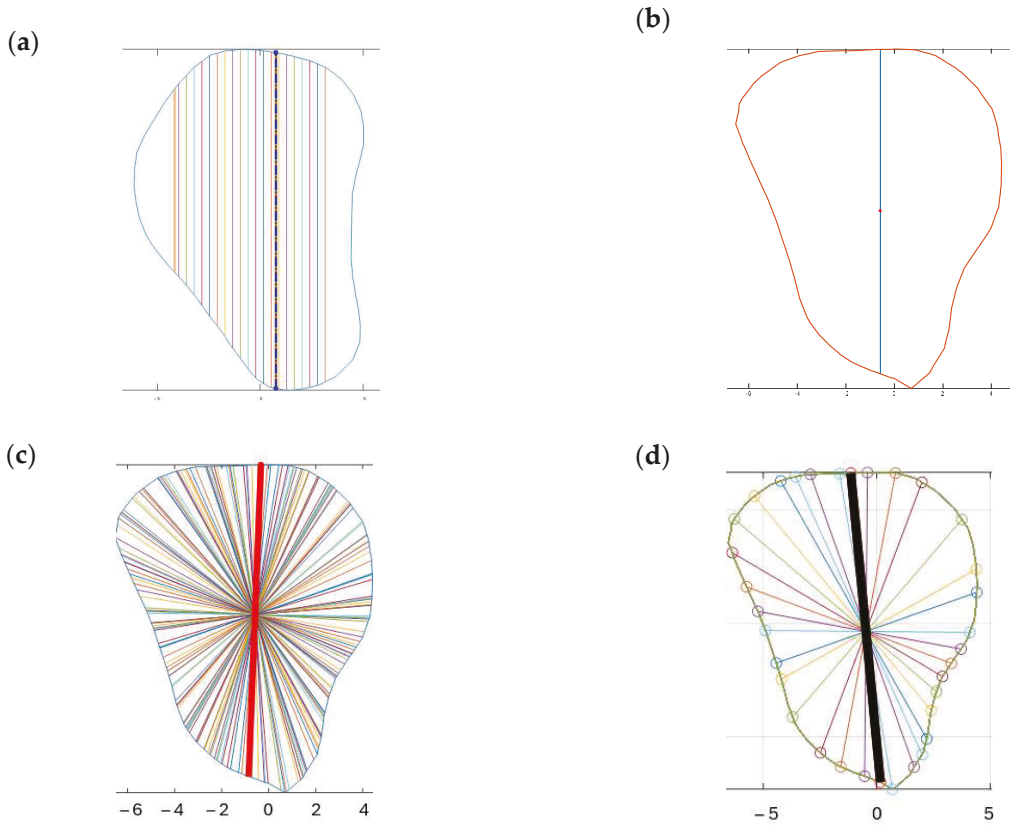

Figure 4. Algorithm for references lines: (**a**) algorithm for red line—grid line with the maximum length; (**b**) algorithm for green line—demonstrating a vertical line that passes through the geometric center of the contour; (**c**) algorithm for blue line—the longest line was highlighted among the different lines that pass through the geometric center of the contour; (**d**) algorithm for black line—blue line was rotated around its midpoint at constant intervals, the highlighted line in black was the identified line for drawing the rectangle.

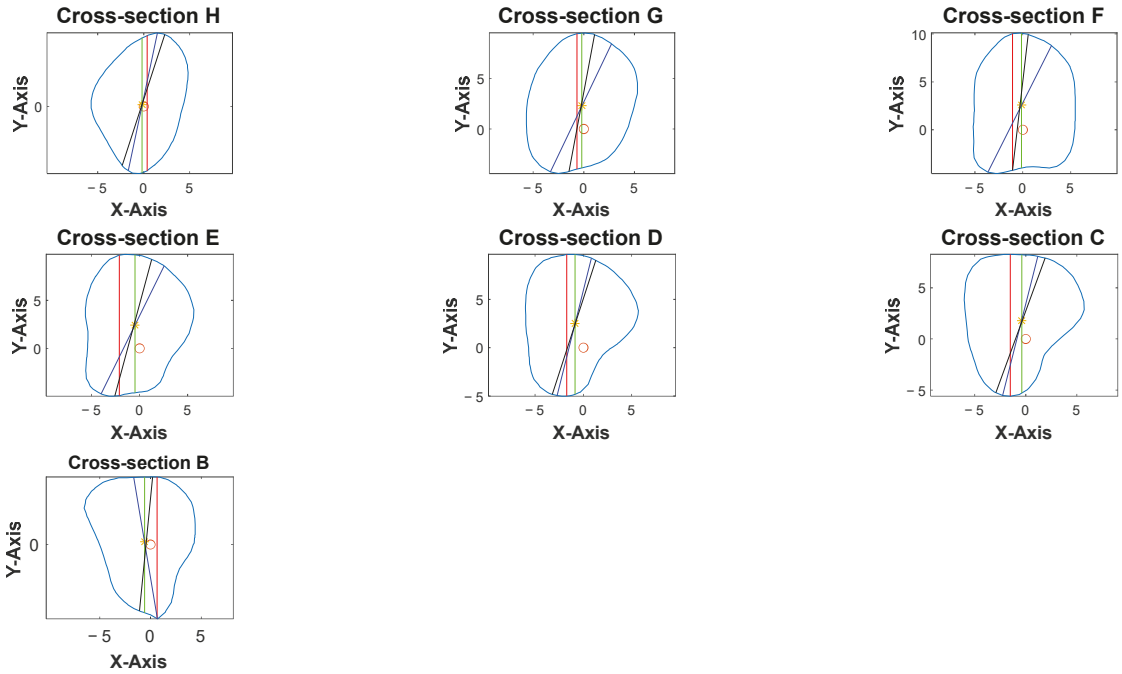

Figure 5. Software interface demonstrating the seven fibula cross-sections with four reference lines. Blue contour represented the outline of each cross-section from point B to H. The *X*-axis represented the anterior aspect of the fibula.

2.3.3. Rectangle Plot

Based on the coordinates of the four reference lines and a user-defined value for the width of the rectangle, four colored rectangle plots would be automatically generated using the corresponding algorithms. Each rectangle represented the greatest dimension of dental implants with the proposed angulation.

2.4. Clinical Considerations

2.4.1. Implant Systems

At our center, the standard dental implant system used for functional jaw reconstruction is the Nobel Parallel Conical Connection TiUltra (Nobel BioCare AB, Göteborg, Sweden). The implant dimensions commonly used were narrow (Ø3.75 mm) and regular (Ø4.3 mm) platforms, with a length of 8.5 mm, 10 mm, 11.5 mm, and 13 mm. However, this number could be easily adjusted in the program with a different implant system. The width of the rectangle represented the user-defined implant diameter with an additional 1.0 mm bony collar included on both sides of the implant (lateral and medial aspects) to ensure no implant thread exposure through the bone [18–20]. Hence, the widths of rectangles for regular and narrow implants were 6.3 mm and 5.75 mm, respectively (Figure 6). This was used as the input value to allow the program to automatically generate the four colored rectangles and calculate the optimal angulation and maximum implant length at sections B, C, D, E, F, G, and H (Figure 7).

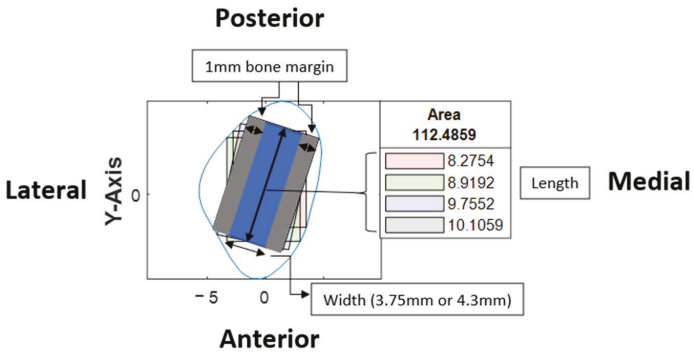

Figure 6. Illustration of rectangles within a cross-section and the orientation of the cross-section.

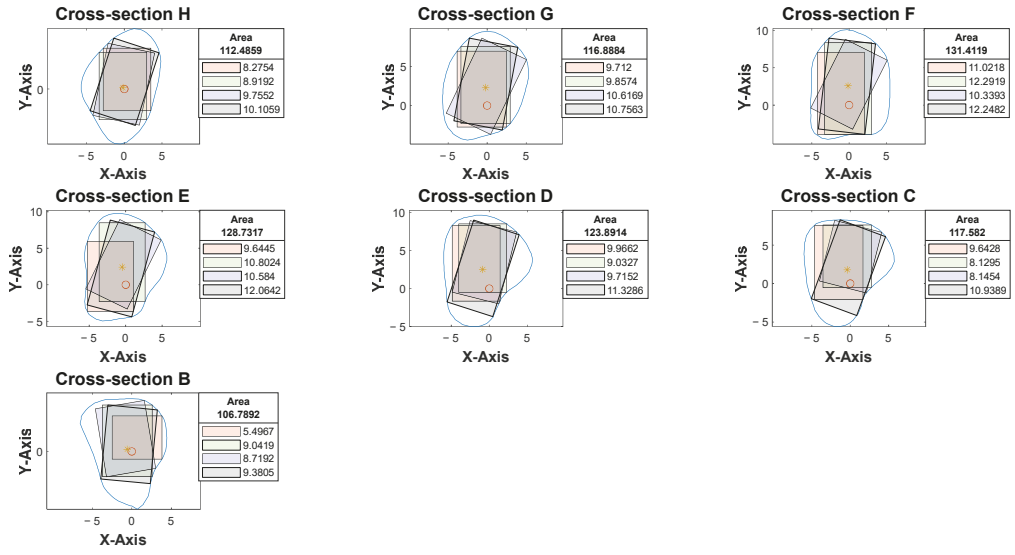

Figure 7. Software interface demonstrating cross-section of fibula segments and four colored rectangles, each representing the different angulation and implant length generated by the four distinct algorithms. The length of each rectangle was automatically generated and shown in the textbox.

2.4.2. Anatomical Considerations for the Fibula Free Flap

The length of the rectangle corresponded to the maximal length of implant possible at each cross-section, with consideration of the surgical feasibility (i.e., from the anterior or lateral aspect of the fibula to the posterior border) and avoidance of the postero-medial portion to prevent interruption to the blood supply from the pedicle.

2.5. Workflow

With the use of MATLAB software R2024a, STL files of the fibula model were imported and analyzed automatically by the program. Each STL file would generate three popup windows, including the 3D bone model (Figure 2), cross-sections with four colored reference lines (Figure 5), as well as the cross-sections with four colored rectangles at seven different heights representing the ideal angulation and length of dental implant for each algorithm (Figure 7). A spreadsheet file would be generated automatically to allow direct observation and comparison of the maximum length of rectangles.

The orientation of fibula bone models was verified by two assessors (M.Y.C. and X.-N.Y.) to evaluate the accuracy level of the program in identifying the anterior edge of the fibula, as this determines the correct insertion angle of the dental implants. The two assessors would then go through the cross-section analysis for each bone model to verify the anatomical considerations of implant insertion in a fibula free flap and select the rectangle with the greatest length. The inter-rater reliability was assessed for each measurement. A third assessor was involved when the discrepancies were out of range.

2.6. Statistical Analysis

Statistical analysis was performed using IBM SPSS Statistics Version 28. The two-way random intraclass correlation coefficient was used to determine the level of agreement between two raters when determining the orientation of the fibula and analyzing the best angulation and dimension of the implant at each cross-section.

3. Results

3.1. Patient's Demographic Background

The demographic data and disease characteristics of patients are presented in Table 1. Of the 91 Chinese patients recruited, 52 (57%) were male and 39 (43%) were female. Patients' ages ranged from 20 to 86 years, with a mean of 58.4 ± 16.7 years. No significant age difference was found between genders (p = 0.882). The majority of the lesions were found in the mandible (77%) and were malignant in nature (68%).

Table 1. Patient demographics and reconstruction characteristics.

Characteristic	Male (n = 52)	Female (n = 39)	p Value
Age (mean)	**58.6 ± 17.7**	**58.2 ± 15.4**	**0.882** [b]
Lesion type			
Benign	21.2% (11/52)	25.6% (10/39)	0.857 [c]
Malignant	69.2% (36/52)	66.7% (26/39)	
Others [a]	9.6% (5/52)	7.7% (3/39)	
Defect site			
Maxilla	19.2% (10/52)	28.2% (11/39)	0.315 [c]
Mandible	80.8% (42/52)	71.8% (28/39)	

[a] Others included secondary reconstruction and osteoradionecrosis; [b] This p-value was calculated by means of the Mann–Whitney U test; [c] This p-value was calculated by means of the chi-square test.

3.2. Program Accuracy

The accuracy level in identifying the orientation and anterior edge of the fibula model was verified before proceeding with cross-sectional analysis. After multiple rounds of optimization of the computer program with human verification, no to minimal manual adjustments were required in orienting the fibula models in the current software version. With the most protruded part method as described earlier, the anterior surface of the lateral malleolus, as highlighted in red in Figure 8, was found to be a reliable benchmark for identifying the inferior and anterior direction of the fibula model. Among the four colored rectangles, the black rectangle demonstrated the maximum length with surgical feasibility in 94% of the cross-sections (Table 2).

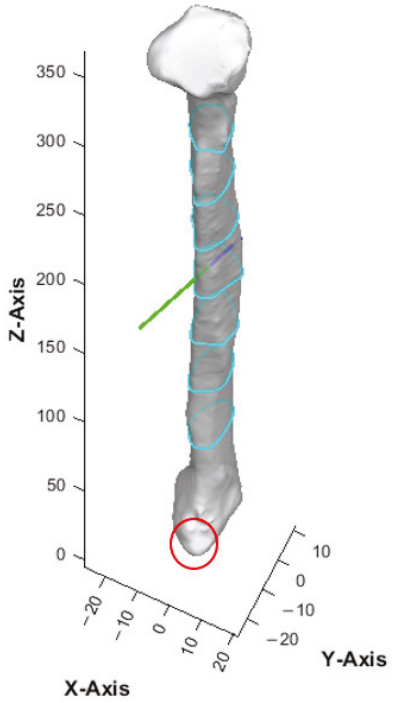

Figure 8. Surface model of fibula bone. The anterior surface of lateral malleolus is circled in red. The green and dark blue lines represented the anterior and posterior aspects of the fibula model respectively.

Table 2. Algorithm selected in fibula cross-sections.

Rectangles Generated by Algorithm	Number of Cross-Sections
Black	94% (1195/1274)
Green	3% (41/1274)
Red	2% (22/1274)
Blue	1% (16/1274)

3.3. Inter-Rater Agreement Measures

A second assessor (X.-N.Y.) conducted the same analysis independently using the customized computer program. Inter-rater agreement was assessed on all STL bone models. The intraclass correlation coefficient was 0.963 with a 95% confidence interval, indicating that the level of agreement and consistency between the two raters when analyzing the best angulation and dimension of the implant at each cross-section was excellent. Among 1274 cross-sections, a different colored rectangle was chosen between the raters in 107 cross-sections (8%) when considering both the maximum possible length of implants and surgical feasibility. Table 3 lists the number of measurements that were not in agree-

ment concerning the location of the cross-section. Cross-section B-C, D-F, G-H correspond to the proximal, middle and distal segments respectively. More discrepancy (52%) was noted towards the proximal end of the fibula, where a more irregular contour was likely to be observed (Figure 9). 48% of the discrepancies had a difference of less than 1.0 mm (as listed in Supplementary Material, Table S1). 79% (85/107) of the disagreements were due to different preferences when determining the ideal implant angulation. Both measurements were surgically feasible; however, one may prefer to insert the implant from the anterior aspect of the fibula (as shown by the black rectangle in Figure 10) and the other from a relatively more lateral aspect (as indicated by the blue rectangle in Figure 10). For the remaining 21% (22/107) of the cases, one may consider that it remains surgically feasible when a small portion of the rectangle (<1.0 mm) exceeded the contour of the cross-section (Figure 11).

Table 3. Number of measurements not in agreement between raters.

		Cross-Section						
		B	**C**	**D**	**E**	**F**	**G**	**H**
Female	5.75 mm	4	2	**4**	**1**	**4**	3	1
	6.3 mm	6	7	**8**	**3**	**3**	5	1
Male	5.75 mm	13	6	**3**	**3**	**2**	0	1
	6.3 mm	15	2	**5**	**3**	**0**	1	1
Total		38	17	**20**	**10**	**9**	9	4
Percentage		36	16	**19**	**9**	**8**	8	4

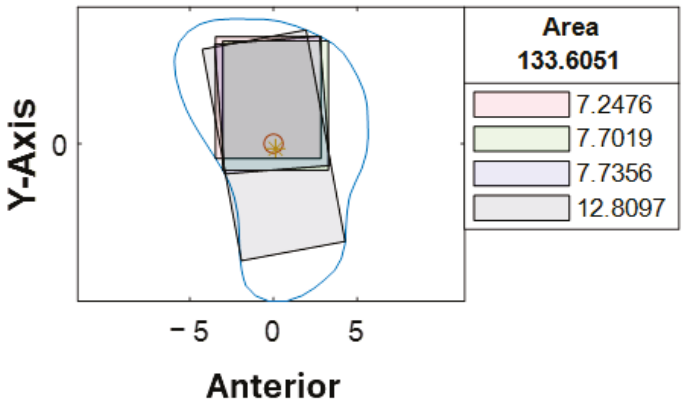

Figure 9. Example of irregular fibula cross-section.

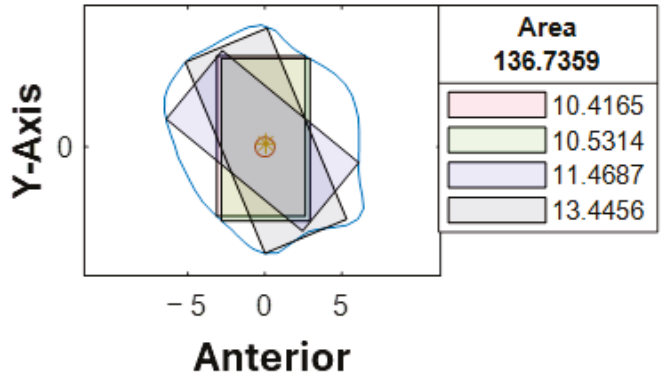

Figure 10. Different implant angulations.

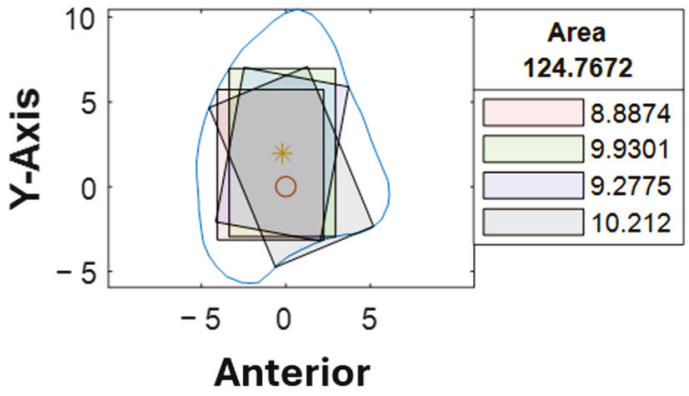

Figure 11. Black rectangle out of contour.

Among the disagreements, 7% of the differences (7/107) were out-of-range based on 95% limits of agreement (as highlighted in Table S1). The location of the fibula segment with the out-of-range differences was recorded, and almost all of those were located towards the proximal end of the fibula (Table S1). A third assessor (J.J.P.) was invited for the assessment. For 5 of them, the black rectangles presented with a slightly insufficient bony collar due to the concave shape of the fibula bone (Figure 9). The surgical feasibility was confirmed by the third assessor. For the other two cases, the cross-section of the fibula presented with a significantly bigger dimension in the mediolateral dimension than in the anteroposterior dimension. The shorter implants were selected for anatomical safety.

4. Discussion

Fibula free flap with simultaneous dental implant placement is now routinely performed for functional jaw reconstruction in our center. However, additional time was needed for preoperative planning, especially in determining the orientation of dental implants and fibula segments, to restore aesthetics and function after ablative surgery. To the best of our knowledge, this is the first study to determine the optimal size and angulation of dental implants using an automatic computer program, while incorporating surgical considerations when harvesting a fibula free flap for jaw reconstruction.

To ensure surgical feasibility, the anterior aspect of the fibula was automatically identified using the program developed, hence the direction of implant installation. Our research has proved that the accuracy and reproducibility of the program in identifying the anterior surface of the fibula were as high as 92%. The ideal location, angulation, and maximum length of implant could be automatically generated based on the selected implant diameter. In addition, the implants' ideal position according to prosthetic considerations predetermines the position of the fibula segments for bony reconstruction [19]. This is an important step towards automatic function-driven fibula reconstruction of the jaw.

In the current study, the specific algorithm for generating the black rectangle proved to be the most effective in representing the ideal angulation with maximum implant length and surgical feasibility in 94% of the cases studied. Based on this significant finding, further efforts could be made to streamline and improve this specific algorithm, aiming to convert implant selection and planning into a fully automated procedure that requires minimal manual adjustments. At the same time, the computer coding could be easily edited to remove the other three algorithms to allow a more focused interpretation using the black algorithm. The automated program could potentially reduce virtual implant planning time, especially in complex cases [21]. To the best of our knowledge, there is no similar automated function in currently available commercial virtual surgical planning software yet.

The inter-rater agreement of 0.963 indicated that rater-related variance and random error were minimal, meaning the raters' measurements were nearly identical across most

cases. It demonstrated that the computer program was user-friendly and could be relied upon to pre-determine the ideal implant angulation based on cross-sectional analysis. Although disagreements (8%) were present between the raters, and 7% of them were out of range, these contributed to 0.5% of all the cross-sections analyzed. The third rater was involved when the discrepancies between the first and second raters were out of range; the results were in line with the first rater. According to our observations, the proximal end of the fibula tends to have a more irregular or triangular cross-sectional shape. Therefore, most of the discrepancies were noted towards the proximal segments, where a slight difference in implant angulation could result in a greater difference in maximum implant length (Figure 9).

We concluded that there were two main reasons for the discrepancies. Different surgeons might have different preferences for ideal implant angulation (Figure 10). One might prefer to insert from the anterior or lateral aspects of the fibula to maximize the possible implant length, while both are surgically acceptable. Secondly, there might be a different opinion on the concept of surgical feasibility [13]. A small portion of the rectangle (<1.0 mm) exceeding the contour of the cross-section might be considered to be surgically acceptable, as the final implant length was determined by subtracting a 1.0 mm bony collar at the apical portion from the maximum length of the rectangle [18]. Furthermore, when referring to the actual clinical application, a smaller implant diameter could be considered in the above scenario to avoid possible implant thread exposure. Implant placement might be avoided in areas with irregular cross-sectional shapes. The cross-sectional analysis allowed clinicians to have a better understanding of the fibula morphology, hence identifying the best segment for implant placement. When the program produces a result as illustrated in Figure 9, this may help to alert the surgeon, and further evaluation should be carried out, as those segments might not be suitable for implant placement. This is why an automated computer program specifically designed for implant planning would be beneficial in VSP for fibula reconstruction.

As with all computer programs or software, regular updates are required to further improve the computer coding and its functionality. This is particularly important when the program is applied to a larger study population, as it would likely require updates to accommodate the anatomical variations in the population for a more reliable and accurate analysis. With significant advances in artificial intelligence and machine learning, this technology can be further integrated into the workflow of automatic virtual surgical planning for functional jaw reconstruction.

Regarding the study limitations, apart from its retrospective nature, switching between different software might be necessary during VSP. Current commercial software is not open source and therefore not available for the integration of third-party developer programming. We recommend using this customized computer program to first analyze the fibula morphology and identify the ideal fibula segments for implant placement before proceeding with the routine VSP with commercial software. To improve clinical integration of the program, the aim is to develop CAS planning software that incorporates the algorithm for implant planning. This is a major step towards a fully integrated automatic surgical planning platform. On the other hand, although the computer program worked for the majority of the cases (92%), for fibula with irregular morphology, especially towards the proximal end, greater differences in maximum possible implant length generated by the algorithms were noted, hence resulting in out-of-range differences in the very limited number of extreme cases. In actual clinical situations, these areas might not be ideal for implant planning. In most of our cases, the proximal end of the fibula was often discarded for the pedicle length. This automatic program currently acts as an aid in analyzing the fibula cross-section with the consideration of the ideal dimension and angulation of dental

implants. Surgeons should make the final clinical decision to ensure intraoperative safety, especially in those extreme cases.

The current study mainly focused on the development and streamlining of the program; clinical validation would be an outcome for future studies. Further prospective clinical studies incorporating this customized computer program are needed to validate the protocol. On the other hand, clinical feasibility or accuracy could be validated by using existing VSP software pre-operatively to check whether the planned implant location with the program could be safely performed during the surgery.

5. Conclusions

This current study describes the development and verification of an automated program to determine the optimal size and angulation of dental implants in functional jaw reconstruction using a fibula free flap. This customized automatic computer program is readily available. It can be incorporated into the current guided implant design workflow to advance developments in function-driven fibula reconstruction of the jaw. Further prospective clinical studies are warranted to validate the clinical performance of the program. This will pave the way towards automatic placement of dental implants during VSP to provide a reliable and efficient solution for functional jaw reconstruction in fibula free flap surgery.

6. Patents

Title of invention: Method and system for automatic identification of a dental implant position on a bone. US 63/754,065. Filing date: 5 Feb 2025.

Supplementary Materials: The following supporting information can be downloaded at https://www.mdpi.com/article/10.3390/cmtr18040046/s1. Table S1: Table showing the differences in measurements between raters.

Author Contributions: Conceptualization, M.Y.C., A.N., Y.-X.S. and J.J.P.; methodology, M.Y.C., A.N., Y.-X.S. and J.J.P.; software, M.Y.C. and A.N.; validation, M.Y.C.; formal analysis, M.Y.C. and X.-N.Y.; investigation, M.Y.C. and X.-N.Y.; data curation, M.Y.C. and K.Y.L.; writing—original draft preparation, M.Y.C. and J.J.P.; writing—review and editing, M.Y.C., Y.-X.S. and J.J.P.; visualization, M.Y.C.; supervision, Y.-X.S. and J.J.P.; funding acquisition, Y.-X.S. All authors have read and agreed to the published version of the manuscript.

Funding: This research was funded by the General Research Fund, Research Grants Council (No. 17114722) and Health and Medical Research Fund (No. 08192096), Health Bureau, Hong Kong.

Institutional Review Board Statement: This study was approved by the Institutional Review Board of the University of Hong Kong/Hospital Authority of Hong Kong West Cluster (IRB: UW 24-121; 13 March 2024).

Informed Consent Statement: Patient consent was waived due to the retrospective nature of the study.

Data Availability Statement: The original data presented in the study are openly available in FigShare at DOI 10.6084/m9.figshare.29413136.

Conflicts of Interest: The authors declare no conflicts of interest.

Abbreviations

The following abbreviations are used in this manuscript:

CAS	Computer-assisted surgery
CT	Computer tomography
CTA	Computer tomography angiography
DICOM	Digital Imaging and Communications in Medicine
FFF	Fibula free flap
STL	Stereolithography
VSP	Virtual surgical planning
3D	Three-dimensional
Ø	Diameter

References

1. Weitz, J.; Bauer, F.J.M.; Hapfelmeier, A.; Rohleder, N.H.; Wolff, K.D.; Kesting, M.R. Accuracy of mandibular reconstruction by three-dimensional guided vascularised fibular free flap after segmental mandibulectomy. *Br. J. Oral Maxillofac. Surg.* **2016**, *54*, 506–510. [CrossRef] [PubMed]
2. Hidalgo, D.A. Fibula free flap: A new method of mandible reconstruction. *Plast. Reconstr. Surg.* **1989**, *84*, 71–79. [CrossRef] [PubMed]
3. Su, Y.R.; Ganry, L.; Ozturk, C.; Lohman, R.; Al Afif, A.; McSpadden, R.; Frias, V.; Pu, J.J. Fibula Flap Reconstruction for the Mandible: Why It Is Still the Workhorse? *Atlas Oral Maxillofac. Surg. Clin. N. Am.* **2023**, *31*, 121–127. [CrossRef] [PubMed]
4. Powcharoen, W.; Yang, W.F.; Li, K.Y.; Zhu, W.; Su, Y.X. Computer-Assisted versus Conventional Freehand Mandibular Reconstruction with Fibula Free Flap: A Systematic Review and Meta-Analysis. *Plast. Reconstr. Surg.* **2019**, *144*, 1417–1428. [CrossRef]
5. Pu, J.J.; Hakim, S.G.; Melville, J.C.; Su, Y.X. Current Trends in the Reconstruction and Rehabilitation of Jaw following Ablative Surgery. *Cancers* **2022**, *14*, 3308. [CrossRef]
6. Pu, J.J.; Choi, W.S.; Yang, W.F.; Zhu, W.Y.; Su, Y.X. Unexpected Change of Surgical Plans and Contingency Strategies in Computer-Assisted Free Flap Jaw Reconstruction: Lessons Learned From 98 Consecutive Cases. *Front. Oncol.* **2022**, *12*, 746952. [CrossRef]
7. Zhu, W.Y.; Su, Y.X.; Pow, E.H.N.; Yang, W.F.; Qin, L.; Choi, W.S. "Three-in-one" patient-specific surgical guides for simultaneous dental implants in fibula flap jaw reconstruction: A prospective case series. *Clin. Implant Dent. Relat. Res.* **2021**, *23*, 43–53. [CrossRef]
8. Pu, J.J.; Lo, A.W.; Wong, M.C.; Choi, W.S.; Ho, G.; Yang, W.F.; Su, Y.X. A quantitative comparison of bone resection margin distances in virtual surgical planning versus histopathology: A prospective study. *Int. J. Surg.* **2024**, *110*, 111–118. [CrossRef]
9. Pu, J.J.; Choi, W.S.; Yu, P.; Wong, M.C.M.; Lo, A.W.; Su, Y.X. Do predetermined surgical margins compromise oncological safety in computer-assisted head and neck reconstruction? *Oral Oncol.* **2020**, *111*, 104914. [CrossRef]
10. Liu, R.; Su, Y.; Pu, J.; Zhang, C.; Yang, W. Cutting-edge patient-specific surgical plates for computer-assisted mandibular reconstruction: The art of matching structures and holes in precise surgery. *Front. Surg.* **2023**, *10*, 1132669. [CrossRef]
11. Pu, J.J.; Choi, W.S.; Yeung, W.K.; Yang, W.F.; Zhu, W.Y.; Su, Y.X. A Comparative Study on a Novel Fibula Malleolus Cap to Increase the Accuracy of Oncologic Jaw Reconstruction. *Front. Oncol.* **2021**, *11*, 743389. [CrossRef]
12. Yang, W.F.; Zhang, C.Y.; Choi, W.S.; Zhu, W.Y.; Li, D.T.S.; Chen, X.S.; Du, R.; Su, Y.X. A novel 'surgeon-dominated' approach to the design of 3D-printed patient-specific surgical plates in mandibular reconstruction: A proof-of-concept study. *Int. J. Oral. Maxillofac. Surg.* **2020**, *49*, 13–21. [CrossRef]
13. Apinhasmit, W.; Sinpitaksakul, P.; Chompoopong, S. Anatomical considerations of the Thai fibula used as a fibula osteocutaneous free flap in mandibular reconstruction and dental implant placement. *J. Med. Assoc. Thai.* **2012**, *95*, 561–568.
14. Matsuura, M.; Ohno, K.; Michi, K.I.; Egawa, K.; Takiguchi, R. Clinicoanatomic examination of the fibula: Anatomic basis for dental implant placement. *Int. J. Oral Maxillofac. Implants* **1999**, *14*, 879–884.
15. Cavalcanti, M.G.; Yang, J.; Ruprecht, A.; Vannier, M.W. Validation of spiral computed tomography for dental implants. *Dentomaxillofac. Radiol.* **1998**, *27*, 329–333. [CrossRef]
16. Choi, S.W.; Kim, H.J.; Koh, K.S.; Chung, I.H.; Cha, I.H. Topographical anatomy of the fibula and peroneal artery in Koreans. *Int. J. Oral Maxillofac. Surg.* **2001**, *30*, 329–332. [CrossRef]
17. Zlotolow, I.M.; Huryn, J.M.; Piro, J.D.; Lenchewski, E.; Hidalgo, D.A. Osseointegrated implants and functional prosthetic rehabilitation in microvascular fibula free flap reconstructed mandibles. *Am. J. Surg.* **1992**, *164*, 677–681. [CrossRef] [PubMed]

18. Klesper, B.; Wahn, J.; Koebke, J. Comparisons of bone volumes and densities relating to osseointegrated implants in microvascularly reconstructed mandibles: A study of cadaveric radius and fibula bones. *J. Craniomaxillofac. Surg.* **2000**, *28*, 110–115. [CrossRef] [PubMed]
19. Ide, Y.; Matsunaga, S.; Harris, J.; Connell, D.O.; Seikaly, H.; Wolfaardt, J. Anatomical examination of the fibula: Digital imaging study for osseointegrated implant installation. *J. Otolaryngol. Head Neck Surg.* **2015**, *44*, 1. [CrossRef] [PubMed]
20. Frodel, J.L., Jr.; Funk, G.F.; Capper, D.T.; Fridrich, K.L.; Blumer, J.R.; Haller, J.R.; Hoffman, H.T. Osseointegrated implants: A comparative study of bone thickness in four vascularized bone flaps. *Plast. Reconstr. Surg.* **1993**, *92*, 449–455; discussion 456–458. [CrossRef]
21. Pu, J.J.; Yu, X.; Pow, E.H.; Lam, W.Y.; Su, Y.X. Single-Double-Single Barrel (1-2-1) Fibula Free Flap Design for Functional and Aesthetic Brown Class III Mandibular Reconstruction. *Plast. Reconstr. Surg.* **2025**, *156*, 407e–411e. [CrossRef]

Disclaimer/Publisher's Note: The statements, opinions and data contained in all publications are solely those of the individual author(s) and contributor(s) and not of MDPI and/or the editor(s). MDPI and/or the editor(s) disclaim responsibility for any injury to people or property resulting from any ideas, methods, instructions or products referred to in the content.

craniomaxillofacial
trauma & reconstruction

MDPI

Article

Integrative Innovation in Genioplasty: Advanced 3D Plate Design: Promoting Stability, Aesthetics, and Harmony Excellence

Bruno Nifossi Prado [1,2], Lucas Cavalieri Pereira [2], Bianca Pulino [1,3,*] and Raphael Capelli Guerra [1,3,4,*]

[1] Hospital Sírio-Libanês, Instituto de Ensino e Pesquisa, São Paulo 01308-050, Brazil; brunoprado8@gmail.com
[2] Oral & Maxillofacial Surgery, São Leopoldo Mandic University, Campinas 13045-755, Brazil; dr.lucasmaxilofacial@hotmail.com
[3] Department of Oral and Maxillofacial Surgery, Hospital Israelita Albert Einstein, São Paulo 05652-900, Brazil
[4] Faculdade Israelita de Ciências da Saúde Albert Einstein, São Paulo 05652-900, Brazil
* Correspondence: biancapulino@icloud.com (B.P.); dr.raphael.guerra@gmail.com (R.C.G.)

Abstract: Background: Genioplasty is a well-established surgical technique for reshaping the chin and enhancing facial harmony. However, conventional fixation methods may present biomechanical and aesthetic limitations. Objective: This study introduces and evaluates a novel Anatomical Chin Plate (ACP), designed to enhance mechanical performance and facial aesthetics compared to the conventional chin plate (CP). Methods: A three-dimensional finite element analysis (FEA) was conducted to compare stress distribution in ACP and CP models under a standardized oblique load of 60 N, simulating muscle forces from the mentalis and digastric muscles. Plates were modeled using Blender and analyzed using ANSYS software 2025 r2. Mechanical behavior was assessed based on von Mises stress, concentration sites, and potential for plastic deformation or fatigue failure. Results: The ACP demonstrated a significantly lower maximum von Mises stress (77.19 MPa) compared to the CP (398.48 MPa). Stress distribution in the ACP was homogeneous, particularly around the lateral fixation holes, while the CP exhibited concentrated stress between central screw holes. These findings indicate that the anatomical geometry of the ACP enhances load dispersion, reduces critical stress concentrations, and minimizes fatigue risk. Conclusions: The ACP design offers superior biomechanical behavior and improved aesthetic potential for genioplasty procedures. Its optimized shape allows for better integration with facial anatomy while providing stable fixation. Further studies are recommended to validate in vitro performance and explore clinical applicability in advanced genioplasty and complex osteotomies.

Keywords: genioplasty; chin osteotomy; finite element analysis; anatomical chin plate; facial aesthetics; plate fixation; mandibular surgery

1. Introduction

The aesthetics of the face have attracted patients since the dawn of humanity. Several techniques have been developed to achieve facial harmony and symmetry. Jaw advancement surgeries, fillers, and genioplasty have been employed in the lower third of the face with excellent outcomes and clear indications [1].

Genioplasty is a well-established surgical procedure. Performed through osteotomies in the mental region of the mandible, this procedure involves separating the bone stumps and repositioning them in the necessary position, followed by a rigid fixation using plates

and screws. This technique allows for advancement, setback, widening, narrowing, and increase or decrease in facial height [2].

An alternative to genioplasty is the placement of anatomical facial prostheses, which increase the volume and contour of the chin region without requiring osteotomies [3].

Finite element analysis (FEA) is commonly performed before in vitro and in vivo studies. In these studies, we can virtually simulate situations where forces are applied in different regions of the plates and evaluate the maximum stress and fatigue of the material [4]. This technique helps guide future studies and assess the feasibility of the product [5].

To revolutionize and improve this surgical approach, we developed an anatomical chin plate that enables multidirectional movement of the bone stumps, offering enhanced contour and anatomy to the facial aesthetic region. In this study, we compared a conventional chin plate (CP) with the new anatomical chin plate (ACP) using finite elements.

2. Materials and Methods

2.1. New Design

In genioplasty procedures, alterations in chin position and morphology are evident; however, deficiencies in the mentolabial region frequently demand adjunctive interventions to achieve optimal facial balance. The ACP was specifically developed to overcome this limitation by providing superior biomechanical performance, including improved load distribution, resistance to torsional and shear stresses, and reduction in stress shielding. These features contribute to enhanced fixation stability, controlled osteotomized segment displacement, and greater long-term predictability of mandibular biomechanics.

The ACP arose from the need to bring a greater aesthetic result to genioplasty, and bone advancement or setback is already well-established in both the literature and clinical practice. The aesthetic complement of the mentolabial sulcus in several patients often requires bone or fat grafts to obtain the desired aesthetic effect.

This new customized plate allows for precise planning of bone advancement or setback while maintaining the aesthetics of the mentolabial fold, which can be seen both in the profile and frontal analysis of the patient (Figure 1). The ACP It was projected and manufactured by EVOLVE®, São Caetano, Brazil.

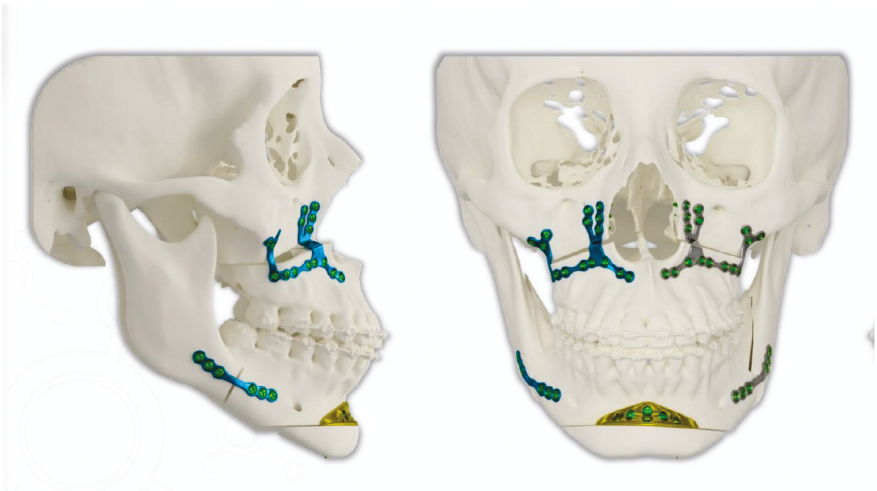

Figure 1. Anatomical Chin Plate (ACP) customized already, providing for the necessary bone advancement and volumization of the labial chin groove.

To ensure the ACP fits accurately and achieves the planned aesthetic outcome, a guided osteotomy must be performed. A surgical guide is fabricated with high precision to match

the planned osteotomy. This guide must be stabilized at both the top (occlusion of the lower teeth) and bottom using a screw (Figure 2). The screw used to stabilize the guide also serves as a drilling guide for the placement of the ACP.



Figure 2. Cutting guide used to perform the correct osteotomy on the chin. This surgical guide has an upper support on the dental elements and a centralized screw at the bottom.

During planning the ACP, the required size of the screws and their relationship with the dental roots were carefully determined to avoid future complications (Figure 3).



Figure 3. Planning of the new ACP in relation to the dental roots and with the planning of the screws necessary for the installation of the plate.

2.2. Modeling and Mechanical Analysis

The plates used in this study were modeled using Blender software version 3.x (Blender Foundation, 2025, Amstedam, The Netherlands). Titanium Ti-6AI-4V plates were used, with an elastic modulus of 110 GPa, Poisson's coefficient of 0.34, and a yield strength of 880 MPa. These three-dimensional models were imported into the ANSYS (Mechanical Finite Element Analysis software 2025 r2) (© 2024 ANSYS, Inc., Canonsburg, PA, USA).

To simulate muscle loading in the chin region, an oblique force vector with a modulus of 60 N was applied, oriented at 45° in the sagittal plane, directed inferoposteriorly. This direction corresponds to the muscular forces exerted primarily by the mental muscles and the anterior belly of the digastric during functional contraction.

Based on the functional anatomy of the mentalis and anterior belly of the digastric muscles, the resulting vector of muscle force acting on the chin can be represented by an oblique vector inclined at 45°, directed inferoposteriorly (i.e., downward and backward).

If we consider a total net force of 60 N, the vector at 45° has equal components in X and Y, as follows:

$$Fx = Fy = F \cdot \cos(45^\circ) = 60 \cdot 22 \approx 42.4\ NFx = Fy = F \cdot \cos(45^\circ) = 60 \cdot 22 \approx 42.4\ N$$

To evaluate the mechanical strength of the titanium plates used in genioplasty, three-dimensional finite element analysis was performed using the von Mises equivalent stress criterion. This criterion was selected because it is widely accepted in the flow prediction of ductile materials such as Ti-6Al-4V.

The plate model was subjected to a vector force of 60 N applied at 45° in the sagittal plane, representing the combined traction of the mentalis muscles and anterior belly of the digastric. Boundary conditions were applied to simulate rigid fixation of the plate to the mandibular blocks using screws that were restricted to all translational degrees of freedom.

The mesh was composed of second-order tetrahedral elements, and the solution was applied until the numerical residuals converged. Von Mises stresses were calculated throughout the body of the plate to identify the regions of stress concentration. Results were expressed in megapascals (MPa) and presented on a continuous chromatic scale.

3. Results

Two different configurations of titanium plates for genioplasty were analyzed with respect to the distribution of von Mises stresses under the same 60 N loading applied at 45°, simulating the combined vector action of the mentalis and anterior digastricus muscles. All models and their characteristics are summarized in Table 1.

Table 1. Comparison between models CP and ACM plates.

Criterion	CP	ACP
	Plate A (Conventional)	**B-Plate (Anatomical)**
Maximum tension (von Mises)	398.48 MPa	77.19 MPa
Critical Concentration Site	Between the center holes	Around the side holes
Risk of plastic deformation	Moderate	Low
Stress distribution	Concentrated	Homogeneous
Potential for fatigue failure	Bigger	Minor

For the conventional plate (Figure 4), the maximum recorded stress was 398.48 MPa, which was in the central region of the plate between the fixing holes. The stress distribution was concentrated in the geometric transition areas and near the orifices, suggesting a possible failure starting point under the cyclic loading. Despite the concentration, the values remained below the yield strength of grade 5 titanium (880 MPa), indicating structural safety under an isolated loading.

In contrast, for the ACP (Figure 5), the maximum stress was 77.19 MPa, distributed around the fixation holes on the lateral portions of the implant. The stress distribution was more homogeneous, with a significant reduction in peak concentrations, particularly in the critical transition regions between the holes and edges. The results suggest that anatomical geometry favors a more efficient dispersion of the load, contributing to greater resistance to fatigue and a reduced risk of local failure.

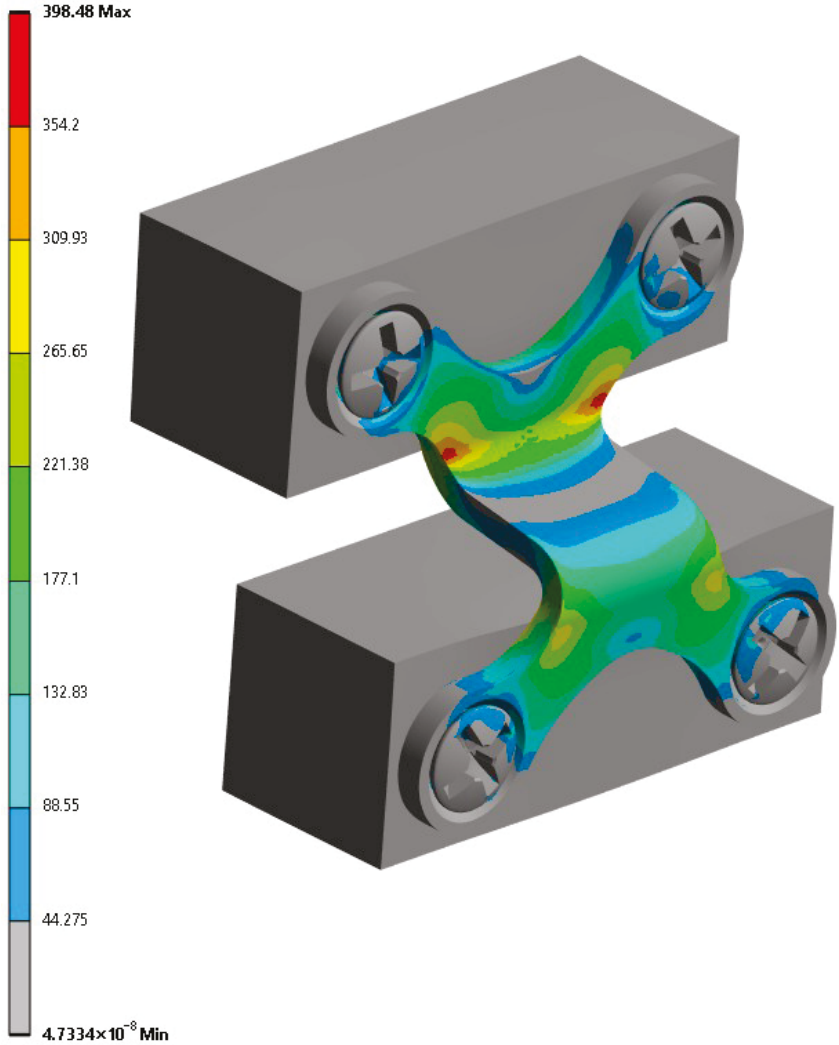

Figure 4. Finite element analysis of the Conventional Plate (CP).

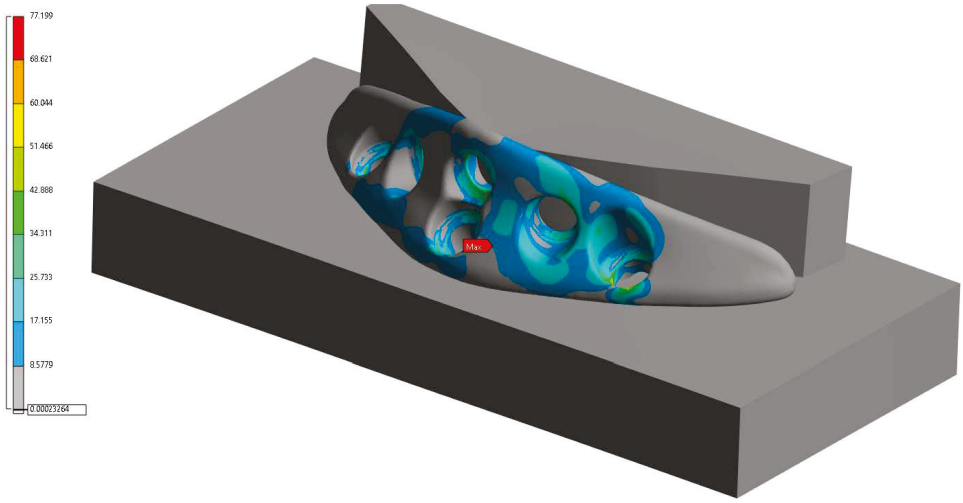

Figure 5. Finite element analysis of the Anatomical Chin Plate (ACP).

4. Discussion

Genioplasty is a surgical procedure that modifies the size, shape, and position of the chin in all directions [2]. When we combined genioplasty with internal fixation, regardless

of the fixation type, the procedure proved to be stable regardless of movement (advance or retreat) when evaluating recurrence in hard and soft tissues [6].

In terms of aesthetics, genioplasty, when compared to chin implants, provided more satisfaction in patients undergoing osteotomy and produced fewer complications [3]. When we think about the osteotomy itself, a modification that has great acceptance is the Chin Wing [7]. Because of its great extension in most cases, it becomes necessary to have extra fixations, which would be an excellent indication for the ACP due to its high degree of resistance. In cases of minimally invasive osteotomies with different shapes [8], the ACP can be used to improve the quality of the soft tissue in the submental region.

We used finite elements as an accurate and cohesive method for evaluating the strength of a plate. It is known that the width, rather than the thickness, of a plate can influence the resistance, making the facts decisive for reducing the maximum stress under bending forces [9]. This is in accordance with the shape of our ACP, which, because it is extended, has 11 fewer tensions than a conventional plate in addition to delivering the necessary aesthetics for the region.

When evaluating the stability of genioplasty, one of the main concerns is the stability of the bone stump in relation to the musculature inserted in the chin. This fixation method is effective in preventing recurrence [5]. Initially, genioplasties were fixed with two bicortical screws; however, FEA has shown that a centrally located conventional plate produced more stability than two bicortical screws [10]. Thus, the placement of a plate, in addition to being more stable, is an easier procedure, particularly in cases of indentation and chin asymmetry.

The ACP was slightly thicker than the conventional plate. Plate thickness can be an important factor influencing the yield threshold and plate deformation. Further studies using plates of different thicknesses should be conducted in the future.

Among the various osteotomy techniques, the T-osteotomy, which removes the central part of the chin, reduces the width, and provides a new contour, is considered one of the least stable and requires fixation with greater stability. A finite element study found that the optimal stability was achieved with either a 1.2 mm plate and five screws or a 0.9 mm plate and seven screws [11]. This suggests that the new ACP, in addition to maintaining a thickness of 1.2 mm, also has six screws, which should be more than ideal to ensure perfect resistance to variations in T-osteotomy.

In advanced genioplasties, customized plates have demonstrated better distribution of strain stress and improved stabilization between the stem and segment [12]. Another benefit of customized plates is the incorporation of nanoparticles such as graphene into their composition; these alloys have been shown to reduce the stress distribution between 5% and 25% in the critical zones of titanium plates [13]. One disadvantage of this customization is that ACP will always depend on centers that work with proper software and a local company that customizes the ACP.

The thickness of the plate is a primary factor for stress distribution on the plates, promoting more resistance in advance [14,15]. The conventional plate has a thickness of 0.8 mm, whereas the customized ACP, at its smallest point, maintains a thickness of 1.2 mm, making it substantially more resistant to titanium fatigue. In addition to the thickness of the ACP board, a crucial change that can be a factor of more resistance can be its geometric shape. No other plate was designed to reproduce the anatomical form, focusing only on fixing the bone stumps letting the bone itself assume the aesthetic role.

5. Conclusions

The results indicate that the ACP model exhibits superior mechanical performance compared to the conventional CP, with significantly lower stress values and improved

load distribution throughout the structure. These findings suggest a more favorable biomechanical behavior, particularly under cyclic or prolonged loading conditions, such as those associated with functional activities of the chin.

Further long-term studies are warranted to validate the effectiveness of the ACP, particularly through advanced biomechanical models and loading simulations, in order to assess the in vitro resistance of this new design. Such investigations may also extend to different types of osteotomies applied in genioplasty.

With validation and eventual clinical adoption, anatomical plates for genioplasty may enable the integration of osteotomy stability with prosthetic contouring, providing a unified technological approach to optimize both biomechanical reliability and facial esthetics.

Author Contributions: Conceptualization, B.N.P., L.C.P. and B.P.; methodology, B.N.P.; software, L.C.P.; validation, R.C.G.; formal analysis, B.N.P.; investigation, B.N.P. and L.C.P.; resources, B.P. and B.N.P.; data curation, L.C.P.; writing—original draft preparation, B.N.P.; writing—review and editing, B.P. and R.C.G.; visualization, B.N.P.; supervision, L.C.P., B.P. and R.C.G.; project administration, R.C.G. All authors have read and agreed to the published version of the manuscript.

Funding: This research received no external funding.

Institutional Review Board Statement: This study was conducted in accordance with the relevant laws and institutional guidelines and was approved by the Ethics Committee of São Leopoldo Mandic University (approval number: 43735621.5.0000.5374, 10 April 2025).

Informed Consent Statement: This is an in vitro computed laboratory study, with digital models.

Data Availability Statement: The raw data supporting the conclusions of this study are available from the authors upon reasonable request.

Conflicts of Interest: The authors declare no conflicts of interest.

References

1. Shokri, T.; Rosi-Schumacher, M.; Petrauskas, L.; Chan, D.; Ducic, Y. Genioplasty and Mandibular Implants. *Facial Plast. Surg.* **2021**, *37*, 709. [CrossRef] [PubMed]
2. Ferretti, C.; Reyneke, J.P. Genioplasty. *Atlas Oral Maxillofac. Surg. Clin. N. Am.* **2016**, *24*, 79–85. [CrossRef] [PubMed]
3. Tabrizi, R.; Behnia, P.; Kavianipour, M.; Behnia, H. Osseous genioplasty versus chin implants: Early complications and patient satisfaction. *Int. J. Oral Maxillofac. Surg.* **2024**, *53*, 141–145. [CrossRef] [PubMed]
4. Choi, A.H.; Ben-Nissan, B.; Conway, R.C. Three-dimensional modelling and finite element analysis of the human mandible during clenching. *Aust. Dent. J.* **2005**, *50*, 42–48. [CrossRef] [PubMed]
5. Stróżyk, P.; Bałchanowski, J. Application of numerical simulation studies to determine dynamic loads acting on the human masticatory system during unilateral chewing of selected foods. *Front. Bioeng. Biotechnol.* **2023**, *11*, 993274. [CrossRef] [PubMed]
6. Kumar, M.; Singh, R.S.; Singh, G.; Raj, P.; Gupta, H.; Kasrija, R. Hard and soft tissue relapse after different genioplasty procedures: A scoping review. *Cureus* **2023**, *15*, e41478. [CrossRef] [PubMed]
7. Cordier, G.; Sigaux, N.; Rasteau, S.; Ibrahim, B.; Cresseaux, P. Long-term stability of basilar mandible osteotomy: Chin Wing. *J. Stomatol. Oral Maxillofac. Surg.* **2022**, *123*, 337–344. [CrossRef] [PubMed]
8. Leon, N.J.; Péres, A.J.P.; Requejo, S.; Goméz, D.; Barros, H.L.M. Telescopic genioplasty: A new concept to reshape the chin. *Adv. Oral Maxillofac. Surg.* **2021**, *4*, 10076. [CrossRef]
9. Guerra, R.C.; de Fátima Borim Pulino, B.; Salomão Júnior, V.F.; Dos Santos Pereira, R.; Thieringer, F.M.; Sacco, R.; Sader, R.; Vieira, E.H. Finite element analysis of low-profile reconstruction plates for atrophic mandibles: A comparison of novel 3D grid and conventional plate designs. *Oral Maxillofac. Surg.* **2024**, *28*, 595–603. [CrossRef] [PubMed]
10. Gulsever, S.; Munevveroglu, S.; Hartomacioglu, S.; Guldiken, I.N.; Uckan, S. Comparison of screw and plate osteosynthesis in advancement genioplasty: A finite element analysis study. *Eur. Oral Res.* **2025**, *59*, 40–45. [CrossRef]
11. Akkoyun, E.F.; Pergel, T. Finite element analysis of shape and thickness variations in patient-specific implants for T-shaped genioplasty. *Med. Oral Patol. Oral Cir. Bucal.* **2025**, *30*, e528–e535. [CrossRef] [PubMed]
12. Ramos, V.F.; Pinto, L.A.P.F.; Basting, R.T. Force and deformation stresses in customized and non-customized plates during simulation of advancement genioplasty. *J. Cranio-Maxillofac. Surg.* **2017**, *45*, 1820–1827. [CrossRef] [PubMed]

13. Jindal, P.; Worcester, F.; Gupta, A.; Breedon, P. Efficiency of nanoparticle reinforcement using finite element analysis of titanium alloy mandible plate. *Proc. Inst. Mech. Eng. H* **2019**, *233*, 309–317. [CrossRef] [PubMed]
14. Tazh, T.; Khorramymehr, S.; Hassani, K.; Nikkhoo, M. Finite element analysis of various fixation patterns in mandible bone fracture. *Comput. Methods Biomech. Biomed. Eng.* **2025**, *13*, 1–16. [CrossRef] [PubMed]
15. da Silveira, M.L.M.; de Oliveira Bueno, M.L.; da Silva, J.S.P.; Germano, A.R. Biomechanical analysis in mandibular advancement and occlusal plane rotation with finite element analysis. *Br. J. Oral Maxillofac. Surg.* **2021**, *59*, 362–367. [CrossRef] [PubMed]

Disclaimer/Publisher's Note: The statements, opinions and data contained in all publications are solely those of the individual author(s) and contributor(s) and not of MDPI and/or the editor(s). MDPI and/or the editor(s) disclaim responsibility for any injury to people or property resulting from any ideas, methods, instructions or products referred to in the content.

craniomaxillofacial
trauma & reconstruction

MDPI

Article

Towards MRI-Only Mandibular Resection Planning: CT-like Bone Segmentation from Routine T1 MRI Images Using Deep Learning

Reinier S. A. ten Brink [1,2,*], Bram J. Merema [1,2], Marith E. den Otter [2], Willemina A. van Veldhuizen [2], Max J. H. Witjes [1,2] and Joep Kraeima [1,2]

[1] Department of Maxillofacial Surgery, University Medical Center Groningen, 9713GZ Groningen, The Netherlands; b.j.merema@umcg.nl (B.J.M.); m.j.h.witjes@umcg.nl (M.J.H.W.); j.kraeima@umcg.nl (J.K.)
[2] 3D Lab, University Medical Center Groningen, 9713GZ Groningen, The Netherlands; w.a.van.veldhuizen@umcg.nl (W.A.v.V.)
* Correspondence: r.s.a.ten.brink@umcg.nl; Tel.: +31-050-3613858

Abstract: We present a deep learning-based approach for accurate bone segmentation directly from routine T1-weighted MRI scans, with the goal of enabling MRI-only virtual surgical planning in head and neck oncology. Current workflows rely on CT for bone modeling and MRI for tumor delineation, introducing challenges related to image registration, radiation exposure, and resource use. To address this, we trained a deep neural network using CT-based segmentations of the mandible, cranium, and inferior alveolar nerve as ground truth. A dataset of 100 patients with paired CT and MRI scans was collected. MRI scans were resampled to the voxel size of CT, and corresponding CT segmentations were rigidly aligned to MRI. The model was trained on 80 cases and evaluated on 20 cases using Dice similarity coefficient, Intersection over Union (IoU), precision, and recall. The network achieved a mean Dice of 0.86 (SD $\pm$ 0.03), IoU of 0.76 (SD $\pm$ 0.05), and both precision and recall of 0.86 (SD $\pm$ 0.05). Surface deviation analysis between CT- and MRI-derived bone models showed a median deviation of 0.21 mm (IQR 0.05) for the mandible and 0.30 mm (IQR 0.05) for the cranium. These results demonstrate that accurate CT-like bone models can be derived from standard MRI, supporting the feasibility of MRI-only surgical planning.

Keywords: deep learning; magnetic resonance imaging; surgery; computer-assisted; surgery; oral

1. Introduction

3D virtual surgical planning (VSP) is applied in the current standard of care for head and neck oncological surgery for more than a decade already [1–3]. This technology enables surgeons to preoperatively visualize complex anatomy, plan surgeries preoperatively, and design 3D printed surgical guides and patient-specific implants (PSIs). This workflow requires rigid matching between MRI and CT, to obtain both soft tissue, tumour and bone tissue delineation, which introduces a 1–2 mm error due to anatomical changes between scans [4]. To mitigate the clinical consequences of these errors misalignments, safety margins are added around the tumour, resulting in unnecessarily larger bone resections.

Furthermore, the requirement for multiple imaging modalities places additional burdens on patients, including increased time and radiation exposure from CT scans. Additionally, the need for extra scans causes strain on hospital resources, contributing to longer waiting times, higher healthcare costs and energy consumption [5].

Given these challenges, a single-modality VSP workflow could significantly reduce the required number of scans needed and remove the error introduced by MRI-CT fusion. MRI, which is better for tumour delineation, is the preferred modality, but accurate bone models from MRI are essential [6,7]. Previous studies have explored the use of blackbone MRI sequences for bone segmentation as a potential solution [8–13]. However, this method adds an additional scan to the already long MRI protocol and requires extensive laborious manual adjustments to accurately segment, limiting clinical feasibility.

This retrospective study investigates whether T1 VIBE Dixon MRI scans, already part of our routine imaging protocol, can be leveraged for bone segmentation. We propose training a deep learning model on MRI scans that uses CT-based bone segmentations as ground truth labels to enable accurate and efficient bone segmentation from these MRI scans. This would lay the foundation for a fully MRI-based VSP workflow that reduces the reliance on CT, minimizes registration errors, and optimizes the overall surgical planning process.

2. Materials and Methods

2.1. Dataset

The retrospective dataset consisted of N = 100 paired T1 MRI scans and CT scans acquired between 2018 and 2025 during routine diagnostic work-up of oncology patients from the department of Oral and Maxillofacial Surgery of the University Medical Center Groningen (UMCG), The Netherlands. Approval for this study was obtained from the Central Ethics Committee of the University Medical Center Groningen (CTc 188984). The included patients were diagnosed with a tumour in the oral cavity region with a planned mandibulectomy or maxillectomy. Patients with dental implants in their jaw were excluded since this causes major artifacts in the MRI. Due to anonymization protocols and the random selection of scans, detailed demographic or pathological information was not available.

The CT scans were acquired in headfirst supine position with either a Siemens SOMATOM Definition AS scanner, or a Siemens SOMATOM Force scanner (Siemens Healthineers, Forchheim, Germany). The resulting CT scans had a median voxel size of $0.6 \times 0.6 \times 0.6$. The MRI scans were acquired in headfirst supine position with a 3.0 Tesla MRI scanner (SIEMENS Magnetom Prisma, Siemens Healthineers, Forchheim, Germany), with a 64-channel head coil. The scans were obtained with the suprahyoid protocol in the T1-weigthed gradient echo (Dixon VIBE) sequence with contrast agent DOTAREM. In-phase scans were used within this study. The parameters of the MRI were: repetition time/echo time, 5.5/2.46 ms; matrix, 256×256 and voxel size $0.9 \times 0.9 \times 0.9$ mm. In order to ensure that the bone models from the CT would fit to the MRI, the MRI scans were resampled to $0.6 \times 0.6 \times 0.6$ mm using linear interpolation and then transformed into nii.gz files.

Manual segmentation of the CT scans was performed using Mimics 26.0 research software (Materialise, Leuven, Belgium). The mandible, cranium and bilateral inferior alveolar nerve (NAI) were segmented. For the thin orbital bone, Mimics' thin bone segment tool was utilized. For the NAI, a spline of 2 mm diameter was drawn through the mandibular canal from the mandibular foramen to the mental foramen. The manual segmentations were performed by a technical physician with 4 years of experience. After creating the 3D models from the segmentations, all segmentations were exported to a standard tessellation language (STL) format and imported into the 3-Matic 18.0 research software (Materialise, Leuven, Belgium). In this software all bones were wrapped with a gap closing distance of 3.0 mm, getting rid of any holes smaller than 3.0 mm, and a detail level of 0.5 mm. These parameters were determined empirically. The resulting models were exported as STL files.

All STL files were uploaded to Brainlab software 4.5 (Brainlab, München, Germany) and linked to the corresponding CT scan. The image fusion tool was then used to align the CT scan with the T1 MRI scan. Since neither the CT or the MRI was acquired in occlusion, this process was repeated twice, to overcome the positional difference in the bones between the MRI and CT, by an experienced operator (RtB): once with the region of interest (ROI) set on the mandible during fusion, after which the mandible and NAI STL files were exported; and once with the ROI set on the cranium, after which the cranium STL file was exported. These STL files were transformed into nii.gz files to serve as a mask in training. The image processing workflow is illustrated in Figure 1.

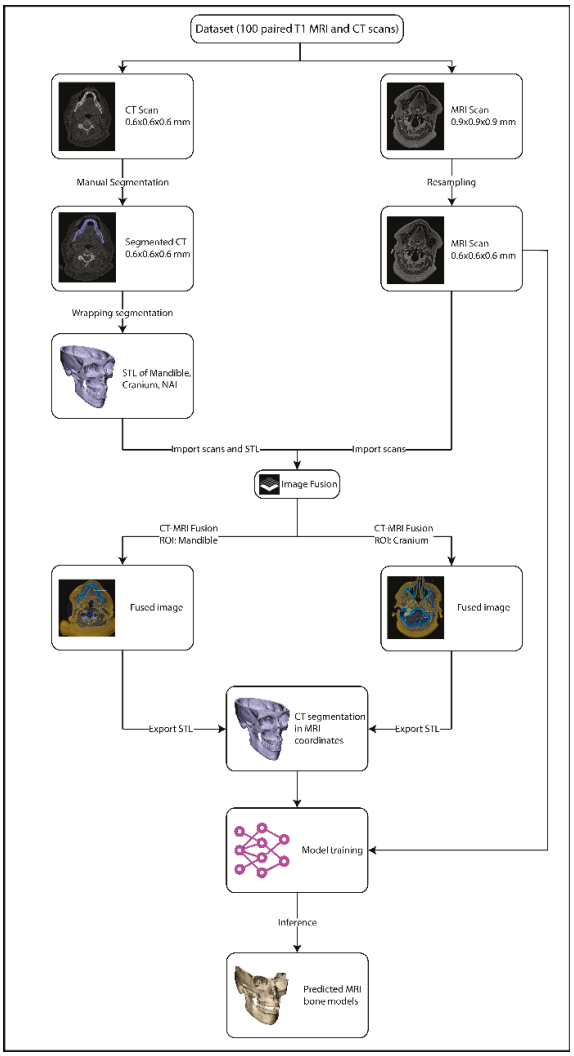

Figure 1. The image processing workflow.

2.2. AI Framework

The nnU-Net convolutional neural network was selected as the framework for automatic segmentation, given its versatility across different datasets [14]. The model was implemented on an Intel® Core™ i9-10980XE CPU with 64 GB RAM and a graphic card of NVIDIA RTX A4000 (NVIDIA Corporation, Santa Clara, CA, USA) with 16 GB GDDR6 memory. A split of 80% for training and 20% for testing was used. Training was carried out using the 3D full resolution configuration with 5-fold cross validation and 1000 epochs per fold using the cross-entropy dice loss function using a polynomial learning rate scheduler with initial learning rate of 0.01. Following the training process, segmentation predictions on the test set were generated by averaging the SoftMax outputs of all 5 trained folds

and selecting the label with the highest probability per voxel to achieve higher accuracy and reliability.

2.3. Evaluation Metrics

Inference on the MRI scans in the test set produced the MRI-based segmentations which were compared against the CT-derived labels rigidly aligned to MRI. The following classification metrics were used to evaluate the performance of the model on the test dataset:

$$\text{Dice} : DSC = \frac{2|A \cap B|}{|A| + |B|}$$

$$\text{Intersection over Union} : \text{IoU} = \frac{|A \cap B|}{|A| \cup |B|}$$

$$\text{Precision} : Precision = \frac{True\ positives}{True\ positives + False\ positives}$$

$$\text{Recall} : Recall = \frac{True\ positives}{True\ positives + False\ negatives}$$

$$\text{95th percentile Hausdorff distance} : H(A, B) = max\ \{h_{95}(A, B), h_{95}(B, A)\}$$

The MRI derived bone models were matched to the original CT bone model using the global registration tool in 3-Matic. To compare the CT and MRI-based bone models, median deviation was calculated and distance maps generated using part-to-part comparison in 3-Matic. The analysis was restricted to bone regions that were present in both the CT and MRI scans to ensure a consistent comparison. A median deviation of $\leq$1 mm between the CT and MRI was deemed acceptable for clinical use based on clinical consensus.

3. Results

20 MRI-based mandible and cranium models were obtained using our deep learning model. The model achieved overall mean Dice similarity coefficient of 0.86 (SD $\pm$ 0.03, range 0.78–0.91), Intersection over Union of 0.76 (SD $\pm$ 0.05, range 0.64–0.84), precision of 0.86 (SD $\pm$ 0.05, range 0.72–0.92) and recall of 0.86 (SD $\pm$ 0.05, range 0.71–0.93) on the test dataset. A summary of the evaluation metrics for each anatomical structure on the test dataset is presented in Figures 2–5 and Table 1.

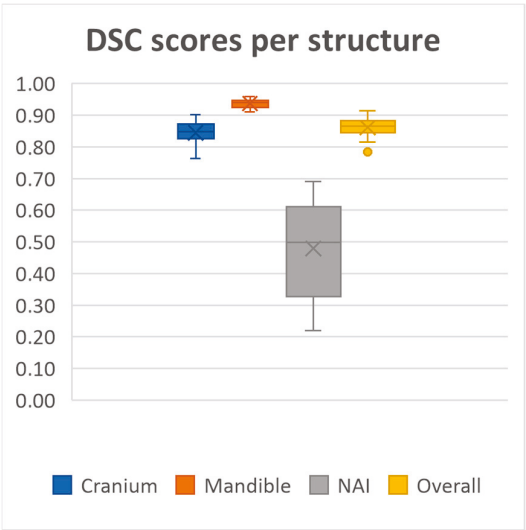

Figure 2. Median Dice scores per structure and all structures combined.

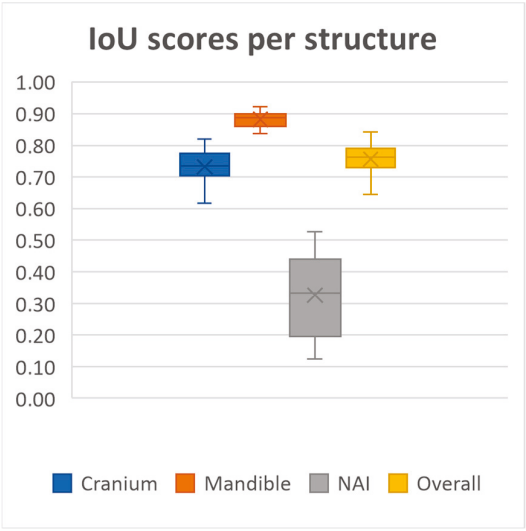

Figure 3. Median Intersection over Union scores per structure and all structures combined.

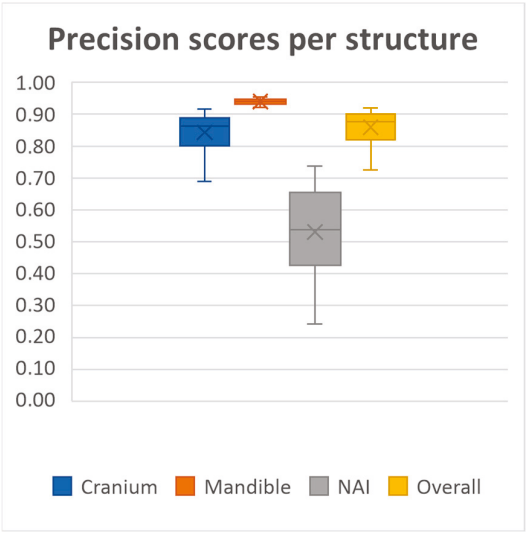

Figure 4. Median precision scores per structure and all structures combined.

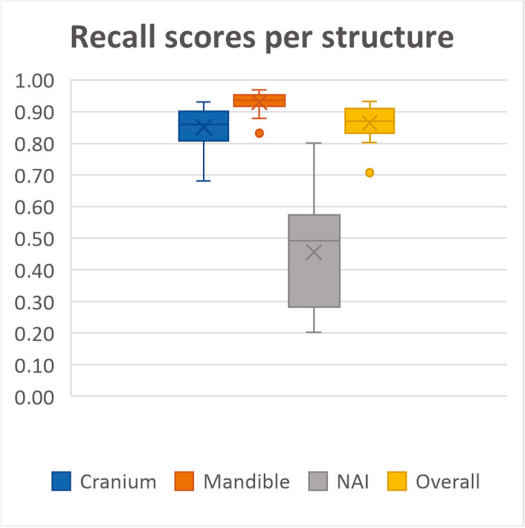

Figure 5. Median recall scores per structure and all structures combined.

Table 1. Mean evaluation metrics of the model performance on the test set.

Metric \ Structure	Mandible	Cranium	Inferior Alveolar Nerve (NAI)	Overall
Dice (SD)	0.94 (±0.01)	0.84 (±0.03)	0.48 (±0.14)	0.86 (±0.03)
IoU (SD)	0.88 (±0.02)	0.73 (±0.05)	0.33 (±0.12)	0.76 (±0.05)
Precision (SD)	0.94 (±0.01)	0.84 (±0.06)	0.53 (±0.14)	0.86 (±0.05)
Recall (SD)	0.93 (±0.03)	0.85 (±0.06)	0.46 (±0.16)	0.86 (±0.05)
95th Hausdorff (HD)	1.60 (±0.42)	4.71 (±2.07)	2.77 (±1.28)	-

Performance was consistently high for both the mandible and cranium, with the mandible achieving the highest scores, as well as the lowest standard deviations across all metrics (Dice 0.94 ± 0.01, IoU, 0.88 ± 0.02, Precision 0.94 ± 0.01, Recall 0.93 ± 0.03, HD95 1.60 ± 0.42). The cranium segmentation performed slightly lower across all metrics, indicating a more variable segmentation performance compared to the mandible (Dice 0.84 ± 0.03, IoU, 0.73 ± 0.05, Precision 0.84 ± 0.06, Recall 0.85 ± 0.06, HD95 4.71 ± 2.07). In contrast, segmentation performance for the NAI was considerably lower than those of the bony structures, highlighting difficulty in accurately segmenting the NAI (Dice 0.48 ± 0.14, IoU, 0.33 ± 0.12, Precision 0.53 ± 0.14, Recall 0.46 ± 0.16, HD95 2.77 ± 1.28).

The median deviation between the CT and MRI-based bone models was 0.21 mm (IQR 0.05) for the mandible and 0.30 mm (IQR 0.08) for the cranium. Visual representations of the MRI-based bone models in Figure 6 illustrates the deviations compared to their CT counterparts. While no separate segmentations of sub anatomy were evaluated, localized larger deviations (>1mm) were qualitatively observed in the dorsal part of the cranium, mandibular condyles, and teeth.

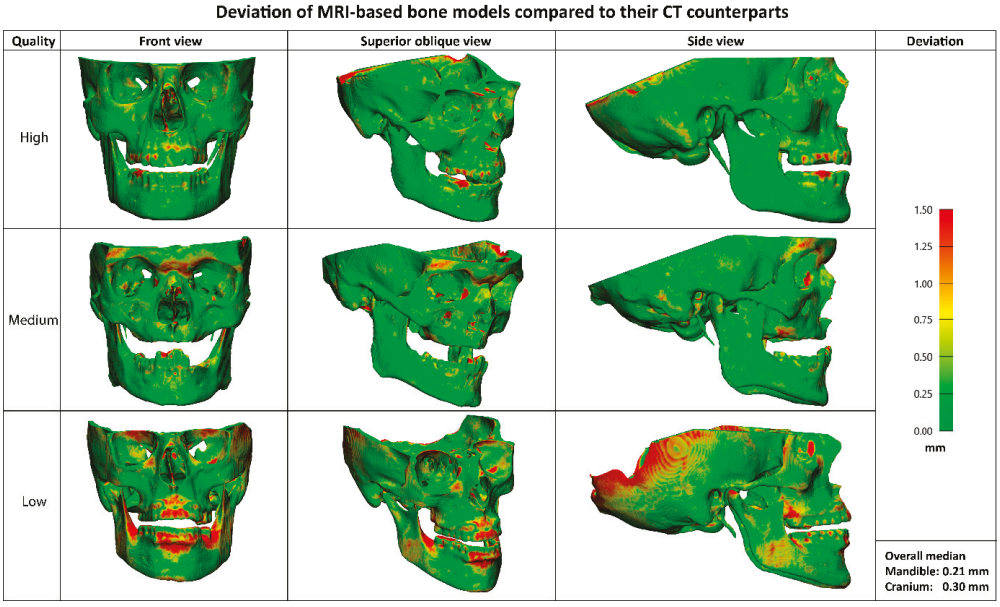

Figure 6. Visualisation of MRI-based bone models for a high-, medium- and low-quality result. The distance map shows deviations compared to their CT counterparts, with green representing small differences (0–0.5 mm) and red representing large differences (>1 mm). Localized larger deviations are qualitatively observed in the dorsal part of the cranium, mandibular condyles, and teeth.

4. Discussion

This study shows that cranium and mandibula models can be segmented accurately and fast from T1 MRI scans with comparable results as CT-based segmentation of bony

tissue and without manually laborious work. This is a significant step towards fully MRI-based VSPs, surgical guide design and incorporating soft tissue into resection and reconstruction planning.

While previous studies have shown that accurate bone segmentation from MRI is possible, it typically involves many laborious steps, such as extensive manual annotation or post-processing due to the lack of a unique intensity range for bone in MRI and resulting in increased risk of variability between observers [7,12]. These approaches have also relied on dedicated MRI sequences, such as Black Bone VIBE, which add to the imaging protocol and may not be widely available or feasible for all patient groups [8–13]. These factors have limited the adoption of MRI-only workflows in 3D VSP. This study preserves the advantages of MRI-only planning and eliminates the need for manual segmentation or specialized sequences, thereby significantly reducing the time and expertise required for bone model generation and making MRI-only workflows accessible and efficient.

The ability to generate accurate bone models from MRI is particularly valuable for designing patient-specific implants and surgical guides for tumour resection. Several studies have explored deep learning-based bone segmentation from MRI, often relying on manual annotations as ground truth or requiring modifications to scanning protocols [11,15,16]. Our method circumvents these limitations by leveraging paired CT and MRI data for deep learning model training, producing bone models form MRI only that are comparable to CT-based reconstructions. These findings could potentially simplify imaging protocols for head and neck cancer patients. This would eliminate the need for MRI-CT matching, creating a more accurate VSP which might reduce the necessary tumour margin and therefore bone resections.

By eliminating the need for a dedicated head CT, radiation exposure to sensitive structures such as the cornea and thyroid gland could be significantly reduced. Reducing the number of necessary CT scans might decrease the strain on hospital resources. Our approach could also be extended to other anatomical regions, provided paired datasets are available.

One important consideration might be the continued necessity of thoracic CT for assessing pulmonary nodules and metastases in oncological cases. Additionally, differences in spatial resolution between CT and MRI may impact the radiological evaluation of subtle bone invasions. To address these challenges, a triage system could be implemented to determine when both CT and MRI are necessary versus when MRI alone is sufficient.

The most significant deviations (>1 mm) between the CT and MRI-derived bone models occur in the dorsal part of the cranium, the mandibular condyles, and the teeth. The missing part of the cranium is likely due to differences in scan coverage between the MRI and CT in the training dataset. It could potentially be improved by manually adding this segmentation to the MRI or building a dataset where the CT fully covers the same area as the MRI. This also explains the higher Hausdorff scores of the cranium. Deviation in the condyles could be explained by the fact that it is difficult to differentiate the condyle from the glenoid fossa due to the articular disc cartilage that is picked up on MRI. [17] The deviation in the teeth can be explained by several aspects. First, the segmentation of the teeth from the CT contains artefacts due to the presence of tooth fillings. Moreover, teeth are relatively small and the original MRI scan has a voxel size of 0.9 mm, thus not capturing the entire tooth. Resampling the scan does not add this data to the scan. All three of these deviations do not affect the clinical usability of the model, as all areas are not essential for designing surgical guides or patient-specific implants.

The accuracy of nerve segmentation remains a challenge. Automatic segmentation of the NAI from MRI is not yet clinically usable with this model (Dice 0.48 ± 0.14). This may be due to the discrepancy between the structures segmented on CT versus MRI. On

CT, the mandibular canal is segmented as a proxy for the nerve, while MRI allows direct visualization of the nerve itself, which is smaller than the canal. This mismatch may have impacted segmentation performance. Given the importance of precise NAI modelling for patient-specific implant design, future work should explore whether increasing the dataset size or manually annotating the NAI on MRI could improve segmentation accuracy. However, manual annotation of the NAI on MRI is a relatively easy and fast task, therefore this does not limit clinical usability of the model.

To fully transition to an MRI-based 3D mandibular reconstruction workflow, segmentation of the fibula from MRI scans is required. Future work should focus on acquiring paired CT and MRI scans of the lower leg to develop a segmentation model for fibular graft planning, currently a study protocol and method is developed in our hospital. A prospective study where an MRI-only workflow will be implemented is needed to test the feasibility of our method in clinical practice.

5. Conclusions

In conclusion, this study shows that a deep learning model, trained on 3D CT reconstructions as input labels, can accurately and fast segment the cranium and mandible from routine T1 MRI scans only, resulting in very accurate bone models. This paves the way for fully MRI-based virtual surgical planning, incorporating soft tissue planning and reducing reliance on CT scans in head and neck cancer treatment.

6. Patents

The authors declare that a patent application related to aspects of this study has been filed but not yet granted.

Author Contributions: R.S.A.t.B.: Conceptualization, Methodology, Software, Writing—Original Draft, Writing—Review and editing B.J.M.: Conceptualization, Writing—Review and editing M.E.d.O.: Methodology, Software, Writing—Review and editing W.A.v.V.: Writing—Review and Editing M.J.H.W.: Supervision, Writing—Review and editing J.K.: Conceptualization, Funding acquisition, Writing—Review and editing. All authors have read and agreed to the published version of the manuscript.

Funding: This work was co-financed by the European Union. The project number of the subsidy is JTFN-00020. The number of the total subsidy is 2021NL16JTPR001.

Institutional Review Board Statement: Approval for this study was obtained from the Central Ethics Committee of the University Medical Center Groningen (CTc 188984) on 31 October 2024.

Informed Consent Statement: Patient consent was waived due to the retrospective design of the study and the impracticability of contacting all eligible patients within a reasonable timeframe, as many are no longer reachable or are deceased.

Data Availability Statement: The data supporting the conclusions of this article will be made available by the authors on reasonable request.

Conflicts of Interest: The authors declare no conflicts of interest.

Abbreviations

The following abbreviations are used in this manuscript:

CT	Computed Tomography
HD	Hausdorff Distance
IoU	Intersection over Union
IQR	Interquartile Range
MRI	Magnetic Resonance Imaging

NAI	Nervus Alveolaris Inferior
ROI	Region of Interest
SD	Standard Deviation
STL	Standard Tesselation Language
UMCG	University Medical Center Groningen
VSP	Virtual Surgical Planning

References

1. Schepers, R.H.; Raghoebar, G.M.; Vissink, A.; Stenekes, M.W.; Kraeima, J.; Roodenburg, J.L.; Reintsema, H.; Witjes, M.J. Accuracy of fibula reconstruction using patient-specific CAD/CAM reconstruction plates and dental implants: A new modality for functional reconstruction of mandibular defects. *J. Cranio-Maxillofac. Surg.* **2015**, *43*, 649–657. [CrossRef] [PubMed]
2. Kraeima, J.; Schepers, R.H.; van Ooijen, P.M.A.; Steenbakkers, R.J.H.M.; Roodenburg, J.L.N.; Witjes, M.J.H. Integration of oncologic margins in three-dimensional virtual planning for head and neck surgery, including a validation of the software pathway. *J. Cranio-Maxillofac. Surg.* **2015**, *43*, 1374–1379. [CrossRef] [PubMed]
3. Brown, J.S.; Griffith, J.F.; Phelps, P.D.; Browne, R.M. A comparison of different imaging modalities and direct inspection after periosteal stripping in predicting the invasion of the mandible by oral squamous cell carcinoma. *Br. J. Oral Maxillofac. Surg.* **1994**, *32*, 347–359. [CrossRef] [PubMed]
4. Dean, C.J.; Sykes, J.R.; Cooper, R.A.; Hatfield, P.; Carey, B.; Swift, S.; Bacon, S.E.; Thwaites, D.; Sebag-Montefiore, D.; Morgan, A.M. An evaluation of four CT–MRI co-registration techniques for radiotherapy treatment planning of prone rectal cancer patients. *Br. J. Radiol.* **2012**, *85*, 61–68. [CrossRef] [PubMed]
5. Ziekenhuischeck.nl. Wachttijden. 2024. Available online: https://www.ziekenhuischeck.nl/ziekenhuizen/umcg/behandeling/wachttijden/ (accessed on 4 March 2025).
6. Neubert, A.; Wilson, K.J.; Engstrom, C.; Surowiec, R.K.; Paproki, A.; Johnson, N.; Crozier, S.; Fripp, J.; Ho, C.P. Comparison of 3D bone models of the knee joint derived from CT and 3T MR imaging. *Eur. J. Radiol.* **2017**, *93*, 178–184. [CrossRef] [PubMed]
7. Kuiper, R.J.A.; Colaris, J.W.; Stockmans, F.; van Es, E.M.; Viergever, M.A.; Seevinck, P.R.; Weinans, H.; Sakkers, R.J. Impact of bone and cartilage segmentation from CT and MRI on both bone forearm osteotomy planning. *Int. J. Comput. Assist. Radiol. Surg.* **2023**, *18*, 2307–2318. [CrossRef] [PubMed]
8. Lethaus, B.; Gruichev, D.; Gräfe, D.; Bartella, A.K.; Hahnel, S.; Yovev, T.; Pausch, N.C.; Krause, M. "Black bone": The new backbone in CAD/CAM-assisted craniosynostosis surgery? *Acta Neurochir.* **2021**, *163*, 1735–1741. [CrossRef] [PubMed]
9. Probst, F.A.; Burian, E.; Malenova, Y.; Lyutskanova, P.; Stumbaum, M.J.; Ritschl, L.M.; Kronthaler, S.; Karampinos, D.; Probst, M. Geometric accuracy of magnetic resonance imaging–derived virtual 3-dimensional bone surface models of the mandible in comparison to computed tomography and cone beam computed tomography: A porcine cadaver study. *Clin. Implant. Dent. Relat. Res.* **2021**, *23*, 779–788. [CrossRef] [PubMed]
10. Eley, K.A.; Watt-Smith, S.R.; Golding, S.J. "Black Bone" MRI: A novel imaging technique for 3D printing. *Dentomaxillofacial Radiol.* **2017**, *46*, 20160407. [CrossRef] [PubMed]
11. Eley, K.A.; Delso, G. Automated 3D MRI rendering of the craniofacial skeleton: Using ZTE to drive the segmentation of black bone and FIESTA-C images. *Neuroradiology* **2021**, *63*, 91–98. [CrossRef] [PubMed]
12. Hoving, A.M.; Kraeima, J.; Schepers, R.H.; Dijkstra, H.; Potze, J.H.; Dorgelo, B.; Witjes, M.J.H. Optimisation of three-dimensional lower jaw resection margin planning using a novel Black Bone magnetic resonance imaging protocol. *PLoS ONE* **2018**, *13*, e0196059. [CrossRef] [PubMed]
13. Vyas, K.S.; Suchyta, M.A.; Hunt, C.H.; Gibreel, W.; Mardini, S. Black Bone MRI for Virtual Surgical Planning in Craniomaxillofacial Surgery. *Semin. Plast. Surg.* **2022**, *36*, 192–198. [CrossRef] [PubMed]
14. Isensee, F.; Jaeger, P.F.; Kohl, S.A.A.; Petersen, J.; Maier-Hein, K.H. nnU-Net: A self-configuring method for deep learning-based biomedical image segmentation. *Nat. Methods* **2021**, *18*, 203–211. [CrossRef] [PubMed]
15. Gu, H.; Colglazier, R.; Dong, H.; Zhang, J.; Chen, Y.; Yildiz, Z.; Chen, Y.; Li, L.; Yang, J.; Willhite, J.; et al. SegmentAnyBone: A Universal Model that Segments Any Bone at Any Location on MRI. *arXiv* **2024**, arXiv:arXiv:240112974. [CrossRef] [PubMed]
16. Almajalid, R.; Zhang, M.; Shan, J. Fully Automatic Knee Bone Detection and Segmentation on Three-Dimensional MRI. *Diagnostics* **2022**, *12*, 123. [CrossRef] [PubMed]
17. Kim, J.J.; Nam, H.; Kaipatur, N.R.; Major, P.W.; Flores-Mir, C.; Lagravere, M.O.; Romanyk, D.L. Reliability and accuracy of segmentation of mandibular condyles from different three-dimensional imaging modalities: A systematic review. *Dentomaxillofacial Radiol.* **2020**, *49*, 20190150. [CrossRef] [PubMed]

Disclaimer/Publisher's Note: The statements, opinions and data contained in all publications are solely those of the individual author(s) and contributor(s) and not of MDPI and/or the editor(s). MDPI and/or the editor(s) disclaim responsibility for any injury to people or property resulting from any ideas, methods, instructions or products referred to in the content.

craniomaxillofacial
trauma & reconstruction

MDPI

Article

Advanced Simulation System for Orbitozygomatic Fracture Reconstruction: Multicenter Validation of a Novel Training and Objective Assessment Platform

Enrique Vargas [1,*], Rodrigo Díaz [1], Juan Pablo Vargas [1], Andrés Campolo [1], Rodrigo Villanueva [1], Carlos Cortéz [1,2] and Salvador Valladares-Pérez [1,2]

[1] School of Dentistry, Pontificia Universidad Catolica de Chile, Santiago 7820436, Chile; rdiag@uc.cl (R.D.); jpvargas@uc.cl (J.P.V.); afcampolo@uc.cl (A.C.); rrvillanueva@uc.cl (R.V.); carlos.cortez@uc.cl (C.C.); salvadorvalladares@gmail.com (S.V.-P.)
[2] Metropolitan Clinical Hospital El Carmen, Maipu, Santiago 9251521, Chile
* Correspondence: eovargas@uc.cl; Tel.: +56-9-96001747

Abstract: Orbitozygomatic fractures represent a complex surgical challenge. Given the urgent need for validated educational tools that surpass traditional learning models, this multicenter study developed and validated a novel synthetic advanced simulation model for the reconstruction of these fractures. The model integrates platinum-cured silicones and 3D-printed bony structures with prefabricated fractures, accurately replicating the anatomy and tactile properties of soft and hard tissues, including simulated herniation of orbital contents. To our knowledge, it is the only available synthetic model combining both tissue types for this training. Ten participants (faculty and residents) completed simulated procedures. Technical performance was assessed using a hand motion tracking system, the global OSATS (Objective Structured Assessment of Technical Skills) scale, and a task-specific error measurement (Specific Fault Measurement, SFM) scale. Statistically significant differences (p = 0.021) were observed in operative time and error count between novices and experts, confirming the model's construct validity. Faculty completed the surgery in significantly less time (mean 18.16 min vs. 37.01 min for residents) and made fewer errors (mean 12.25 vs. 53.25). Face and content validity were strongly supported by participant surveys, with 100% stating they would use the simulator to practice before real surgery. A strong inverse correlation (r = –0.786, p = 0.021) between OSATS and SFM scores demonstrated concurrent validity. This model enables ethical, repeatable, and cost-effective training, supporting its implementation into surgical curricula to enhance competence and provide objective skill assessment in orbitozygomatic trauma surgery.

Keywords: surgical education; technical skills; synthetic surgical model; performance feedback; patient safety; OSATS

1. Introduction

According to facial architecture, a direct impact on the eye and/or the orbital rim with sufficient energy to cause fractures typically results in fractures occurring in areas of least resistance [1], primarily the orbital floor and medial wall. However, due to the dynamics of traumatic forces, it is common for the lateral wall to be involved, resulting from a zygomatic displacement that compromises the fronto-zygomatic and spheno-zygomatic sutures.

High-energy trauma (such as motor vehicle accidents) has increased the incidence of this type of fracture [2]. Post-traumatic enophthalmos remains one of the most challenging complications to treat [3], and of particular importance are patients with an orbital

floor fracture and an associated inferior rectus entrapment, as this condition constitutes a surgical emergency.

Complex orbital fractures present significant surgical challenges due to the presence of multiple anatomical structures within the orbital cavity and the limited visibility during surgery [3]. As such, the operative management of facial trauma requires a high level of clinical expertise and advanced decision-making skills [4].

Reconstruction of orbitozygomatic fractures demands not only surgical proficiency but also specialized training in minimally invasive techniques [5,6], which are essential for restoring function while minimizing aesthetic sequelae in the facial region [7].

In this context, surgical simulation has been demonstrated to be an efficient and effective tool for acquiring surgical skills. It offers a safe and realistic environment where trainees can practice surgical techniques, thereby reducing patient risk and improving the confidence and performance of surgical residents [8–10]. Considering that simulation-based teaching tools have proven effective in various educational settings, their incorporation into surgical training programs has become increasingly essential [11,12].

Previous educational models for orbitozygomatic anatomy [13], soft tissue management [14–18], and fracture reconstruction [19,20] have been developed for training purposes. However, to date, soft tissue models lack the capability to simulate deep orbital structures, and 3D-printed orbital models remain insufficient, as they have not been able to replicate the experience of reducing entrapped orbital soft tissues [19].

To our knowledge, no synthetic simulation models combining both soft and hard tissues are currently available for training residents in orbitozygomatic fracture reconstruction techniques [8]. Given that proper handling of soft tissues is crucial to achieving optimal aesthetic outcomes, specialized training is required. Simulation models provide an opportunity for deliberate practice [9], an objective and structured form of training that includes real-time feedback and unbiased evaluation [4].

Thus, we present the development and validation of a novel high-fidelity simulation model and training program through a simulation-based research design in which simulation serves as the subject of investigation rather than merely as a research method. The objectives of this study are to assess face and construct validity, validate a specific rating scale for each task, and describe the development of a high-fidelity synthetic orbitozygomatic reconstruction training model for maxillofacial trainees.

The primary objective of this study is to develop a synthetic simulation model and associated training program for orbitozygomatic fracture reconstruction, with a focus on evaluating its face, content, and construct validity. To achieve this, this study has several specific aims: first, to test the simulation model with a sample of faculty and residents (n = 10) and to determine whether there are statistically significant differences in performance between the two groups; second, to evaluate face and content validity through a structured questionnaire administered to participants; and third, to assess construct validity by measuring surgeons' hand motion parameters using the ICSAD (Imperial College Surgical Assessment Device), evaluating overall surgical performance with the 5-point Likert-based OSATS (Objective Structured Assessment of Technical Skills) scale, and quantifying technical errors in key surgical domains through expert evaluation and a complementary error-specific measurement system.

2. Materials and Methods

This study was written in accordance with the reporting guidelines for simulation-based research, extensions of the CONSORT and STROBE statements [21].

2.1. Simulation Model Construction

The development of the simulation model began by deconstructing orbitozygomatic fracture reconstruction surgery into essential procedural tasks that trainees must master within the training program. These tasks were organized into a standardized surgical protocol, designed to be applied consistently across all evaluated procedures. Two expert maxillofacial surgeons from the Faculty of Medicine at Pontificia Universidad Católica de Chile identified the critical stages of the reconstruction and established a detailed protocol encompassing all steps necessary to complete the surgery, from incision to final closure.

Based on this protocol—and supported by 3D image processing techniques, as well as direct observation of anatomical dissections and live surgical procedures (Figure 1)—a synthetic model was developed to incorporate expert-driven anatomical and procedural recommendations (Figures 2 and 3).



(**a**) (**b**)

Figure 1. The design of the simulator was based on the analysis and observation of anatomical models from the anatomy laboratory of the School of Medicine at the Pontificia Universidad Católica de Chile, as well as in vivo procedures: (**a**) dry human skull specimen; (**b**) anatomical dissection of orbital soft tissues.



Figure 2. Screenshot from an actual training session video analyzed by experts. The video presents two simultaneous views of the phantom during the simulated surgery, allowing experts to evaluate the procedure without any visual obstruction at any point.

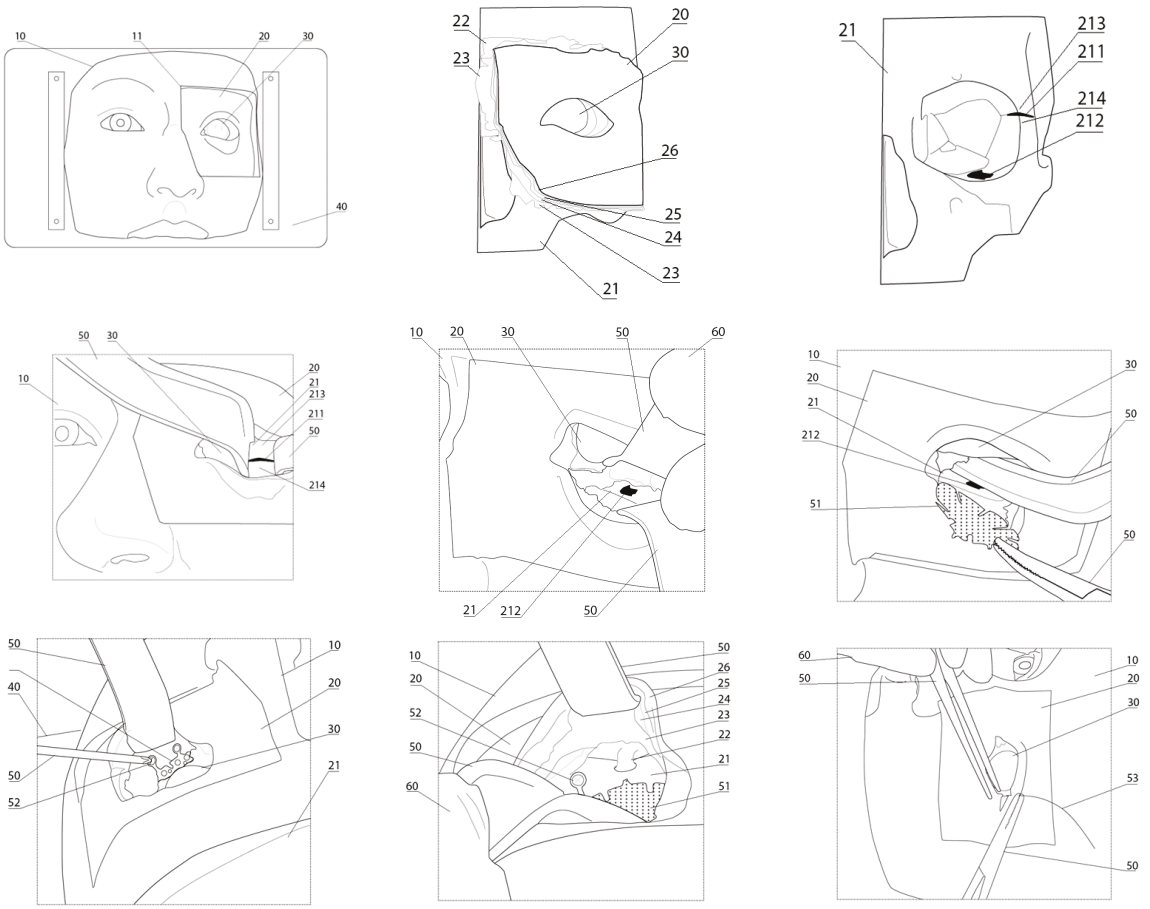

10. Facial structure (PLA).
>11. Opening to access the interchangeable model.
20. Interchangeable model.
>21. Simulated bone (polyurethane-12).
- 211. Frontozygomatic fracture.
- 212. Orbital floor fracture defect.
- 213. Zygomatic process of the frontal bone.
- 214. Frontal process of the zygomatic bone.
>22. Simulated periosteum (silicone).
>23. Simulated connective tissue (silicone).
>24. Orbicularis oculi muscle (silicone).
>25. Subcutaneous tissue (silicone).
>26. Skin (silicone).
30. Eye (silicone).
40. Acrylic stabilization base.
50. Surgical instruments.
>51. Titanium reconstruction mesh.
>52. Osteosynthesis screws.
>53. Suture.
60. Surgeon's gloves.

Figure 3. Description of the simulator components.

To replicate the anatomical characteristics of the human orbitozygomatic region, 3D printing technology was used to fabricate negative molds that accurately reproduced the morphology of both hard and soft midfacial tissues. The digital models were designed and processed using the following 3D modeling and slicing software: Blender 4.2 LTS, Autodesk Fusion 360, Autodesk Meshmixer 3.5.0, Ultimaker Cura 5.7.2, and Bambu Studio v2.1.1. Physical fabrication was performed using Artillery Sidewinder X1 (Artillery, Shenzhen, China), Creality CR-10 Pro (Creality, Shenzhen, China), and Bambu Lab A1 (Bambu Lab, Shenzhen, China) 3D printers, selected based on convenience and the specific technical requirements of each component.

The simulation of hard tissues was achieved using polyurethane-12, while the soft tissues were recreated through incremental layering of platinum-cured silicones, ensuring anatomical and tactile fidelity. The resulting model replicated with high precision the anatomical structures of the midface, particularly the periorbital region and its components. The simulation included representations of the skin, subcutaneous tissue, fat, muscle, periosteum, sclera, conjunctiva, and the infraorbital neurovascular bundle. Each layer was engineered to exhibit the appropriate consistency, color, elasticity, and mechanical resistance of its real-life counterpart. The soft tissues were fabricated using platinum-catalyzed silicone, as follows. For the eyeball, Ecoflex 00:10 silicone (Smooth-On; Macungie, PA, USA) was used with a 20:1 ratio of white to yellow pigment for the sclera. Periorbital fat was simulated using Ecoflex Gel (Smooth-On; Macungie, PA, USA) with 20% Slacker and a 10:1 ratio of yellow to white pigment. Muscle tissue was created using Ecoflex 00:50 (Smooth-On; Macungie, PA, USA) silicone pigmented in blood red. Subcutaneous tissue was produced using Ecoflex Gel with a 5:1 ratio of blood-red to skin-tone pigment. Finally, the skin layer was fabricated using 5% Ecoflex 00:50 silicone with skin-tone pigment. Furthermore, prefabricated fractures were incorporated into the frontozygomatic suture and orbital floor to ensure uniformity across models and to simulate the herniation of orbital contents into the maxillary sinus.

This design enables trainees to become familiar with the use of osteosynthesis materials—including orbital floor mesh, plates, screws, and the corresponding surgical instruments—but, more importantly, it allows them to simultaneously integrate proper technique in soft tissue handling while coordinating all these elements in a cohesive manner. This comprehensive approach significantly enhances both the realism and the educational effectiveness of the surgical training experience.

2.2. Ethics and Participants

This study was formally reviewed and approved by the Institutional Review Board of the Faculty of Medicine at Pontificia Universidad Católica de Chile, Santiago, Chile (approval ID: 230809001).

Prior to participation, all individuals enrolled in the training program completed an initial questionnaire aimed at collecting background information regarding their surgical experience and prior exposure to simulation-based training. The full questionnaire is presented in Table 1.

Sample size estimation was informed by previous validation studies, indicating a minimum requirement of three participants per group (trainees and non-trainees) [22]. Based on a standard deviation of 3.1 and a mean difference of 13.5 from previous findings, a power analysis indicated that at least three experts and three non-expert participants were required to achieve sufficient statistical power [23].

Participants were classified into two groups according to their clinical experience: trainees and faculty. The trainee group consisted of maxillofacial surgery residents in postgraduate years 2 through 4, each having participated in no more than three orbitozygomatic fracture reconstruction procedures. The faculty group included board-certified maxillofacial surgeons with clinical teaching experience; each having performed at least 30 orbitozygomatic reconstruction procedures. All faculty members were affiliated with one of three leading Chilean institutions recognized for their expertise in maxillofacial trauma: Hospital Clínico Mutual de Seguridad (CChC), Hospital de Carabineros (HOSCAR), and Pontificia Universidad Católica de Chile (PUC).

Exclusion criteria included any interruption of clinical activities for a period exceeding six months within the last two years.

Before participating in the simulation session, all individuals completed a standardized orientation session, filled out a demographic survey, and provided written informed consent.

Table 1. Preliminary questionnaire.

Initial Survey—Assessment of Surgical Experience
1. Level of Training in Oral and Maxillofacial Surgery and Traumatology:
☐ Resident ☐ Specialist
2. Years of Experience:
How many years have you been practicing as a Resident or Specialist?
_____years.
3. Current Areas of Professional Practice:
Mark with an X all the areas in which you are currently active:
☐ Teaching activities
☐ Non-surgical clinical practice
☐ Operating room activities
☐ Administrative duties
4. Career Interruptions:
Please indicate whether you have had to suspend your clinical or surgical activities for a period longer than 6 months during your career:
☐ I have never suspended activities for more than 6 months
☐ I have suspended clinical/surgical activities for more than 6 months
Reason: _____
5. Experience with Surgical Simulation:
Have you previously performed surgical simulation using high-fidelity mannequins (phantoms)?
☐ Yes
☐ No
6. Knowledge of the Surgical Procedures to Be Simulated:
Are you familiar with the surgical procedures that will be simulated during the practical session?
☐ Yes, I am familiar with them and have practiced them before
☐ Yes, I am familiar with them, but I have not had the opportunity to practice them
☐ No, I am not familiar with them
7. Practical Experience in Surgical Procedures:
If you had to estimate the number of surgeries in which you have performed these procedures on real patients during your career, what would that number be?
Number of surgeries: _____

2.3. Simulation Assessment

The assessment of the simulation training program was conducted in five phases:

1. Simulated surgeries were performed, during which performance data was collected for each participant. Procedures were video-recorded and assessed with ICSAD to measure performance metrics and evaluate construct validity through motion analysis.
2. Immediately following the procedures, participants completed structured satisfaction surveys aimed at evaluating the face and content validity of the simulation model.
3. Postoperative CBCT evaluation by a blinded radiologist assessed six key aspects using standardized criteria.
4. In the fourth stage, two expert surgeon evaluators, blinded to participant identity and group allocation, reviewed the performance data collected during the first stage. Each participant was assessed using both a global rating scale (OSATS) and a specific objective, fault-based scale (Specific Fault Measurement, SFM) to evaluate technical performance.

5. In the final phase, statistical comparisons were conducted between groups to determine whether significant differences in performance outcomes could be identified.

2.3.1. First Stage: Simulated Surgeries

Participants were paired in dyads, each composed of one trainee and one faculty member, emulating the traditional surgical training model in which an expert supervises and guides a novice through a clinical procedure [24]. In this format, the expert provided real-time guidance to address any gaps in knowledge not explicitly covered by the standardized surgical protocol.

Both participants worked on identical synthetic simulators and were instructed to follow the same standardized surgical protocol to treat an orbitozygomatic complex fracture, which included a blowout fracture of the orbital floor and a frontozygomatic suture fracture. The reconstruction was performed using a minimally invasive technique, employing real surgical instruments on the simulation model.

Construct validity, defined as the simulation system's ability to distinguish between novice and expert performance under standardized, controlled conditions, was assessed by evaluating whether the system could identify performance differences between trainees and faculty—and whether trainees could, over time, approach expert-level proficiency.

In this study, all participants were instructed to follow the procedural steps of the standardized surgical protocol without prior rehearsal.

Each simulation was timed and video-recorded from at least two perspectives, including a first-person point of view and a fixed-camera angle, to ensure comprehensive visualization of the procedure.

Meanwhile, motion tracking data was simultaneously collected using the ICSAD (Imperial College Surgical Assessment Device). Sensors placed on the dorsum of participants' hands (beneath surgical gloves) tracked the position and movement of both hands across three spatial axes.

These metrics were obtained using the ICSAD system, a validated tool for surgical motion analysis that captures spatial and temporal hand performance parameters via inertial sensors [25,26].

Key performance metrics were recorded, including total operative time (in seconds), path length traveled by both hands (in meters), and number of hand movements.

2.3.2. Second Stage: Structured Satisfaction Surveys

Face and Content Validity

The survey consisted of 12 structured items designed to evaluate the simulator's fidelity in replicating real-life surgical procedures. All items were rated using a 5-point Likert scale, with higher scores indicating greater agreement or satisfaction.

This instrument was specifically developed to measure Level 1 (Reaction) of Kirkpatrick's Four-Level Model of training evaluation [27], providing information about participants' perceptions of realism, educational value, and overall satisfaction with the simulation-based experience.

- The Face Validity Survey (Table 2) evaluated the anatomical accuracy and realism of the simulator, assessing whether it provided a convincing surgical environment.
- The Content Validity Survey (Table 3) assessed the simulator's ability to effectively convey the procedural knowledge and technical skills necessary for a successful orbitozygomatic fracture reconstruction.

Table 2. Face validity questionnaire.

Face Validity Statement	Strongly Agree	Agree	Neutral	Disagree	Strongly Disagree
1. The visual appearance of the blow-out fracture looks realistic.					
2. The visual appearance of the frontozygomatic fracture looks realistic.					
3. The phantom accurately simulates the depth and shape of the orbitozygomatic anatomy.					
4. The soft tissues of the orbitozygomatic complex feel realistic when performing the minimally invasive surgical approach.					
5. The cortical bone and cancellous bone feel realistic when drilling and inserting screws.					
6. I believe I would practice with this simulator before performing an actual orbitozygomatic fracture surgery.					

Table 3. Content validity questionnaire.

Content Validity Statement	Strongly Agree	Agree	Neutral	Disagree	Strongly Disagree
7. The simulator achieves overall realism for practicing reconstruction, reduction, and fixation of orbitozygomatic complex fractures.					
8. This simulator is a useful tool for residents to learn how to perform reconstruction, reduction, and fixation of orbitozygomatic complex fractures.					
9. This simulator is a useful tool for training surgeons with prior experience in maxillofacial trauma.					
10. You would consider implementing this simulator as a training model for maxillofacial surgery residents.					
11. This simulator can be used to learn how to perform surgical access to orbitozygomatic complex fractures.					
12. This simulator is suitable for learning how to use the screw, plate, and mesh systems specific to orbitozygomatic complex fractures.					

2.3.3. Third Stage: Cone-Beam Tomography Ancillary Assessment (CBCT)

Postoperative CBCT was captured (Figure 4) and an objective evaluation was conducted by an experienced maxillofacial radiologist, who served as a blinded assessor. The

radiologist systematically assessed six key postoperative outcome aspects in the models using standardized criteria (Table 4), indicating whether each criterion was satisfactorily met.

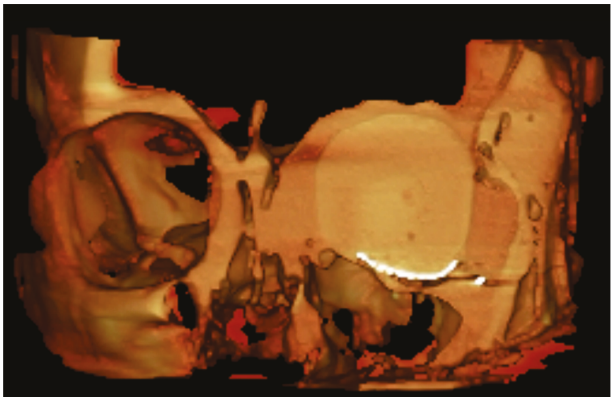

Figure 4. CBCT virtual rendering of the mesh, anterior coronal section.

Table 4. CBCT evaluated categories and their corresponding criteria.

Category	Evaluated Aspect
1. Mesh–bone interface.	Presence or absence of soft tissue at the mesh–bone interface.
2. Mesh/function.	Mesh position preventing or allowing orbital fat protrusion into the maxillary sinus.
3. Mesh/position.	Complete coverage of the orbital floor
4. Mesh adaptation.	Proper anatomical adaptation to the orbital cavity.
5. Mesh positional integrity.	Evidence of displacement, deformation, or rotation.
6. Relationship with maxillary sinus.	Presence or absence of sinus invasion.

2.3.4. Fourth Stage: Evaluation by Expert Surgeons

After the simulation, blinded expert raters—selected from the original faculty group—evaluated each performance using two complementary tools:

a. The OSATS (Objective Structured Assessment of Technical Skills) scale, a 5-point Likert scale evaluating overall surgical competence.
b. The Specific Fault Measurement (SFM) system records and quantifies each procedural error throughout the entire surgery, within the same five defined domains evaluated globally by the OSATS framework.

The evaluators were blinded to participant identity and group assignment and were previously trained in both the protocol and use of the simulation training system. Evaluations were based on multi-angle video footage of each procedure, including point-of-view recordings, to ensure uninterrupted visualization of the surgical field. Videos contained no identifying information about the participants.

OSATS Global Rating Scale (GRS)

Surgical performance was evaluated using the Global Rating Scale (GRS), derived from the widely validated Objective Structured Assessment of Technical Skills (OSATS) framework [28,29]. The scale comprises five key performance domains, each rated on a 5-point Likert scale, where a score of 5 indicates optimal performance in the corresponding domain.

The five domains assessed were

1. Respect for tissue integrity.
2. Avoidance of unnecessary movements.
3. Absence of hesitant or awkward movements.

4. Maintenance of a steady operative flow.
5. Demonstrated procedural knowledge.

Each evaluation could range from a minimum of 5 points to a maximum of 25 points. Since performance was assessed independently by two expert evaluators, the combined score for each participant could vary between a minimum of 10 points and a maximum of 50 points.

To facilitate interpretation of the results, OSATS scores were further categorized into three performance tiers—low, intermediate, and high—based on a standardized performance conversion scale (Table 5).

Table 5. Three-level performance conversion scale.

Performance Level	Score Range
Low	10–23
Intermediate	24–37
High	38–50

Specific Fault Measurement (SFM) Scale

To complement the OSATS framework, a novel evaluation tool was developed as part of this training program: The Specific Fault Measurement (SFM) scale. This complementary assessment instrument was designed to quantify specific technical errors in a detailed and objective manner, addressing the same five core surgical principles evaluated by OSATS but through a fault-based, quantitative lens.

Unlike the global judgment required by the OSATS, the SFM provides a time-stamped recording of procedural transgressions throughout the surgical task. Evaluators documented each error as it occurred, noting both the precise time (minutes and seconds) and the specific domain in which it was committed. All errors were recorded in an error log table, enabling a cumulative error count for each of the five domains.

The total number of errors yielded a numerical SFM score, where higher scores indicate poorer performance. This system enhances the granularity and objectivity of the assessment, and it was specifically designed to improve post-procedural debriefing and feedback. By identifying exact moments and areas of deficiency, instructors are better equipped to guide trainees in developing targeted strategies for improvement and preventing the recurrence of the same errors in future sessions.

The SFM scale was thus developed to serve not only as a validation tool but also as a pedagogical aid, promoting reflective learning and facilitating the design of individualized training plans (Table 6).

Table 6. Surgical error record, organized by five assessment domains contributing to the SFM score.

Category	Type of Error Committed	Number of Errors Observed
1. Respect for Tissue	Violation of appropriate tissue handling.	
2. Unnecessary Movements	Performs unnecessary or non-purposeful movements.	
3. Hesitant or Clumsy Movements	Exhibits hesitation or clumsiness during any part of the procedure.	
4. Operative Flow	Interrupts or disrupts the surgical workflow.	
5. Procedural Knowledge	Demonstrates lack of procedural knowledge by making an error, expressing uncertainty, or requiring clarification on the next steps.	
Total Errors (SFM Score)	**Sum of all errors committed across categories.**	

2.3.5. Fifth Stage: Statistical Comparisons

Statistical comparisons between the trainee and faculty groups were conducted to determine whether the simulator could effectively distinguish between different levels of surgical expertise in search of evidence of construct, face, and content validity.

All data were analyzed using IBM SPSS Statistics, version 27.0.1.0. Descriptive statistics were calculated for all variables. Given the small sample size and the nonparametric nature of the data, construct validity was assessed using the Mann–Whitney U test to identify statistically significant differences in performance between independent groups (trainees vs. faculty). A p-value < 0.05 was considered statistically significant.

The relationship between SFM (Specific Fault Measurement) scores and OSATS (Objective Structured Assessment of Technical Skills) scores was assessed using Spearman's rank correlation coefficient.

To evaluate the internal consistency of the face and content validity questionnaires, Cronbach's alpha was used as a reliability coefficient.

3. Results

A total of 10 participants were recruited for this study, including 6 faculty members (board-certified maxillofacial surgeons) and 4 residents currently enrolled in a maxillofacial surgery training program. Of the total participants, only two reported prior experience with simulation-based training—both from the faculty group, with none of the residents having such experience.

Participant demographic data and clinical experience are summarized (Table 7).

Table 7. Summary of participant demographic characteristics and clinical experience.

Group	n	Age, Mean (Range)	Years in Practice, Mean (Range)	No. of Orbitozygomatic Surgeries, Mean (Range)	No. of Surgeries per Year, Mean (Range)
Trainees	4	33 (29–36)	2.5 (2–4)	0.75 (0–3)	0.19 (0–0.75)
Faculty	6	47 (39–63)	14.8 (7–26)	351.67 (30–1600)	17.12 (4–61.53)

3.1. Construct Validity

Assessment of performance quality using the Global Rating Scale (GRS) from the Objective Structured Assessment of Technical Skills (OSATS) revealed significantly higher scores among faculty members compared to trainees.

As shown in Figure 5, 75% of participants in the trainee group fell within the lowest performance tier, while the remaining 25% were categorized in the intermediate stratum. In contrast, 100% of faculty participants scored within the intermediate or high-performance tiers, with an even distribution of 50% in each category.

The faculty group achieved a median GRS score of 19.5 out of 30 (range: 9–23), whereas the trainee group obtained a median score of 11 (range: 9–20). The mean score difference between the groups was 8.5 points.

The Specific Fault Measurement (SFM), developed to assess the simulation model, demonstrated high internal consistency, with a Cronbach's alpha of 0.8288, indicating strong reliability of the instrument.

Higher SFM scores were observed among trainee participants, whereas all faculty members obtained lower scores, reflecting superior technical performance.

A strong negative correlation was found between SFM and OSATS scores ($r = -0.786$, $p = 0.021$). Given the significance level ($p < 0.05$), the null hypothesis was rejected (Figure 6).

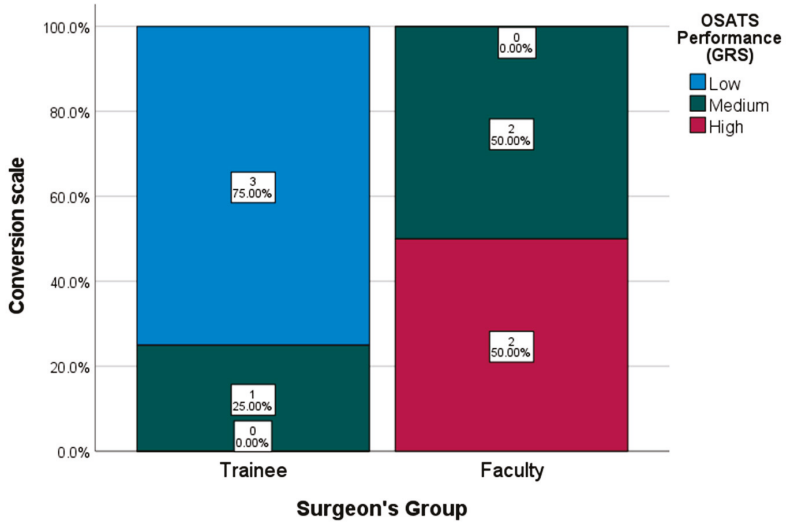

Figure 5. OSATS Performance Conversion Scale (GRS).

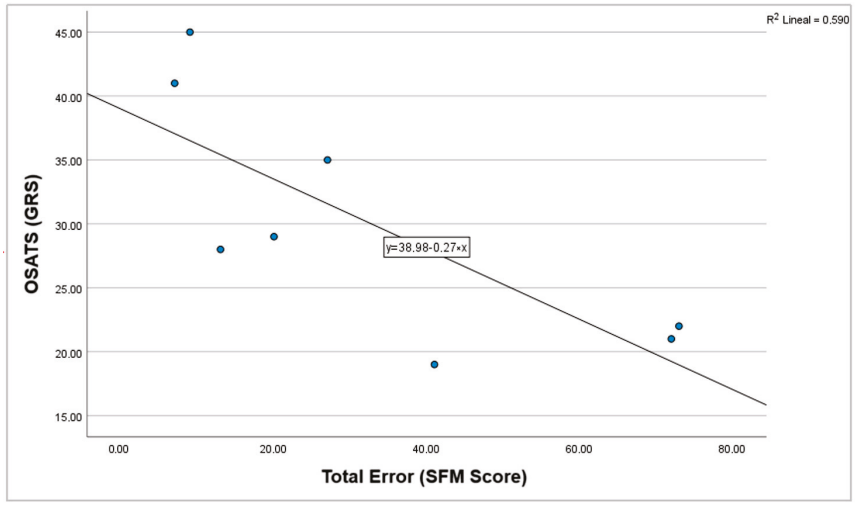

Figure 6. Correlation graph between OSATS (GRS) and total errors (SFM score).

Further analysis confirmed these findings: the faculty group exhibited a significantly lower number of procedural faults compared to the trainee group. The mean number of faults recorded per procedure was 53.25 (SD = 22.95) for the trainee group, compared to 12.25 (SD = 5.73) for the faculty group (p = 0.021). (Figure 7) (Table 8).

Table 8. Specific Fault Measurement (SFM) test statistics.

Statistics			
Specific Fault Measurement (SFM)			
Trainees	N	Valid	4
		Missing	0
	Mean		53.25
	Std. Deviation		22.955
	Minimum		27
	Maximum		73
	Percentiles	25	30.50
		50	56.50
		75	72.75

Table 8. *Cont.*

Statistics			
Specific Fault Measurement (SFM)			
Faculty	N	Valid	4
		Missing	0
	Mean		12.25
	Std. Deviation		5.737
	Minimum		7
	Maximum		20
	Percentiles	25	7.50
		50	11.00
		75	18.25

Test Statistics [a]	
	Specific Fault Measurement (SFM)
Mann–Whitney U	0.000
Wilcoxon W	10.000
Z	−2.309
Asymp. Sig. (2-tailed)	0.021
Exact Sig. [2(1-tailed Sig.)]	0.029 [b]

[a]. Grouping variable: surgeon. [b]. Not corrected for ties.

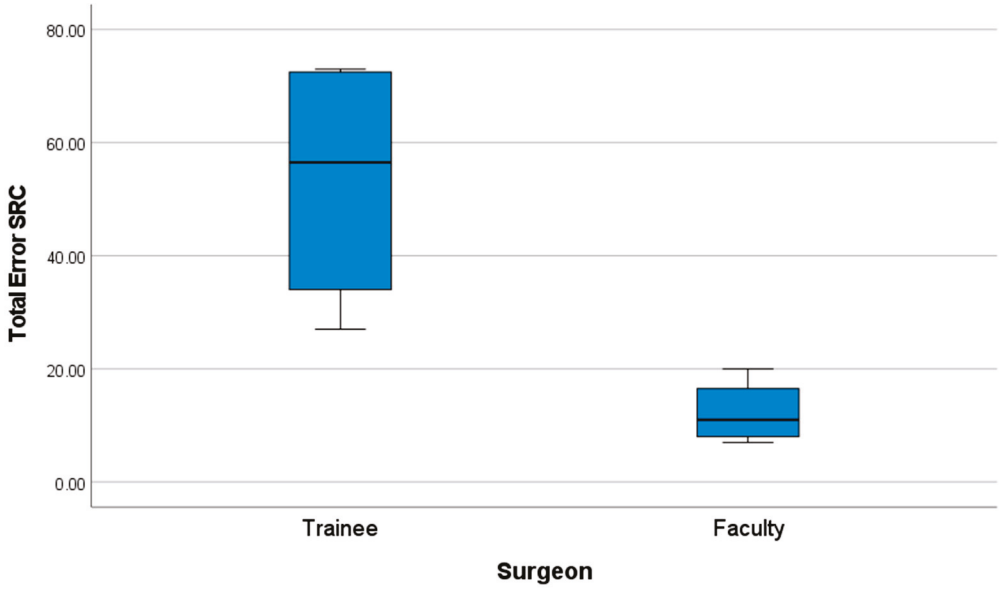

Figure 7. Performance graph of total errors (SFM score).

These results indicate a statistically significant difference in performance between novice and expert surgeons.

3.2. Operative Time Comparison

Faculty members completed the surgical simulation in a significantly shorter time compared to trainees. The mean operative time for the faculty group was 18.16 min (SD = 5.15), whereas for the trainee group, it was 37.01 min (SD = 11.13).

A non-parametric Mann–Whitney U test was conducted to compare operative times between the two groups, revealing a mean difference of 18.85 min. The results confirmed

a statistically significant difference, with a p-value of 0.021 ($p \leq 0.05$), allowing for the rejection of the null hypothesis (Figure 8) (Table 9).

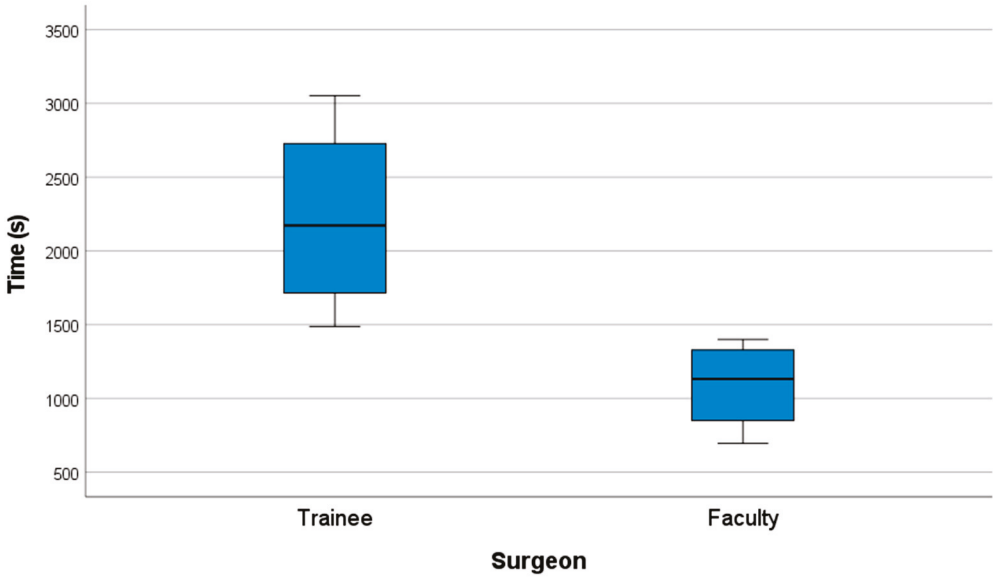

Figure 8. Performance graph of time (s).

Table 9. Operative time comparison test statistics.

Statistics			
Time			
Trainees	N	Valid	4
		Missing	0
	Mean		2221.25
	Std. Deviation		668.360
	Minimum		1488
	Maximum		3053
	Percentiles	25	1601.50
		50	2172.00
		75	2890.25
Faculty	N	Valid	4
		Missing	0
	Mean		1089.75
	Std. Deviation		309.518
	Minimum		695
	Maximum		1400
	Percentiles	25	772.75
		50	1132.00
		75	1364.50
Test Statistics [a]			
			Time
Mann–Whitney U			0.000

Table 9. *Cont.*

Statistics	
Time	
Wilcoxon W	10.000
Z	−2.309
Asymp. Sig. (2-tailed)	0.021
Exact Sig. [2(1-tailed Sig.)]	0.029 [b]

[a]. Grouping variable: surgeon. [b]. Not corrected for ties.

These results indicate a statistically significant difference in performance between novice and expert surgeons.

3.3. Hand Movement and Path Length Analysis

Data on hand movements and path length, collected via the Imperial College Surgical Assessment Device (ICSAD), were available for 8 out of 10 participants. Two faculty members were excluded from this analysis due to technical difficulties: in one case, the sensor detached from the participant's hand, and in the other, a voltage drop caused the ICSAD device to stop recording. As a result, statistical comparisons were conducted on data from four trainees and four faculty members.

Faculty members showed greater economy of motion throughout the procedure.

The mean number of hand movements (movements currently displayed) was 3914.75 (SD = 2341.24) in the faculty group, compared to 5850 (SD = 4074.82) in the trainee group (Figure 9).

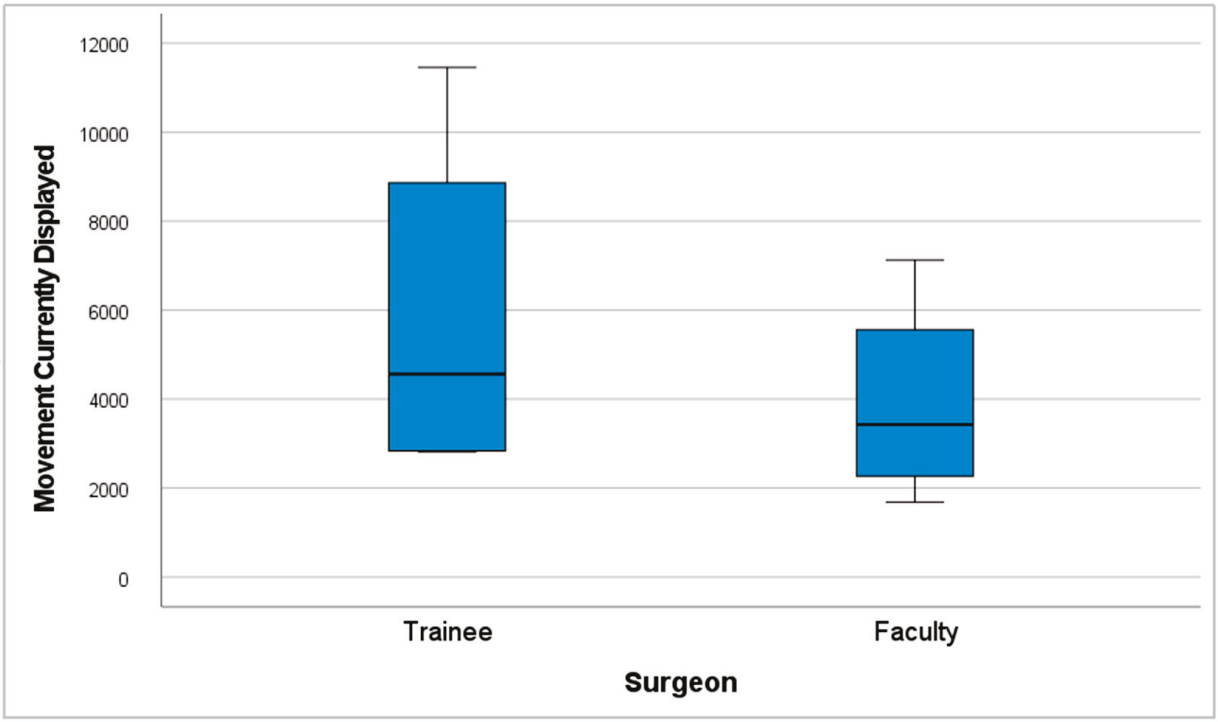

Figure 9. Performance graph of movements currently displayed.

Likewise, the total path length traveled by both hands was shorter among faculty, with a mean of 413.41 m (SD = 208.1), versus 630.66 m (SD = 372.64) for trainees (Figure 10).

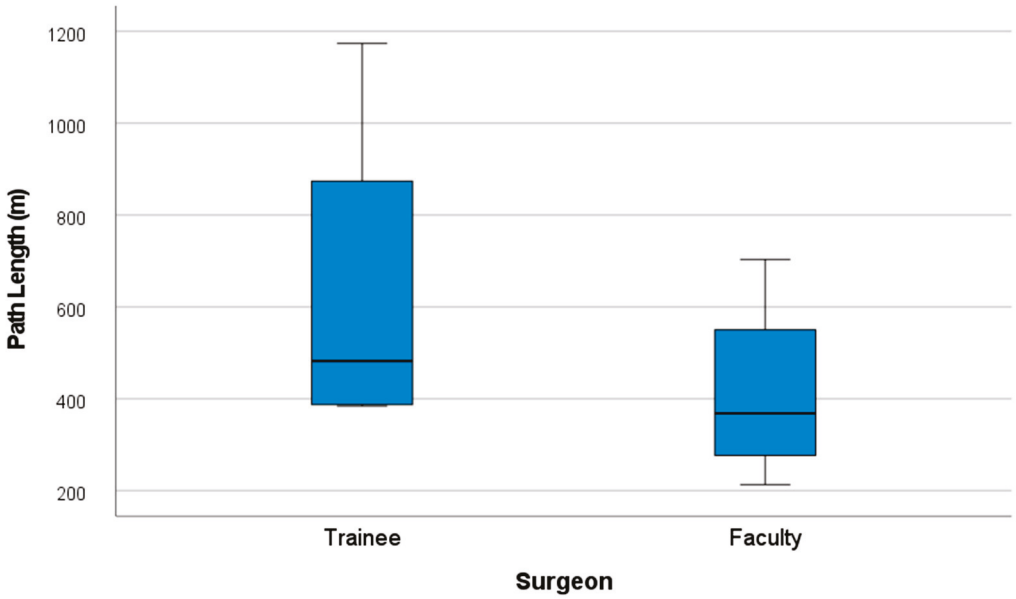

Figure 10. Performance graph of path length (m).

Despite the faculty group showing greater economy of movements with 33.08% fewer movements currently displayed and 34.44% less total path length, a ($p \leq 0.05$) was not obtained in these categories.

3.4. Content and Face Validity

Tables 10 and 11 present the results of the Likert-scale survey used to evaluate both content and face validity, respectively, detailing participants' perceptions regarding the realism and educational relevance of the simulation model.

Table 10. Table shows content validity results.

Content Validity Questions Statement/Answers (N = 10)	Strongly Agree	Agree	Neutral	Disagree	Strongly Disagree
This simulator can be used to learn how to perform surgical access to fractures of the orbitozygomatic complex.	7 (70%)	3 (30%)	0 (0%)	0 (0%)	0 (0%)
I would consider it appropriate to implement this simulator as a training model for maxillofacial surgery residents.	8 (80%)	2 (20%)	0 (0%)	0 (0%)	0 (0%)
The simulator achieves general realism for practicing reconstruction, reduction, and fixation of fractures of the orbitozygomatic complex.	5 (50%)	2 (20%)	3 (30%)	0 (0%)	0 (0%)
This simulator is suitable for learning how to use the screw, plate, and mesh system specific for fractures of the orbitozygomatic complex.	7 (70%)	1 (10%)	1 (10%)	0 (0%)	1 (10%)
This simulator is a useful tool for residents to learn how to perform reconstruction, reduction, and fixation of orbitozygomatic complex fractures.	8 (80%)	2 (20%)	0 (0%)	0 (0%)	0 (0%)
This simulator is a useful tool for training surgeons with previous experience in maxillofacial trauma.	3 (30%)	4 (40%)	1 (10%)	1 (10%)	1 (10%)

Table 11. Table shows face validity results.

Face Validity Questions Statement/Answers (*N* = 10)	Strongly Agree	Agree	Neutral	Disagree	Strongly Disagree
The visual appearance of the Blow out Fracture looks realistic	5 (50%)	4 (40%)	0 (0%)	1 (10%)	0 (0%)
The visual appearance of the frontozygomatic fracture looks realistic.	5 (50%)	3 (30%)	2 (20%)	0 (0%)	0 (0%)
The model adequately simulates the depth and shape of the orbitozygomatic anatomy	6 (60%)	4 (40%)	0 (0%)	0 (0%)	0 (0%)
The soft tissues of the Zygomatic-orbital complex feel realistic when performing minimally invasive surgical access.	1 (10%)	6 (60%)	2 (20%)	1 (10%)	0 (0%)
Realistic cortical bone and cancellous bone feel when drilling and inserting screws	6 (60%)	1 (10%)	1 (10%)	2 (20%)	0 (0%)
Do you think you would practice with this simulator before an actual orbitozygomatic complex fracture surgery?	6 (60%)	4 (40%)	0 (0%)	0 (0%)	0 (0%)

3.4.1. Content Validity

The internal consistency of the content validity questionnaire was evaluated using Cronbach's alpha, which yielded a value of 0.879, indicating good reliability of the instrument.

As shown in Table 10,

- In terms of surgical approach training, 100% of respondents agreed that the simulator could be effectively used to teach access to orbitozygomatic fractures (mean = 4.7 out of 5; SD = 0.48).
- When asked about its applicability to real clinical settings, all participants (100%) agreed that the simulator could be effectively implemented as a training model in maxillofacial surgery residency programs, with the highest possible score in this item (mean = 4.8 out of 5; SD = 0.42).
- A total of 70% of respondents strongly agreed that the simulator achieved an appropriate level of realism for practicing fracture reduction, reconstruction, and fixation in this anatomical region (mean of 4.2 out of 5; SD = 0.92).
- Furthermore, 80% of participants agreed or strongly agreed that the simulator was suitable for learning the application of specific fixation systems, such as screws, plates, and meshes, relevant to the treatment of orbitozygomatic fractures (mean = 4.3 out of 5; SD = 1.34).
- Regarding its educational utility, 80% of participants strongly agreed that the simulator represents a valuable tool for training residents in performing reconstruction, reduction, and fixation procedures for orbitozygomatic fractures (mean = 4.7 out of 5; SD = 0.48).
- Lastly, 70% agreed or strongly agreed that the model is also useful for training surgeons with prior experience in maxillofacial trauma, highlighting its potential for continuing surgical education (mean = 3.7 out of 5; SD = 1.34).

3.4.2. Face Validity

Internal consistency for the face validity questionnaire was assessed using Cronbach's alpha, yielding a value of 0.790, which is considered acceptable reliability for the instrument.

The satisfaction survey results are shown in Table 11.

The results of the satisfaction survey reflected a high perceived level of realism among participants regarding the evaluated simulator.

- A total of 90% of respondents agreed or strongly agreed that the visual appearance of the blow-out fracture was realistic, with a mean score of 4.3 out of 5 (SD = 0.95).
- Similarly, 80% of participants agreed or strongly agreed that the visual representation of the frontozygomatic fracture appeared realistic, with a mean score of 4.3 out of 5 (SD = 0.82).
- Regarding anatomical representation, 100% of participants agreed or strongly agreed that the phantom accurately simulated the depth and anatomy of the orbitozygomatic region, achieving a mean score of 4.6 out of 5 (SD = 0.52).
- For soft tissue realism, 70% of participants reported that soft tissues felt realistic during the minimally invasive surgical approach, with a mean score of 3.7 out of 5 (SD = 0.82).
- In terms of bone structure simulation, 60% of respondents strongly agreed that both cortical and cancellous bone provided a realistic tactile experience during drilling and screw placement, with a mean score of 4.1 out of 5 (SD = 1.29).

Finally, overall acceptance of the simulator: 100% of participants stated that they would use the model as a practice tool prior to performing real orbitozygomatic fracture surgery. This statement also received the highest rating, with a mean score of 4.6 out of 5 (SD = 0.52), reinforcing the simulator's perceived educational value and clinical relevance.

3.5. Cone-Beam Tomography Ancillary Assessment (CBCT)

From this evaluation, four phantoms achieved a flawless outcome, with no errors observed in any of the assessed characteristics; all belonged to the expert group. In contrast, within the novice group, two cases were noteworthy. One case failed to achieve optimal coverage of the bony defect, resulting in only partial coverage. This incomplete coverage led to localized soft tissue infiltration beneath the mesh–bone interface, which subsequently allowed orbital fat herniation into the maxillary sinus cavity.

Additionally, a second novice case showed superior displacement of the reconstruction mesh, secondary to inadequate adaptation along the lateral orbital wall. This mispositioning resulted in soft tissue interposition at the mesh–bone interface and subsequent partial orbital fat protrusion into the maxillary sinus cavity. In both cases, the novices' performance was classified as unfavorable surgical outcomes.

The dataset supporting the findings of this study has been published and is publicly available in the Dataverse repository.

4. Discussion

As shown in Section 3.5 of the Results, novice participants may commit surgical errors during their learning process which, if occurring in real patients, could lead to unfavorable outcomes or postoperative complications—potentially even requiring revision surgery to correct defects. This underscores the critical importance of initial training on phantoms before transitioning acquired skills to real surgical environments.

Clinical skills are typically acquired more rapidly than manual surgical skills, which require extensive training and practice. Consequently, maxillofacial trainees must develop a combination of theoretical knowledge and hands-on surgical experience [30].

Simulation-based education has been shown to effectively transfer technical skills to the operating room [31]. Additionally, previous studies have reported that simulation

programs reduce learning curves [4,9,32], lower surgical training costs [33], and minimize complications associated with medical errors [20,34,35]. Given these advantages, the development of this simulation model may facilitate the practice of key steps in orbitozygomatic fracture reconstruction, particularly for novice trainees, shortening the learning curve.

In this study, we developed a synthetic and anatomically accurate orbitozygomatic fracture reconstruction simulation model as a training tool for maxillofacial surgery trainees. This approach enables the production of multiple identical phantom models, each with the same fractures and preoperative conditions, ensuring repeatability and consistency. These characteristics make the model particularly suitable for maxillofacial training programs, serving both as a training tool and an objective assessment platform for maxillofacial surgery skills.

To the best of our knowledge and based on previously published findings included in patent No. 3766-2024 [36], published on February 14 in the Chilean Official Gazette (CVE 2609714), which is provided as an annex to this manuscript, no other orbitozygomatic fracture simulation model combining both soft and hard tissues currently exists.

This high-fidelity model may be particularly beneficial for junior residents, allowing them to acquire basic competencies more rapidly and take greater advantage of real surgical opportunities [37]. The results of this study demonstrate that training with this simulation model exhibits construct validity, as it successfully differentiates between varying levels of surgical expertise. Specifically, SFM scores and operative time revealed statistically significant differences between faculty members and trainees, underscoring the model's potential as an objective assessment tool for orbitozygomatic fracture reconstruction skills.

All study participants agreed that the phantom accurately simulated the anatomy of the orbitozygomatic region and reported they would use the simulator for practice prior to performing the procedure in real-life surgical scenarios. The mean scores exceeded 4.6 out of 5, indicating high levels of user satisfaction and supporting the model's face validity.

Regarding content validity, all participants evaluated the model's educational effectiveness, stating they would recommend it to peers and support its implementation in maxillofacial surgery residency programs. Additionally, all participants rated the model as a valuable tool for training residents in performing reconstruction procedures for orbitozygomatic fractures, with mean scores above 4.7 out of 5, further demonstrating strong user satisfaction and content validity.

Our findings regarding the model's construct validity, evidenced by significant differences in OSATS scores, SFM (error count), and operative time between faculty and trainees, are consistent with validated simulation training systems across various surgical specialties. For instance, a high-fidelity model for minimally invasive hallux valgus surgery effectively differentiated experts from novices based on Objective Structured Assessment of Technical Skills (OSATS) scores and surgical time [38]. Similarly, a simulation module for ileo-transverse intracorporeal anastomosis demonstrated construct validity through significant differences in OSATS scores and operative times between experience levels [39]. In laryngeal microsurgery, a synthetic model successfully distinguished experts from residents using global rating scales (GRSs), specific rating scales (SRSs), execution time, and path length [22]. Furthermore, a model for endoscopic rectus sheath plication showed that experts achieved significantly higher OSATS and procedure-specific checklist scores than non-experts [40]. These consistent findings across diverse surgical fields underscore the reliability and utility of advanced simulation models in objectively assessing technical skills and differentiating between levels of surgical expertise.

Thus, such validated models actively contribute to improving training standards across surgical specialties, with scientific validation serving as a foundational step in the

development of innovative educational strategies within residency programs, both for teaching and for the summative assessment of trainees.

Beyond construct validity, these studies are increasingly complemented by evaluations of user satisfaction and perceived realism, as these features are essential for engaging both trainees and instructors while enhancing the authenticity of surgical simulation. For example, the laryngeal microsurgery simulation system and the endoscopic rectus sheath plication model both achieved high scores for face and content validity among participating experts [22,40]. Similarly, evaluation of the hallux valgus MIS model revealed high satisfaction with its anatomical representation, handling characteristics, and utility as a training tool [38]. Collectively, these findings reinforce the critical role of simulation in modern surgical education, particularly for complex procedures such as orbitozygomatic fracture repair.

In an era where surgical exposure for residents must be regarded as a limited and valuable resource, simulation provides an accessible and ethical alternative for skill acquisition [41] prior to real surgical procedures. It enables trainees to practice fundamental skills in a controlled environment, ensuring that their initial operative experiences focus on advanced tasks, having already mastered basic techniques on the simulator. This ethical and cost-effective approach to surgical skill acquisition is rapidly evolving across all areas of medicine, and maxillofacial surgery should be no exception. It is expected to become increasingly widespread, supported by multiple studies demonstrating its effectiveness even in unsupervised settings with remote asynchronous feedback [42].

The integration of detailed feedback mechanisms, such as our Specific Fault Measurement (SFM) scale, further enhances its educational value by providing targeted areas for improvement and fostering personalized learning experiences [43]. Looking ahead, this approach aligns seamlessly with broader advancements in educational technologies, including the proven effectiveness of unsupervised simulation with remote asynchronous feedback [42] and the emerging potential of artificial intelligence to provide valuable, objective feedback in surgical scenarios [44]. This evolution in training allows residents to develop proficiency more efficiently, potentially reducing learning curves [38] and boosting self-confidence [41] in a safe, repeatable environment.

4.1. Specific Rating Scale Validation

To ensure a robust evaluation framework, we also developed a Specific Rating Scale (Specific Fault Measurement (SFM) Scale) based on OSATS-defined criteria.

A strong negative correlation was observed between SFM and OSATS scores. Given the significance level ($p < 0.05$), the null hypothesis was rejected, indicating that a high-intensity inverse relationship exists between the two scores. This result supports the convergent validity of the newly developed scale, which aligns with the conceptual framework of both assessment tools. While OSATS scores reflect overall surgical proficiency—with higher scores indicating better performance—the SFM scale quantifies technical errors, where higher scores indicate a greater number of procedural faults; conversely, participants with higher OSATS scores—indicative of superior surgical performance—committed fewer errors on the SFM scale.

Given that the SFM provides granular and domain-specific feedback, it serves as a valuable tool for post-simulation debriefing, helping educators identify precise areas for improvement and tailor feedback more effectively.

Concurrent validity was demonstrated by a strong inverse correlation between SFM and OSATS scores, and construct validity was supported by the significant differences observed between the faculty group and trainee group. Additionally, internal consistency, which measures the reliability of different items within a composite score, was high for

both the SFM and OSATS, indicating that all assessment items contribute meaningfully to the final score.

The traditional apprenticeship model remains the standard method for training surgeons in orbitozygomatic fracture reconstruction, wherein inexperienced surgeons operate on live patients under supervision [24,45].

However, this traditional approach presents significant ethical, logistical, and financial challenges, making it increasingly difficult to justify as the sole training method in modern surgical education.

Moreover, previously developed simulation training models for the maxillofacial region are often low-fidelity, which results in limited educational outcomes and very limited effectiveness in replicating real surgical conditions [8,14–20,46,47]. Alternatively, high-fidelity simulation methods, such as the use of cadaveric specimens, while offering anatomical realism, suffer from major cost-related limitations, with some reports indicating costs exceeding USS 1500 per simulation station used by just two trainees [4].

This synthetic model offers a cost-effective, reproducible, and ethically viable alternative to traditional training approaches, avoiding the drawbacks associated with cadaveric, animal, or virtual reality models.

Despite its advantages, some limitations of the model were noted. One concern raised by participants was the lack of intraoperative bleeding, which facilitated visualization of deep structures and potentially simplified the procedure. Future iterations of the model should incorporate mechanisms to enhance realism by simulating surgical bleeding.

Technical difficulties also affected data collection, as two of ten participants could not be evaluated using the ICSAD tracking system due to unforeseen malfunctions. Despite these exclusions, differences in hand movements and path length were still observed between the trainee and faculty groups.

Thus, a potential limitation lies in the influence of the assessment tools on surgical performance. The use of ICSAD motion sensors and first-person recording cameras, which are not typically employed in live surgical settings, may have affected participant performance. To mitigate this risk, all recording devices were carefully positioned before the procedure, ensuring that the surgeon was comfortable and that no loose or obstructive elements interfered with the surgical process, and pairs of one faculty and one trainee participant always used the exact same equipment to avoid introducing performance bias between groups. At the end, all participants reported feeling comfortable with the setup during surgery, except for one case, in which a motion sensor detached mid-procedure, resulting in the exclusion of that data from analysis. A second exclusion occurred due to a voltage drop that rendered the ICSAD system inoperable for the remainder of the simulation.

Additionally, this study acknowledges that the sample size was relatively small due to the limited availability of surgeons from participating institutions. This limitation indicates that the reliability of the performance-related conclusions is constrained and should be interpreted with caution. This point is further reinforced by our recommendation that future studies include larger sample sizes to enhance the generalizability of the findings. To minimize variability, a standardized assessment protocol was implemented, ensuring that all participants were evaluated under identical conditions using identical fracture models with consistent anatomical characteristics. This approach provided a level of uniformity that is impossible to achieve in live patient surgeries, where anatomical and fracture variations introduce significant confounding factors.

Similarly, a clear advantage arises over cadaveric simulation models—whether human or animal—as, although these can be prepared using standardized protocols, their inherent anatomical variability undermines sample uniformity. As noted in a previous study in

otolaryngology simulation, notable differences in porcine ear specimens were observed, illustrating the challenges posed by biological variability in surgical training [48].

A notable strength of the present study is the consistency and predictability of the synthetic model, which enables repeated training and assessment under standardized conditions. As a result, the only differentiating variable in this study was the surgeons' performance, thereby enhancing the reliability of the assessment outcomes.

4.2. Future Directions

Future studies should incorporate larger sample sizes to improve the generalizability of the findings. Additionally, further research is needed to explore learning curves, as well as the model's external and predictive validity, through applicability studies that assess how skills acquired in simulation translate to real operating room performance, ultimately enabling generalization to patient-based outcomes.

This study is intended to lay the groundwork for a subsequent longitudinal investigation aimed at evaluating residents through repeated performance assessments across multiple sessions. This approach will allow us to accurately determine their learning curve and later assess the impact on their performance in a real clinical setting.

5. Conclusions

The orbitozygomatic fracture simulation model and SFM developed in this study serve as surgical assessment tools for maxillofacial training programs. This low-cost, synthetic model is widely accessible and can be integrated into maxillofacial surgical training programs for skill development and assessment.

In an era of increasing awareness of medical errors and patient safety, there is a pressing need for continuous training of both students and specialists. Ethical constraints prohibit trainees from learning complex procedures directly on patients, while cadaveric and animal-based simulators present inherent accessibility, ethical, and financial challenges. This synthetic model offers a feasible, reproducible, and ethical solution, addressing the limitations of traditional training approaches while providing an objective, standardized, and cost-effective platform for maxillofacial surgical education.

6. Patents

This simulation model was the winner of the LXX Concurso Patentar para Transferir at Pontificia Universidad Católica de Chile and has been granted patent No. 3766-2024 [36], published on February 14 in the Chilean Official Gazette (CVE 2609714).

Author Contributions: Conceptualization, E.V. and S.V.-P.; methodology, E.V. and A.C.; validation, E.V., R.D. and J.P.V.; formal analysis, R.V., C.C. and S.V.-P.; investigation, E.V.; data curation, E.V. and J.P.V.; writing—original draft preparation, E.V.; writing—review and editing, R.D., J.P.V., A.C., C.C. and S.V.-P.; supervision, A.C. and S.V.-P. All authors have read and agreed to the published version of the manuscript.

Funding: This research received no external funding.

Institutional Review Board Statement: This study was conducted in accordance with the Declaration of Helsinki and formally reviewed and approved by the Institutional Review Board of the Faculty of Medicine at Pontificia Universidad Católica de Chile, Santiago, Chile (approval ID: 230809001). Date of approval 2 August 2024.

Informed Consent Statement: Informed consent was obtained from all subjects involved in this study.

Data Availability Statement: The dataset supporting the findings of this study has been published and is publicly available in the Dataverse repository. It can be accessed through the following:

https://doi.org/10.60525/04teye511/CUDFRE. The dataset is licensed under the Creative Commons Attribution-ShareAlike 4.0 International License (https://creativecommons.org/licenses/by-sa/4.0/deed.es) (accessed on 3 June 2025), which permits sharing and adaptation with appropriate credit and under the same license terms. This open access availability supports transparency, reproducibility, and collaborative use within the research community.

Acknowledgments: We express our sincere gratitude for the support and contributions of the following doctors: Ilich Vargas (OMFS), Christian Pedemonte (OMFS), José Ignacio Barrios (OMFS), Alfredo Noguera (OMFS), Juan Alberto O'Ryan, Ramses Palma, and Carlos Ulloa. We are grateful for their valuable input and support throughout the project.

Conflicts of Interest: The only conflict to declare is the intellectual property ownership of the orbitozygomatic fracture reconstruction simulation phantom, which is held 10% by Pontificia Universidad Católica de Chile and 90% by Enrique Octavio Vargas Becerra. None of the other authors or participants declares any additional conflicts of interest.

Abbreviations

The following abbreviations are used in this manuscript:

ICSAD	Imperial College Surgical Assessment Device
OSATS	Objective Structured Assessment of Technical Skills
CONSORT	Consolidated Standards of Reporting Trials
STROBE	Strengthening the Reporting of Observational studies in Epidemiology
PLA	Polylactic Acid
CChC	Hospital Clínico Mutual de Seguridad
HOSCAR	Hospital de Carabineros
PUC	Pontificia Universidad Católica de Chile
SFM	Specific Fault Measurement
GRS	Global Rating Scale
SD	Standard Deviation

References

1. Carl-Peter, C.; Nils, G.; Søren, H.; Kenji, K.; Warren, S. Surgery Reference CMF Trauma Midface Introduction. Surgery Reference AO Fundation. 2025. Available online: https://surgeryreference.aofoundation.org/cmf/trauma/midface/further-reading/introduction?searchurl=/searchresults (accessed on 18 March 2025).
2. Dhar, P.; Jones, J. Electric scooter-related oral and maxillofacial injuries in Oxfordshire. *Br. J. Oral Maxillofac. Surg.* **2024**, *62*, 826–830. [CrossRef]
3. Azarmehr, I.; Stokbro, K.; Bell, R.B.; Thygesen, T. Contemporary Techniques in Orbital Reconstruction: A Review of the Literature and Report of a Case Combining Surgical Navigation, Computer-Aided Surgical Simulation, and a Patient-Specific Implant. *J. Oral Maxillofac. Surg.* **2020**, *78*, 594–609. [CrossRef] [PubMed]
4. Christophel, J.J.; Park, S.S.; Nogan, S.J.; Essig, G.F. A Facial Trauma Simulation Course for Evaluation and Treatment of Facial Fractures. *JAMA Facial Plast. Surg.* **2017**, *19*, 464–467. [CrossRef] [PubMed]
5. Pérez, S.V.; Correa, D.B.; Fuentes, C.C.; Mori, F.A.; Troncoso, G.S.; Sirandoni, R.F. Transconjunctival Approach Using Lateral Skin Extension for Reconstruction of Orbit Zygomatic Complex Fractures: Technique Description and a Case Series Analysis. *Craniomaxillofacial Trauma Reconstr.* **2021**, *14*, 246–253. [CrossRef] [PubMed]
6. Dhupar, V.; Akkara, F.; Gavhane, S.S.; Chodankar, N.U. 'Y' Modification of the cutaneous incision of the preseptal transconjunctival approach for the management of zygomatico-maxillary complex fractures: A prospective clinical study. *J. Stomatol. Oral Maxillofac. Surg.* **2024**, *125*, 101927. [CrossRef]
7. Alshalah, M.E.; Enezei, H.H.; Aldaghir, O.M.; Khalil, A.A.; Aldelaimi, T.N.; Al-Ani, R.M. Direct or Indirect Surgical Approach of Zygomatic Complex Fracture: A Comparative Study. *J Craniofac Surg.* **2023**, *34*, 2433–2436. [CrossRef]
8. Lee, R.; Raison, N.; Lau, W.Y.; Aydin, A.; Dasgupta, P.; Ahmed, K. A systematic review of simulation-based training tools for technical and non-technical skills in ophthalmology. *Eye* **2020**, *34*, 1737–1759. [CrossRef]
9. Meara, D.J.; Coffey Zern, S. Simulation in craniomaxillofacial training. *Curr. Opin. Otolaryngol. Head Neck Surg.* **2016**, *24*, 376–380. [CrossRef]
10. Borgersen, N.J.; Naur, T.M.H.; Sørensen, S.M.D.; Bjerrum, F.; Konge, L.; Subhi, Y. Gathering Validity Evidence for Surgical Simulation. *Ann. Surg.* **2018**, *267*, 1063–1068. [CrossRef]

11. Zargaran, A.; Hirniak, J.; Zargaran, D. Oral and Maxillofacial Surgical simulation: Efficacy for medical students. *Br. J. Oral Maxillofac. Surg.* **2020**, *58*, 1251–1254. [CrossRef]
12. Rojas, F.; Tapia, S.; Campolo, A.; Vargas, A.; Ramírez, H.; Benitez, B.K.; Teuber, C.E. Simulating A Subcondylar Mandibular Fracture With Intraoral Open Reduction and Internal Fixation: A Novel Education Tool for Residents. *Craniomaxillofacial Trauma Reconstr.* **2023**, *16*, 275–280. [CrossRef]
13. Adams, J.W.; Paxton, L.; Dawes, K.; Burlak, K.; Quayle, M.; McMenamin, P.G. 3D printed reproductions of orbital dissections: A novel mode of visualising anatomy for trainees in ophthalmology or optometry. *Br. J. Ophthalmol.* **2015**, *99*, 1162–1167. [CrossRef]
14. Segall, S.C.; Lavell, K.; Brody, A. Lateral Canthotomy and Cantholysis Simulation Device. United States; US11710425B2. 2023. Available online: https://patentimages.storage.googleapis.com/c2/f6/2d/23169e4478b8cb/US11710425.pdf (accessed on 23 May 2025).
15. Ottensmeyer, M.P.; de Novi, G.; Loan, G.J.; Scott Bardsley, R.; Cho Moore, J. Trauma Training Simulator with Event-Based Gesture Detection and Instrument-Motion Tracking. United States; US9595208B2. 2017. Available online: https://patentimages.storage.googleapis.com/03/ee/d6/2f3604d2d8fad7/US9595208.pdf (accessed on 23 May 2025).
16. Hine, J.F. Anatomical Head and Neck Simulator Apparatus. United States; US20240233579A9. 2024. Available online: https://patentimages.storage.googleapis.com/44/9f/6c/d2064605250ada/US20240233579A9.pdf (accessed on 23 May 2025).
17. Gada, S.M.; Liacouras, P.C.; Wyn, M.J.; Garnes, J.A. Ophthalmic Training Simulator. United States; US10410543B2. 2019. Available online: https://patentimages.storage.googleapis.com/60/46/01/8027a0979b8fba/US10410543.pdf (accessed on 23 May 2025).
18. Marson, B.A.; Sutton, L.J. The Newport eye: Design and initial evaluation of a novel foreign body training phantom. *Emerg. Med. J.* **2014**, *31*, 329–330. [CrossRef]
19. Scawn, R.L.; Foster, A.; Lee, B.W.; Kikkawa, D.O.; Korn, B.S. Customised 3D Printing: An Innovative Training Tool for the Next Generation of Orbital Surgeons. *Orbit* **2015**, *34*, 216–269. [CrossRef] [PubMed]
20. Jacobo, O.M.; Giachero, V.E.; Hartwig, D.K.; Mantrana, G.A. Three-dimensional printing modeling: Application in maxillofacial and hand fractures and resident training. *Eur. J. Plast. Surg.* **2018**, *41*, 137–146. [CrossRef]
21. Cheng, A.; Kessler, D.; Mackinnon, R.; Chang, T.P.; Nadkarni, V.M.; Hunt, E.A. Reporting guidelines for health care simulation research: Extensions to the CONSORT and STROBE statements. *Adv. Simul.* **2016**, *1*, 25. [CrossRef] [PubMed]
22. Santander, M.J.; Sepúlveda, V.; Iribarren, J.; Rosenbaum, A.; Albrich, D.; Varas, J.; Napolitano, C. Development and Validation of a Laryngeal Microsurgery Simulation Training System for Otolaryngology Residents. *Otolaryngol. Head Neck Surg.* **2023**, *169*, 971–987. [CrossRef]
23. Kazan, R.; Viezel-Mathieu, A.; Cyr, S.; Hemmerling, T.M.; Gilardino, M.S. The Montreal Augmentation Mammaplasty Operation (MAMO) Simulator: An Alternative Method to Train and Assess Competence in Breast Augmentation Procedures. *Aesthetic Surg. J.* **2018**, *38*, 835–849. [CrossRef]
24. Ayub, S.M. "See one, do one, teach one": Balancing patient care and surgical training in an emergency trauma department. *J. Glob. Health* **2022**, *12*, 03051. [CrossRef]
25. Datta, V.; Mackay, S.; Mandalia, M.; Darzi, A. The Use of Electromagnetic Motion Tracking Analysis to Objectively Measure Open Surgical Skill in The Laboratory-Based Model. *J. Am. Coll. Surg.* **2001**, *193*, 479–485. [CrossRef]
26. Corvetto, M.A.; Fuentes, C.; Araneda, A.; Achurra, P.; Miranda, P.; Viviani, P.; Altermatt, F.R. Validation of the imperial college surgical assessment device for spinal anesthesia. *BMC Anesthesiol.* **2017**, *17*, 131. [CrossRef] [PubMed]
27. Johnston, S.; Coyer, F.M.; Nash, R. Kirkpatrick's Evaluation of Simulation and Debriefing in Health Care Education: A Systematic Review. *J. Nurs. Educ.* **2018**, *57*, 393–398. [CrossRef] [PubMed]
28. Niitsu, H.; Hirabayashi, N.; Yoshimitsu, M.; Mimura, T.; Taomoto, J.; Sugiyama, Y.; Takiyama, W. Using the Objective Structured Assessment of Technical Skills (OSATS) global rating scale to evaluate the skills of surgical trainees in the operating room. *Surg. Today* **2013**, *43*, 271–275. [CrossRef] [PubMed]
29. Martin, J.A.; Regehr, G.; Reznick, R.; Macrae, H.; Murnaghan, J.; Hutchison, C.; Brown, M. Objective structured assessment of technical skill (OSATS) for surgical residents. *Br. J. Surg.* **1997**, *84*, 273–278. [CrossRef]
30. Consorti, G.; Paglianiti, M.; Monarchi, G.; de Tomaso, S.; Cirignaco, G.; Gasperoni, M.; Gennaro, P. New test for systematic skills enhancement and improvement in maxillofacial surgery training: Multicentre pilot study. *Br. J. Oral Maxillofac. Surg.* **2024**, *2*, 716–721. [CrossRef]
31. Boza, C.; León, F.; Buckel, E.; Riquelme, A.; Crovari, F.; Martínez, J.; Gennaro, P. Simulation-trained junior residents perform better than general surgeons on advanced laparoscopic cases. *Surg. Endosc.* **2017**, *31*, 135–141. [CrossRef]
32. Kolozsvari, N.O.; Feldman, L.S.; Vassiliou, M.C.; Demyttenaere, S.; Hoover, M.L. Sim One, Do One, Teach One: Considerations in Designing Training Curricula for Surgical Simulation. *J. Surg. Educ.* **2011**, *68*, 421–427. [CrossRef]
33. Cohen, E.R.; Feinglass, J.; Barsuk, J.H.; Barnard, C.; O'Donnell, A.; McGaghie, W.C.; Wayne, D.B. Cost Savings from Reduced Catheter-Related Bloodstream Infection After Simulation-Based Education for Residents in a Medical Intensive Care Unit. *Simul. Healthc. J. Soc. Simul. Healthc.* **2010**, *5*, 98–102. [CrossRef]

34. Bae, D.S.; Lynch, H.; Jamieson, K.; Yu-Moe, C.W.; Roussin, C. Improved Safety and Cost Savings from Reductions in Cast-Saw Burns After Simulation-Based Education for Orthopaedic Surgery Residents. *J. Bone Jt. Surg.* **2017**, *99*, e94. [CrossRef] [PubMed]
35. Aggarwal, R.; Darzi, A. Simulation to Enhance Patient Safety. *Chest* **2011**, *140*, 854–858. [CrossRef]
36. Vargas, E. *Fantoma Personalizable de Tercio Medio Facial Para Simulación de Reconstrucción de Fracturas Orbito Cigomáticas*; Díaz, F.A.P., Ed.; CVE 2609714; Diario Oficial de la República de Chile, Ministerio del Interior: Santiago, Chile, 2025; p. 1.
37. Coronel, B.V.; Álvarez, R.I.S.; Riveros, F.B.; Schilling, M.M.; Espinoza, V.D.; Jaras, I.M.; Cohen, J.V. Minor surgery course using remote and asynchronous feedback: Training wherever, whenever. *Glob. Surg. Educ. J. Assoc. Surg. Educ.* **2023**, *2*, 109. [CrossRef]
38. Morales, S.; Lam, P.; Cerrato, R.; Mococain, P.; Ruz, C.; Filippi, J.; Villa, A.; Varas, J. A novel simulation model and training program for minimally invasive surgery of hallux valgus. *J. Am. Acad. Orthop. Surg.* **2024**, *32*, e816–e825. [CrossRef] [PubMed]
39. Jarry, C.; Varas, J.; Inzunza, M.; Escalona, G.; Machuca, E.; Vela, J.; Bellolio, F.; Larach, J.T. Design and validation of a simulation-based training module for ileo-transverse intracorporeal anastomosis. *Surg Endosc.* **2025**, *39*. [CrossRef]
40. Rojas, M.F.; Torres, J.; Figueroa, U.; Varas, J.; Achurra, P.; Navia, A.; Cuadra, A.; Searle, S. Validation of a synthetic simulation model of endoscopic rectus sheath plication. *Hernia* **2024**, *28*, 1381–1390. [CrossRef] [PubMed]
41. Ortiz, C.; Vela, J.; Contreras, C.; Belmar, F.; Paul, I.; Zinco, A.; Ramos, J.P.; Ottolino, P.; Achurra-Tirado, P.A.; Jarufe, N.; et al. A new approach for the acquisition of trauma surgical skills: An OSCE type of simulation training program. *Surg. Endosc.* **2022**, *36*, 8441–8550. [CrossRef]
42. Varas, J.; Belmar, F.; Fuentes, J.; Vela, J.; Contreras, C.; Letelier, L.M.; Riquelme, A.; Asbun, D.; Abbott, E.F.; Escalona, G.; et al. Improving medical student performance with unsupervised simulation and remote asynchronous feedback. *J. Surg. Educ.* **2024**, *81*. [CrossRef] [PubMed]
43. Fried, G.M.; Varas, J.; Telem, D.A.; Greenberg, C.C.; Hashimoto, D.A.; Paige, J.T.; Pugh, C. Opportunities and applications of educational technologies in surgical education and assessment. *Ann. Surg.* **2025**, *281*, 34–39. [CrossRef]
44. Trujillo, C.J.; Ulloa, J.V.; Vivas, G.E.; Escobar, E.G.; Gutiérrez, I.V.; Tirado, P.A.; Cohen, J.V. Surgeons vs ChatGPT: Assessment and feedback performance based on real surgical scenarios. *J. Surg. Educ.* **2024**, *81*, 960–966. [CrossRef]
45. Coffey-Zern, S.; Calvi, R.M.D.; Vorrasi, J.S.; Meara, D.J. Incorporating Simulation into Oral and Maxillofacial Surgery Residency Education and Training: Christiana Care's Method. *J. Oral Maxillofac. Surg.* **2015**, *73*, 1244–1245. [CrossRef]
46. Peserico-DalFarra, P.; Gagliardi-Lugo, A.F. Training simulation for oral and maxillofacial surgeons based on the techniques of arthroscopy in the temporomandibular joint. *Br. J. Oral Maxillofac. Surg.* **2019**, *57*, 929–931. [CrossRef]
47. Bertin, H.; Huon, J.F.; Praud, M.; Fauvel, F.; Salagnac, J.M.; Perrin, J.P.; Corre, P. Bilateral sagittal split osteotomy training on mandibular 3-dimensional printed models for maxillofacial surgical residents. *Br. J. Oral Maxillofac. Surg.* **2020**, *58*, 953–958. [CrossRef] [PubMed]
48. Rosenbaum, A.; Faba, G.; Varas, J.; Andrade, T. Septoplasty Training During the COVID-19 Era: Development and Validation of a Novel Low-Cost Simulation Model. *OTO Open* **2022**, *6*. [CrossRef] [PubMed]

Disclaimer/Publisher's Note: The statements, opinions and data contained in all publications are solely those of the individual author(s) and contributor(s) and not of MDPI and/or the editor(s). MDPI and/or the editor(s) disclaim responsibility for any injury to people or property resulting from any ideas, methods, instructions or products referred to in the content.

craniomaxillofacial
trauma & reconstruction

MDPI

Review

Innovations in Clinical Maxillofacial Tissue Engineering and Reconstruction: Cellular Bone Matrix Allografts, Autografts, and Growth Factors

Jeffrey S. Marschall

Department of Oral and Maxillofacial Surgery, University of Iowa Hospital and Clinics, Iowa City, IA 52242, USA; jeffrey-marschall@uiowa.edu

Abstract

Reconstruction of craniomaxillofacial (CMF) bony defects requires individualized strategies based on defect characteristics and graft bed biology, with traditional approaches relying on autogenous non-vascularized bone grafts or vascularized free flaps that, while reliable, are associated with donor-site morbidity and operative complexity. Biologically driven reconstructive strategies, including tissue engineering, cellular bone matrix allografts (CBMs), and growth factor adjuncts, have emerged as alternatives or complements to autograft-based reconstruction. This review introduces and details these new innovations with emphasis on the current literature, thus empowering surgeons to enhance their clinical armamentarium.

Keywords: tissue engineering; bone grafting; cellular bone matrix; growth factors

1. Introduction

Regeneration and reconstruction of bone is a central focus for craniomaxillofacial (CMF) surgeons. The etiology, size, location, and tissues removed and/or missing guide the reconstructive approach. Reconstruction of the craniofacial complex can consist of non-vascularized bone grafts and vascularized tissue transfer. Recently, tissue engineering and allogenic grafts have risen as alternatives for bony reconstruction of the face.

Tissue engineering is the use of a scaffold, cells, and bioactive molecules, such as growth factors, to promote regeneration of a target tissue—specifically, in this case, bone. Two major benefits of using tissue engineering techniques and allogenic components are a possible decrease in operative time and eliminating the need for a second surgical site. Current methods of maxillofacial tissue engineering have been referred to as "in situ tissue engineering" [1–3]. In this scenario, the matrix is generally supplied using allogenic bone, which is osteoconductive; stem cells are provided by a bone marrow aspirate concentrate, which is osteogenic; and the bioactive molecule (growth factor) is rhBMP-2, which is osteoinductive [1–3]. Notably, as with the aforementioned method, a second minor surgical site is required, and multiple adjunctive materials are used. Ideally, a single reconstructive material would be osteoconductive, osteogenic, and osteoinductive. An allogenic material that provides all three components is the cellular bone matrix allograft (CBM, e.g., ViviGen™, LifeNet Health, Virginia Beach, VA, USA). CBMs have been demonstrated to have viable, lineage-committed bone-forming cells within a bony matrix; bone morphogenetic proteins (BMP)-2 and BMP-7; vascular endothelial growth factor (VEGF); and angiogenin [4].

There have been few studies demonstrating the use of CBMs for maxillofacial tissue engineering [5–7]. The purpose of this article is to demonstrate the effectiveness of CBM-based maxillofacial tissue engineering by reviewing the current literature and providing case examples.

2. Cellular Bone Matrix Allografts

Traditional mandibular reconstruction had relied heavily on autologous vascularized bone flaps such as fibula free flaps [8]. These flaps have been reconstructive surgeons' go-to due to reliable revascularization for composite defects. However, donor-site morbidity, operative complexity, and limitations in certain patient populations have motivated the search for alternative biomaterials.

Tissue engineering approaches aim to provide a biologically active scaffold capable of supporting new bone formation while minimizing surgical morbidity. Three major strategies dominate current clinical efforts: 1. cellular bone matrix allografts, which deliver viable osteogenic cells within a preserved extracellular matrix scaffold; 2. non-vascularized bone-grafting techniques that leverage autologous or allogenic bone; and 3. adjunctive biological agents—most notably bone morphogenetic proteins (BMPs)—that stimulate osteoinduction and enhance graft incorporation. Together, these strategies represent a continuum of biologically driven mandibular reconstruction modalities that may augment or replace traditional mandibular reconstruction.

Cellular bone matrices (CBMs) represent a major evolution in allogeneic graft technology and have gained increasing attention as potential alternatives to autogenous bone grafts for maxillofacial reconstruction. Unlike traditional demineralized bone matrix (DBM) or mineralized allograft chips, CBMs are processed to preserve living-donor-derived mesenchymal cells (MSCs) or lineage-committed bone cells (Osteoblasts and Osteocytes) within the native extracellular matrix. These constructs deliver all three essential elements of bone regeneration—osteoconduction, osteoinduction, and osteogenesis—positioning them as a promising modality for craniomaxillofacial applications where volume stability and biologic integration are critical. Commercial CBMs such as Osteocel^{TM} (Globus Medical, Audubon, PA, USA), ViviGen^{TM} (Virginia Beach, VA, USA), and Trinity Elite^{TM} (Orthofix Medical, Lewisville, TX, USA) have been used extensively in spine and orthopedic surgery [9–12], and increasingly in craniofacial applications [5,6].

The biologic basis for CBM or non-vascular bone graft use is simple: the soft tissue bed must be adequate in both quality and quantity (Figure 1) [7,13–15]. Large composite defects and sites that have had previous radiation treatment are contraindications to this reconstructive modality due to inadequate soft tissue and destruction of the microvasculature that will support the CBM or graft. Successful graft incorporation requires rapid revascularization and the recruitment of osteogenic cells capable of producing woven and lamellar bone. CBMs are designed to provide an immediate reservoir of viable cells that may enhance early osteogenesis and accelerate graft integration compared with acellular allografts [16].

Despite CBMs stemming from the same fundamental idea—that is, an allogenic source of osteogenic cells—CBMs can differ substantially across multiple practical and biologic dimensions. These differences influence handling characteristics and cell type; understanding these differences is essential when selecting a CBM for mandibular tissue engineering.

One difference is the composition of the bone matrix that carries the viable cells. Some CBMs are formulated primarily from cortical cancellous allograft chips (e.g., Vivigen^{TM}, Virginia Beach, VA, USA). To enhance handling characteristics, some products contain demineralized fibers (Vivigen Formable^{TM}, Virginia Beach, VA, USA; Trinity Elite^{TM} Orthofix Medical, Lewisville, TX, USA). These products are designed to be easily packed into

https://doi.org/10.3390/cmtr19020018

irregular alveolar or cystic defects and to remain cohesive within titanium mesh constructs. Some manufacturers offer both a solid chip form and a formable variant achieved by adding a carrier that confers malleability without significantly altering osteoconductivity. It is this author's preference to use CBMs that have a fiber component as the handling characteristics are excellent [5,6].

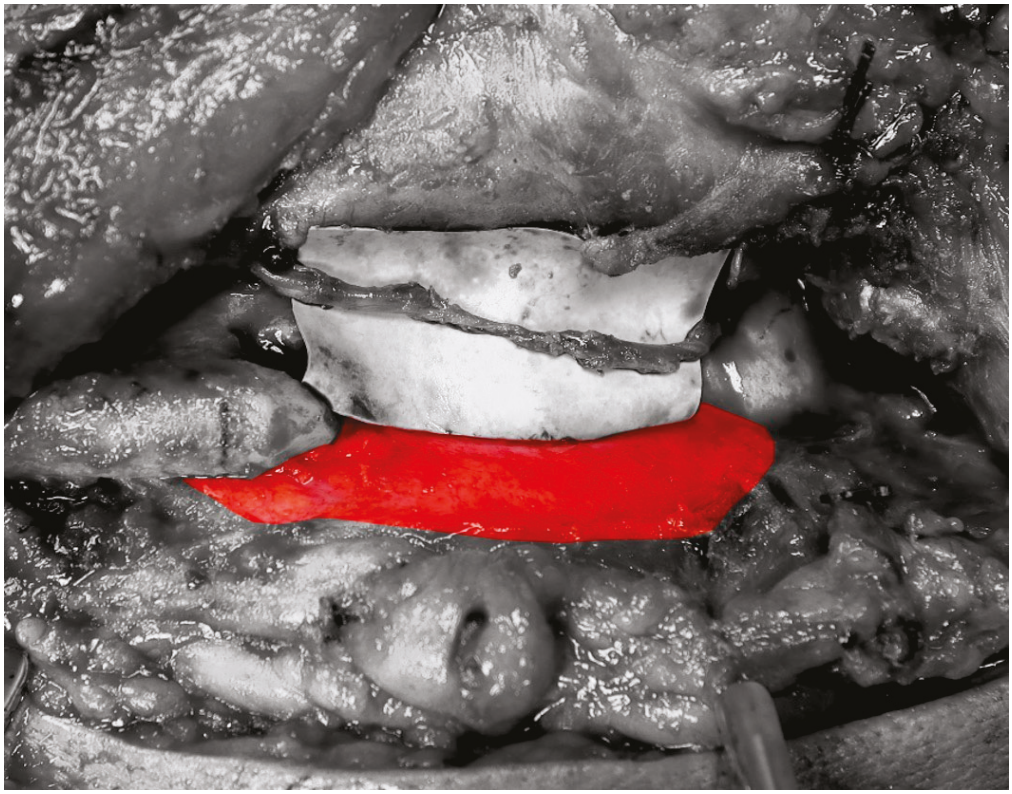

Figure 1. Highlighted area demonstrates healthy periosteum. Graft bed vasculature is essential for mandibular tissue engineering. Radiation and/or composite defects can jeopardize the quantity and quality of the graft bed.

Manufacturing processes are another major point of divergence. CBMs are typically processed using proprietary aseptic techniques prior to cryopreservation. Manufacturers utilize controlled-rate freezing with cryoprotectants (for example, dimethyl sulfoxide, DMSO) or other proprietary formulations; controlled-rate freezing may help minimize cell damage from osmotic membrane imbalance and may reduce ice crystal formation within the cell [17]. For long-term storage prior to shipping to the hospital or point of care, CBMs are maintained in vapor-phase liquid nitrogen tanks, usually around −185 degrees Celsius. Shipping occurs as quickly as possible, usually next-day shipping, with dry ice and special packaging. CBMs are generally maintained in the tissue banks of the medical center at at least −70 degrees Celsius. To maintain cellular viability within the CBMs, rapid-thaw processes are usually implemented. The process is manufacture-specific; therefore, it is important to know the specifics of the product.

Perhaps the most profound differences among CBMs relate to the cellular populations in the product. Some products describe their cellular component as a mixture of viable mesenchymal stromal cells (MSCs), osteoprogenitors, and osteoblast-lineage cells (e.g., Osteocel^{TM} Globus Medical, Audubon, PA, USA); others emphasize lineage-committed bone cells rather than multipotent MSCs (ViviGen^{TM}, Virginia Beach, VA, USA). The distinction matters: MSCs are multipotent and can contribute to osteogenesis (or adipogenesis), whereas lineage-committed bone cells may be more immediately osteogenic but potentially

https://doi.org/10.3390/cmtr19020018

less proliferative [18,19]. Reported post-thaw cell viabilities and cell counts vary both between products and between lots of the same product. There is a range of viable cell yields, with some products reporting higher viable cell counts and in vitro proliferative potential than others [20,21]. MSC-containing products generally have higher cell counts compared to lineage-committed cellular products, but the viability of these cells is lower [20,21]. It is important to note, however, that viability assays do not directly equate to clinical efficacy; viable cell counts are only one determinant of whether a CBM will contribute meaningfully to bone formation in vivo.

CBM safety is a major concern for manufactures, clinicians, and patients. This is influenced by donor screening, aseptic processing, and terminal sterilization (when applied). CBMs generally avoid terminal sterilization to preserve cell viability and are therefore processed aseptically with validated sterility testing. The absence of terminal sterilization raises theoretical infection concerns; in practice, published surveillance and registry data report low rates of infectious transmission with modern tissue banking and donor-screening protocols, although vigilance is warranted [17,22]. Immunogenicity is typically low because mesenchymal-lineage cells express low levels of HLA class II and have immunomodulatory properties; nevertheless, product processing that depletes hematopoietic cells is often highlighted by manufacturers to minimize immune activation [17,22,23].

Preserving viability necessitates cold-chain logistics and on-site thaw protocols. Some CBMs require ultra-low-temperature storage (−70 degrees Celsius) and are delivered on dry ice with immediate thawing during the procedure. Cost per unit varies considerably among products and often exceeds that of conventional allograft, with prices depending on hospital contracting and formulation (formable vs. particulate). Cost-effectiveness analyses are limited; clinicians must weigh the potential reduction in donor-site morbidity and operative time against higher graft acquisition costs.

Selection of a CBM for mandibular tissue engineering should be individualized (Figure 2). Considerations include the defect biology and size (well-vascularized defects may be amenable to CBMs; large composite and/or radiated defects typically require vascularized transfer) and the available clinical evidence for the anatomic site. In practice, CBMs are frequently chosen when the goal is to avoid autograft harvest for lateral/linear continuity defects, whereas surgeons confronting larger mandibular continuity defects may rely on hybrid approaches combining CBMs with autograft [5,7].

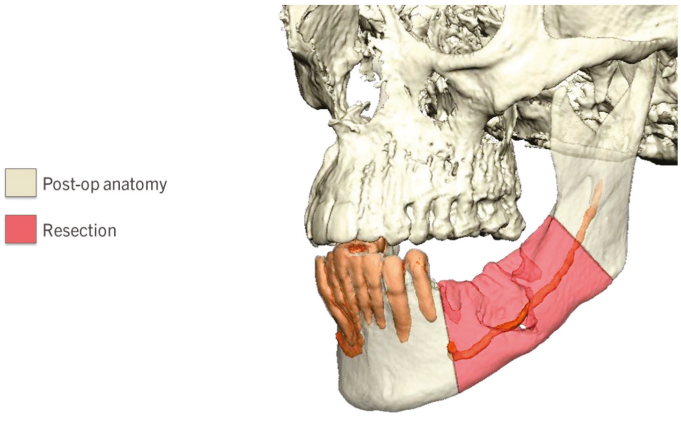

(**A**)

Figure 2. *Cont.*

https://doi.org/10.3390/cmtr19020018

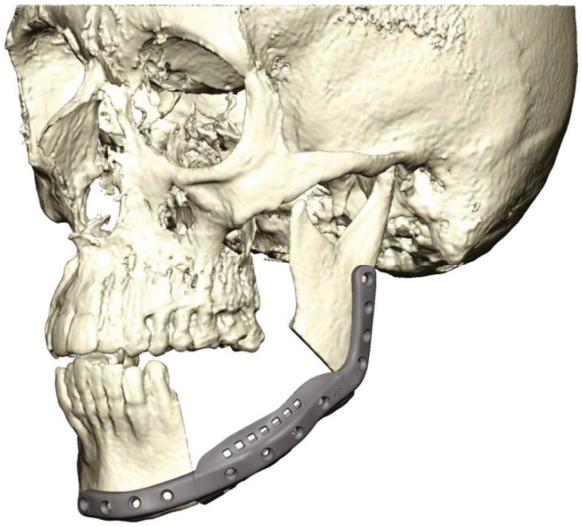

(**B**)

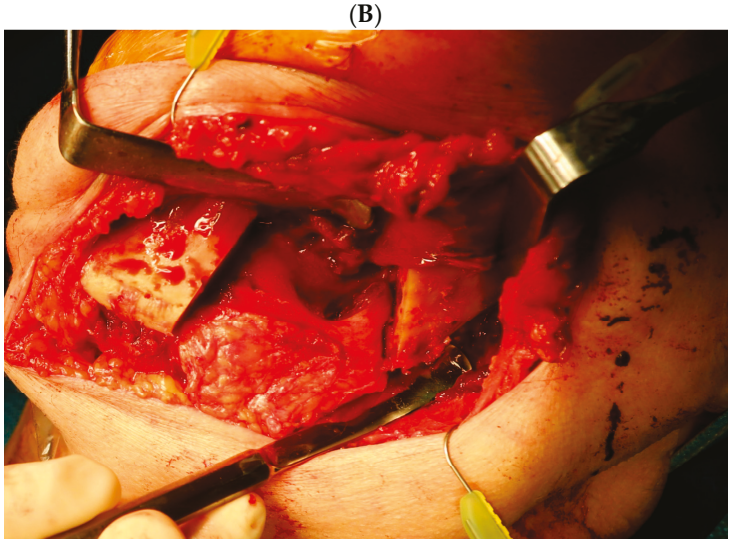

(**C**)

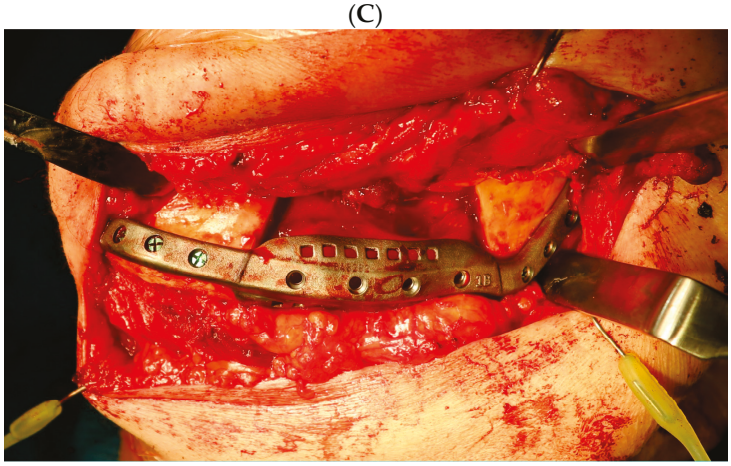

(**D**)

Figure 2. *Cont.*

https://doi.org/10.3390/cmtr19020018

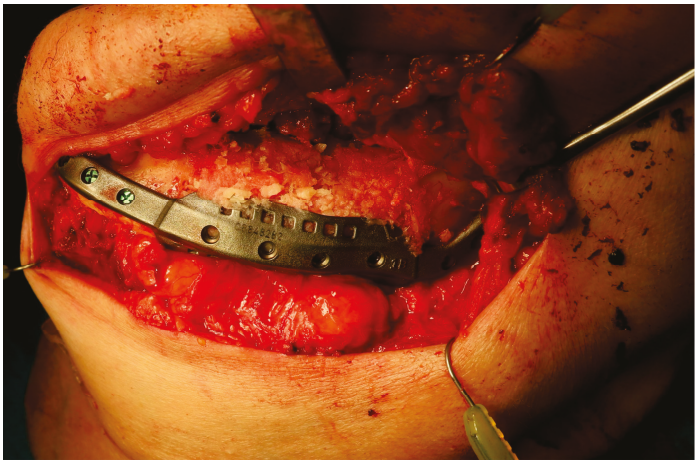

(**E**)

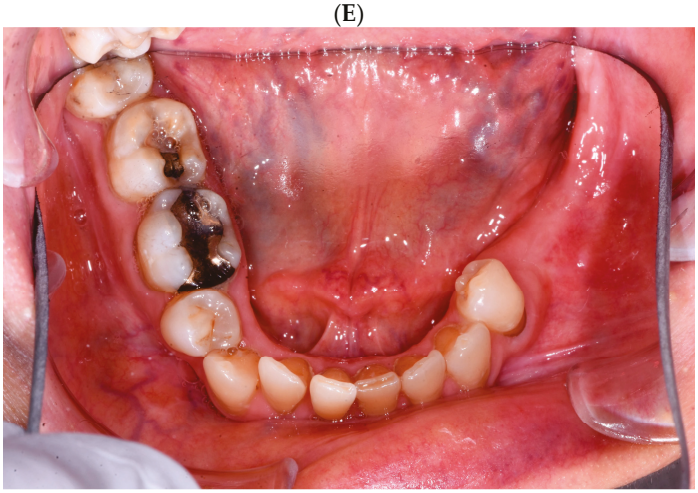

(**F**)



(**G**)

Figure 2. *Cont.*

https://doi.org/10.3390/cmtr19020018

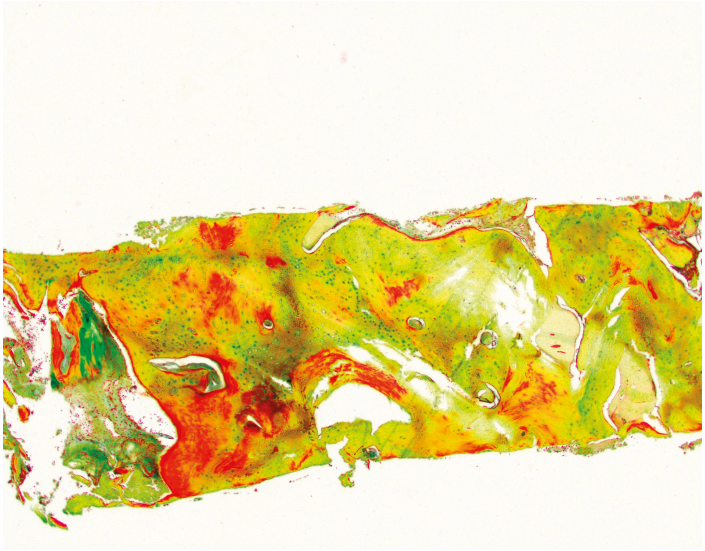

(**H**)

Figure 2. A 78-year-old female with left mandibular pathologic fracture secondary to osteomyelitis that was reconstructed with cellular bone matrix and rh-BMP-2. (**A**) Preoperative imaging from planning session demonstrating area of bone to be resected. (**B**) Resected bone with patient-specific locking reconstruction plate with mesh. (**C**) Clinical photograph of resected mandible and healthy soft tissue bed. (**D**) Patient-specific mandibular reconstruction plate in place. (**E**) Tissue engineering construct (cellular bone matrix and rh-BMP-2) placed into defect site. (**F**) Intra-oral photograph taken 11 months after resection. (**G**) Cone-beam computed tomography scan 3D reconstruction 11 months after resection demonstrating excellent consolidation of bone. (**H**) Bone core taken during endosseous implant placement in a separate patient in a site reconstructed with cellular bone matrix; Orange/red = osteoid; yellow = calcified bone.

Overall, the literature for CBM-based mandibular reconstruction and tissue engineering is limited but growing. The largest series by Marschall et al. [5] included 38 subjects. In total, 50% of the subjects were reconstructed with CBM plus an autograft. Overall success of the reconstructions was 73.7%. Interestingly, subjects with a reported penicillin allergy or a history of diabetes had significantly lower success [5]. This investigation demonstrated the viability of CBM/autograft combination and CBM-based mandibular reconstruction for the first time. There have been several other case reports demonstrating success in geriatric and pediatric patients as well [24,25].

CBM-based reconstruction has also found a niche in maxillary bone defect repair (Figure 3). A recent report demonstrated 87.5% success in 48 subjects. Most of the defects reported in this study were sites reconstructed after extirpation of odontogenic cysts, representing simple bone defects. However, CBMs have been used in cleft orthognathic surgery, and in the management of bilateral oro-sino orbital fistula in bilateral Tessier IV clefts [26,27]. Another intriguing application of CBMs is in cleft maxilla reconstruction [28]. Indeed, this is one of the areas where the author is using this reconstructive modality the most.

CBMs will likely play a larger role in craniomaxillofacial reconstruction. Further investigations are needed to determine the limits of their use. Regardless, the fundamental biologic principles pertaining to their success are similar to those of autograft, which will be discussed next.

https://doi.org/10.3390/cmtr19020018



(**A**)

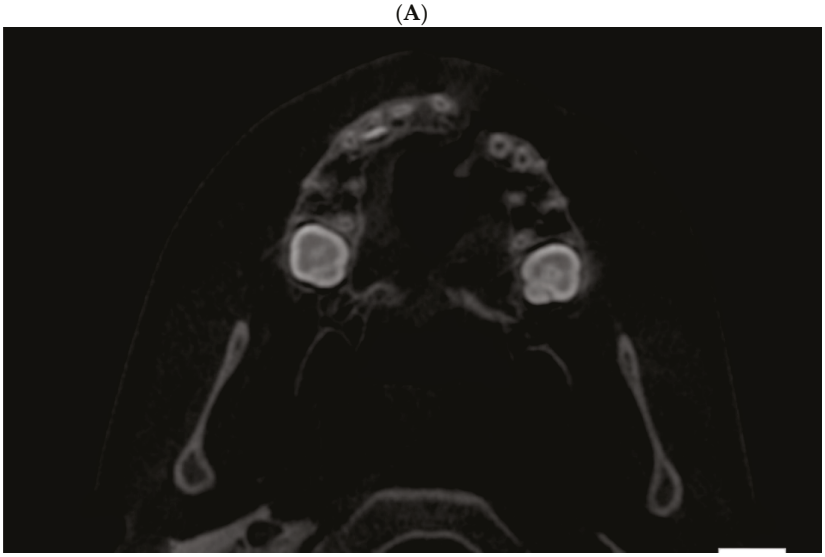

(**B**)

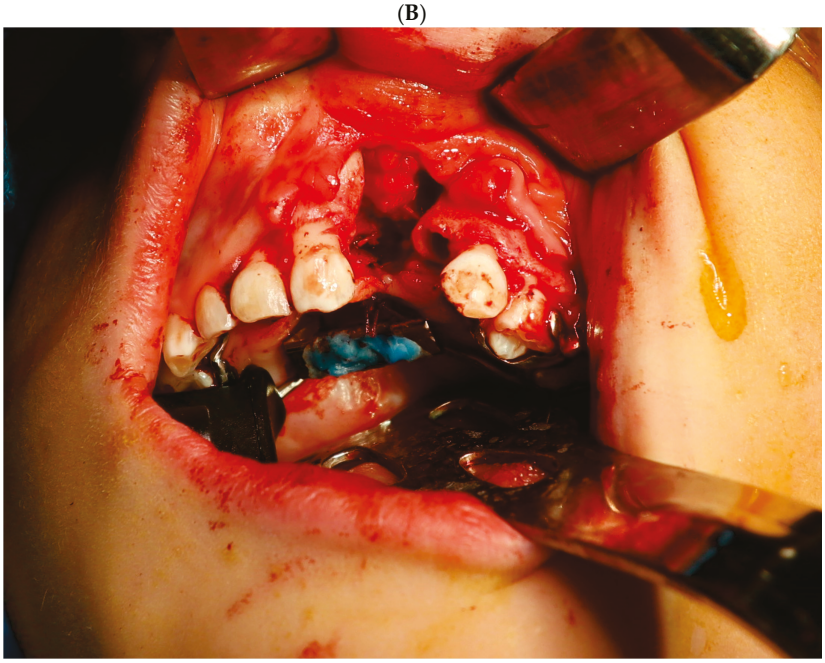

(**C**)

Figure 3. *Cont.*

https://doi.org/10.3390/cmtr19020018

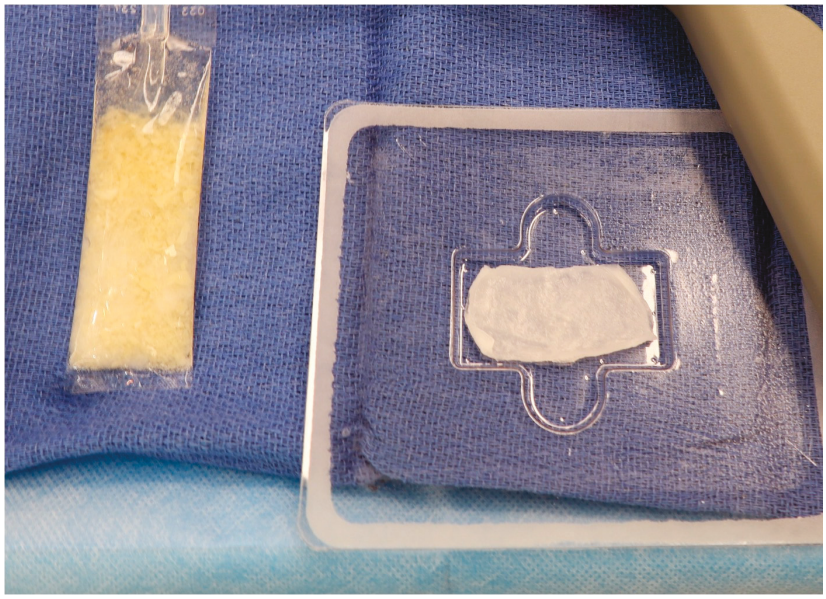

(**D**)

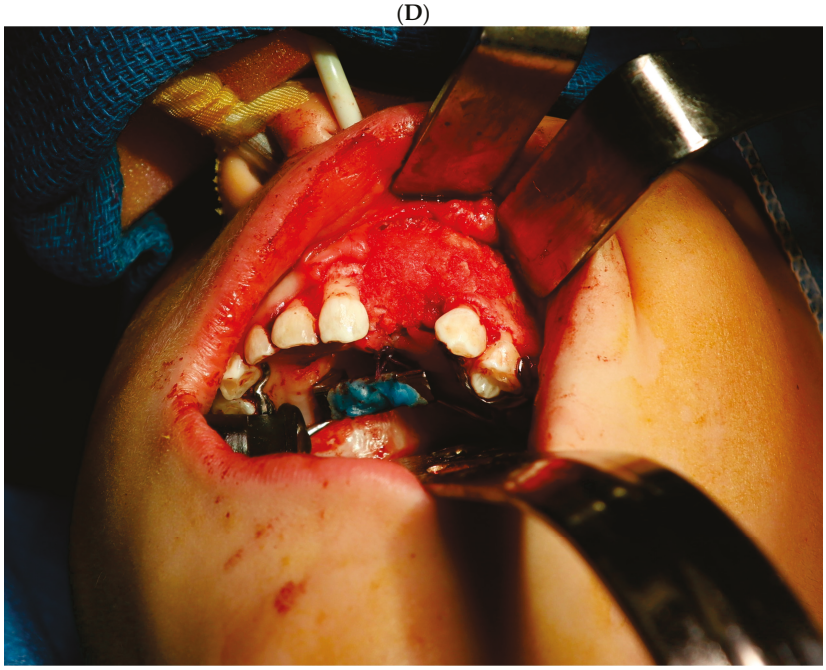

(**E**)

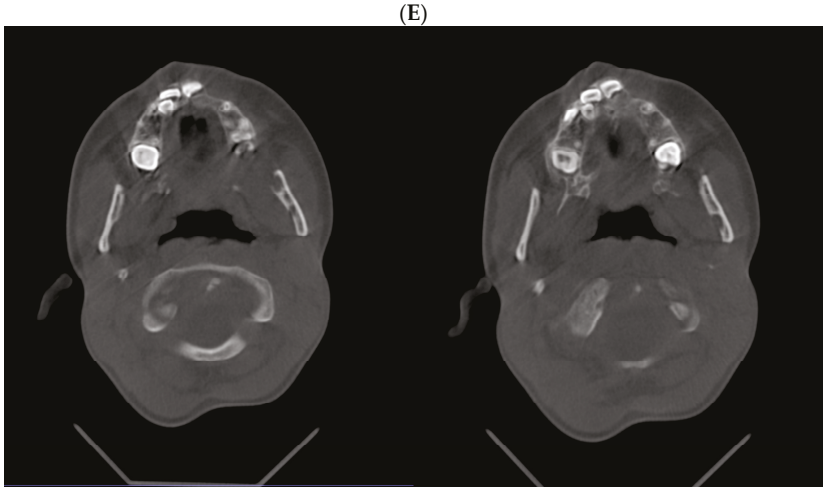

(**F**)

Figure 3. *Cont.*

https://doi.org/10.3390/cmtr19020018



(**G**)

Figure 3. A 6-year-old male with left complete cleft lip and palate that was reconstructed with cellular bone matrix and rh-BMP-2. (**A**) Pre-operative intra-oral photographs. (**B**) Axial cone-beam computed tomography scan demonstrating cleft. (**C**) Intra-operative photograph demonstrating fistula repair and cleft defect. (**D**) Photograph of tissue engineering materials: left—cellular bone matrix, right—rh-BMP-2 sponge. (**E**) Tissue engineering construct placed into cleft maxilla. (**F**) Axial CT scan taken 6 months after surgery demonstrating excellent continuity of the maxilla. (**G**) Intra-oral photograph taken 6 months after surgery demonstrating excellent healing.

3. Autografts

Non-vascularized bone grafts are still an excellent source of cells and bone for mandibular reconstruction. While CBMs are challenging the status quo, autogenous bone remains the gold standard (Figure 4). Non-vascular free bone grafts have traditionally been used for reconstruction of mandibular defects less than 6 cm in length in healthy soft tissue beds that have not been subjected to radiation [15,29]. Recently, the long-standing "6 cm rule" is being challenged [2,7,30–32]. Autogenous non-vascular bone grafts can be harvested as cancellous bone and marrow and cortical and corticocancellous bone. Common locations include the iliac crest and proximal tibia. The tibia bone graft is an excellent source for cancellous bone and is the author's go-to for adult non-vascular bone harvest. This procedure is relatively easy to perform with a low complication rate [33]. Twenty-five cubic centimeters of cancellous bone can be harvested from a single site [33]. Interestingly, an investigation by Engelstad and Morse demonstrated that the proximal tibia yielded a significantly greater mean volume of compressed cancellous bone when compared to the anterior iliac crest [34]. Cancellous bone from the proximal tibia has been demonstrated to be a predictable graft for a variety of mandibular defects, both large and small [5,7,30,35].

As mentioned above, surgeons are challenging the "6 cm rule". Deeper understanding of bone graft biology and new adjuncts are extending the predictability of non-vascularized bone regeneration and reconstruction. Nandra et al. [31] reported that 13 of 14 bone grafts were successful in defects greater than 6 cm. Schlieve et al. [32] reported that of 11 grafts larger than 6.38 cm, 9 were successful and 2 were failures. Marechek et al. [14] added further evidence that non-vascular bone grafts are effective for defects greater than 6 cm. Furthermore, another author has demonstrated predictable reconstruction with autograft alone, CBMs, and growth factors for large segmental defects [5,7,30]. Melville et al. has also demonstrated large mandibular reconstruction via "in situ" tissue engineering methods, which use a combination of rhBMP-2, bone marrow aspirate concentrate, and off-the-shelf allograft [1–3,36]. A common thread from all these studies is that none of the patients

https://doi.org/10.3390/cmtr19020018

had undergone radiotherapy, demonstrating the importance of the graft bed biology and healthy microvasculature.

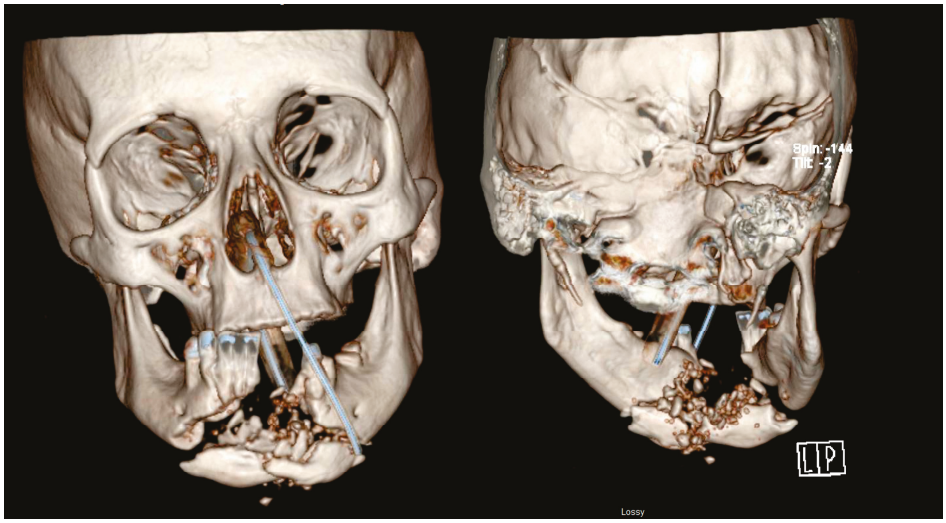

(**A**)

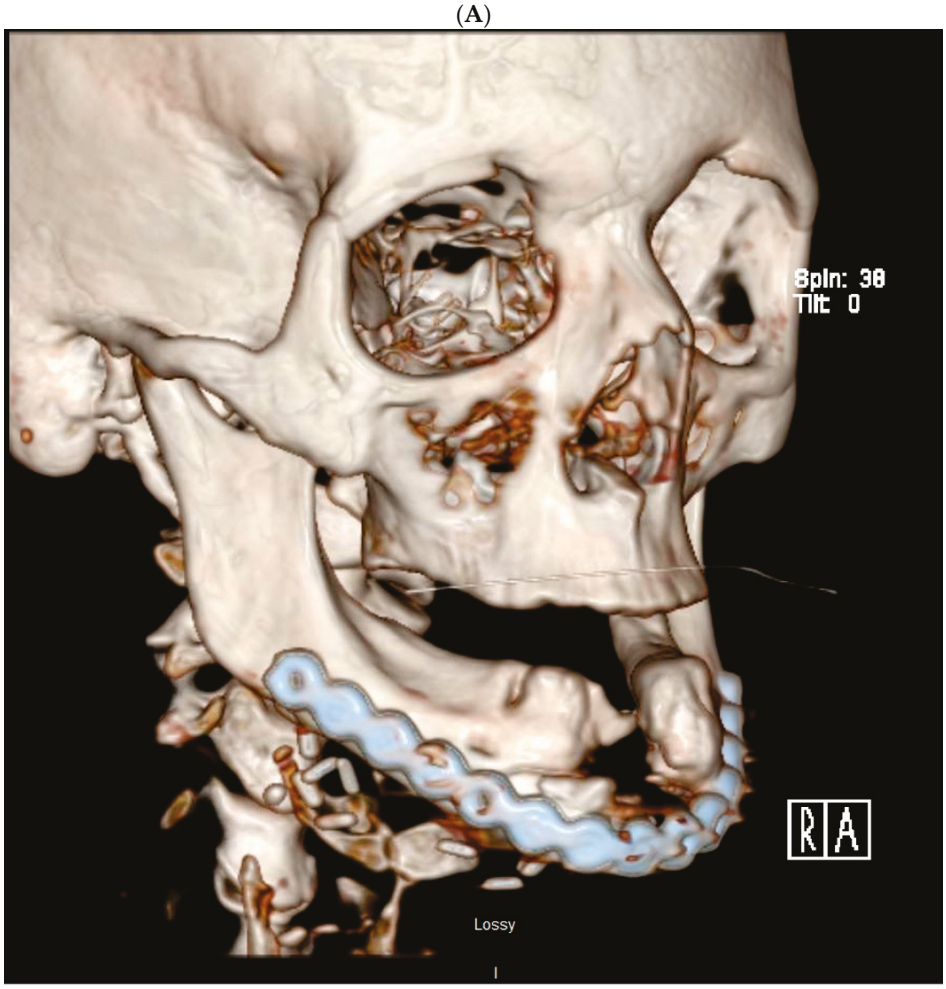

(**B**)

Figure 4. *Cont.*

https://doi.org/10.3390/cmtr19020018

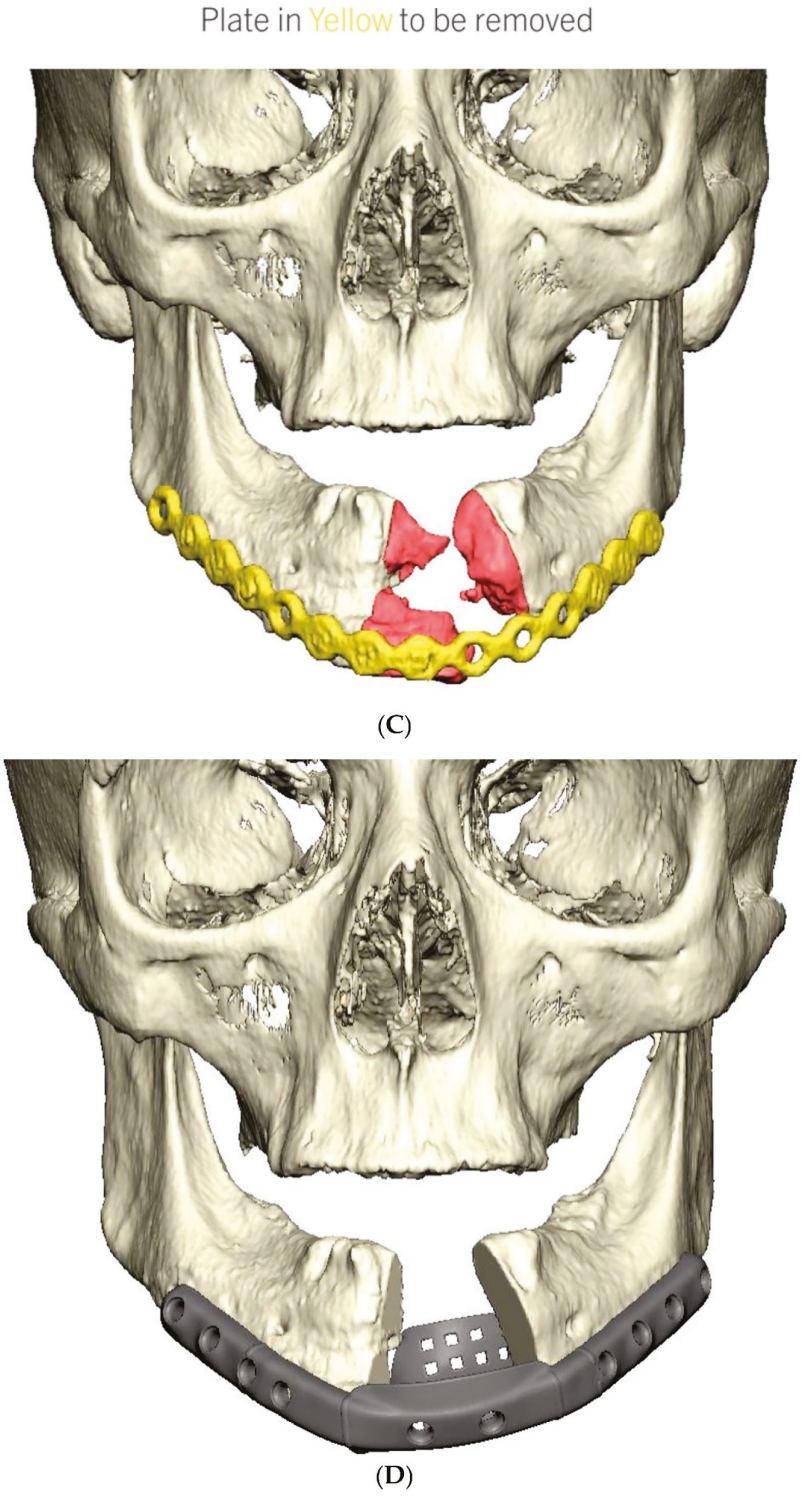

(**C**)

(**D**)

Figure 4. *Cont.*

https://doi.org/10.3390/cmtr19020018



(E)

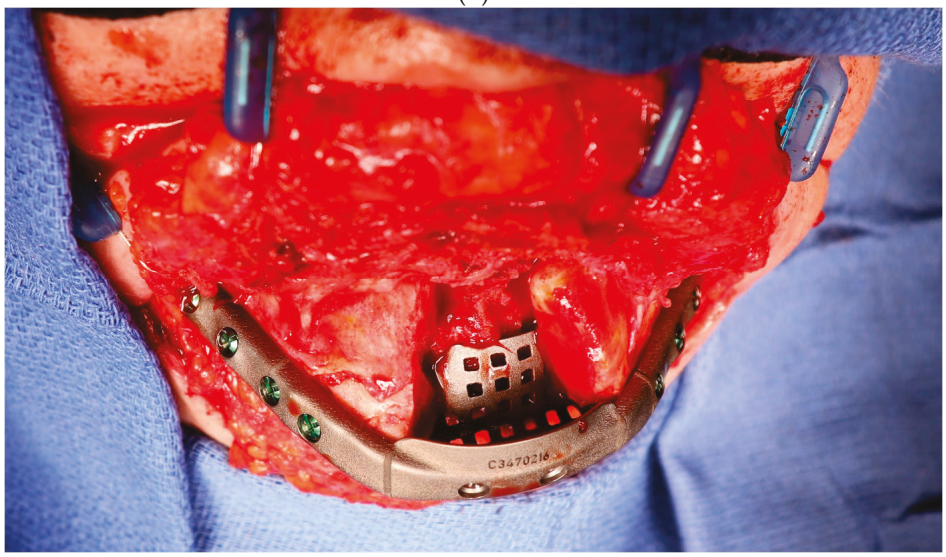

(F)

Figure 4. *Cont.*

https://doi.org/10.3390/cmtr19020018



(**G**)

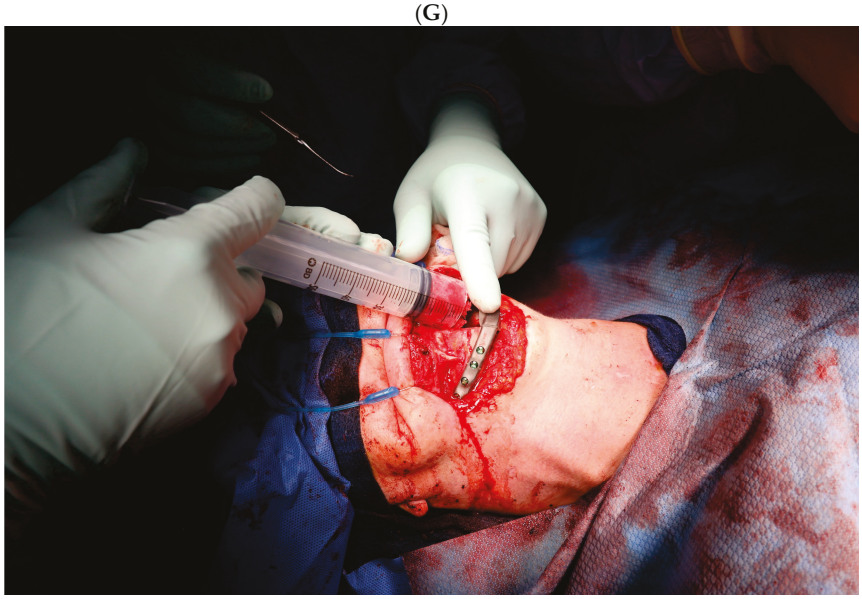

(**H**)

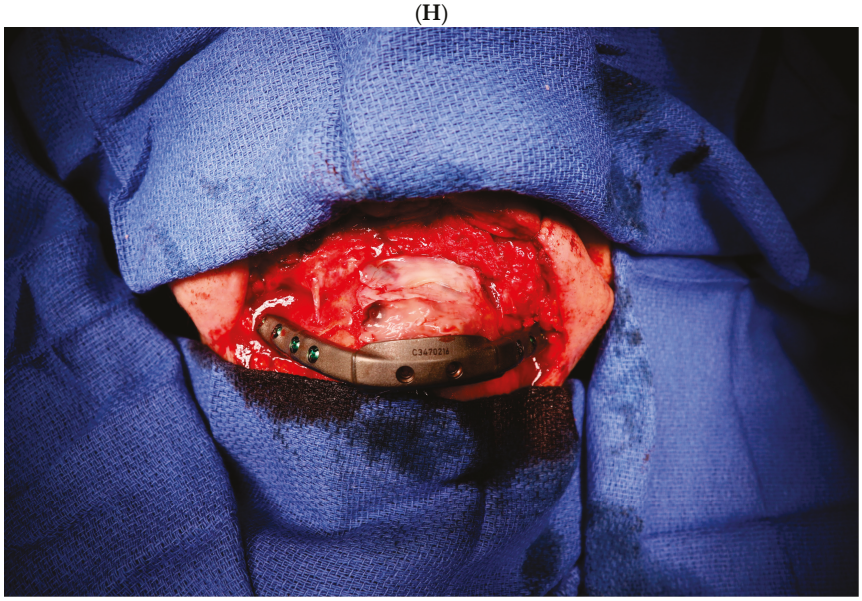

(**I**)

Figure 4. *Cont.*

https://doi.org/10.3390/cmtr19020018

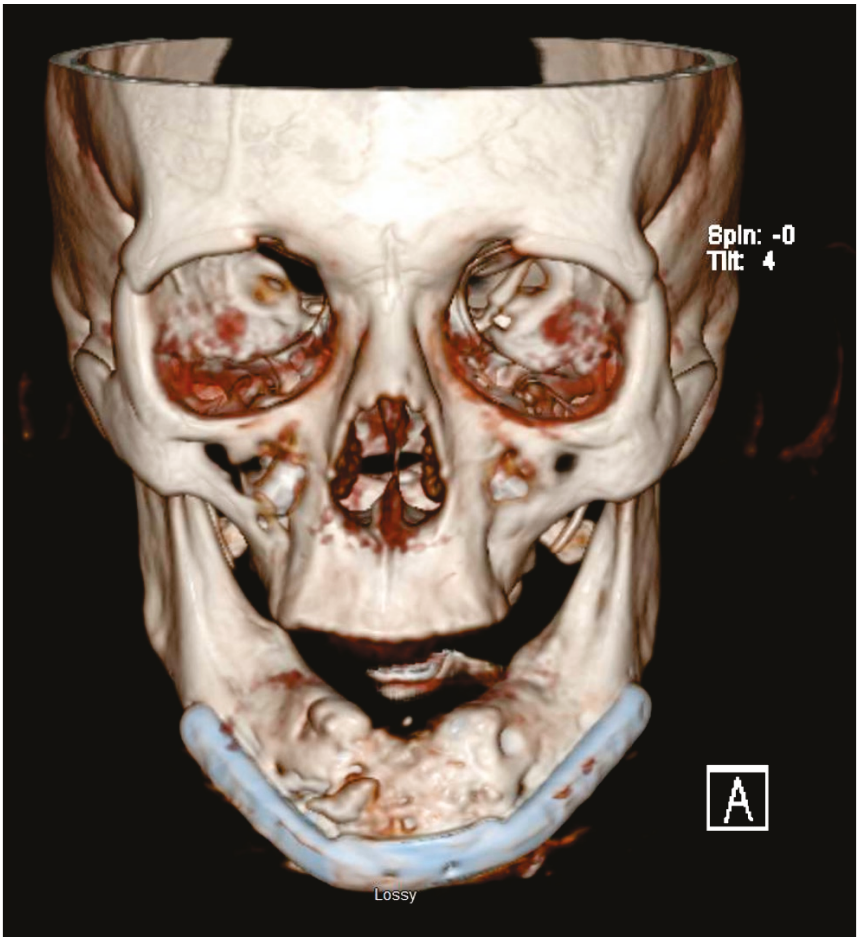

(**J**)

Figure 4. A 44-year-old female that was shot in the face that had original reconstruction plate removed secondary to intra-oral exposure and infection with reconstruction with autogenous bone graft and platelet-rich fibrin. (**A**) Initial CT scan demonstrating mandibular fracture. (**B**) Post-operative CT scan completed by another surgeon demonstrating continuity defect. (**C**) Planned removal of infected plate and bone. (**D**) Patient-specific reconstruction plate and titanium crib. (**E**) Intra-operative photograph demonstrating infected-plate removal. (**F**) Patient-specific reconstruction plate in place. (**G**) Autogenous bone graft in syringe and platelet-rich fibrin membranes. (**H**) Bone graft being placed into defect. (**I**) Bone graft in place with platelet-rich fibrin membranes over graft. (**J**) Post-operative CT scan demonstrating reconstruction of mandibular continuity defect.

4. Growth Factors

Bone regeneration is a dynamic biological process that occurs in three stages: an initial inflammatory response, a subsequent reparative phase, and a final period of remodeling [35,37]. Progression through these stages depends on tightly regulated interactions between signaling molecules and the cellular populations they recruit. Because growth factors play a central role in coordinating inflammation, angiogenesis, and osteogenesis, they have been widely investigated as therapeutic adjuncts to enhance bone healing. Beyond their role in skeletal repair, growth factors govern fundamental cellular behaviors—including proliferation, migration, and lineage commitment—making controlled delivery strategies particularly relevant in regenerative medicine. In oral and maxillofacial surgery, clinically utilized growth factors are generally divided into autologous, blood-derived biologic modifiers and exogenously produced recombinant proteins.

Among autologous biologics, platelet-rich plasma (PRP) represents one of the earliest growth-factor-based therapies to gain broad clinical acceptance [38]. PRP is readily ob-

https://doi.org/10.3390/cmtr19020018

tained via routine venipuncture and contains multiple signaling molecules with known roles in tissue repair, including platelet-derived growth factor, transforming growth factor-β, fibroblast growth factor, insulin-like growth factors 1 and 2, and vascular endothelial growth factor [39,40]. Despite these advantages, PRP is limited by considerable interpatient variability and a rapid, short-lived release of growth factors. In physiologic wound healing, growth factors are embedded within the extracellular matrix and exert their effects over extended periods, often lasting days to weeks [41]. Platelet-rich fibrin (PRF) was subsequently introduced to better approximate this natural release profile (Figure 4) [42]. Contemporary tissue engineering principles emphasize the importance of a three-dimensional scaffold capable of supporting cellular infiltration and differentiation, ideally with incorporated biochemical cues. In PRF, a fibrin-based matrix functions as both a scaffold and a reservoir for platelets and leukocytes, creating a biologically active construct rich in growth factors. The entrapment of these signaling molecules within the fibrin network results in more sustained and physiologically relevant release kinetics [40]. These features have contributed to the expanding clinical use of PRF in procedures such as reconstruction following extensive mandibular resection [5,13,30].

Bone morphogenetic proteins (BMPs) were first described in the mid-twentieth century and are now recognized as members of the transforming growth factor-β superfamily. This group consists of approximately 20 related proteins with demonstrated roles in angiogenesis, inflammation, programmed cell death, and the formation of bone and cartilage [43]. BMP-2, in particular, has emerged as one of the most potent osteoinductive agents identified to date [44]. Its biological activity is mediated through binding to specific receptors on undifferentiated mesenchymal cells, triggering intracellular signaling via SMAD transcription factors [43]. Activation of this pathway promotes osteoblastic differentiation, directed cell migration, new bone formation, and synthesis of extracellular matrix [43]. The ability of BMP-2 to induce bone formation is especially valuable when used in conjunction with allograft or xenograft materials, which lack inherent osteoinductive properties; in this context, BMP-2 may enhance host cell infiltration and render these substitutes functionally closer to autologous bone [2,3,35,45–48]. Recombinant human BMP-2 (rhBMP-2; Infuse, Medtronic) is currently available for clinical use. Multiple studies have shown that rhBMP-2, delivered on an absorbable collagen sponge and combined with allo- and/or xenografts, achieves outcomes comparable to, and in certain scenarios superior to, autologous grafting in alveolar cleft repair [49] and reconstruction of critically sized defects of the maxilla and mandible [44,45]. In maxillofacial surgery, the most commonly described complications include pronounced post-operative edema, erythema, and dysphagia [49]; however, these effects are typically transient, rarely compromise overall graft success, and are likely due to supraphysiologic dosing. The author recommends not exceeding a medium-size BMP sponge. Indeed, an extra-extra-small or extra-small BMP sponge is adequate for most maxillofacial applications.

5. Conclusions

Reconstruction of maxillofacial bony defects requires careful consideration of defect characteristics, soft-tissue-bed biology, and the biologic properties of the reconstructive material. Autogenous bone grafting, cellular bone matrix allografts, and growth-factor-based adjuncts each represent distinct but overlapping strategies grounded in the fundamental principles of osteoconduction, osteoinduction, and osteogenesis. Autogenous non-vascularized bone grafts remain a reliable and well-established option for appropriately selected defects in well-vascularized tissue beds, and recent evidence suggests their utility may extend beyond traditionally accepted size limitations when host biology is favorable.

https://doi.org/10.3390/cmtr19020018

Cellular bone matrix allografts represent an evolution in allogeneic graft technology, offering the potential to deliver viable osteogenic cells within an extracellular matrix while avoiding donor-site morbidity. Although CBMs differ in matrix composition, cellular content, processing, and handling characteristics, early clinical experience in mandibular and maxillary reconstruction demonstrates that they may be effective in selected non-radiated defects, either alone or in combination with autograft. Growth factors, including platelet-derived products and recombinant BMPs, further augment reconstructive strategies by modulating the biologic environment and enhancing osteogenesis, particularly when used within appropriate dosing parameters.

The author's preferred mandibular reconstructive strategy is summarized in Figure 5. In defects with compromised graft bed biology—such as those associated with prior radiation therapy and/or composite tissue loss—vascularized free tissue transfer is favored. For defects measuring <8 cm, a tissue engineering approach using CBM combined with a growth factor source (rhBMP-2 and/or PRF) is employed. For defects measuring 8–10 cm, autologous bone grafting from the proximal tibia or iliac crest is incorporated into the construct. For defects >10 cm, free tissue transfer remains the most reliable and predictable reconstructive modality [5,7,30].

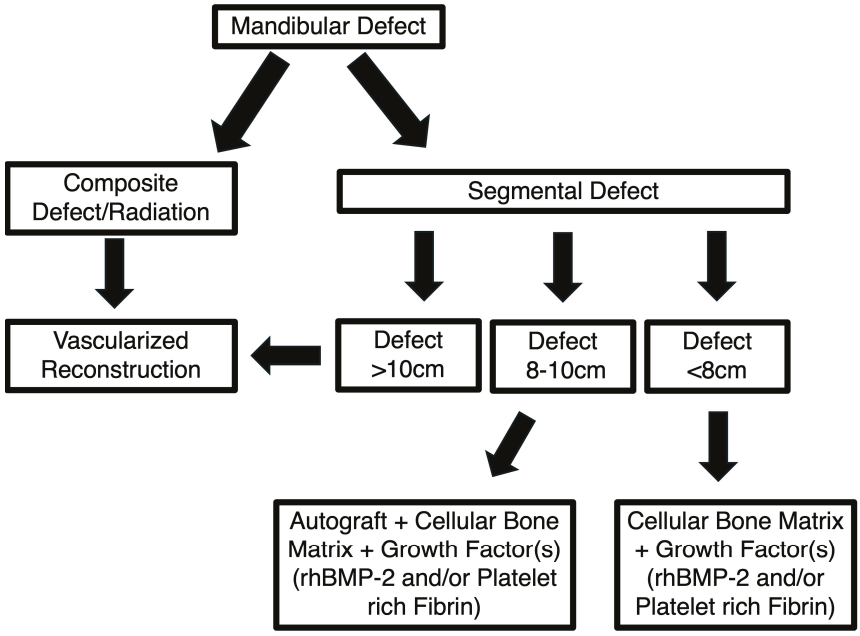

Figure 5. The author's treatment algorithm for mandibular reconstruction.

Collectively, these biologically driven approaches expand the reconstructive armamentarium available to craniomaxillofacial surgeons and underscore the importance of defect-specific planning and soft-tissue-bed quality. While the existing clinical literature remains limited, current evidence supports the selective use of CBMs, autografts, and growth factor adjuncts as complementary tools. Continued clinical investigation and longer-term outcome data will further define their respective roles and limitations in craniomaxillofacial reconstruction.

Funding: This research received no external funding.

Institutional Review Board Statement: Ethical review and approval were waived for this study because the manuscript is a review.

Informed Consent Statement: Patient consent was waived due as patients cannot be identified.

https://doi.org/10.3390/cmtr19020018

Data Availability Statement: No new data were created or analyzed in this study.

Conflicts of Interest: Dr. Marschall serves as a consultant for LifeNet Health.

References

1. Melville, J.C.; Tran, H.Q.; Bhatti, A.K.; Manon, V.; Young, S.; Wong, M.E. Is Reconstruction of Large Mandibular Defects Using Bioengineering Materials Effective? *J. Oral Maxillofac. Surg.* **2020**, *78*, 661.e1–661.e29. [CrossRef]
2. Melville, J.C.; Nassari, N.N.; Hanna, I.A.; Shum, J.W.; Wong, M.E.; Young, S. Immediate Transoral Allogeneic Bone Grafting for Large Mandibular Defects. Less Morbidity, More Bone. A Paradigm in Benign Tumor Mandibular Reconstruction? *J. Oral Maxillofac. Surg.* **2017**, *75*, 828–838. [CrossRef]
3. Melville, J.C.; Rethman, B.; Kaleem, A.; Patel, N.; Marx, R.E.; Tursun, R.; Shum, J.; Wong, M.E.; Young, S. Tissue Engineering for Mandibular Reconstruction. *Atlas Oral Maxillofac. Surg. Clin. N. Am.* **2023**, *31*, 165–176. [CrossRef]
4. Gianulis, E.; Wetzell, B.; Scheunemann, D.; Gazzolo, P.; Sohoni, P.; Moore, M.A.; Chen, J. Characterization of an advanced viable bone allograft with preserved native bone-forming cells. *Cell Tissue Bank.* **2023**, *24*, 417–434. [CrossRef]
5. Marschall, J.S.; Davis, S.S.; Jones, L.; Kushner, G.M. Are Cellular Bone Matrix Allografts a Viable Option for Mandibular Tissue Engineering and Reconstruction? *J. Oral Maxillofac. Surg.* **2024**, *82*, 1163–1175. [CrossRef] [PubMed]
6. Marschall, J.S.; Davis, S.S.; Rysavy, O.; Kushner, G.M. Reconstruction of Maxillary Bone Defects with Cellular Bone Matrix Allografts. *Craniomaxillofac. Trauma Reconstr.* **2024**, *17*, NP263–NP270. [CrossRef] [PubMed]
7. Marschall, J.S.; Kushner, G.M.; Flint, R.L.; Jones, L.C.; Alpert, B. Immediate Reconstruction of Segmental Mandibular Defects with Nonvascular Bone Grafts: A 30-Year Perspective. *J. Oral Maxillofac. Surg.* **2020**, *78*, 2099.e1–2099.e9. [CrossRef] [PubMed]
8. Hidalgo, D.A. Fibula free flap: A new method of mandible reconstruction. *Plast. Reconstr. Surg.* **1989**, *84*, 71–79. [CrossRef]
9. Elgafy, H.; Wetzell, B.; Gillette, M.; Semaan, H.; Rowland, A.; Balboa, C.A.; Mierzwa, T.A.; McLean, J.B.; Dorsch, K.; Moore, M.A. Lumbar spine fusion outcomes using a cellular bone allograft with lineage-committed bone-forming cells in 96 patients. *BMC Musculoskelet. Disord.* **2021**, *22*, 699. [CrossRef]
10. Moran, T.E.; Sequeira, S.; Cooper, M.T.; Park, J. A Retrospective Analysis of Outcomes from Foot and Ankle Arthrodesis and Open Reduction and Internal Fixation Using Cellular Bone Allograft Augmentation. *Foot Ankle Spec.* **2022**, *15*, 312–320. [CrossRef]
11. Jones, C.P.; Loveland, J.; Atkinson, B.L.; Ryaby, J.T.; Linovitz, R.J.; Nunley, J.A. Prospective, Multicenter Evaluation of Allogeneic Bone Matrix Containing Viable Osteogenic Cells in Foot and/or Ankle Arthrodesis. *Foot Ankle Int.* **2015**, *36*, 1129–1137. [CrossRef]
12. Pinter, Z.W.; Elder, B.D.; Kaye, I.D.; Kepler, C.K.; Wagner, S.; Freedman, B.A.; Sebastian, A.S. A Review of Commercially Available Cellular-based Allografts. *Clin. Spine Surg.* **2022**, *35*, E77–E86. [CrossRef]
13. Marschall, J.S.; Flint, R.L.; Kushner, G.M.; Alpert, B. Management of Mandibular Osteomyelitis with Segmental Resection, Nerve Preservation, and Immediate Reconstruction. *J. Oral Maxillofac. Surg.* **2019**, *77*, 1490–1504. [CrossRef]
14. Marechek, A.; Ahmad, A.; Pack, S.; Demko, C.; Quereshy, F.; Baur, D. Nonvascularized Bone Grafts for Reconstruction of Segmental Mandibular Defects: Is Length of Graft a Factor of Success? *J. Oral Maxillofac. Surg.* **2019**, *77*, 2557–2566. [CrossRef] [PubMed]
15. Pogrel, M.A.; Podlesh, S.; Anthony, J.P.; Alexander, J. A comparison of vascularized and nonvascularized bone grafts for reconstruction of mandibular continuity defects. *J. Oral Maxillofac. Surg.* **1997**, *55*, 1200–1206. [CrossRef] [PubMed]
16. Darveau, S.C.; Leary, O.P.; Persad-Paisley, E.M.; Shaaya, E.A.; Oyelese, A.A.; Fridley, J.S.; Sampath, P.; Camara-Quintana, J.Q.; Gokaslan, Z.L.; Niu, T. Existing clinical evidence on the use of cellular bone matrix grafts in spinal fusion: Updated systematic review of the literature. *Neurosurg. Focus* **2021**, *50*, E12. [CrossRef] [PubMed]
17. MBTATETEplaces. Available online: https://www.mtfbiologics.org/docs/default-source/mbot/orthopedics/viable-bone-allograft/tt-1614---trinty-elite-technical-monograph-update-dfnl.pdf?sfvrsn=16b6b3ef_4 (accessed on 1 December 2025).
18. Neman, J.; Duenas, V.; Kowolik, C.; Hambrecht, A.; Chen, M.; Jandial, R. Lineage mapping and characterization of the native progenitor population in cellular allograft. *Spine J.* **2013**, *13*, 162–174. [CrossRef]
19. Johnstone, B.; Zhang, N.; Waldorff, E.I.; Semler, E.; Dasgupta, A.; Betsch, M.; Punsalan, P.; Cho, H.; Ryaby, J.T.; Yoo, J. A Comparative Evaluation of Commercially Available Cell-Based Allografts in a Rat Spinal Fusion Model. *Int. J. Spine Surg.* **2020**, *14*, 213–221. [CrossRef]
20. Skovrlj, B.; Guzman, J.Z.; Al Maaieh, M.; Cho, S.K.; Iatridis, J.C.; Qureshi, S.A. Cellular bone matrices: Viable stem cell-containing bone graft substitutes. *Spine J.* **2014**, *14*, 2763–2772. [CrossRef]
21. Govoni, M.; Vivarelli, L.; Mazzotta, A.; Stagni, C.; Maso, A.; Dallari, D. Commercial Bone Grafts Claimed as an Alternative to Autografts: Current Trends for Clinical Applications in Orthopaedics. *Materials* **2021**, *14*, 3290. [CrossRef]
22. Available online: https://stage-corporate.lifenethealth.org/sites/default/files/files/68-40-254%20Technical%20Monograph.pdf?_gl=1*1rw6rek*_gcl_au*MTU1NzM3MzE2NS4xNzY0NDU3MzAx (accessed on 1 December 2025).
23. Ammerman, J.M.; Libricz, J.; Ammerman, M.D. The role of Osteocel Plus as a fusion substrate in minimally invasive instrumented transforaminal lumbar interbody fusion. *Clin. Neurol. Neurosurg.* **2013**, *115*, 991–994. [CrossRef]

https://doi.org/10.3390/cmtr19020018

24. Alfi, D.M.; Hassan, A.; East, S.M.; Gianulis, E.C. Immediate Mandibular Reconstruction Using a Cellular Bone Allograft Following Tumor Resection in a Pediatric Patient. *FACE* **2021**, *2*, 490–495. [CrossRef]
25. Ryu, B.; Abraham, C., III; Polido, W.D. Treatment of mandibular non-union using patient specific crib cage plates and cellular bone allograft: A case report. *Craniomaxillofac. Trauma Reconstr. Open* **2021**, *6*, 24727512211005949. [CrossRef]
26. Parsaei, Y.; Maniskas, S.; Reategui, A.; Lopez, J.; Steinbacher, D. Segmental Cleft-orthognathic Surgery to Achieve Facial Balance, Fistula Closure, and Arch Unification. *Plast. Reconstr. Surg.–Glob. Open* **2022**, *10*, e3948. [CrossRef] [PubMed]
27. Pontell, M.E.; Barahimi, B.; Golinko, M.S. Managing Bilateral Oro-Sino-Orbital Fistulae in the Setting of Bilateral Tessier IV Clefts. *J. Craniofac. Surg.* **2022**, *33*, e73–e76. [CrossRef]
28. Roe, R.M.; Farsi, S.; Brown, M.C.; Flowers, J.; Hartzell, L.D. Surgical Repair of Unilateral Cleft Alveolus Using Viable Bone Allograft in Pediatrics: A Case Report. *Facial Plast. Surg. Aesthet. Med.* **2025**. [CrossRef]
29. Foster, R.D.; Anthony, J.P.; Sharma, A.; Pogrel, M.A. Vascularized bone flaps versus nonvascularized bone grafts for mandibular reconstruction: An outcome analysis of primary bony union and endosseous implant success. *Head Neck* **1999**, *21*, 66–71. [CrossRef]
30. Nandra, B.; Fattahi, T.; Martin, T.; Praveen, P.; Fernandes, R.; Parmar, S. Free Bone Grafts for Mandibular Reconstruction in Patients Who Have not Received Radiotherapy: The 6-cm Rule-Myth or Reality? *Craniomaxillofac. Trauma Reconstr.* **2017**, *10*, 117–122. [CrossRef]
31. Schlieve, T.; Hull, W.; Miloro, M.; Kolokythas, A. Is immediate reconstruction of the mandible with nonvascularized bone graft following resection of benign pathology a viable treatment option? *J. Oral Maxillofac. Surg.* **2015**, *73*, 541–549. [CrossRef]
32. Kushner, G.M. Tibia bone graft harvest technique. *Atlas Oral Maxillofac. Surg. Clin. N. Am.* **2005**, *13*, 119–126. [CrossRef]
33. Engelstad, M.E.; Morse, T. Anterior iliac crest, posterior iliac crest, and proximal tibia donor sites: A comparison of cancellous bone volumes in fresh cadavers. *J. Oral Maxillofac. Surg.* **2010**, *68*, 3015–3021. [CrossRef] [PubMed]
34. Marschall, J.S.; Wong, M.E.; Young, S.; Marx, R.E.; Viet, C.T.; Morlandt, A.B.; Melville, J.C. Tissue engineering in maxillofacial reconstruction: Past, present, and future. In *Advancements and Innovations in OMFS, ENT, and Facial Plastic Surgery*; Springer: Berlin/Heidelberg, Germany, 2023; pp. 309–322.
35. Melville, J.C.; Manon, V.A.; Blackburn, C.; Young, S. Current Methods of Maxillofacial Tissue Engineering. *Oral Maxillofac. Surg. Clin. N. Am.* **2019**, *31*, 579–591. [CrossRef] [PubMed]
36. Lienemann, P.S.; Lutolf, M.P.; Ehrbar, M. Biomimetic hydrogels for controlled biomolecule delivery to augment bone regeneration. *Adv. Drug Deliv. Rev.* **2012**, *64*, 1078–1089. [CrossRef] [PubMed]
37. Marx, R.E.; Carlson, E.R.; Eichstaedt, R.M.; Schimmele, S.R.; Strauss, J.E.; Georgeff, K.R. Platelet-rich plasma: Growth factor enhancement for bone grafts. *Oral Surg. Oral Med. Oral Pathol. Oral Radiol. Endod.* **1998**, *85*, 638–646. [CrossRef]
38. Freymiller, E.G.; Aghaloo, T.L. Platelet-rich plasma: Ready or not? *J. Oral Maxillofac. Surg.* **2004**, *62*, 484–488. [CrossRef]
39. Kobayashi, E.; Fluckiger, L.; Fujioka-Kobayashi, M.; Sawada, K.; Sculean, A.; Schaller, B.; Miron, R.J. Comparative release of growth factors from PRP, PRF, and advanced-PRF. *Clin. Oral Investig.* **2016**, *20*, 2353–2360. [CrossRef]
40. Zisch, A.H.; Lutolf, M.P.; Ehrbar, M.; Raeber, G.P.; Rizzi, S.C.; Davies, N.; Schmokel, H.; Bezuidenhout, D.; Djonov, V.; Zilla, P.; et al. Cell-demanded release of VEGF from synthetic, biointeractive cell ingrowth matrices for vascularized tissue growth. *FASEB J.* **2003**, *17*, 2260–2262. [CrossRef]
41. Dohan, D.M.; Choukroun, J.; Diss, A.; Dohan, S.L.; Dohan, A.J.; Mouhyi, J.; Gogly, B. Platelet-rich fibrin (PRF): A second-generation platelet concentrate. Part II: Platelet-related biologic features. *Oral Surg. Oral Med. Oral Pathol. Oral Radiol. Endod.* **2006**, *101*, e45–e50. [CrossRef]
42. Reddi, A.H. Bone morphogenetic proteins and skeletal development: The kidney-bone connection. *Pediatr. Nephrol.* **2000**, *14*, 598–601. [CrossRef]
43. Cicciu, M.; Herford, A.S.; Cicciu, D.; Tandon, R.; Maiorana, C. Recombinant human bone morphogenetic protein-2 promote and stabilize hard and soft tissue healing for large mandibular new bone reconstruction defects. *J. Craniofac. Surg.* **2014**, *25*, 860–862. [CrossRef]
44. Herford, A.S.; Boyne, P.J. Reconstruction of mandibular continuity defects with bone morphogenetic protein-2 (rhBMP-2). *J. Oral Maxillofac. Surg.* **2008**, *66*, 616–624. [CrossRef] [PubMed]
45. Herford, A.S.; Cicciu, M. Recombinant human bone morphogenetic protein type 2 jaw reconstruction in patients affected by giant cell tumor. *J. Craniofac. Surg.* **2010**, *21*, 1970–1975. [CrossRef] [PubMed]
46. Herford, A.S.; Lowe, I.; Jung, P. Titanium Mesh Grafting Combined with Recombinant Human Bone Morphogenetic Protein 2 for Alveolar Reconstruction. *Oral Maxillofac. Surg. Clin. N. Am.* **2019**, *31*, 309–315. [CrossRef] [PubMed]
47. Herford, A.S.; Lu, M.; Buxton, A.N.; Kim, J.; Henkin, J.; Boyne, P.J.; Caruso, J.M.; Rungcharassaeng, K.; Hong, J. Recombinant human bone morphogenetic protein 2 combined with an osteoconductive bulking agent for mandibular continuity defects in nonhuman primates. *J. Oral Maxillofac. Surg.* **2012**, *70*, 703–716. [CrossRef]

https://doi.org/10.3390/cmtr19020018

48. Hammoudeh, J.A.; Fahradyan, A.; Gould, D.J.; Liang, F.; Imahiyerobo, T.; Urbinelli, L.; Nguyen, J.T.; Magee, W., 3rd; Yen, S.; Urata, M.M. A Comparative Analysis of Recombinant Human Bone Morphogenetic Protein-2 with a Demineralized Bone Matrix versus Iliac Crest Bone Graft for Secondary Alveolar Bone Grafts in Patients with Cleft Lip and Palate: Review of 501 Cases. *Plast. Reconstr. Surg.* **2017**, *140*, 318e–325e. [CrossRef]
49. Boyne, P.J. Animal studies of application of rhBMP-2 in maxillofacial reconstruction. *Bone* **1996**, *19*, 83S–92S. [CrossRef]

Disclaimer/Publisher's Note: The statements, opinions and data contained in all publications are solely those of the individual author(s) and contributor(s) and not of MDPI and/or the editor(s). MDPI and/or the editor(s) disclaim responsibility for any injury to people or property resulting from any ideas, methods, instructions or products referred to in the content.

https://doi.org/10.3390/cmtr19020018

craniomaxillofacial
trauma & reconstruction

MDPI

Review

Facial Contouring in Orthognathic Surgery: The Role of Facial Implants

Gabriel Conceição Brito [1], Márcio de Moraes [1], Leonardo Faverani [1] and Sergio Olate [1,2,*]

[1] Division of Oral and Maxillofacial Surgery, Department of Oral Diagnosis, Piracicaba School of Dentistry, State University of Campinas, São Paulo 13414-903, Brazil; gabriel.bucomaxilo@gmail.com (G.C.B.); mmoraes@unicamp.br (M.d.M.); faverani@unicamp.br (L.F.)
[2] Center for Research in Morphology and Surgery (CEMyQ), University of La Frontera, Temuco 4780000, Chile
* Correspondence: sergio.olate@ufrontera.cl

Abstract

Orthognathic surgery restores functional balance and facial esthetics in patients with dentofacial deformities. The use of adjunctive facial implants—made from materials such as porous polyethylene, titanium, or polyetheretherketone (PEEK)—has increased to enhance contour and projection, although standardized guidelines for their selection and integration remain scarce. Following PRISMA-ScR guidelines, a systematic search of PubMed, Scopus, Embase, and LILACS identified studies reporting facial implants placed concomitantly with orthognathic surgery. Eligible studies included case reports, case series, observational studies, clinical trials, and reviews involving human patients, without language or date restrictions. Seventeen studies published between 1998 and 2025 met the inclusion criteria, comprising retrospective and prospective designs, case series, and one technical note. Implants were used in the malar, infraorbital, paranasal, chin, mandibular body, and angle regions. Materials included PEEK, porous polyethylene, silicone, hydroxyapatite, polymethylmethacrylate, and titanium. PEEK was mainly used for patient-specific implants, while porous polyethylene was commonly used as stock implants. Follow-up time, outcome reporting, and study design varied widely, reflecting substantial methodological heterogeneity and predominantly observational evidence. As a result, outcomes were primarily reported qualitatively, limiting comparative assessment and long-term inference. Overall, the available literature suggests that alloplastic facial implants may serve as useful adjuncts to orthognathic surgery for contour enhancement, with outcomes influenced by implant design, surgical expertise, fixation, and soft tissue conditions. However, the current evidence base remains limited, underscoring the need for standardized outcome measures, comparative studies, and longer follow-up to better inform clinical decision-making and future research.

Keywords: facial implants; orthognathic surgery; facial esthetic

1. Introduction

Patients presenting with dentofacial deformities are candidates for orthognathic surgery, a procedure primarily intended to reestablish functional balance by improving occlusion, mastication, and speech [1–3]. Nevertheless, the esthetic dimension of orthognathic surgery remains undeniable, and comprehensive treatment planning has increasingly focused on optimizing both functional restoration and facial harmony [3–5].

Over recent decades, adjunctive procedures to orthognathic surgery have evolved in response to rising esthetic expectations and the continuous pursuit of more refined,

individualized outcomes [5–7]. These combined approaches are particularly valuable in complex clinical scenarios, such as patients with facial asymmetry or craniofacial syndromes, in whom achieving correction across the three anatomical planes—axial, sagittal, and coronal—poses a significant challenge [8–10]. In such contexts, the integration of complementary techniques may reduce the need for more extensive skeletal movements or invasive osteotomies, such as the Le Fort III procedure [11,12].

The objective of facial implants in orthognathic surgery is to achieve a visible and long-lasting increase in facial soft-tissue volume. Soft-tissue response following orthognathic procedures has also demonstrated a degree of unpredictability [13,14], indicating that the esthetic impact of complementary procedures cannot be fully anticipated. Nevertheless, in addition to facial implants, the use of fat grafts and other alloplastic materials has been reported [15], supporting the notion that volume enhancement represents a key step in optimizing the esthetic outcomes of orthognathic treatment.

Facial implants, introduced in the early 1970s, are now well-established for skeletal reconstruction and esthetic contouring [16,17], and their combined use with orthognathic surgery has gained increasing attention [5,12,18]. They are applied in both the midface and lower face to enhance contour and projection of areas such as the malar eminence, paranasal region, orbital rim, chin, and mandibular angle [11,18,19]. However, evidence remains limited regarding standardized assessment, planning methodologies, and clinical rationale within orthognathic surgery frameworks.

Facial implants may be fabricated from various materials—such as porous polyethylene, titanium, and polyetheretherketone (PEEK)—and are available as either prefabricated (stock) or patient-specific implants (PSIs), the latter designed to conform precisely to individual skeletal anatomy through digital planning and additive manufacturing technologies [20,21].

Given the multifactorial complexity of these cases—including indication criteria, implant selection, surgical approach, and postoperative evaluation—there remains a clear need to define evidence-based strategies for integrating facial implants into single-stage orthognathic procedures. Such strategies aim to maximize both functional stability and esthetic refinement.

Accordingly, the present scoping review aims to map and synthesize the existing evidence regarding the use of facial implants in patients undergoing orthognathic surgery, with particular emphasis on indications, implant materials and designs, clinical outcomes, and their functional and esthetic implications.

2. Materials and Methods

2.1. Study Design

This study was designed and reported in accordance with the Preferred Reporting Items for Systematic Reviews and Meta-Analyses extension for Scoping Reviews (PRISMA-ScR) guidelines [22]. In accordance with PRISMA-ScR recommendations for transparency and methodological rigor, the protocol for this scoping review was registered in the Open Science Framework (OSF) (Registration ID: 10.17605/OSF.IO/4MG27; available at https://osf.io/4mg27 (accessed on 19 November 2025).

2.2. Research Question

The following research question guided the review:

What are the types, indications, surgical techniques, and clinical outcomes reported in the literature for facial implants used concomitantly with orthognathic surgery?

This question was structured using the PCC (Population, Concept, Context) framework:

- Population (P): Patients undergoing orthognathic surgery

https://doi.org/10.3390/cmtr19010002

- Concept (C): Facial implants (custom-made or conventional)
- Context (C): Simultaneous placement during orthognathic surgery.

2.3. Eligibility Criteria

Studies were included if they met the following criteria:

- Involved human patients who underwent orthognathic surgery with simultaneous placement of facial implants (in a single surgical procedure)
- Included study designs such as case reports, case series, observational studies, clinical trials, and reviews
- No restriction on publication date or language.

Exclusion criteria included:

- Studies focused exclusively on orthognathic surgery without reporting any details regarding facial implants
- Narrative reviews without primary data
- In vitro or animal studies
- Studies involving syndromic patients (e.g., craniofacial syndromes).

2.4. Information Sources and Search Strategy

An electronic literature search was performed across the following databases: PubMed, Scopus, Embase, and LILACS.

The primary search strategy included combinations of Medical Subject Headings (MeSH) and free-text terms. An example of the search query used in PubMed is ("Prostheses and Implants" [MeSH Terms]) AND ("Orthognathic Surgery" [MeSH Terms] OR "Osteotomy, Sagittal Split Ramus" [MeSH Terms] OR "Osteotomy, Le Fort" [MeSH Terms]) adapted for each database platform.

A. Study Selection and Data Extraction Process

All identified records were imported into START (State of the Art through Systematic Review Tool, LaPES-UFSCar) for management and screening.

Two independent reviewers (GCB and SO) conducted the initial screening by title and abstract. Full texts of potentially eligible studies were then retrieved and assessed against the inclusion and exclusion criteria. Disagreements between reviewers were resolved through discussion and, when necessary, by a third reviewer (MM).

The selection process will be illustrated using a PRISMA-ScR flow diagram. This dual-review process was designed to ensure consistency and minimize selection bias.

B. Data Charting and Synthesis

Data extraction was conducted using a standardized Excel spreadsheet. The following variables were collected from each included study:

- Author(s), year of publication, and country
- Study design
- Patient demographics (age, sex)
- Type of facial implant used (e.g., custom-made, stock)
- Purpose and anatomical region of the implant
- Indication for implant placement (esthetic and/or functional)
- Associated orthognathic surgical procedure
- Clinical and esthetic/functional outcomes
- Reported complications
- Main conclusions.

https://doi.org/10.3390/cmtr19010002

Descriptive data synthesis will be performed in both quantitative and qualitative formats. The findings will be presented using tables, charts, and narrative summaries, aiming to map the current evidence landscape on this topic.

In accordance with scoping review methodology, the Discussion integrates findings from the included studies with relevant external literature to contextualize the results and support clinical interpretation. This additional literature was not intended to expand the evidence base of the review, but rather to aid in the discussion of key themes identified through the scoping process.

C. Risk of Bias and Quality Assessment

In line with the objectives and methodological framework of a scoping review, no formal assessment of methodological quality or risk of bias was conducted, as recommended by the PRISMA-ScR guidelines.

3. Results

3.1. Included Studies and Data Extraction

According to the established inclusion criteria, a total of 17 studies were selected for data extraction [7,10,11,18,19,21,23–33]. The overall design and selection process of the included articles are summarized in the flow chart (Figure 1). The studies were published between 1998 and 2025, comprising six retrospective studies [11,20,26,27,32,33], two prospective studies [18,25], seven case series or clinical case reports [7,10,19,21,24,28,29,31], and one technical note [23].

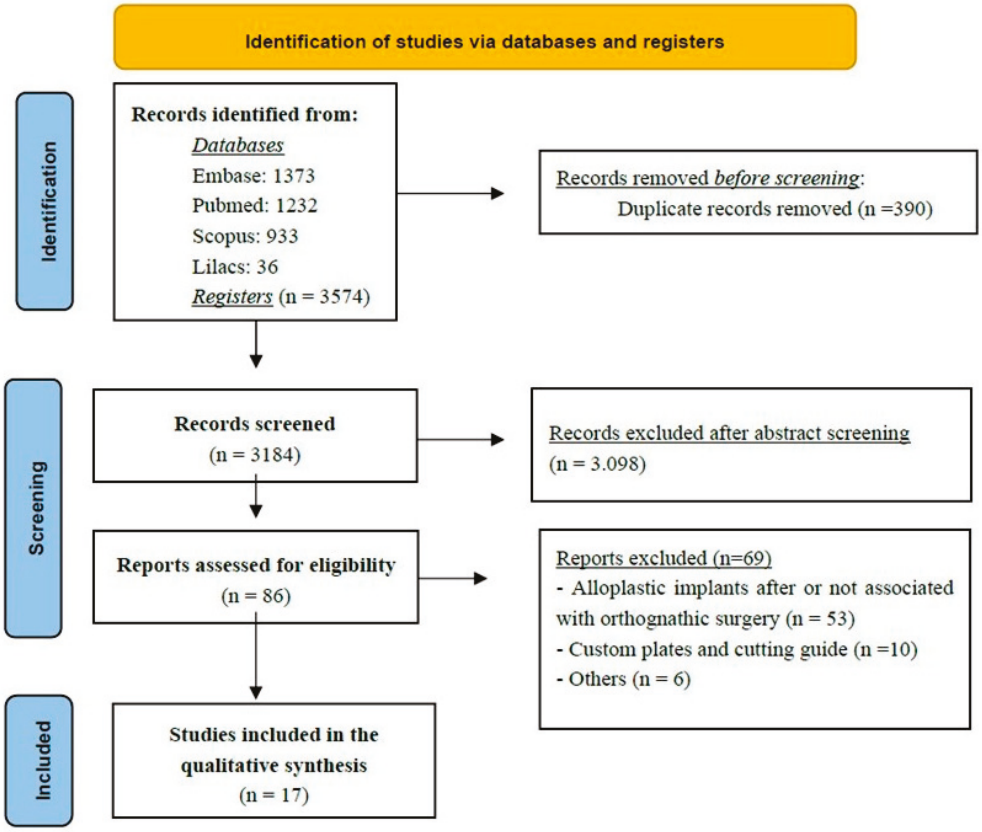

Figure 1. The Flowchart summarizes the study selection process, including identification, screening, eligibility assessment, and final inclusion of studies in the scoping review.

https://doi.org/10.3390/cmtr19010002

3.2. Anatomical Regions and Implant Materials

Among the anatomical regions treated with facial prostheses in conjunction with orthognathic surgery, the included studies reported interventions involving implants designed to modify or enhance the projection of the malar region [11,18,19,26,29,31], infraorbital rim [23], paranasal area [26–28], chin (menton) [7,11,19,32], mandibular body [7,10,25,32], and mandibular angle [7,10,11,21,25,26,30,33].

Regarding the materials used for the fabrication of facial implants, the studies described the application of polyetheretherketone (PEEK) [21,26,32], porous polyethylene [11,19,21,25,27–29,31], silicone [23], hydroxyapatite granules [18], polymethylmethacrylate (PMMA) [7], and titanium [10,30,33]. PEEK implants were typically associated with patient-specific implants (PSI) manufactured through digital design and additive fabrication technologies, whereas porous polyethylene implants were most often employed as stock implants.

Some studies conducted comparative analyses between different types of facial implant materials, while others focused on the long-term biological behavior and clinical performance of a single material. The key characteristics of each selected study—including the implant material, anatomical region, and notable findings—are summarized in Table 1.

Table 1. Characteristics of the facial implants used and clinical aspects of its application.

Author (Year)	Implant Material	Anatomical Region	Key Distinctive Findings
Marano et al. (2025) [7]	Polymethylmethacrylate	Mandibular angle to the chin	(1) Lower-third volume augmentation with Le Fort I, stable at 1-year follow-up. (2) Following virtual implant design, positive and negative muffle templates were 3D printed using light-curing biocompatible resins
Ramieri et al. (2025) [10]	Titanium (PSI)	Inferior border of the mandible and the posterior margin of the ramus	(1) Simultaneous correction of mandibular advancement, transverse widening, and vertical ramus augmentation. (2) Mean mandibular width gain of 18.1 $\pm$ 6.2 mm, with vertical ramus increases of ~6 mm bilaterally.
Rios et al. (2025) [30]	Titanium (PSI)	Mandibular angle implants	(1) BSSO tends to increase intergonial distance $\rightarrow$ must be considered in implant design. (2) In orthognathic surgery, inserted at the end, after occlusion is established.
Genc et al. (2022) [25]	Porous Polyethylene	Mandibular body and angle implants	(1) BSSO performed first to correct malocclusion. (2) Prefabricated Medpor implants trimmed according to the surgical template. (3) Implants heated in 90 °C saline and molded to fit the mandibular cortex
Kerkfeld et al. (2022) [26]	Polyetheretherketone (PEEK)	Mandibular, maxillary, temporal, zygomatic, periorbital	(1) PEEK implants were virtually planned in a second step (mirroring/superimposition strategy). (2) All patients underwent bimaxillary surgery (Le Fort I + bilateral sagittal split osteotomy), and after the PEEK implant placement
Olate et al. (2021) [21]	Medpor (stock) and PEEK (PSI)	Mandibular angle implants	(1) Stock implants: Triangle shape with ramus and body coverage. size confirmed with a template; implant modified when necessary. Fixed with 1–2 titanium screws. (2) Patient-Specific Implants: Adaptation obtained directly from CAD/CAM (no template needed). Fixed with 1 titanium screw.
Lutz et al. (2020) [11]	High-density porous polyethylene	Malar implants	(1) Simultaneous placement showed no significant difference, but delayed placement was preferred (2) Rationale: gradual facial change, reduced infection risk, short operative time (3) Implants support the lower eyelid in older patients $\rightarrow$ rejuvenating effect
Findikcioglu el al. (2018) [24]	Porous polyethylene	Genioplasty (chin)	(1) Horizontal sliding osteotomy with 8 mm advancement plus an implant adding 9 mm projection. (2) Mean soft-tissue advancement of 13 mm at the menton region.
Fattahi et al. (2017) [23]	Silicone	Infraorbital rim	(1) It was chosen using sizers (small or medium) for harmony with maxillary osteotomy correction. (2) Implant inserted and positioned as superiorly as possible to augment the entire infraorbital rim length, may rest on Le Fort I fixation plates and secured with titanium screws.
Menezes et al. (2016) [28]	Porous polyethylene	Improvement of the paranasal area	Effect of implants: significant improvement in nasolabial angle and columella inclination in cases of midface hypoplasia

https://doi.org/10.3390/cmtr19010002

Table 1. *Cont.*

Author (Year)	Implant Material	Anatomical Region	Key Distinctive Findings
D'Agostino et al. (2016) [18]	Porous HA granules	zygomatic region	(1) Shaping is performed at the end of the Le Fort I orthognathic procedure. (2) Pockets created within the zygomatic bones match implant size (prevent displacement). (3) No internal fixation needed to stabilize implants.
Scolozzi et al. (2015) [32]	polyetheretherketone-PSI	Chin and mandibular defects.	(1) Rapid workflow: Models reviewed, marked, and approved by the surgeon before final manufacturing. (2) Intraoral incision and implants matched bone defect dimensions perfectly; no modifications required 3. Fixation with 1.5 titanium-plate lag screws.
Kwon et al. (2014) [27]	Porous polyethylene	Paranasal	(1) Sub-periosteal reflection performed in the paranasal/piriform area, no need to reflect the anterior nasal spine (2) Thin margins trimmed for anatomical fit; smooth graft transition verified (3) Fixation with 7–9 mm miniscrew
Nocini et al. (2011) [19]	Porous polyethylene	Improvement of the malar area	(1) Clinical parameters for indication: marked mandibular excess, midface hypoplasia, retropositioned upper lip, severe bimaxillary discrepancy, infraorbital shadows (2) Analysis tool: grid-plan midfacial analysis (developed at Verona University).
Stringer et al. (2009) [33]	TiMesh titanium mesh	Mandibular angle	(1) Implant positioning: Medial aspect of mesh tray locked along the medial surface of the posterior border of the ramus and the inferior border of the mandible. (2) Fixation: Only 2 screws required. Minimal forces were applied to the titanium mesh implant.
Nocini et al. (2009) [29]	Porous polyethylene	Improvement of the malar area	(1) Advantages: stability, lower infection risk, fixation with titanium miniscrews, easy to insert and shape (2) Disadvantages: wider intraoral incisions sometimes required (for multiple areas), risk of exposure in thin or scarred skin under tension.
Robiony et al. (1998) [31]	Porous polyethylene	Malar implants	(1) Clinical evaluation and positioning reference by Mladick's Method (2) Subperiosteal placement via incision from Le Fort I osteotomy and fixed with screws (3) Insertion: anteromedial, anterolateral, or both. The average implant size was 4 ± 0.5 mm.

3.3. Follow-Up Periods

The follow-up durations varied considerably among the studies and were closely related to their respective study designs. The mean follow-up times (in years) across the studies ranged from 0.5 [25] to 6 [18]. Follow-up protocols were not standardized, showing considerable variability among studies. In most cases, follow-up was limited to the feasible observation period—particularly in case reports and case series—thereby restricting the interpretation of long-term outcomes.

4. Discussion

The following sections are structured around key themes identified during data charting of the included studies. Where appropriate, additional literature is cited to contextualize and expand upon these findings.

4.1. Indications

Facial implants have emerged as a less invasive alternative to extensive skeletal surgeries such as the Le Fort III osteotomy or zygoma osteotomy, which (initially used to correct midfacial deficiencies and improve esthetics), involved high morbidity, extraoral/intraoral approaches, and significant technical challenges [11,12]. With advancements in biomaterials, the use of alloplastic implants has largely replaced these aggressive techniques for enhancing midface projection and correcting infraorbital and zygomatic deficiencies [18,19]. Simultaneous orthognathic surgery combined with patient-specific implant (PSI) placement has been shown to improve facial symmetry and esthetic outcomes [21,26].

The midface is key for facial contour, zygomatic projection, and a youthful appearance. Hypoplasia, malar deficiency, and maxillary retrusion disrupt harmony and accentuate infraorbital shadows [18,19]. Correction often involves infraorbital, zygomatic, and paranasal

https://doi.org/10.3390/cmtr19010002

implants to restore malar volume and projection, enhancing facial balance and esthetics [19,28], as demonstrated in Figure 2.

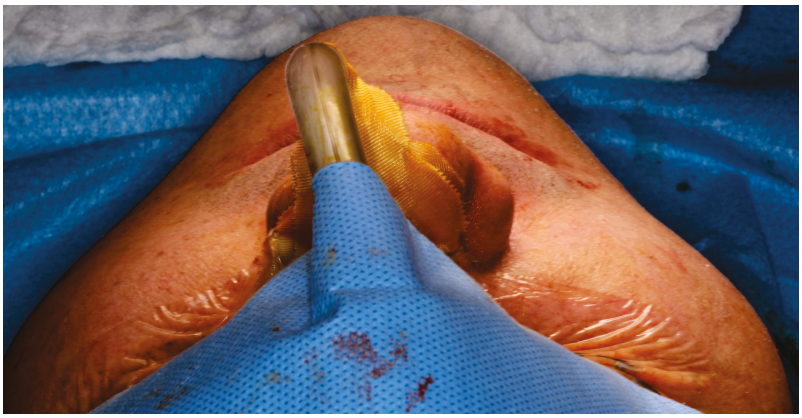

Figure 2. Intraoperative view following Le Fort I osteotomy. A right-side zygomatic implant has been positioned to enhance midfacial projection, while the left side remains without augmentation. The comparison demonstrates an augmentation in zygomatic contour and anterior midfacial projection before bilateral implant placement—Image from the authors' personal archive.

In particular, infraorbital rim deficiency is often associated with a concave facial profile, Class III malocclusion, a shortened upper lip, and prominent nasolabial folds [23]. Additional features such as scleral show, prominent lower eyelid fat pads, and altered globe orientation relative to the infraorbital region are also commonly observed, supporting the indication for implant placement [12,23,34].

Several techniques have been proposed to identify the ideal point for malar augmentation, including those described by Mladick [35], Pendergast [36], Terino [37], and other authors [38,39] who employ different anatomic landmarks and facial lines to determine the most prominent zone. Most recently, the Gridplan method stands out due to its systematic and reproducible approach, dividing the midface into defined areas through a framework of perpendicular vertical and horizontal lines [29]. This grid-based analysis allows three-dimensional evaluation of the relationships between the zygomatic arch, paranasal area, and infraorbital rim, and can be applied both in isolated implant procedures and in conjunction with orthognathic surgery [19,29].

In recent years, the mandibular jawline has emerged as a key determinant of facial attractiveness and perceived youth. There is growing recognition that jawline balance—particularly in patients with facial asymmetry, reduced ramus height, or gonial angle discrepancies—is crucial to overall facial harmony [10,33,40]. To optimize esthetic outcomes, surgeons increasingly combine orthognathic procedures with targeted mandibular augmentation (chin and/or jaw angle) using alloplastic or PSI designs to harmonize chin projection and mandibular angles in height, width, and lateral projection [10,30,40].

Anatomical and esthetic analyses indicate that the ideal gonial angle averages approximately 130°, with sex-related variations influencing mandibular contour and lower-third facial esthetics. The intergonial width should maintain proportionality to the interzygomatic width, typically at a ratio of about 0.83:1, ensuring transverse facial harmony [41]. Proper alignment of the mandibular angles with key facial landmarks—such as the oral commissure and lip level—further contributes to balanced facial proportions [30,41]. In female patients, the gonial angle tends to measure approximately 142° in the frontal view and 125.5° in the profile view, with its vertical position generally aligning with the stomion or upper lip, reinforcing a softer and more harmonious lower facial contour [30,41,42].

Mandibular angle augmentation can be planned using the triangle area concept, defined by lines through the lower incisor apex and posterior ramus to delineate the

https://doi.org/10.3390/cmtr19010002

target region for contour implants. Vertical ramus augmentation restores facial symmetry, aligns the mandibular plane with the Frankfurt plane, and integrates the symphysis and body [21]. Adjustments to the mandibular angle and body width further harmonize intergonial distance and ensure bilateral symmetry.

4.2. Implant Materials

A variety of materials have been described for use in facial augmentation and reconstruction procedures associated with orthognathic surgery, particularly in the midface and lower facial thirds [6,12,19]. Fattahi et al. (2017) [23] described the use of silicone implants for infraorbital rim augmentation to correct deficiencies around the infraorbital foramen. Silicone remains popular due to its availability in preformed shapes, ease of placement, and lack of fixation requirements (in some cases). However, its limitations include poor integration, fibrous capsule formation, underlying bone resorption, and a potential for displacement or extrusion over time (Figure 3).

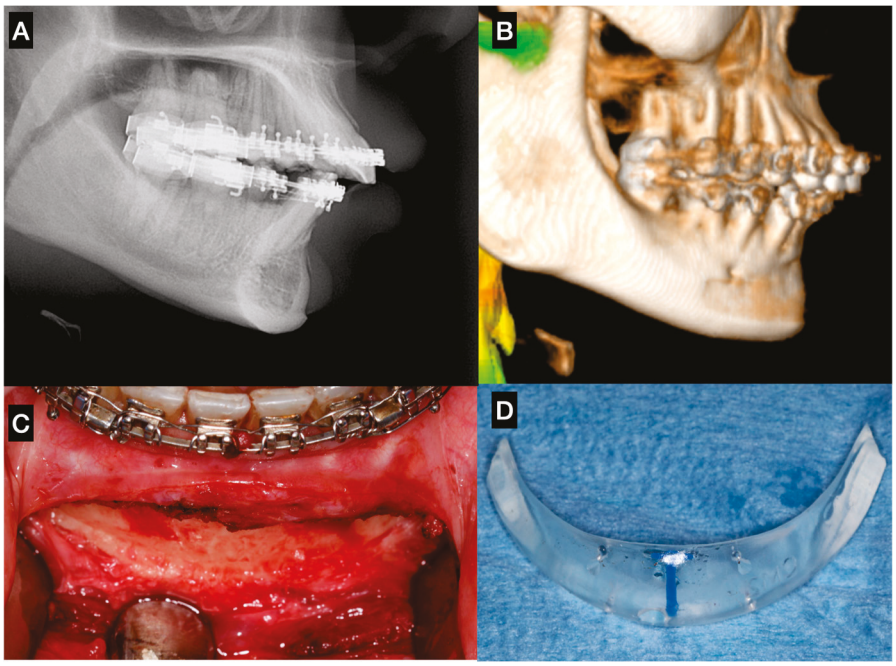

Figure 3. Sagittal chin augmentation using a standard silicone implant in a patient presenting with a Class II skeletal deformity. The patient sought evaluation due to implant mobility detected clinically four years after placement. (**A**) Lateral cephalometric radiograph showing pronounced bone resorption beneath the implant, with proximity to the apices of the mandibular incisors. (**B**) 3D reconstruction confirming a well-defined resorption defect extending toward the mental foramen. (**C**) Post-explantation intraoperative image demonstrating the full extent and depth of the osseous defect. (**D**) Removed standard silicone implant, evidencing its non-anatomic contour and excessive posterior extension, factors that likely contributed to instability and bone resorption—Image from the authors' personal archive.

In the study by D'Agostino et al. (2016) [18], porous hydroxyapatite (HA) implants in the midfacial region demonstrated excellent biocompatibility and osteoconductive properties, resulting in stable long-term esthetic outcomes. However, the technique presents certain drawbacks, including the relatively long time required for prosthesis fabrication, a steep learning curve for creating the subperiosteal pocket, and the need for slight overcorrection to compensate for early postoperative volumetric reduction.

High-density porous polyethylene is stable and biocompatible, but it is difficult to adapt due to its rigidity and the need for screw fixation. The reported complication rate

https://doi.org/10.3390/cmtr19010002

is expected to be very low [27]. Nevertheless, the porous structure (100–300 μm) allows fibrovascular and osseous ingrowth, enhancing implant stabilization and resistance to infection—clear advantages over silicone [21]. Other materials have also been described, such as a non-resorbable porous polymeric composite based on polymethylmethacrylate (PMMA) with pore sizes between 150 and 350 μm, as well as silicone, which remains widely used due to its chemical inertness and ease of handling [7].

In the lower facial third, polyetheretherketone (PEEK) and titanium have been extensively studied, particularly in PSI and mandibular augmentation procedures. PEEK offers several advantages, including light weight, radiolucency, and an elastic modulus similar to bone, while not interfering with imaging modalities such as CT or MRI [21,30].

Studies have reported satisfactory esthetic results and comparable symmetry between stock polyethylene implants and customized PEEK implants, with PEEK being more favorable in patient-specific mandibular angle implants [21,26]. However, the lack of osseointegration in PEEK remains a concern among European surgeons, who prefer titanium due to its long-term integration, despite the potential complications associated with osseointegrated materials [43].

Smooth-surfaced titanium implants reduce bacterial adhesion and biofilm formation by 80–90% compared with porous coatings while supporting osteogenic cell compatibility [30]. Patient-specific titanium angle implants further lower displacement risk through precise anatomic fit [10,30]. Titanium also ensures durable outcomes via osseointegration, unlike porous polyethylene, and porous titanium closely matches human bone mechanics, providing structural stability and long-term integration [10,30].

CAD/CAM-designed patient-specific implants (PSIs) enable greater precision and planning, particularly in complex or asymmetric facial cases, offsetting increased cost and planning time by reducing surgical duration and improving esthetic predictability [21,26]. Unlike stock implants, which often require intraoperative trimming and risk asymmetry, PSIs provide faster, more predictable symmetry and volumetric restoration. Screw fixation—usually one or two per implant—ensures stability and prevents postoperative displacement [21]. However, the design of customized implants must account for the practical feasibility of intraoperative positioning and stabilization. If these considerations are overlooked, the implant may not be clinically executable when transitioning from virtual planning to surgical application (Figure 4). Therefore, the surgeon must closely monitor and actively participate in the design process to ensure that the final construct is surgically achievable.

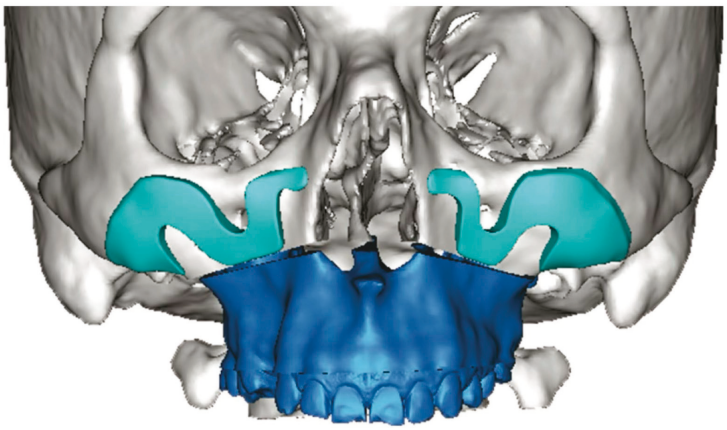

Figure 4. Three-dimensional computer-assisted design illustrates the potential for highly customized implant geometry. However, in this case, the virtual planning lacked adequate anatomical assessment and did not include a rigorous evaluation of the surgical access or the feasibility of implant insertion within the available soft-tissue pocket. These oversights contributed to limitations in the clinical applicability of the proposed design—Image from the authors' personal archive.

https://doi.org/10.3390/cmtr19010002

4.3. Intraoperative Technical Considerations

Placement of facial implants during orthognathic surgery requires precise planning and delicate technique. Infraorbital rim augmentation after Le Fort I osteotomy with silicone implants is technically demanding, as dissection must expose the infraorbital rim while preserving the neurovascular bundle and periosteal integrity. The implant is contoured to accommodate the infraorbital nerve and positioned flush with the rim to avoid mid-cheek over augmentation. Secure fixation with titanium screws is recommended, particularly when the implant overlaps the Le Fort I plates [11].

Placement of malar implants is technically challenging due to the limited surgical field and the need for precise, symmetric bilateral dissection along the zygomatic body and arch. Careful subperiosteal pocket creation is essential to avoid injury to the infraorbital and zygomaticofacial nerves (Figure 5). Slight overcorrection (1 mm) is recommended to account for postoperative tissue adaptation [18,19,28].

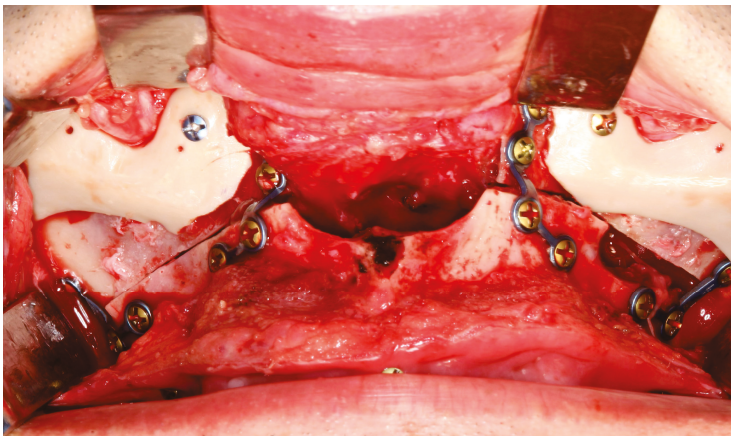

Figure 5. Personalized midfacial implants designed to enhance zygomatic and perinasal projection. Internal fixation was achieved with two screws, and the customized design prevents contact with the titanium plates—Image from the authors' personal archive.

Porous polyethylene implants, while promoting tissue integration, require meticulous pocket preparation and a thick soft tissue envelope to avoid erosion or exposure. Excessive handling can damage the implant or surrounding tissues. The introduction of preformed PEEK-PSI has improved intraoperative efficiency by minimizing trimming and manipulation, though precise alignment within the surgical field remains technically demanding [21].

For genioplasty, the intraoral approach is favored to avoid external scarring in patients undergoing concurrent orthognathic procedures [11]. However, this approach restricts visualization and increases soft tissue tension, particularly when inserting large or rigid implants. Dissection must remain strictly subperiosteal to preserve the mental nerves and ensure stable pocket formation [24]. Overextension of the incision or excessive traction may compromise wound closure and elevate infection risk. Proper screw fixation is crucial to counteract dynamic muscular forces during mastication and speech [11,24].

Mandibular angle augmentation during orthognathic surgery is technically demanding (Figure 6) due to the complex anatomy of the pterygomasseteric sling and its functional relationship with the masseter muscle [30]. Careful subperiosteal dissection along the inferior mandibular border is required to preserve the muscular sling, as disruption may cause superior masseter retraction and hollowing of the angle [10,30,33]. Intraoperative strategies to minimize complications include epinephrine infiltration, wide intraoral incisions for visualization, strict subperiosteal dissection, and stable screw fixation. Augmentation should respect the patient's soft-tissue envelope and masseter strength, particularly in

https://doi.org/10.3390/cmtr19010002

hypodivergent or brachyfacial patients, to avoid over-contouring or implant stress, thereby reducing the risk of malposition, asymmetry, and revision [10,33].



Figure 6. Standard mandibular angle implants. When used in combination with a mandibular osteotomy, adaptation of the implant design is required. Although this remains a viable surgical alternative, it demands additional operative time and meticulous positioning to ensure adequate bone contact and stability. Using PSI, this adaptation can be planned in advance, positioned safely away from the osteotomy line and the fixation point—Image from the authors' personal archive.

4.4. Outcomes

Outcome reporting across the included studies was primarily qualitative, reflecting the absence of standardized outcome measures and the limited availability of comparative data in the current literature. This limitation precludes meaningful quantitative comparison and underscores the exploratory nature of the present scoping review.

Facial implants combined with orthognathic surgery yield predictable and esthetically favorable outcomes when careful technique and sufficient soft tissue coverage are ensured. Porous polyethylene implants perform best under healthy mucoperiosteum, particularly in the paranasal region, with low complication rates. Reported issues, such as excessive prominence or minor asymmetry, may require revision, but proper tissue ingrowth and stable fixation minimize these risks [28].

In a large clinical series, Medpor implants had an overall complication rate of 8.8%, including rare infection, delayed hematoma, transient paresthesia, and mild disproportion, with implant removal required in only 0.7% of cases [19]. Pain and sensory changes were transient, and no long-term migration or allergic reactions occurred. Similarly, Lutz et al. (2020) [11] reported no physical complications over a mean follow-up of 41 months, with an 8% esthetic complication rate that resolved after minor revisions and over 80% patient satisfaction. Malar augmentation performed alongside orthognathic surgery achieved excellent facial symmetry with minimal morbidity.

Patient-specific PEEK implants have emerged as a promising alternative for facial skeletal reconstruction due to their anatomic accuracy, biocompatibility, and intraoperative efficiency. Kerkfeld et al. (2022) [26] reported intraoral exposure in two patients, which was corrected by in situ grinding without further complications. No cases of infection, inflammation, or fracture were noted. Scolozzi et al. (2015) [32] reported no complications in 10 patients with a mean age of 21.3 years who underwent PEEK implants for correction of residual contour chin and/or mandibular defects concomitantly with orthognathic surgery, with a mean follow-up of 1 year.

https://doi.org/10.3390/cmtr19010002

Titanium patient-specific implants (PSIs) and mesh have shown reliable outcomes when combined with orthognathic surgery for mandibular contour correction. Ramieri et al. (2025) [10] reported stable volumetric augmentation with minimal complications using the Implate system, while Rios et al. (2025) [30] highlighted titanium's osseointegration and low long-term risk. Stringer and Brown (2009) [33] also confirmed effective mandibular asymmetry correction with angled titanium mesh. Overall, titanium implants—custom or mesh-based—offer predictable, stable results and improved mandibular definition when integrated into the surgical plan.

Despite the potential advantages of simultaneous facial implant placement during orthognathic surgery, several limitations and challenges have been reported. In the acute surgical setting, postoperative edema and ongoing soft tissue adaptation may compromise accurate intraoperative assessment of implant size, contour, and three-dimensional positioning, particularly when stock implants are used [44,45]. This limitation may increase the risk of suboptimal esthetic outcomes, implant malposition, or the need for secondary revision procedures [46]. Consequently, several authors have advocated a staged approach, in which facial implants are placed after completion of orthognathic surgery and stabilization of the soft tissues, allowing for more precise esthetic evaluation, improved surgical planning, and greater predictability of outcomes [20,47,48].

4.5. Summary and Future Perspectives

Current evidence suggests that alloplastic facial implants may serve as useful adjuncts to orthognathic surgery, with reported improvements in skeletal contour and soft tissue profile. However, the available data are largely derived from case reports and small observational series, which limits the strength of conclusions regarding safety, effectiveness, and predictability. The growing use of customized, patient-specific implants (PSIs)—particularly those fabricated from PEEK or titanium—appears to offer potential advantages in terms of anatomical fit and surgical planning, although these observations are based on limited clinical evidence. Importantly, reported outcomes remain closely dependent on surgical expertise, appropriate implant fixation, and the condition of the overlying soft tissues. Future studies employing standardized outcome measures, comparative designs, and longer follow-up periods are needed to better evaluate long-term stability, cost-effectiveness, and the impact of digital planning advancements, including more accurate simulation of soft tissue behavior. As the evidence base evolves, these developments may help clarify the role of PSI-based facial augmentation in orthognathic and reconstructive facial surgery.

Author Contributions: Conceptualization, G.C.B. and S.O.; methodology, G.C.B. and S.O.; software, G.C.B. and S.O.; validation, M.d.M., L.F. and S.O.; formal analysis, G.C.B. and S.O.; investigation, G.C.B. and S.O.; resources, S.O.; data curation, G.C.B. and S.O.; writing—original draft preparation, G.C.B.; writing—review and editing, M.d.M., L.F. and S.O.; visualization, G.C.B. and S.O.; supervision, S.O.; project administration, G.C.B. and S.O. All authors have read and agreed to the published version of the manuscript.

Funding: This research received no external funding.

Institutional Review Board Statement: Ethical review and approval were waived for this study due to the review nature of the article. The clinical images used were obtained from the author's own archive and correspond to patients who had previously undergone surgical procedures and had signed informed consent forms authorizing the use of their images for scientific research purposes.

Informed Consent Statement: Due to the nature and methodology applied in this study, informed consent from participants is not required.

https://doi.org/10.3390/cmtr19010002

Data Availability Statement: The original contributions presented in this study are included in the article. Further inquiries can be directed to the corresponding author.

Conflicts of Interest: The authors declare no conflicts of interest.

References

1. Simões, J.C.M.; Garcia, D.M.; De Mello-Filho, F.V.; De Felício, C.M.; Trawitzki, L.V.V. Masticatory function and three-dimensional facial morphology of soft tissues: One year after orthognathic surgery. *Arch. Oral Biol.* **2025**, *169*, 106103. [CrossRef]
2. Lin, C.; Zhang, J.; Zheng, M.; Li, M.; Zhu, C.; Wan, Q. Factors influencing the quality of life among orthognathic patients: A systematic review and meta-analysis. *Eur. J. Orthod.* **2025**, *47*, cjaf034. [CrossRef]
3. Kao, C.Y.; Huang, T.H.; Ho, C.T.; Hsieh, Y.H.; Kao, C.T. Evaluating the impact of orthognathic surgery on mental health, function, and quality of life. *J. Dent. Sci.* **2025**, *20*, 2292–2300. [CrossRef]
4. Avrămuț, R.-P.; Stăncioiu, A.-A.; Talpos, S.; Motofelea, A.C.; Popa, M.; Szuhanek, C. Quantitative Evaluation of Skeletal, Dental, and Soft Tissue Changes After Orthognathic Surgery: A Cephalometric and Statistical Analysis. *J. Clin. Med.* **2025**, *14*, 7336. [CrossRef]
5. Grillo, R. Harmonizing aesthetics and function in orthognathic surgery: An evolving evidence-based dialogue. *J. Stomatol. Oral Maxillofac. Surg.* **2025**, *126*, 102482. [CrossRef]
6. Jansma, J.; Schepers, R.H. Adjunctive Aesthetic Procedures in Orthognathic Surgery. *Oral Maxillofac. Surg. Clin. N. Am.* **2023**, *35*, 139–152. [CrossRef] [PubMed]
7. Marano, R.; Leite, M.G.; de Oliveira Gorla, L.F.; Daroz, B.G.; de Oliveira, R.P. Complementing Orthognathic Surgery Esthetic Outcomes with Facial Prosthesis. *J. Craniofac. Surg.* **2025**. [CrossRef]
8. Zheng, Z.; Saito, D.; Hasebe, D.; Funayama, A.; Nihara, J.; Kobayashi, T. Three-dimensional evaluation of maxillofacial symmetry improvement following orthognathic surgery in patients with asymmetrical jaw deformities. *Oral Maxillofac. Surg.* **2024**, *29*, 8. [CrossRef] [PubMed]
9. Sun, X.; Han, J.; Wang, J.; Lian, J.; Liu, J.; Li, S.; Liu, S.; Zhou, H. Precision and Efficacy of Digital Technology in Orthognathic Surgery for Facial Asymmetry Correction: A Quantitative Analysis. *Aesthetic Plast. Surg.* **2025**, *49*, 4587–4596. [CrossRef]
10. Ramieri, V.; Pignataro, L.V.; Marianetti, T.M.; Spadoni, D.; Frosolini, A.; Gennaro, P. Overcoming the Limitations of Conventional Orthognathic Surgery: A Novel Approach Using Implate. *J. Clin. Med.* **2025**, *14*, 5012. [CrossRef] [PubMed]
11. Lutz, J.C.; Assouline Vitale, L.S.; Graillon, N.; Foletti, J.M.; Schouman, T. Standard and Customized Alloplastic Facial Implants Refining Orthognathic Surgery: Outcome Evaluation. *J. Oral Maxillofac. Surg. Off. J. Am. Assoc. Oral Maxillofac. Surg.* **2020**, *78*, 1832.e1–1832.e12. [CrossRef]
12. Yaremchuk, M.J.; Doumit, G.; Thomas, M.A. Alloplastic augmentation of the facial skeleton: An occasional adjunct or alternative to orthognathic surgery. *Plast. Reconstr. Surg.* **2011**, *127*, 2021–2030. [CrossRef]
13. Olate, S.; Zaror, C.; Mommaerts, M.Y. A systematic review of soft-to-hard tissue ratios in orthognathic surgery. Part IV: 3D analysis—Is there evidence? *J. Cranio-Maxillofac. Surg.* **2017**, *45*, 1278–1286. [CrossRef] [PubMed]
14. Ravelo, V.; Olate, S.; Bravo-Soto, G.; Zaror, C.; Mommaerts, M. Systematic review of soft-to-hard tissue ratios in orthognathic surgery: 3D analysis-update of scientific evidence. *Int. J. Oral Maxillofac. Surg.* **2025**, *54*, 819–829. [CrossRef] [PubMed]
15. Raffaini, M.; Pisani, C. Orthognathic surgery with or without autologous fat micrograft injection: Preliminary report on aesthetic outcomes and patient satisfaction. *Int. J. Oral Maxillofac. Surg.* **2015**, *44*, 362–370. [CrossRef]
16. Rees, T.D. *Wood Smith D: Cosmetic Facial Surgery*, 1st ed.; Saunders: Philadelphia, PA, USA, 1973.
17. Arem, A.J.; Rasmussen, D.; Madden, J.W. Soft tissue response to Proplast: Quantitation of scar ingrowth. *Plast. Reconstr. Surg.* **1978**, *61*, 214. [CrossRef]
18. D'Agostino, A.; Trevisiol, L.; Favero, V.; Gunson, M.J.; Pedica, F.; Nocini, P.F.; Arnett, G.W. Hydroxyapatite/Collagen Composite Is a Reliable Material for Malar Augmentation. *J. Oral Maxillofac. Surg. Off. J. Am. Assoc. Oral Maxillofac. Surg.* **2016**, *74*, 1238.e1–1238.e15. [CrossRef]
19. Nocini, P.F.; Chiarini, L.; Bertossi, D. Cosmetic procedures in orthognathic surgery. *J. Oral Maxillofac. Surg. Off. J. Am. Assoc. Oral Maxillofac. Surg.* **2011**, *69*, 716–723. [CrossRef]
20. Kauke-Navarro, M.; Knoedler, L.; Baecher, H.; Sherwani, K.; Knoedler, S.; Allam, O.; Diatta, F.; Alperovich, M.; Safi, A.F. A systematic review of implant materials for facial reconstructive and aesthetic surgery. *Front. Surg.* **2025**, *12*, 1548597. [CrossRef] [PubMed]
21. Olate, S.; Uribe, F.; Huentequeo-Molina, C.; Goulart, D.R.; Sigua-Rodriguez, E.A.; Alister, J.P. Mandibular Angle Contouring Using Porous Polyethylene Stock or PEEK-based Patient Specific Implants. A Critical Analysis. *J. Craniofacial Surg.* **2021**, *32*, 242–246. [CrossRef]
22. Tricco, A.C.; Lillie, E.; Zarin, W.; O'Brien, K.K.; Colquhoun, H.; Levac, D.; Moher, D.; Peters, M.D.; Horsley, T.; Weeks, L.; et al. PRISMA extension for scoping reviews (PRISMA-ScR): Checklist and explanation. *Ann. Intern. Med.* **2018**, *169*, 467–473. [CrossRef]

https://doi.org/10.3390/cmtr19010002

23. Fattahi, T.; Salman, S.; Steinberg, B. Augmentation of the infraorbital rim in orthognathic surgery. *Int. J. Oral Maxillofac. Surg.* **2017**, *46*, 1315–1318. [CrossRef] [PubMed]
24. Findikcioglu, K.; Sibar, S.; Gulsen, A. Treatment Approach to Severe Microgenia Cases: Combined Use of Osseous and Implant Genioplasty. *J. Craniofacial Surg.* **2018**, *29*, e175–e179. [CrossRef]
25. Genc, A.; Isler, S.C.; Oge, A.E.; Matur, Z. Effect of Sagittal Split Osteotomy with Medpor® Porous Polyethylene Implant on Masticatory Reflex. *Ann. Dent. Spec.* **2022**, *10*, 12–16. [CrossRef]
26. Kerkfeld, V.; Schorn, L.; Depprich, R.; Lommen, J.; Wilkat, M.; Kübler, N.; Rana, M.; Meyer, U. Simultaneous PSI-Based Orthognathic and PEEK Bone Augmentation Surgery Leads to Improved Symmetric Facial Appearance in Craniofacial Malformations. *J. Pers. Med.* **2022**, *12*, 1653. [CrossRef] [PubMed]
27. Kwon, T.G.; Kang, S.M.; Hwang, H.D. Three-dimensional soft tissue change after paranasal augmentation with porous polyethylene. *Int. J. Oral Maxillofac. Surg.* **2014**, *43*, 816–823. [CrossRef]
28. da Silva de Menezes, J.D.; Moura, L.B.; Martins, R.P.; Hochuli-Vieira, E. Porous Polyethylene Implant as Aesthetic Complement in Orthognathic Surgery. *J. Craniofacial Surg.* **2016**, *27*, e790–e791. [CrossRef]
29. Nocini, P.F.; Boccieri, A.; Bertossi, D. Gridplan midfacial analysis for alloplastic implants at the time of jaw surgery. *Plast. Reconstr. Surg.* **2009**, *123*, 670–679. [CrossRef]
30. Rios, O.; Pradel, R.; Pradel, J.; Lerhe, B.; Savoldelli, C. Jawline improvement using patient-specific angle implants with virtual planning in orthognathic surgery. *J. Craniomaxillofac Surg.* **2025**, *53*, 507–515. [CrossRef]
31. Robiony, M.; Costa, F.; Demitri, V.; Politi, M. Simultaneous malaroplasty with porous polyethylene implants and orthognathic surgery for correction of malar deficiency. *J. Oral Maxillofac. Surg.* **1998**, *56*, 734–742. [CrossRef]
32. Scolozzi, P. Computer-aided design and computer-aided modeling (CAD/CAM) generated surgical splints, cutting guides and custom-made implants: Which indications in orthognathic surgery? *Rev. Stomatol. Chir. Maxillofac. Chir. Orale* **2015**, *116*, 343–349. [CrossRef]
33. Stringer, D.; Brown, B. Correction of mandibular asymmetry using angled titanium mesh. *J. Oral Maxillofac. Surg.* **2009**, *67*, 1619–1627. [CrossRef]
34. Hwang, S.M.; Park, S.H.; Lee, J.S.; Kim, H.D.; Hwang, M.K.; Kim, M.W. Improvement of Infraorbital Rim contour Using Medpor. *Arch. Craniofacial Surg.* **2016**, *17*, 77–81. [CrossRef] [PubMed] [PubMed Central]
35. Mladick, R.A. Alloplastic cheek augmentation. *Clin. Plast. Surg.* **1991**, *18*, 29. [CrossRef]
36. Pendergast, M.; Schoenrock, L.D. Malar augmentation: Patient classification and placement. *Arch. Otolaryngol. Head Neck Surg.* **1989**, *115*, 964–969. [CrossRef]
37. Terino, E.O. Alloplastic facial contouring by zonal principles of skeletal anatomy. *Clin. Plast. Surg.* **1992**, *19*, 487. [CrossRef]
38. Sylver, W.F. The use of alloplastic material in contouring the face. *Facial Plast. Surg.* **1986**, *3*, 81. [CrossRef]
39. Powell, N.B.; Riley, R.W.; Laub, D.R. A new approach to evaluation and surgery of the malar complex. *Ann. Plast. Surg.* **1988**, *20*, 206. [CrossRef] [PubMed]
40. Moradi, A.; Montes, J.R.; Humphrey, S.; Grunebaum, L.D.; Bertossi, D.; Dimitrijevic, E.; Sangha, S. A Unified Approach to Facial Contours and Volume Correction: The Role of the Cheek and the Chin. *Plast. Reconstr. Surg. Glob. Open* **2024**, *12*, e6219. [CrossRef] [PubMed] [PubMed Central]
41. Mommaerts, M.Y. The ideal male jaw angle—An internet survey. *J. Cranio-Maxillofac. Surg.* **2016**, *44*, 381–391. [CrossRef]
42. Mommaerts, M.Y.; Cleymaet, R. The ideal shape of the female jaw angle: An online survey. *J. Cranio-Maxillofac. Surg.* **2023**, *51*, 597–602. [CrossRef]
43. Mommaerts, M.Y. Guidelines for patient-specific jawline definition with titanium implants in esthetic, deformity, and malformation surgery. *Ann. Maxillofac. Surg.* **2016**, *6*, 287–291. [CrossRef] [PubMed]
44. Guyuron, B.; Raszewski, R. Aesthetic considerations in orthognathic surgery. *Clin. Plast. Surg.* **2007**, *34*, 469–479.
45. Binder, W.J. The use of alloplastic implants in facial skeletal augmentation. *Clin. Plast. Surg.* **2009**, *36*, 1–14.
46. Mommaerts, M.Y. Facial implants: Indications, techniques, and pitfalls. *J. Craniofacial Surg.* **2001**, *12*, 297–303.
47. Eppley, B.L. Combined orthognathic and aesthetic surgery: Indications and outcomes. *Oral Maxillofac. Surg. Clin. N. Am.* **2014**, *26*, 557–564.
48. Villarreal Renedo, P.; Gancedo Pérez, B.; Villarreal-González, A.; Roldán-Otero, P.; Fernández-González, V.; Requena-Pérez, M.V. Simultaneous orthognathic surgery and implant-supported rehabilitation using customized subperiosteal or supraosseous implants: Clinical case series. *Rev. Esp. Cir. Oral Maxilofac.* **2023**, *45*, 26–30. [CrossRef]

Disclaimer/Publisher's Note: The statements, opinions and data contained in all publications are solely those of the individual author(s) and contributor(s) and not of MDPI and/or the editor(s). MDPI and/or the editor(s) disclaim responsibility for any injury to people or property resulting from any ideas, methods, instructions or products referred to in the content.

https://doi.org/10.3390/cmtr19010002

craniomaxillofacial
trauma & reconstruction

MDPI

Technical Note

Preoperative Near-Infrared (NIR) Vein Visualization in Zygomatic Implant Perforated (ZIP) Flap †

Yoram Fleissig [1,*], Jhonatan Elia [2], Nir Hirshoren [3], Amalia Sabato [4], Eleonora Ginzburg [4], Jawad Abu Tair [1], Jeffrey M. Weinberger [3] and Shay Sharon [1]

[1] Department of Oral and Maxillofacial Surgery, Hadassah Medical Center, Faculty of Dental Medicine, Hebrew University of Jerusalem, P.O. Box 12272, Jerusalem 9112102, Israel
[2] Department of Plastic Surgery, Hadassah Medical Center, Faculty of Medicine, Hebrew University of Jerusalem, P.O. Box 12272, Jerusalem 9112102, Israel
[3] Department of Otolaryngology—Head and Neck Surgery, Hadassah Medical Center, Faculty of Medicine, Hebrew University of Jerusalem, P.O. Box 12272, Jerusalem 9112102, Israel
[4] Maxillofacial Rehabilitation Unit, Hadassah Medical Center, Faculty of Dental Medicine, Hebrew University of Jerusalem, P.O. Box 12272, Jerusalem 9112102, Israel
* Correspondence: yoram77@gmail.com
† Near-Infrared Vein Visualization in ZIP Flap Reconstruction.

Abstract

Zygomatic implant perforated (ZIP) flap reconstruction offers immediate surgical rehabilitation following maxillectomy, integrating oncologic zygomatic implants with a fasciocutaneous free flap. A critical technical challenge is safely perforating the free flap skin paddle to accommodate implants' abutments without damaging its vasculature. Near-infrared (NIR) vein visualization technology provides real-time mapping of subcutaneous vessels and has been widely investigated in settings such as pediatric intravenous (IV) cannulation. By projecting vein pathways onto the skin, NIR visualization facilitates precise vascular identification, potentially reducing complications. We describe a case of ZIP flap reconstruction in a 25-year-old patient utilizing NIR vein visualization to preemptively locate flap vasculature and minimize the risk of vessel puncture. Our discussion places these findings within the context of the existing literature on NIR devices, underscoring their benefits of non-invasive operation, rapid imaging, and minimal need for advanced operator skills, and highlighting their utility in microvascular reconstructive surgery.

Keywords: zygomatic implant perforated flap; near-infrared vein visualization; maxillectomy reconstruction

1. Introduction

Surgical reconstruction following maxillectomy is both complex and challenging, with ongoing debate regarding the optimal reconstruction approach. Each method has distinct advantages and disadvantages [1]. While obturators can provide satisfactory outcomes, issues such as nasal leakage, retention, and resistance often arise. In certain cases, reconstruction using composite microvascular free tissue transfer is preferred, yielding excellent results. However, it is estimated that fewer than 50% of patients achieve dental rehabilitation following maxillary free flap reconstruction due to various challenges [2]. Even when successful, composite free flap reconstructions often delay dental rehabilitation by 12 to 18 months [3]. While the concept of a maxillary jaw in a day offers a promising solution, it is not extensively reported in the literature, and concerns about higher flap failure rates were raised, especially in malignant cases [2]. Edentulism has a well-documented negative

impact on patients' quality of life. Achieving acceptable functional and aesthetic outcomes through microvascular reconstruction, dental implants, and prostheses can significantly enhance patient well-being [4].

Rogers and Butterworth introduced the zygomatic implant perforated (ZIP) flap technique, a method for immediate surgical reconstruction and rapid postoperative prosthodontic rehabilitation with a fixed dental prosthesis following low-level maxillectomy [5]. Although Hirsch et al. previously described a similar approach, their method involved placing the zygomatic implants at a second stage [6]. In the ZIP flap technique, zygomatic oncologic implants are inserted immediately after maxillary tumor ablation, while a second surgical team simultaneously harvests a fascio-cutaneous free flap, typically from the radial forearm.

The free flap is meticulously perforated to accommodate the zygomatic implant abutments before being anastomosed. Recent outcomes from a series of 35 cases highlight the potential of this technique, demonstrating its predictability, rapid return to function, and high levels of patient satisfaction [7].

Although this technique is relatively straightforward, microvascular surgeons may find the perforation of the free flap skin paddle challenging, particularly when the flap has not yet been anastomosed, and the superficial vasculature is inadequately visible.

Near-infrared (NIR) vein visualization technology allows for the real-time mapping of subcutaneous vasculature directly onto the skin's surface. NIR light penetrates the skin and subcutaneous fat, where it is absorbed by blood flowing through the veins, making the veins appear dark against the lighter background of the surrounding tissues. NIR vein visualization technology is widely used in modern hospitals, particularly in emergency medicine and pediatric departments, as well as in anesthesiology, intensive care, and oncology units.

This paper aims to describe the utility of near-infrared (NIR) vein visualization in preventing vessel puncture during flap skin paddle perforation.

2. Case Presentation

A 25-year-old male presented to our outpatient clinic with a two-year history of a growing mass in his left palate (Figure 1). An incisional biopsy confirmed a diagnosis of low-grade mucoepidermoid carcinoma. Oncologic workup included CT, MRI, CBCT, and dental scans. The CAD-CAM workflow (Figure 2) involved using ProPlan CMF software (Materialise, Leuven, Belgium) to plan for a marking jig for performing the planned resection with adequate margins and low-level maxillectomy. The EZplan Real Guide planning software (Noris Medical zygomatic implants, Noris Medical, Nesher, Israel) was used to plan the placement of two oncologic zygomatic implants (50 mm and 37.5 mm long), and a standard 16 mm long implant at the upper left second incisor site, which was sacrificed to enhance dental prosthesis stability. A patient-specific titanium surgical guide was fabricated to ensure precise implant placement, and the dental prosthesis was designed using Meshmixer ver. 3.5 (Autodesk Inc., San Francisco, CA, USA) software and manufactured by a 3D printer (Formlabs, Somerville, MA, USA). To mark preferred skin paddle perforation sites for zygomatic implants' abutments, we used a free-flap 3D printed elastic template that could transfer the specific location.

https://doi.org/10.3390/cmtr19020019



Figure 1. A 25-year-old male with a two-year history of a growing mass in the left palate.

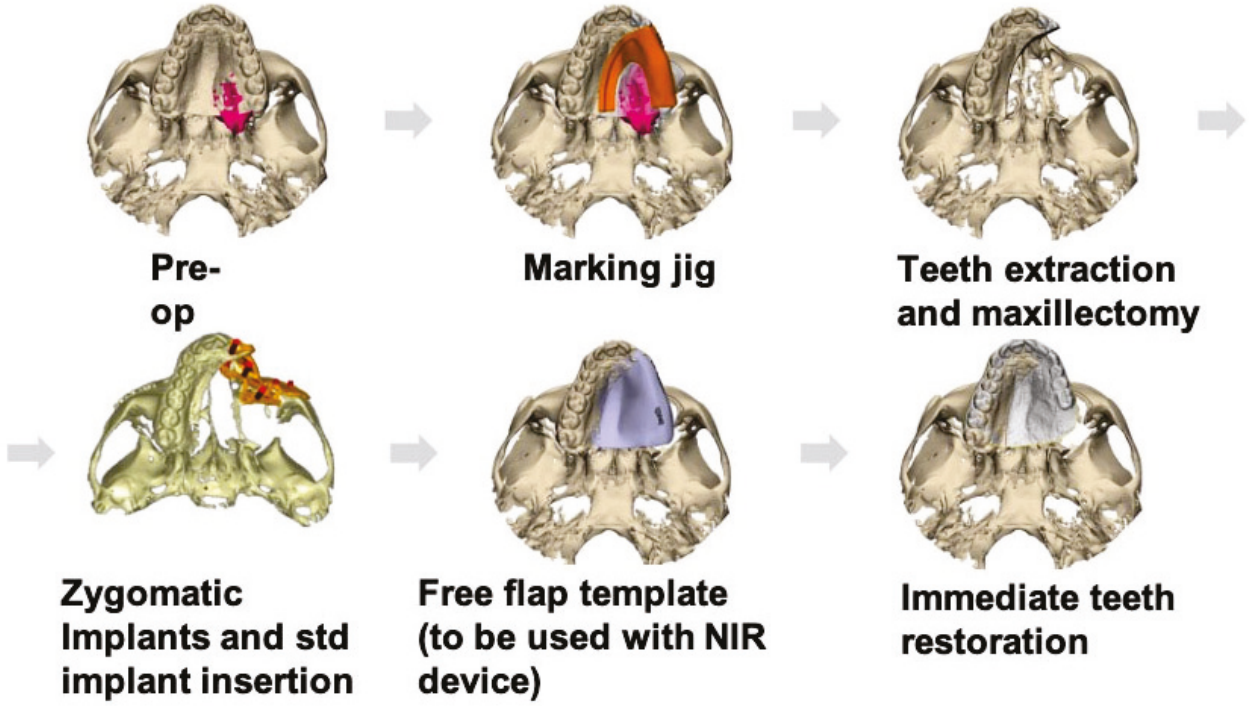

Figure 2. CAD-CAM workflow planning, marking jig, low-level maxillectomy, placement of two oncologic zygomatic implants and a standard long implant at the upper left second incisor site, free-flap template to transfer perforation sites to the skin paddle in conjunction with vasculature mapping using NIR vein visualization, and plan for immediate teeth restoration.

The surgical procedure included a tracheostomy, elective selective neck dissection at level Ib, and vessel preparation. A low-level hemi-maxillectomy (Brown IIB) was performed

https://doi.org/10.3390/cmtr19020019

through an intraoral approach, extending over the midline and including part of the soft palate and through the upper left canine socket. The marking jig was used to delineate the specific soft tissue resection border (Figure 3). The upper left second incisor was extracted, and the surgical guide was used to place the dental implant and two zygomatic implants, all achieving excellent primary stability (Figure 4). Before harvesting the radial forearm free flap, near-infrared vein visualization was utilized to map the superficial vein network and perforators from the radial artery, marking vascular-free area and optimal perforation locations for the zygomatic implants' abutments. A CAD-CAM free-flap template was used to verify and transfer the preferred perforation sites for the zygomatic implants' abutments (Figure 5a,b). In this case, according to the surgical resection site, expected emergence of the implants, flap geometry and the chosen direction of the vascular pedicle (posteriorly), perforations were planned at the medial side of the radial forearm free flap, far from the radial artery, but adjacent to the entangled superficial vein network (Figure 5c). The vascular pedicle was tunneled to the left neck, and flap insetting was completed with perforations at the pre-marked sites. Before perforating the skin paddle, the zygomatic implants' abutments were palpated, and we verified that their actual placement fits the plan and skin markings. Perforation was done meticulously using blade #11 and fine Mosquito forceps (Figure 6). After vascular anastomosis, the prefabricated dental prosthesis was fixed to the implants using a multi-unit system (Figure 7). Final pathology report described intermediate to high-grade mucoepidermoid carcinoma with perineural invasion and free surgical margins. Postoperative panoramic x-ray presents the implant location and temporary restoration (Figure 8).



Figure 3. Marking jig used to mark the specific soft tissue resection border.

https://doi.org/10.3390/cmtr19020019

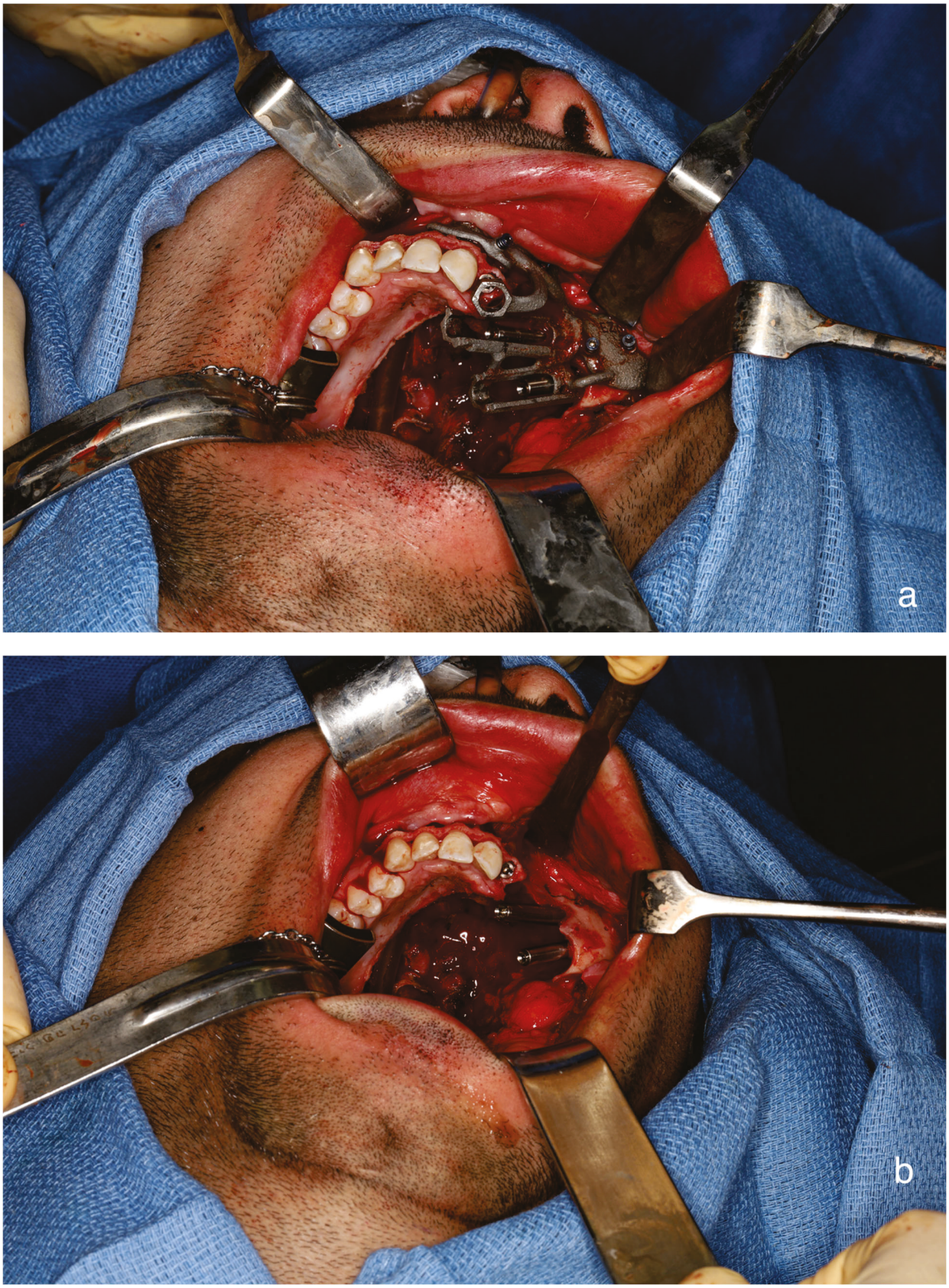

Figure 4. (**a**) Surgical guide for zygomatic implants and standard implant, fits well to post-resection maxillary and zygomatic defect boundaries. (**b**) Inserted dental implant and two zygomatic implants, all achieving excellent primary stability.

https://doi.org/10.3390/cmtr19020019

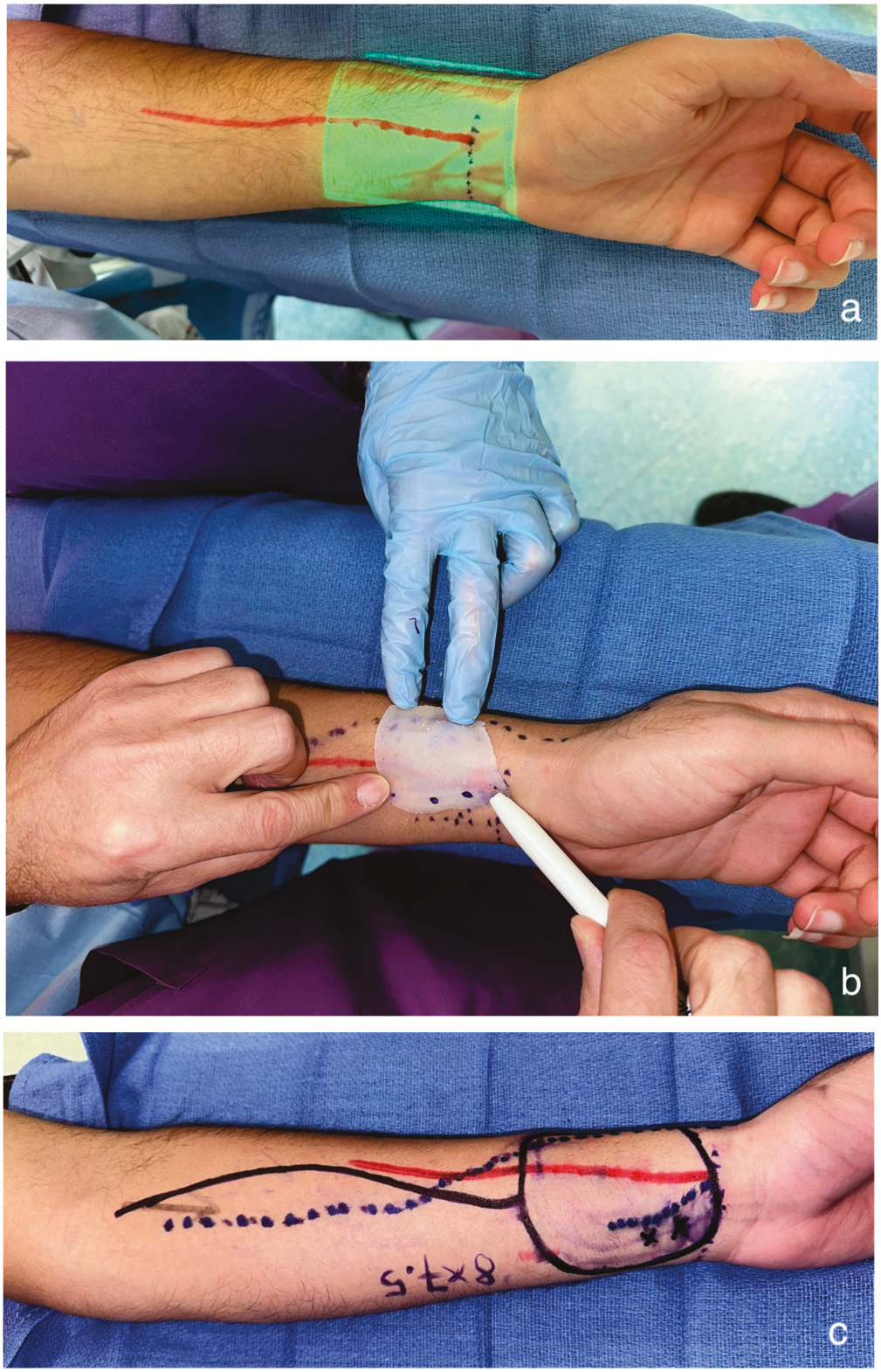

Figure 5. (**a**) Near-infrared vein visualization mapping the superficial vasculature of the radial forearm. Red line marks represent the radial artery. (**b**) A free-flap template was used to verify and transfer the preferred perforation sites (dot marks) for the zygomatic implants' abutments. (**c**) Radial forearm free flap markings (black marker). Red line marks the radial artery, blue dotted line marks the cephalic vein, and black asterisks mark the planned flap perforation for zygomatic implants, selected in a vascular-safe area.

https://doi.org/10.3390/cmtr19020019



Figure 6. Insetting of radial forearm free flap into maxillectomy defect and perforating two zygomatic implants and one standard dental implant.



Figure 7. Immediate rehabilitation with a prefabricated dental prosthesis that was fixed to the implants using a multi-unit system.

https://doi.org/10.3390/cmtr19020019

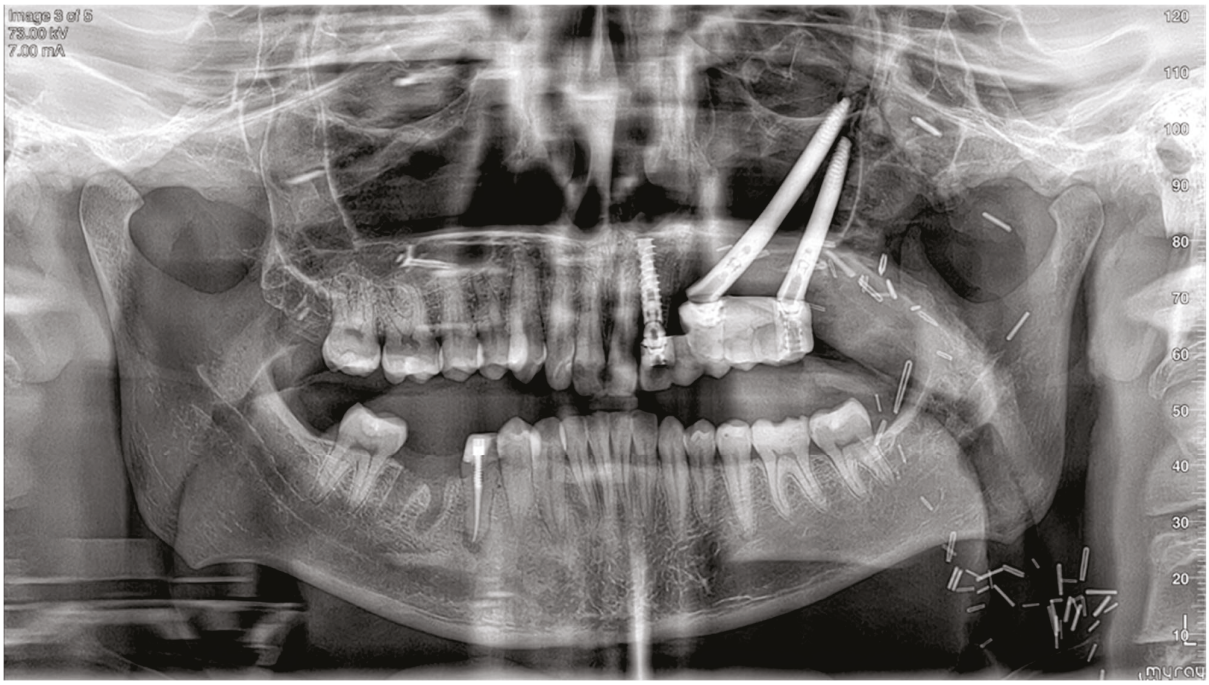

Figure 8. Postoperative panoramic X-ray.

3. Technique

To facilitate reproducibility, the CAD-CAM workflow is described step by step (Figure 2).

1. Tumor marking and resection planning: Using CAD-CAM, mark the tumor and plan sufficient oncologic resection margins using a marking jig.
2. Virtual resection: Execute virtual resection according to the tumor size and planned margins.
3. Implant planning: Using a dental scan of both jaws, plan the positions of zygomatic implants and abutment emergence to fit the dental arch and occlusion. As a guideline, we aim for 15 mm vertical distance between the implant platform and opposing teeth.
4. Surgical guide preparation: Plan a surgical guide for both zygomatic and standard implants (Figure 9). Ensure that the guide fits accurately to the post-resection maxillary and zygomatic defect boundaries. We recommend printing a 3D model to help the surgeon visualize the expected surgical defect (Figure 10). For cases with high uncertainty, surgical cutting guides can be printed (though they were not used in this case).
5. Free flap template planning: Print a free-flap template from elastic material to precisely measure flap size and geometry (Figure 11). After determining the side of vascular pedicle emergence, mark the preferred perforation sites for zygomatic implants on the template.
6. Vascular mapping: Using an NIR vein visualization device, mark the superficial vasculature on the skin paddle. Place the free flap template over the skin paddle, aligning the preferred perforation sites with a vascular-safe area.
7. Pre-perforation verification: After free flap harvesting and insetting, palpate the abutments over the zygomatic implant just before perforating the flap to ensure proper alignment of the planned perforation site.
8. Flap Perforation: Create a stab incision with a #11 blade and gently dilate with fine Mosquito forceps. Avoid over-enlarging the perforation, maintaining soft tissue tension to allow abutment insertion while preventing outward displacement. Use sutures as needed to reinforce tissue tension around the abutment.

https://doi.org/10.3390/cmtr19020019

9. Immediate restoration: Following free flap anastomosis, the prosthodontic team can proceed with immediate dental restoration. This restoration can be planned using CAD-CAM, based on the planned zygomatic implants, abutment emergence, and the patient's occlusion.

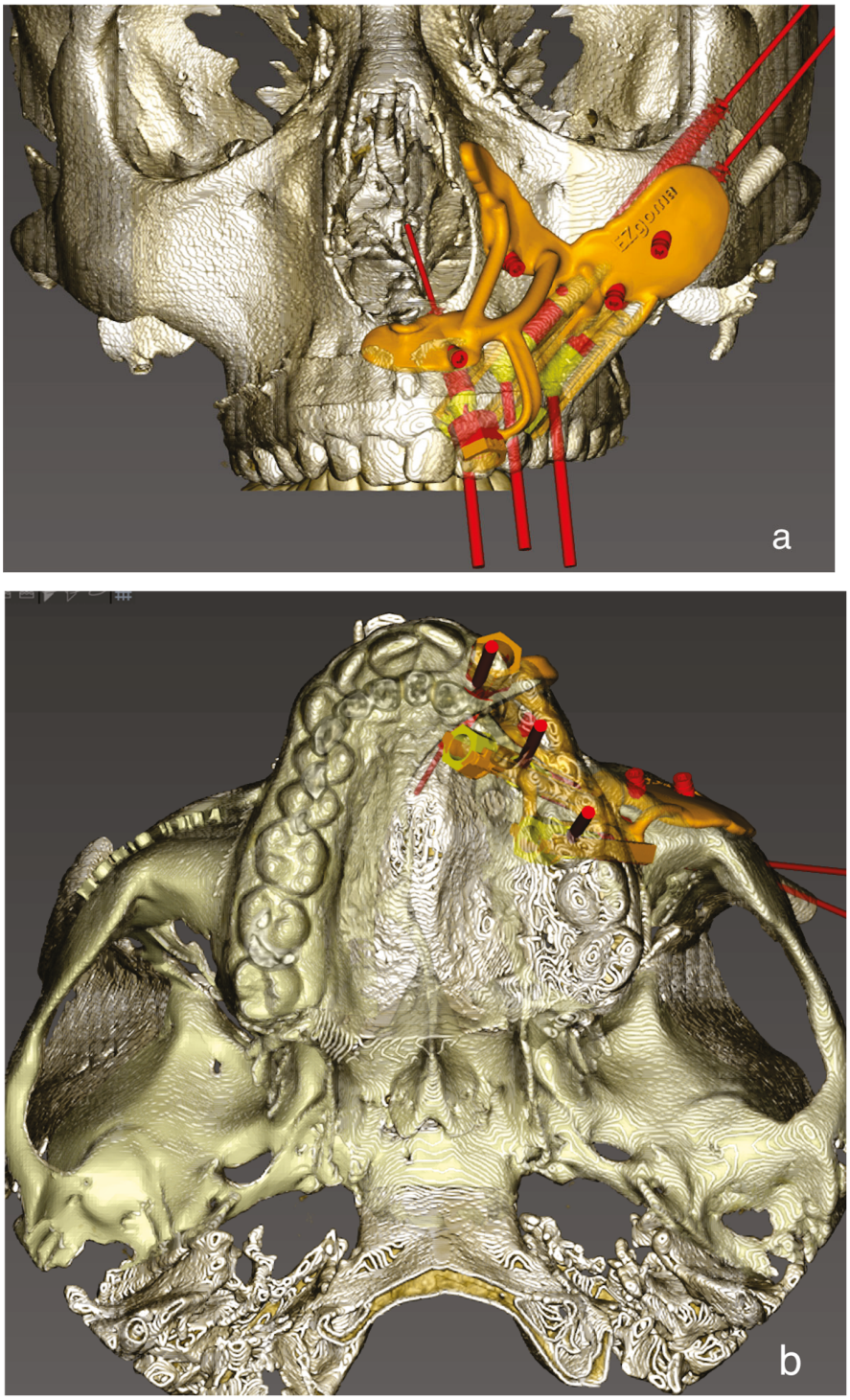

Figure 9. (**a**) Plan for surgical guide for zygomatic implants and standard implants—frontal view, demonstrating angulated and parallel abutments. (**b**) Plan for surgical guide for zygomatic implants and standard implants—inferior view, demonstrating abutment angles coinciding with the dental arch. A thin red line indicates the long axis of the implant.

https://doi.org/10.3390/cmtr19020019

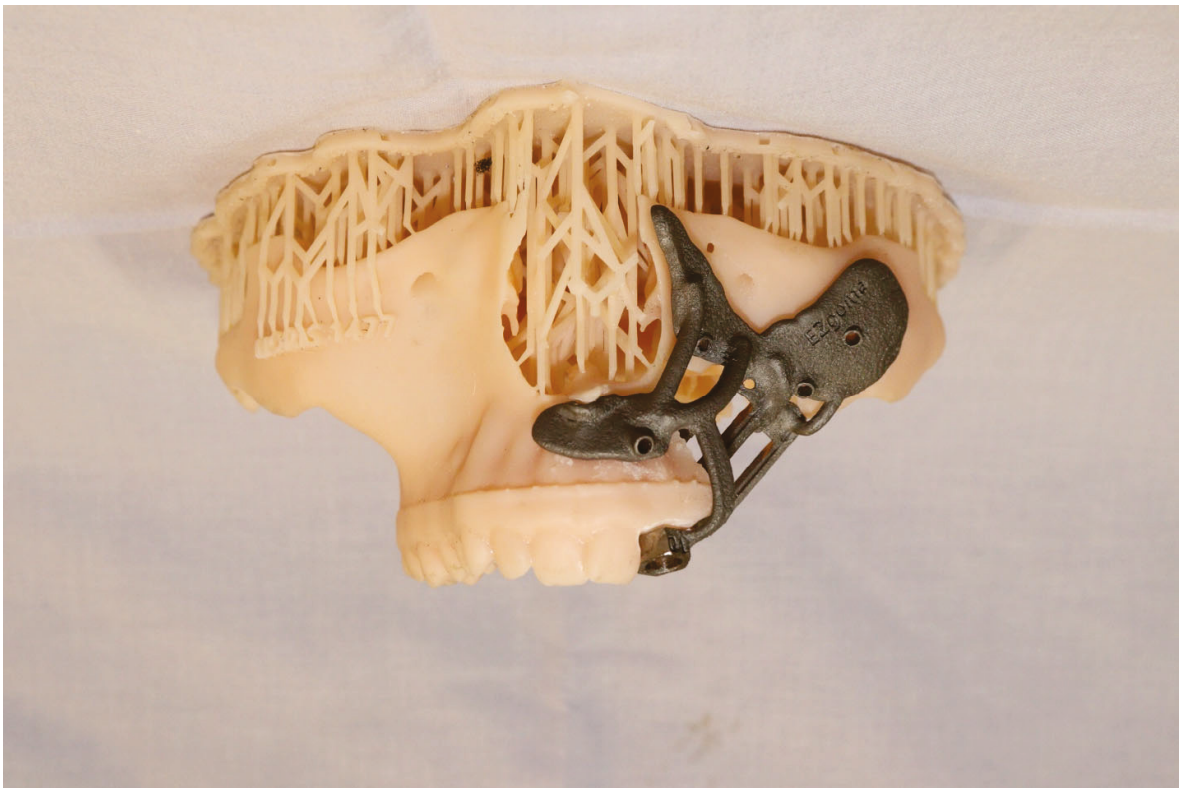

Figure 10. Printed 3D model to assist the surgeon in understanding what surgical defect to expect and how to fit the surgical guide.

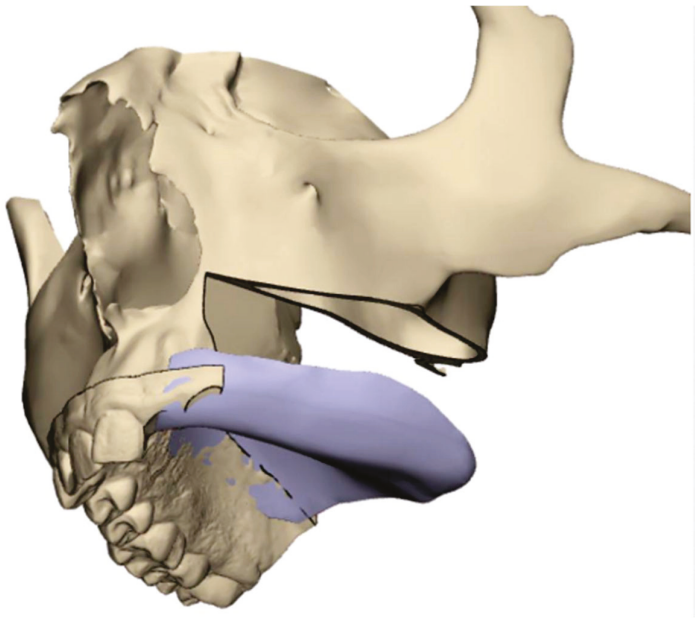

Figure 11. Plan for a free-flap template (printed from elastic material) to measure precisely for free flap size and geometry, and for transferring the preferred sites of perforation to the skin paddle.

4. Discussion

The NIR vein visualization device has been previously employed in reconstructive procedures, such as the design of a venous flap [8]. Its ability to enhance precision in identifying vascular structures makes it an invaluable tool in both routine and specialized medical applications. Much of the existing literature on NIR vein visualization focuses on intravenous (IV) cannulation, particularly in pediatric patients, where the aim is to

https://doi.org/10.3390/cmtr19020019

shorten cannulation time, reduce the number of attempts, and minimize pain or anxiety [9–11]. Although many of these studies show mixed or inconclusive results, likely due to population heterogeneity and varying operator skill, some also suggest potential benefits for individuals with difficult venous access, such as reduced complications like hematomas [12,13]. Crucially, the core principle remains the same: direct visualization of otherwise obscured veins can expedite procedures and lower the risk of vascular injury.

These insights align with our use of NIR vein visualization technology in flap surgery. In the pediatric realm, the key advantages include non-contact operation, real-time imaging, ease of learning, and no requirement for injected agents [9,14]. The same features can be highly beneficial when performing delicate procedures such as perforating a free flap skin paddle. By providing a clear visualization of the superficial vasculature, NIR vein visualization devices help avoid accidental vessel puncture, minimize bleeding, and potentially shorten operative time. The device is simple to use, typically with a working distance of 20–30 cm. It does not require a tourniquet, and no special setting is necessary to gain a good image quality.

Recent studies in adult and elderly populations [13] have further underlined the role of NIR vein visualization devices in reducing complications and patient distress. While some randomized trials found no significant improvement in first-attempt success rates or procedure duration, these devices were nonetheless associated with decreased hematoma formation and lower anxiety or depression scores, pointing toward improved overall patient comfort [13]. Although these findings stem from IV cannulation contexts, the underlying principle of careful vascular visualization can be readily translated to surgical procedures like ZIP flap reconstruction.

The radial forearm free flap is commonly the preferred choice for ZIP flap reconstruction due to its favorable thickness and pliability. Its superficial vasculature consists of the cephalic and basilic veins, which are typically visible to the naked eye. However, smaller intercommunicating veins on the volar side, as well as radial artery perforators, may be overlooked due to their random distribution and size. After harvesting the radial forearm flap, the veins become depleted and are no longer visible, making NIR vein visualization particularly useful preoperatively. This straightforward, non-invasive technique is time-efficient and can prevent vascular puncture and the complications of uncontrolled bleeding, especially when the flap is already sutured in place within the oral cavity. The device is relatively inexpensive and widely available in hospital settings. Although never discussed, we believe that perforating the free flap skin paddle is a challenging step. Incorporating the NIR vein visualization method could help address the concerns of reconstructive surgeons, particularly during their initial cases, and reduce the likelihood of abandoning this effective reconstruction option.

The practical advantages of NIR vein visualization devices, like non-invasiveness, ease of use, and immediate visualization, make them well-suited for incorporation into ZIP flap workflows. Although more comparative research is warranted, our experience suggests that the principles underlying the NIR vein visualization device's success in venous cannulation can indeed inform and improve surgical flap handling.

This case is notable for being performed on a young patient (25 years old), whereas most reported cases involve individuals in their seventh decade of life [7]. Additionally, ZIP flap reconstructions are typically bilateral, involving quad zygomatic implants. These two factors raise concerns about the long-term success and durability of this case. We also highlight the utility of CAD-CAM technology in the ZIP flap procedure, a concept previously suggested [15]. It is important to note in this context that the use of NIR vein visualization technology for skin-paddle perforation in free flap is independent of the CAD-CAM workflow and can be applied without it. However, since zygomatic implant

https://doi.org/10.3390/cmtr19020019

placement requires a high level of technical skill, the use of CAD-CAM and surgical guides can be an excellent option for young surgeons. Although this approach demands significant time and resources preoperatively, it simplifies the execution of initial cases and enhances surgical precision.

5. Conclusions

NIR vein visualization can significantly aid in the perforation of a radial forearm free flap during zygomatic implant perforated (ZIP) flap reconstruction. By clearly delineating superficial vasculature in real time, it helps avoid vessel injury and reduces the risk of complications, which can be especially advantageous for surgeons undertaking this procedure for the first time. Although the literature on NIR devices spans diverse clinical contexts, particularly pediatric venous cannulation, its core benefits of non-invasive operation, ease of use, and rapid vascular mapping are directly applicable to complex reconstructive surgery. Incorporating NIR vein visualization into ZIP flap workflows can streamline the surgical process, contribute to flap integrity, and potentially accelerate patient recovery.

Author Contributions: Conceptualization, Y.F., A.S., E.G., J.A.T. and S.S.; methodology, Y.F., J.E., N.H., A.S., E.G. and S.S.; software, Y.F., E.G. and S.S.; writing—original draft preparation, Y.F. and S.S.; writing—review and editing, Y.F., J.E., N.H. and J.M.W.; supervision, J.A.T. and J.M.W.; All authors have read and agreed to the published version of the manuscript.

Funding: This research received no external funding.

Institutional Review Board Statement: Ethical approval was waived for this study, as it is a technical note.

Informed Consent Statement: Informed consent was obtained from all subjects involved in the study.

Data Availability Statement: No new data were created or analyzed in this study.

Conflicts of Interest: The authors declare no conflict of interest.

References

1. Hanasono, M.M.; Silva, A.K.; Yu, P.; Skoracki, R.J. A comprehensive algorithm for oncologic maxillary reconstruction. *Plast. Reconstr. Surg.* **2013**, *131*, 47–60. [CrossRef] [PubMed]
2. Betz, S.; Kim, R.Y.; Jelmini, J.; Williams, F.C.; Hammer, D.A. Is Maxillary Jaw in a Day Feasible? *Atlas Oral Maxillofac. Surg. Clin. N. Am.* **2024**, *32*, 141–149. [CrossRef] [PubMed]
3. Ettinger, K.S.; Arce, K.; Bunnell, A.M.; Nedrud, S.M. Mandibular Reconstruction: When to Graft, When to Flap, and When to Say No. *Atlas Oral Maxillofac. Surg. Clin. N. Am.* **2023**, *31*, 91–104. [CrossRef] [PubMed]
4. Kanatas, A.; Ghazali, N.; Lowe, D.; Udberg, M.; Heseltine, J.; O'Mahony, E.; Rogers, S.N. Issues patients would like to discuss at their review consultation: Variation by early and late stage oral, oropharyngeal and laryngeal subsites. *Eur. Arch. Oto-Rhino-Laryngol.* **2013**, *270*, 1067–1074. [CrossRef] [PubMed]
5. Dattani, A.; Richardson, D.; Butterworth, C.J. A novel report on the use of an oncology zygomatic implant-retained maxillary obturator in a paediatric patient. *Int. J. Implant. Dent.* **2017**, *3*, 37. [CrossRef] [PubMed]
6. Hirsch, D.L.; Howell, K.L.; Levine, J.P. A novel approach to palatomaxillary reconstruction: Use of radial forearm free tissue transfer combined with zygomaticus implants. *J. Oral Maxillofac. Surg.* **2009**, *67*, 2466–2472. [CrossRef] [PubMed]
7. Butterworth, C.J.; Lowe, D.; Rogers, S.N. The Zygomatic Implant Perforated (ZIP) flap reconstructive technique for the management of low-level maxillary malignancy—Clinical & patient related outcomes on 35 consecutively treated patients. *Head Neck* **2022**, *44*, 345–358. [PubMed]
8. Karaaltin, M.V. Utilizing the vein viewer technology to map out a venous flap preoperatively. *J. Reconstr. Microsurg.* **2013**, *29*, 423–424. [CrossRef] [PubMed]
9. Vyas, V.; Sharma, A.; Goyal, S.; Kothari, N. Infrared vein visualization devices for ease of intravenous access in children: Hope versus hype. *Anaesthesiol. Intensive Ther.* **2021**, *53*, 69–78. [CrossRef] [PubMed]

https://doi.org/10.3390/cmtr19020019

10. Ferrario, S.; Sorrentino, G.; Cavallaro, G.; Cortinovis, I.; Traina, S.; Muscolo, S.; Agosteo, A.; Santini, G.; Lagostina, E.; Mosca, F. Near-infrared system's efficiency for peripheral intravenous cannulation in a level III neonatal intensive care unit: A cross-sectional study. *Eur. J. Pediatr.* **2022**, *181*, 2747–2755. [CrossRef] [PubMed]
11. Cuper, N.J.; de Graaff, J.C.; Verdaasdonk, R.M.; Kalman, C.J. Near-infrared imaging in intravenous cannulation in children: A cluster randomized clinical trial. *Pediatrics* **2013**, *131*, e191–e197. [CrossRef] [PubMed]
12. Hattori, Y.; Imai, S.; Nakamura, R.; Niu, A. Use of a near-infrared vein visualization device in partial second toe pulp flap transfer for fingertip reconstruction. *Microsurgery* **2020**, *40*, 719–720. [CrossRef] [PubMed]
13. Edge, R.; Butcher, R. Vein Illumination Devices in Long-Term and Acute Care Settings: A Review of Clinical Effectiveness, Cost-Effectiveness and Guidelines. Canadian Agency for Drugs and Technologies in Health. 2020. Available online: https://europepmc.org/article/NBK/nbk563452 (accessed on 11 January 2026). [PubMed]
14. Lida, T.; Mihara, M.; Yoshimatsu, H.; Hara, H.; Narushima, M.; Koshima, I. Versatility of a Near-Infrared Vein Visualization Device in Plastic and Reconstructive Surgery. *Plast. Reconstr. Surg.* **2012**, *130*, 637e–638e. [CrossRef] [PubMed]
15. Vosselman, N.; Glas, H.H.; de Visscher, S.A.H.; Kraeima, J.; Merema, B.J.; Reintsema, H.; Raghoebar, G.M.; Witjes, M.J.H. Immediate implant-retained prosthetic obturation after maxillectomy based on zygomatic implant placement by 3D-guided surgery: A cadaver study. *Int. J. Implant. Dent.* **2021**, *7*, 54. [CrossRef] [PubMed]

Disclaimer/Publisher's Note: The statements, opinions and data contained in all publications are solely those of the individual author(s) and contributor(s) and not of MDPI and/or the editor(s). MDPI and/or the editor(s) disclaim responsibility for any injury to people or property resulting from any ideas, methods, instructions or products referred to in the content.

https://doi.org/10.3390/cmtr19020019

craniomaxillofacial
trauma & reconstruction

MDPI

Technical Note

From Resection to Rehabilitation in One Day: Digital Workflow for Mandibular Reconstruction with Fibular Free Flap and Immediate Dental Rehabilitation Using CAD/CAM Guides at the Point of Care

Matthias Ureel [1,*], Benjamin Denoiseux [1], Katrien Brijs [1], Pieter-Jan Boderé [2], Nicolas Dhooghe [3] and Renaat Coopman [1]

[1] Department of Oral & Craniomaxillofacial Surgery, Ghent University Hospital, C. Heymanslaan 10, 9000 Ghent, Belgium; benjamin.denoiseux@uzgent.be (B.D.); katrien.brijs@uzgent.be (K.B.); renaat.coopman@uzgent.be (R.C.)
[2] Department of Dentistry, Ghent University Hospital, C. Heymanslaan 10, 9000 Ghent, Belgium; pieter-jan.bodere@uzgent.be
[3] Department of Plastic and Reconstructive Surgery, Ghent University Hospital, C. Heymanslaan 10, 9000 Ghent, Belgium; nicolas.dhooghe@uzgent.be
* Correspondence: matthias.ureel@uzgent.be; Tel.: +32-9-332-32-05

Abstract

By using virtual surgical planning (VSP) and 3D printed guides, complex maxillofacial defects can be reconstructed with high accuracy and predictability. A fully digital workflow resulting in a modular all-in-one 3D printed guide system for fibula osteotomies, bone segment positioning, fully guided dental implant placement and dental prosthesis fixation for mandibular reconstruction was developed at Ghent University Hospital. A follicular ameloblastoma of the left mandible was resected in a 28-year-old male. The defect was reconstructed with a two-segment fibular free flap with immediate placement of three dental implants and immediate implant loading with a screw-retained bridge. A split thickness skin graft and Elemental PerioPlast were used as wound dressing. Comparison of the preoperative planning with the postoperative CT-scan showed a deviation immediately after surgery, which was no longer present at the 6-month follow-up. The patient achieved a stable occlusion and 44 mm mouth opening and reported high satisfaction. This case illustrates that fully digital, immediate mandibular reconstruction with simultaneous implant placement and prosthetic rehabilitation is feasible and accurate and enhances early functional recovery. Future improvements in intraoperative validation may further refine accuracy and reproducibility in complex oncologic reconstructions.

Keywords: three-dimensional (MESH); 3D printing; surgical cutting guide; free vascularised fibula graft; virtual surgical planning; mandibular reconstruction (MESH); immediate dental implant loading (MESH)

1. Introduction

Oral malignancies and aggressive benign lesions may infiltrate the maxilla and mandible, necessitating continuity resection and subsequent complex reconstruction. The fibular free flap (FFF) remains the gold standard for mandibular reconstruction due to its reliable vascular supply, adequate bone length, and favorable osteointegrative properties [1].

Over the past decades, the integration of virtual surgical planning (VSP) and patient-specific cutting and positioning guides has significantly enhanced precision, accuracy, and efficiency while reducing technical complexity [2].

Despite these improvements, a major limitation is still the delayed restoration of oral function, particularly dental occlusion and masticatory capacity. In response, 'jaw-in-a-day' (JIAD) protocols have emerged, aiming to achieve immediate oral rehabilitation and improved postoperative quality of life within a single surgical stage. Recent studies have confirmed that JIAD is no longer limited to benign cases but is a safe and feasible approach for malignant indications, provided there is meticulous planning for oncological margins [3,4].

A secondary challenge remains the reconstruction of the mandibular condyle. Restoring correct spatial orientation within the glenoid fossa is technically demanding [5]. The combination of microvascular mandibular reconstruction and alloplastic TMJ prosthesis has been described in the literature. To our knowledge, there has not been a report describing alloplastic TMJ reconstruction within the JIAD protocol [6–8].

Several techniques to perform the JIAD protocol such as the analog Rohner technique, stackable guides and 3D-printed patient specific osteosynthesis plates or a combination have been described [9–17]. Contemporary research highlights the superiority of fully digital workflows resulting in logical, robust and reproducible solutions for immediate functional rehabilitation [17].

In this report, we present a case of immediate mandibular reconstruction using a fibular free flap combined with simultaneous dental implant placement and prosthetic rehabilitation, based on a fully digital preoperative workflow at the point of care. This approach aims to integrate surgical precision with functional immediacy.

2. Materials and Methods

2.1. Patient Presentation and Preoperative Work-Up

A 28-year-old male presented with unilateral swelling and discomfort on the left side of the mandible (Figure 1). Clinical examination revealed a palpable buccal expansion in the left retromolar region. An orthopantomogram demonstrated a well-defined radiolucent lesion in the left mandibular body (Figure 2).



Figure 1. Initial clinical presentation with swelling of the left jaw. (**A**) Extra-oral swelling of the left jaw; (**B**) distortion of the occlusion due to the swelling.

https://doi.org/10.3390/cmtr19010015



Figure 2. Preoperative orthopantomogram. A well-defined, scalloped radiolucent area is visible in the left mandible, extending towards the coronoid process. Teeth 37 and 38 are involved in the lesion.

Radiographic evaluation with contrast-enhanced CT revealed a 6.6 cm × 2.5 cm expansile, lytic lesion located in the left mandibular body, extending posteriorly into the angle and ascending ramus. The lesion showed signs of cortical thinning, focal cortical perforation, and involvement of the roots of teeth 37 and 38. The mandibular canal was not clearly delineated within the lesion. No radiographic evidence of locoregional soft tissue invasion or thoracic metastases was observed.

An incisional biopsy confirmed the diagnosis of a follicular-type ameloblastoma. Genetic analysis for BRAF mutation was negative. A multidisciplinary surgical approach was planned involving both maxillofacial and reconstructive plastic surgery teams and consisted of a segmental mandibular resection, reconstruction with a fibular free flap and immediate prosthetic rehabilitation with dental implants and a screw-retained prosthetic bridge.

Prior to surgery, standardized clinical photographs were taken, and an occlusal registration in centric relation was obtained using a wax bite. Additionally, a facial scan (Metismile 3D Face Scanner, Shining 3D®, Hangzhou, China) and intraoral scans of both arches (Medit i500®, Medit, Seoul, Republic of Korea) were performed. A high-resolution thin-slice (0.6mm) maxillofacial CT scan (Somatom, Siemens, Munich, Germany) with the wax bite in situ, ensuring appropriate condylar seating and jaw relation, was taken. A CT angiography (dual-energy spiral CT, arterial phase of contrast injection) of the lower limbs was performed to assess vascular anatomy and donor site perfusion.

Using Materialise Enlight v6.0® (Materialise NV, Leuven, Belgium), DICOM images were segmented and aligned with the intraoral scans to generate a virtual 3D twin of the patient's maxillofacial and lower extremity structures.

2.2. Virtual Surgical Planning and 3D Printing

Given the extent of the lesion, the decision was made to place the resection margin distal to tooth 33 (Figure 3A–C), according to the Brown classification class Ic [18]. The left mandibular condyle was not preserved due to oncological considerations. Mandibular reconstruction was planned with a two-segment fibula graft from the right leg.

https://doi.org/10.3390/cmtr19010015

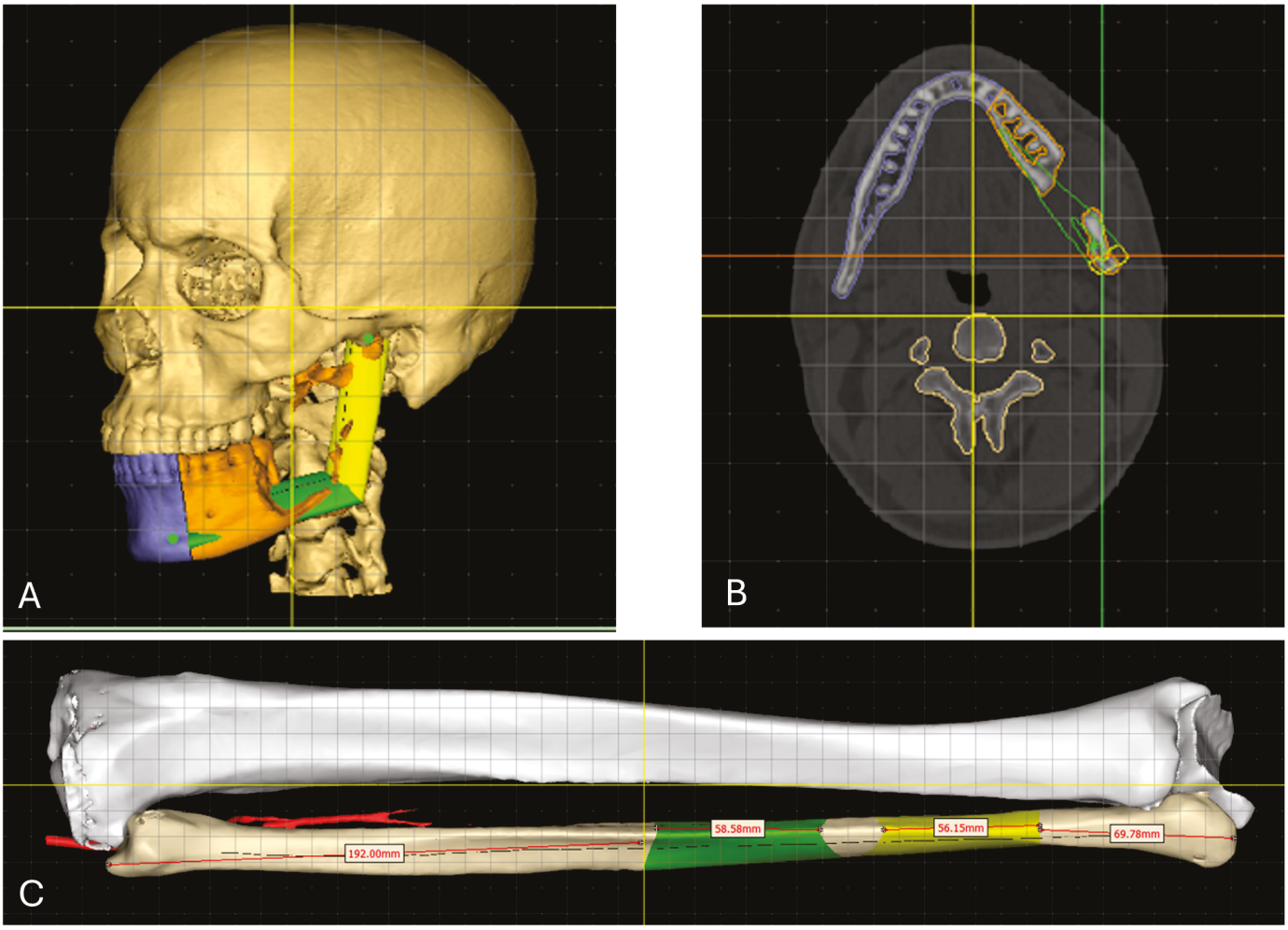

Figure 3. (**A**) Segmented 3D reconstruction of the skull (beige) and mandible, showing the native mandibular segment (purple) and the portion planned for resection (orange). The projected reconstruction with the free vascularized fibular graft is also visualized, with planned fibular segments shown in yellow and green. Reference lines in yellow.; (**B**) axial CT image with corresponding segmented overlays, color-coded to match the schematic in panel A. Reference lines in yellow, green and orange; (**C**) segmented CT angiography of the right lower leg, showing the tibia (white), native fibula and fibula segments (beige, yellow, and green). The vascular supply via the peroneal artery (a. fibularis) is indicated in red. The length of the fibula segments is visualized in white rectangles. Reference lines in yellow.

The alignment of the fibula segments was decided based on the anatomy of the patient and the position of the teeth (backward prosthetic planning). The intraoral scan and the dentition of the resected portion of the mandible (highlighted in orange in Figure 3A) served as anatomical reference points for segment positioning.

The virtual surgical plan (VSP) created in Materialise Enlight v6.0® (Materialise NV, Leuven, Belgium) was exported to Materialise 3-Matic v18.0® (Materialise NV, Leuven, Belgium) for the design and development of all surgical guides.

The following guides were created:

1/The Neomandible: This anatomical model served as a template for pre-bending the 2.3 mm reconstruction plate prior to surgery. To increase structural rigidity during manipulation, an intercondyle cylindrical support (8 mm diameter) was incorporated (Figure 4A).

https://doi.org/10.3390/cmtr19010015

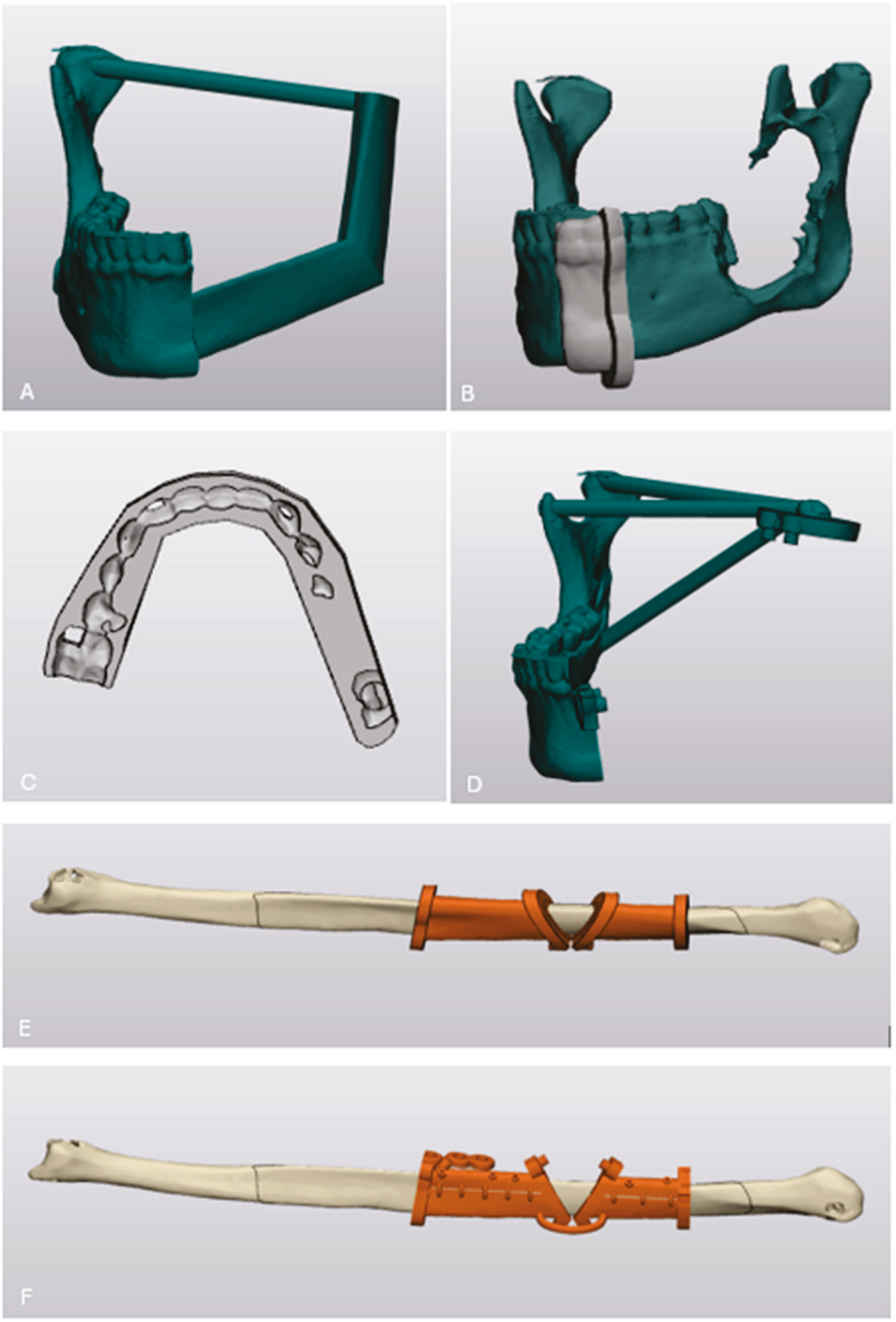

Figure 4. (**A**) Neomandible with an intercondylar reinforcement cylinder: (**B**) Gray cutting guide for mandibular osteotomy positioned on the neomandible (green); (**C**) interdental wafer to ensure correct positioning of reconstructed segments and screw-retained bridge; (**D**) mandibular repositioning guide; (**E**) basic version of fibula cutting guide (orange) positioned on the fibula bone (beige); (**F**) fibula cutting guide with modifications (orange) positioned on the fibula bone (beige).

2/Cutting Guide for Mandibular Osteotomy: The cutting guide for oncologic resection of the left mandible consisted of a base plate (3 mm thickness) and a flange marking the osteotomy line distal to tooth 33 (Figure 4B).

3/Interdental Wafer: Using the Orthognatic module of Materialise Enlight v6.0®, a surgical wafer was designed based on the patient's intraoral scans and preoperative occlusion. This wafer was intended to be used intraoperatively as a positioning guide to ensure accurate spatial orientation of the reconstructed segments (Figure 4C).

https://doi.org/10.3390/cmtr19010015

4/Mandibular Repositioning Guide: To ensure accurate positioning of the condylar segment, a dedicated repositioning guide was developed (Figure 4D). This guide was designed to interlock with the fibula cutting guide via matching pins and holes, allowing for precise seating of the condylar segment. Once the construct was stabilized, the pre-bent osteosynthesis plate could be positioned and fixated with KLS Martin 2.3 mm screws.

5/All-in-One Fibula Guide System: The fibula guide was designed in Materialise 3-Matic® v18.0 using a standard workflow: the desired surface on the fibula was marked, a base plate with 3 mm thickness and an offset of 0.2 mm was created, and directional flanges to define the osteotomy lines were added. This guide served as the base for further adaptations (Figure 4E,F).

5a/The first adaptation of the fibula guide involved dividing the guide into superior and inferior parts using the 'trim' function. The inferior portion was designed to be removed intraoperatively after the osteotomy was performed, thereby creating space for placement of the pre-bent osteosynthesis plate. The superior and inferior parts were connected with 2 mm diameter cylinders using the 'bridge' module. Additional drill holes were incorporated into the superior parts to allow fixation of the guide onto the FFF graft using KLS Martin 2.0 mm screws. The guides of each fibula segment were connected with a larger 4 mm diameter cylinder on the inferior parts.

5b/Secondly, to prevent rotational displacement of the individual fibula segments, pins and holes were added to the flanges. The pins measured 3 mm in height and diameter, and the holes measured 3.1 mm in height and 3.1 mm in diameter. These components ensure that both fibula segments fit together in a mechanically interlocked and rotationally stable configuration. This pin-and-hole system was also added to the mandibular repositioning guide.

5c/The final adaptation involved the integration of fully guided implant sleeves (Figure 5A,B) for accurate dental implant placement. For this step, the coDiagnostiX® software platform version 10.9 (Dental Wings GmbH, Berlin, Germany) was used. The relevant STL models were exported from Materialise Enlight® v6.0 and imported into coDiagnostiX®. The intraoral scan of the mandible was used to determine the ideal implant positions. Three Bredent SKY Classic 4.0 × 10mm (Bredent medical, Senden, Germany) implants were virtually planned at positions 34, 36, and 37 (Figure 5A). A fully guided implant drill guide was designed and subsequently exported for further processing in Materialise 3-Matic® v18.0. Using N-point alignment, the implant drill guide was accurately transferred onto the fibula cutting guide.

The provisional dental bridge was designed in Exocad® (Exocad GmbH, Darmstadt, Germany) and based on the patient's original dentition and anatomical references. Existing teeth served as the template for the occlusal morphology. The STL-file of the provisional bridge was imported into the virtual surgical plan (VSP), where it was digitally aligned with the pre-designed implant and fibular cutting guides. By subtracting the fibula guide from the provisional bridge, the bridge could be securely seated onto the fibula guide during surgery, enabling precise intraoperative fixation and immediate prosthetic loading (Figure 5B). This adaptation ensured precise spatial alignment and intraoperative control, allowing the correct occlusal vertical dimension (OVD) to be established during surgery.

All guides were 3D-printed in Ultrasint® polyamide 11 (Forward AM Technologies, Heidelberg, Germany) with a Farsoon SS403P 3D printer (Farsoon Europe, Stuttgart, Germany). The provisional dental bridge was 3D-printed in polymer (Ultraprint Dental Denture UV, Heygears, Guangzhou, China—C&B Microfilled Hybrid, Nextdent, Soesterberg, The Netherlands) with a Heygears A3D 3D printer (Heygears, Guangzhou, China). The gingival component was colored manually to achieve an anatomically realistic appearance.

https://doi.org/10.3390/cmtr19010015

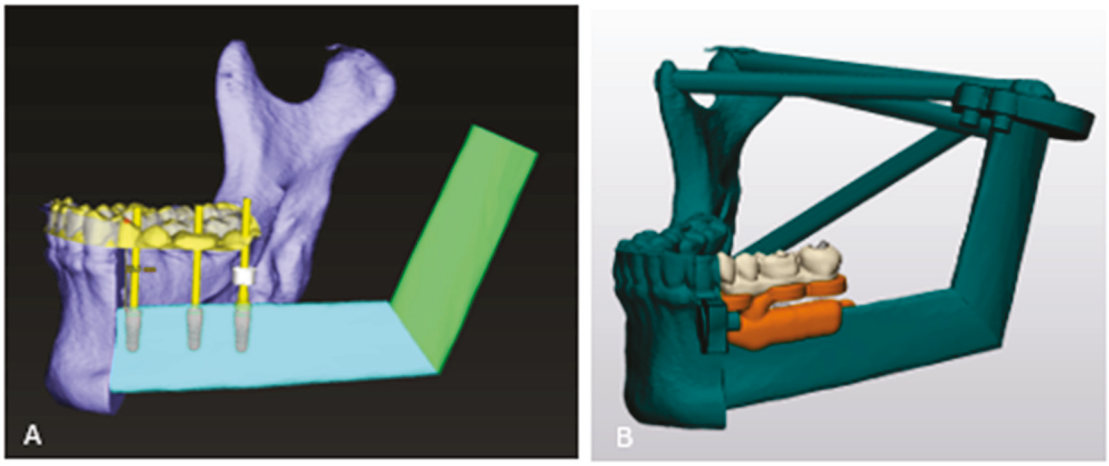

Figure 5. (**A**) Preoperative virtual surgical planning (VSP) for dental implant placement in the neomandible (purple, blue and green). Bredent® implants (gray) are planned on teeth positions 34, 36 and 37. The intraoral scan (yellow) was used as a reference for positioning the dental implants in the fibula; (**B**) in Materialise 3-Matic®, the STL-file of the provisional bridge (beige) was imported and the fully guided implant drill guide (orange) was accurately transferred onto the fibula bone (green).

2.3. Surgery

2.3.1. Tumor Resection

A submandibular Risdon approach was used, and by ligating the facial vessels, the marginal facial nerve was preserved. Supraperiosteal dissection was preferred due to perforation of the mandibular cortex. A segmental mandibulectomy was performed starting from tooth 33 posteriorly, including the left condyle using the mandibular cutting guide. The mental nerve was transected and the lingual nerve, encased by the tumor, was sacrificed. The resection preserved the temporomandibular joint capsule. The resection specimen was submitted for histopathology (Figure 6).



Figure 6. Surgical resection specimen of the ameloblastoma in the left mandible. The left condyle was completely resected.

https://doi.org/10.3390/cmtr19010015

2.3.2. Fibular Free Flap Harvest

The osteomyocutaneous fibula free flap (FFF) was prepared from the right leg in a supraperiosteal plane with a mobile skin island.

The FFF all-in-one guide was then secured to the fibula using KLS Martin 2.0 screws (length: 9 mm). In accordance with the Bredent® fully guided drilling protocol, three Bredent Classic SKY® implants (4.0 × 10 mm, REF: kSKY4010) were placed into the fibula. Subsequently, four osteotomies were performed using soft tissue-friendly piezoelectric surgical instruments to avoid deperiostation of the fibula (Piezosurgery Flex, Mectron spa, Carasco, Italy) (Figure 7A,B). The provisional prosthetic bridge was accurately positioned on the all-in-one guide, restoring the dental anatomy of the patient and ensuring a correct vertical dimension (Figure 7B). Immediate loading was achieved with 3 mm straight unicone abutments (Ref: SKYUC003, Bredent medical, Senden, Germany) and plastic prosthetic cylinders (Ref: SKYUCPKK, Bredent medical, Senden, Germany). The prosthetic bridge was fixed using a light-cured flowable composite (G-ænial Universal Injectable, GC Europe, Leuven, Belgium) (Figure 7C).

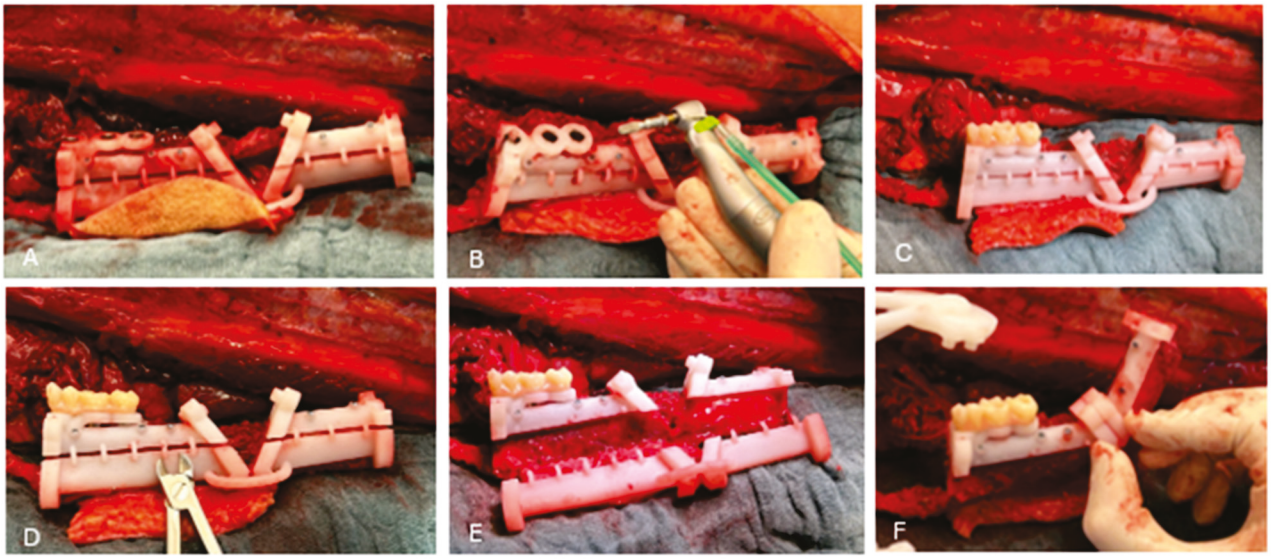

Figure 7. Osteotomy of the FFF and placement of dental implants according to the immediate loading protocol. (**A**) The fibular cutting guide was fixed to the right fibula using five KLS Martin 2.0 screws. The flanges were used to mark the osteotomy lines on the fibula with a piezotome. (**B**) The fully guided drilling protocol for the Bredent implants was executed using the incorporated drill sleeves. Three implants were placed. The implant drill guide was positioned at the correct height during the virtual surgical planning (VSP). (**C**) The provisional prosthesis was anchored to the three implants via 3mm unicone abutments and prosthetic cylinders using composite resin. Note that the prosthesis was seated directly onto the guide structure to ensure accurate positioning and vertical dimension. (**D**) The 2mm guide bridges were cut. (**E**) The lower part of the fibular cutting guide was removed. (**F**) The pin and hole connection system allowed accurate positioning of the two fibula flap segments. The fibula flap remained vascularized throughout the entire process.

The 2 mm connecting cylinders of the guide were cut, and the inferior part of the fibula guide was removed, hereby mobilizing the fibula segments (Figure 7D–F). Both segments were positioned in the mandibular repositioning guide using pin-and-hole connections (Figure 8A).

https://doi.org/10.3390/cmtr19010015

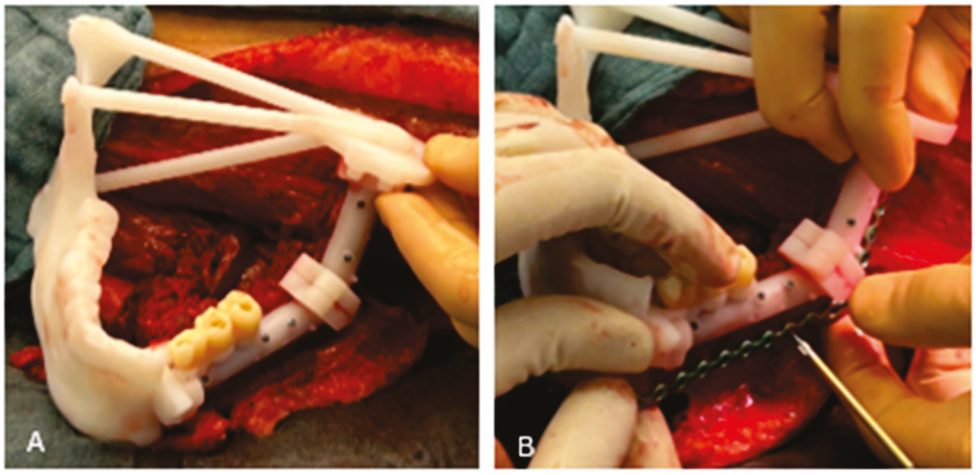

Figure 8. (**A**) The mandibular repositioning guide and fibular guide were connected via the pin-and-hole system. The fibula segments were now correctly positioned according to the VSP. (**B**) Removal of the lower portion of the fibular cutting guide created space for the placement of a reconstruction plate (KLS Martin 2.3®). This plate had been pre-bent on an anatomical model of the neomandible. Fixation was performed using KLS Martin 2.3® screws. The FFF remained attached to its vascular pedicle during this step.

The pre-bent KLS Martin 2.3mm reconstruction plate was secured to the fibula with locking and non-locking screws (Figure 8B). An additional 2.0 mm miniplate was placed anteriorly (KLS Martin 2.0®). The fibula construct was ready for transfer to the mandibula defect.

2.3.3. Reconstruction

The vascular pedicle was cut, the fibula guide was removed and the fibula construct, including the screw-retained prosthetic bridge, was transferred as a single unit into the oral cavity. The provisional prosthetic bridge served as an intraoperative guide to position the fibula construct in the occlusal plane to ensure proper alignment. Once optimal occlusion was confirmed, the reconstruction plate was fixated to the native mandible using KLS Martin 2.3 mm screws (Figure 9A,B). An additional KLS Martin 1.5 mm miniplate was placed for increased stability. Dental occlusion was verified using the interdental wafer.

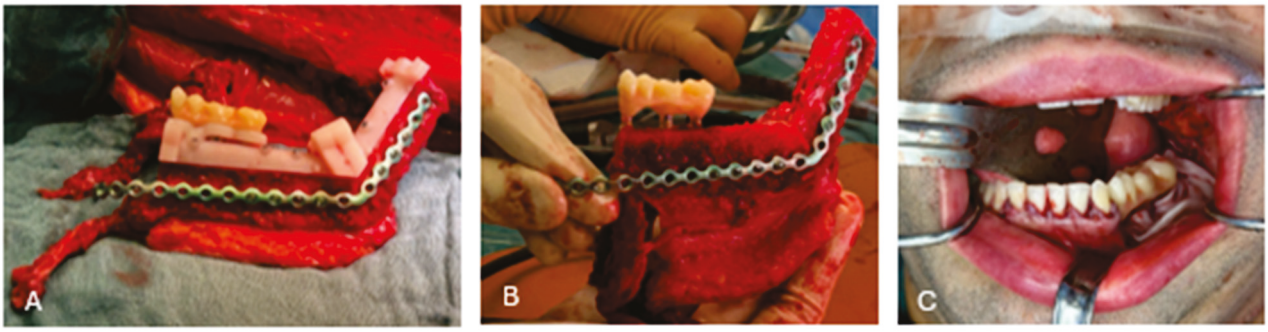

Figure 9. The completed fibular reconstruction. (**A**) After removing the mandibular repositioning guide, the fibula construct was visible. (**B**) The prosthetic restoration was removed from the implants to allow full removal of the fibula guide. Final adjustments were made to the dental bridge; the prosthesis was then polished and repositioned on the implants. (**C**) Intraoral image of the final situation. A split-thickness skin graft was placed around the dental implants and kept in place with an Elemental PerioPlast wound dressing placed below the screw-retained bridge.

Microvascular anastomoses were performed by the plastic surgery team, resulting in a total ischemia time of 115 min.

https://doi.org/10.3390/cmtr19010015

To optimize long-term implant maintenance, a split-thickness skin graft (STSG) was harvested from the right lower leg and placed intraorally over the implants to cover and protect the FFF periosteum. Fenestrations were created for implant emergence. Surfasoft and Elemental® Perioplast (Withelemental, Ghent, Belgium) dressings were applied around the implants to stabilize the STSG and maintain a buccal vestibule [19]. The skin paddle of the FFF was sutured posteriorly to the implants in the retromolar area.

The remaining intraoral wounds were closed primarily, and the cervical and donor-site wounds were closed in a layered fashion (Figure 9C).

2.4. Postoperative Care Protocol and Flap Monitoring

The patient remained intubated overnight with planned extubation in the ICU the following day. Surgical drains were placed in the neck and fibular donor site. Prophylactic antibiotics (amoxicillin-clavulanic acid 1 g four times daily) were continued for seven days. The patient was kept nil per os (NPO) for the first five postoperative days. Oral hygiene began on postoperative day one using a sponge brush. Enoxaparin (Clexane®, Sanofi, Paris, France) was started eight hours postoperatively to prevent thromboembolism. Corticosteroids (methylprednisolone, Solumedrol®, Pfizer Inc., New York, NY, USA) were given to reduce edema.

Flap monitoring followed standard microvascular protocols. A MAP > 75 mmHg or systolic BP > 130 mmHg was maintained. The patient was positioned in a 30° Fowler position with the head in neutral midline orientation. Head rotation toward the flap side was avoided. Doppler ultrasound of the vascular pedicle was performed hourly for the first 24 h and then every two hours up to 72 h to detect early vascular compromise.

3. Results

Immediate postoperative occlusion was deemed adequate, and as the postoperative edema subsided, the patient achieved a stable and functional occlusion. The Elemental® Perioplast wound dressing was removed 12 days after surgery (Figure 10A).

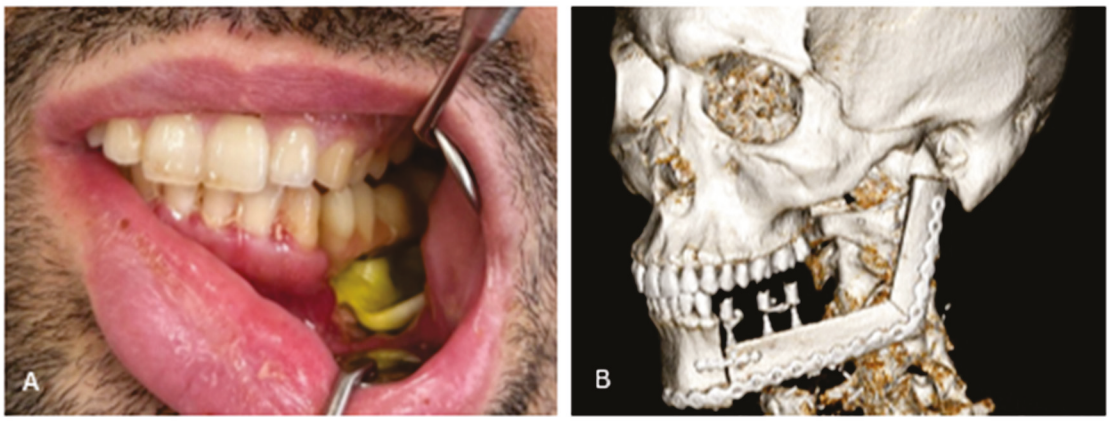

Figure 10. Clinical and radiological situation one week postoperatively. (**A**) Clinical picture with provisional screw-retained bridge. There was no dental occlusion posteriorly, most likely caused due to postoperative swelling. The Elemental® wound dressing is visible under the provisional bridge and keeps the skin graft in place. (**B**) Aside from a small opening between the native mandible and the fibula graft, the postoperative CT scan shows a good alignment of the fibular graft with the native mandible. There is a diastasis between the distal end of the FFF and the glenoid fossa.

The postoperative CT and orthopanthomogram demonstrated satisfactory alignment of the fibular graft with the native mandible (Figure 10B). A small gap between the fibula graft and native mandible was noticed. There was no evidence of loosening or mechanical

https://doi.org/10.3390/cmtr19010015

failure. The dental implants were visualized in the correct position. On the postoperative CT scan, a diastasis was observed between the distal end of the FFF graft and the glenoid fossa.

Using the 'Part comparison' module in Materialise 3-Matic® v18.0 (Materialise NV, Leuven, Belgium), the preoperative virtual surgical plan (VSP) and the postoperative CT scan were analyzed to assess surgical accuracy. A maximal deviation of approximately 7 mm is seen at the free-ending fibula construct compared to the preoperative planning. The construct is positioned more laterally than planned (Figure 11A).

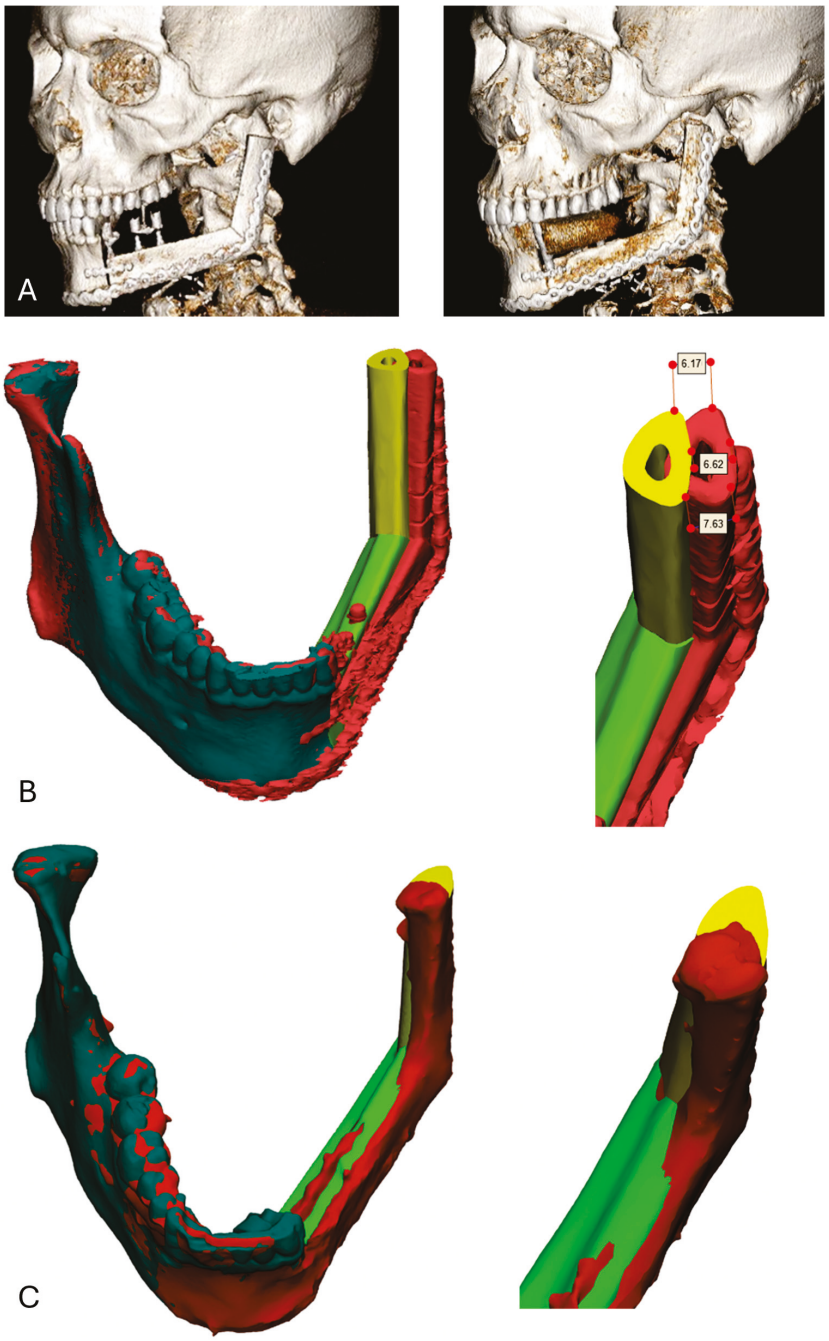

Figure 11. Postoperative analysis. Postoperative CT scan after one week and 6 months (**A**). (**B**) Comparison between the postoperative result (red) and the preoperative planning (mandible in green and yellow). A deviation of around 7 mm was observed due to a more lateral and caudal position of the neomandible compared to the preoperative planning. (**C**) Comparison after 6 months with a minimal deviation between postoperative result (red) and preoperative planning (green and yellow).

https://doi.org/10.3390/cmtr19010015

After six months, a new CT was performed to evaluate the position of the fibular fragments and osseous healing. A good osseous union was now observed, as well as beginning neocondylar formation due to the remodeling of the free end of the fibula [20]. The free end of the fibula had also shifted cranially towards the fossa as a result of the disappearance of oedema and medially probably due to occlusal guidance by the provisional dental bridge. A new comparison analysis showed a nearly perfect alignment between the preoperative planning and the postoperative result (Figure 11B).

Five months after surgery, the definitive prosthetic restoration was fabricated. High implant stability and healthy peri-implant soft tissues were observed. An intraoral digital impression was taken using Primescan® (Dentsply Sirona, Mölndal, Sweden). A milled try-in was produced to evaluate occlusal relationships, vertical dimension, and esthetic parameters. Minor adjustments were performed as needed to optimize the functional and esthetic outcome.

Given the patient's young age and demonstrated ability to maintain proper oral hygiene, a screw-retained fixed prosthesis was chosen to maximize function, stability, and long-term tissue health. The final bridge consisted of a custom CAD/CAM-milled titanium framework onto which a full-contour zirconia bridge was bonded. The patient expressed high satisfaction with the efficiency and rapidity of the surgical recovery (Figure 12).



Figure 12. Clinical situation at 5 months postoperatively. (**A**) Excellent keratinization of the peri-implant mucosa is observed, facilitating adequate oral hygiene. (**B**) Clinical view showing the dental elements and prosthetic bridge in stable occlusion. (**C**) Close-up view of the definitive prosthetic bridge.

4. Discussion

This case illustrates the efficacy of a multidisciplinary approach in the management of head and neck reconstruction. The integration of virtual surgical planning (VSP), in-house 3D-printed surgical guides, and immediate dental rehabilitation enabled both functional and esthetic reconstruction. The fibular free flap (FFF) remains the preferred reconstructive option due to its osteointegrative capacity and adaptability to mandibular defects. Importantly, the placement of dental implants and immediate loading during the primary surgery significantly reduced overall rehabilitation time and improved the patient's quality of life.

The evolution of 3D printing and VSP technologies has significantly expanded the possibilities of mandibular reconstruction. In contrast to earlier analog workflows such as the Rohner technique [10,21], which relied on plaster casts and manual planning, contemporary digital methods offer greater precision and reproducibility. The authors advocate for VSP protocols that adhere to four essential principles: accuracy, speed, reproducibility, and immediate rehabilitation.

- Accuracy: Surgeons must continuously strive for the highest level of accuracy in VSP execution. When surgical outcomes deviate from the plan, critical assessment of the VSP and refinement of clinical workflows are required.

https://doi.org/10.3390/cmtr19010015

- Speed: VSP should demonstrably reduce operative and ischemia time. Shorter ischemia times improve flap survival, and reduced operative durations limit anesthetic exposure and enhance postoperative recovery.
- Reproducibility: VSP must be embedded in a coherent digital workflow that is transferable to the surgical team, including residents and nursing staff. This enables consistent surgical outcomes and contributes to institutional learning.
- Immediate Rehabilitation: Particularly in oncological cases where adjuvant radiotherapy may hinder postoperative dental rehabilitation, immediate implant placement represents the future of jaw reconstruction [3,22,23]. While implants are often placed but not yet loaded, the proposed technique allows for controlled, reproducible, and accurate immediate functional rehabilitation—even in patients with limited prognosis—thus contributing to quality of life.

Certain considerations must be acknowledged regarding this approach. The guides must be designed with awareness of the surrounding soft tissues. The position of the vascular pedicle and potential perforators of the skin island or a muscle flap need to be taken into account. In cases necessitating a lot of soft tissue, it is sometimes difficult to position the fibula segments in the mandibular repositioning guide. Precautions not to rotate or compress the vascular pedicle should be taken. Also, during the preparation of the fibula construct, the pedicle should always be watched to avoid traction. Accurate positioning of the fibula all-in-one guide is important for adequate implant placement as the fibula is often thin and osseous perforations of the implants can occur. In Ghent University Hospital, all guides are designed by the surgeons themselves. While time-consuming, this approach fosters clinically driven innovation and enhances intraoperative adaptability by intimately understanding the limitations of the planning.

Another point of concern is the final positioning of the FF flap relative to the virtual plan. Although significant deviations were observed, they were not clinically relevant. This phenomenon has been reported by other authors as well [24–26]. While the condylar repositioning guide likely preserved correct spatial orientation, challenges persist during fixation to the native mandible, particularly in seating the distal segment accurately within the glenoid fossa. This final step often occurs after prolonged surgery, further complicated by soft tissue edema.

In this case, the provisional prosthetic bridge fractured under occlusal load a few days postoperatively. Two causes were identified: the use of plastic prosthetic components, which lacked mechanical strength, and reduced occlusal awareness due to postoperative sensory deficits. In consultation with the implant manufacturer, the plastic connectors were replaced with metallic components.

An interesting observation is the evolution of the spatial changes in the fibula construct over time. The postoperative CT scan after one week showed a significant lateral and caudal deviation of approximately 7 mm in the most distal part of the fibula construct compared to the preoperative planning. A small gap between the fibula and the native mandible was noticed at the fibula, suggesting suboptimal positioning of the fibula construct, although the occlusion was used as a guidance. Over time, six months later, the fibula construct positioned itself according to the virtual plan. The authors hypothesize that this change was induced by an optimalisation of the interdigitation of the prosthetic bridge with the native dentition in combination with intraoral muscle balances. The immediate placement of the prosthetic bridge served as a guide for correct osseous positioning; i.e., form follows function. This aspect warrants further investigation in future studies.

Future directions include refinements in surgical guide design and intraoperative validation workflows. A small window will be integrated into the implant drill guide to enable real-time visualization of implant placement and guide positioning on the fibula

https://doi.org/10.3390/cmtr19010015

bone. The authors emphasize that achieving surgical outcomes significantly deviating from the original VSP undermines its purpose. Therefore, intraoperative imaging could serve as a valuable tool for immediate verification and adjustment of the plan. To enhance efficiency and precision, artificial intelligence may play a pivotal role in accelerating intraoperative image processing, currently limited by slow surface-based segmentation techniques.

5. Conclusions

Digital workflows enable accurate, single-stage mandibular reconstruction with simultaneous implant placement and immediate prosthetic rehabilitation (jaw-in-a-day). Dental occlusion can serve as a positioning tool for osseous reconstruction as form follows function. A functionally and esthetically stable result was achieved. Surgeon-driven VSP fosters innovation but requires experience and time investment. Future improvements should focus on intraoperative validation, potentially supported by artificial intelligence.

Author Contributions: Conceptualization, M.U., B.D., P.-J.B. and N.D.; methodology, M.U., B.D., P.-J.B. and N.D.; software, M.U., B.D. and P.-J.B.; validation, M.U., B.D. and P.-J.B.; formal analysis, M.U.; investigation, M.U., B.D., P.-J.B. and R.C.; resources, K.B.; writing—original draft preparation, M.U., B.D., K.B., P.-J.B. and R.C.; writing—review and editing, all authors; visualization, M.U. and K.B.; supervision, R.C.; project administration, M.U. All authors have read and agreed to the published version of the manuscript.

Funding: This research received no external funding.

Institutional Review Board Statement: The study was conducted in accordance with the Declaration of Helsinki, and approved by the Ethics Committee of Ghent University Hospital (CR-2025-0014; 1 December 2025).

Informed Consent Statement: Written informed consent has been obtained from the patient to publish this paper.

Data Availability Statement: The original contributions presented in this study are included in the article; further inquiries can be directed to the corresponding author.

Conflicts of Interest: The authors declare no conflicts of interest.

Abbreviations

The following abbreviations are used in this manuscript:

CAD/CAM	Computer-aided design/computer-aided manufacturing
FFF	Fibular free flap
ICU	Intensive care unit
NPO	Nil per os
OVD	Occlusal vertical dimension
QID	Quater in die
STSG	Split thickness skin graft
VSP	Virtual surgical planning

References

1. Hidalgo, D.A. Fibula free flap: A new method of mandible reconstruction. *Plast. Reconstr. Surg.* **1989**, *1*, 71–79. [CrossRef]
2. Barr, M.L.; Haveles, C.S.; Rezzadeh, K.S.; Nolan, I.T.; Castro, R.; Lee, J.C.; Steinbacher, D.; Pfaff, M.J. Virtual Surgical Planning for Mandibular Reconstruction with the Fibula Free Flap: A Systematic Review and Meta-analysis. *Ann. Plast. Surg.* **2020**, *84*, 117–122. [CrossRef]
3. Trac, J.; Ramchandani, R.; Dutta, P.; Sarkis, L.; Calvisi, R.; Villemure-Poliquin, N.; Davies, J.; Somogyi-Ganss, E.; Blanas, N.; Cuddy, K.; et al. Jaw-in-a-day (JIAD) for malignant indications: A systematic review. *Oral Oncol.* **2026**, *173*, 107823. [CrossRef] [PubMed]

https://doi.org/10.3390/cmtr19010015

4. Omole, D.; Khatib, B.; Patel, A.A.; Cheng, A.; Salama, A.; Brecht, L.E.; Hirsch, D.L. Reconstructing the Mandible: Jaw-In-A-Day: Where We Were, Where We Are, and the Future. *Atlas Oral. Maxillofac. Surg. Clin.* **2023**, *31*, 153–164. [CrossRef] [PubMed]
5. Lee, Z.H.; Avraham, T.; Monaco, C.; Patel, A.A.; Hirsch, D.L.; Levine, J.P. Optimizing Functional Outcomes in Mandibular Condyle Reconstruction With the Free Fibula Flap Using Computer-Aided Design and Manufacturing Technology. *J. Oral Maxillofac. Surg.* **2018**, *76*, 1098–1106. [CrossRef] [PubMed]
6. Chauvel-Picard, J.; Kreutzer, K.; Heiland, M.; Kreusch, T.; Ebker, T.; Beck-Broichsitter, B. One stage microvascular mandible reconstruction by using scapula chimeric flap combined with computer-aided-design and computer-aided-manufacturing plate including bilateral alloplastic TMJ prosthesis: A case report. *Microsurgery* **2021**, *41*, 263–269. [CrossRef]
7. Landes, C.; Korzinskas, T.; Dehner, J.F.; Santo, G.; Ghanaati, S.; Sader, R. One-stage microvascular mandible reconstruction and alloplastic TMJ prosthesis. *J. Cranio-Maxillofac. Surg.* **2014**, *42*, 28–34. [CrossRef]
8. Pyne, J.M.; Davis, C.M.; Kelm, R.; Bussolaro, C.; Dobrovolsky, W.; Seikaly, H. Advanced mandibular reconstruction with fibular free flap and alloplastic TMJ prosthesis with digital planning. *J. Otolaryngol.—Head Neck Surg.* **2023**, *52*, s40463-023. [CrossRef]
9. Ureel, M.; Boderé, P.J.; Denoiseux, B.; Corthouts, P.; Coopman, R. Mandibular Reconstruction with Osseous Free Flap and Immediate Prosthetic Rehabilitation (Jaw-in-a-Day): In-House Manufactured Innovative Modular Stackable Guide System. *Bioengineering* **2024**, *11*, 1254. [CrossRef]
10. Rohner, D.; Guijarro-Martínez, R.; Bucher, P.; Hammer, B. Importance of patient-specific intraoperative guides in complex maxillofacial reconstruction. *J. Cranio-Maxillofac. Surg.* **2013**, *41*, 382–390. [CrossRef]
11. Williams, F.C. History of the Jaw in a Day. *Oral Maxillofac. Surg. Cases* **2023**, *9*, 100306. [CrossRef]
12. Sukato, D.C.; Hammer, D.; Wang, W.; Shokri, T.; Williams, F.; Ducic, Y. Experience With "Jaw in a Day" Technique. *J. Craniofac. Surg.* **2020**, *31*, 1212–1217. [CrossRef]
13. Schepers, R.H.; Raghoebar, G.M.; Vissink, A.; Lahoda, L.U.; Van der Meer, W.J.; Roodenburg, J.L.; Reintsema, H.; Witjes, M.J. Fully 3-dimensional digitally planned reconstruction of a mandible with a free vascularized fibula and immediate placement of an implant-supported prosthetic construction. *Head Neck* **2013**, *35*, E109–E114. [CrossRef]
14. Khatib, B.; Cheng, A.; Sim, F.; Bray, B.; Patel, A. Challenges With the Jaw in a Day Technique. *J. Oral Maxillofac. Surg.* **2020**, *78*, 1869.e1–1869.e10. [CrossRef]
15. Nayar, S. Current concepts and novel techniques in the prosthodontic management of head and neck cancer patients. *Br. Dent. J.* **2019**, *226*, 725–737. [CrossRef]
16. Jeong, Y.J.; Dunn, M.; Manzie, T.; Howes, D.; Wykes, J.; Palme, C.E.; Leinkram, D.; Low, T.; Oberoi, R.; Aung, Y.M.; et al. Jaw in a day surgery: Early experience with 19 patients at an Australian tertiary referral center. *ANZ J. Surg.* **2024**, *94*, 1531–1538. [CrossRef] [PubMed]
17. Van, T.D.; Khanh, L.N.; Dinh, H.N.; Phong, M.H.; Duc, C.C. Fully Digital Workflow for Immediate Prosthetic Implant on Microsurgery Fibula Flap for Mandibular Reconstruction. *Med. Arch.* **2025**, *79*, 215–219. [CrossRef]
18. Brown, J.S.; Barry, C.; Ho, M.; Shaw, R. Review A New classification for Mandibular Defects after Oncological Resection. *Lancet Oncol.* **2016**, *17*, e23–e30. Available online: www.thelancet.com/oncology (accessed on 5 November 2025). [CrossRef]
19. Van Der Kelen, L.; Ureel, M.; Denoiseux, B.; Boderé, P.-J.; Matthys, C.; Vermeersch, H.; Coopman, R. Enhancing Implant Success in Mandibular Reconstruction: A Novel Approach Combining Implant-Retained Splint and Vestibuloplasty—A Case Series. *J. Clin. Med.* **2025**, *14*, 1298. [CrossRef] [PubMed]
20. Lim, M.; Martinez, I.A.V.; Woods, T.; McIntyre, B.; Bayrakdar, I.S.; Kurt-Bayrakdar, S.; Jagtap, R. Neocondylar Formation with Vascularized Fibular Free Flap: A Report of Three Rare Cases and Review of Literature. *Surgeries* **2025**, *6*, 34. [CrossRef]
21. Rohner, D.; Bucher, P.; Kunz, C.; Hammer, B.; Schenk, R.K.; Prein, J. Treatment of severe atrophy of the maxilla with the prefabricated free vascularized fibula flap. *Clin. Oral Implant. Res.* **2002**, *13*, 44–52. [CrossRef]
22. Wetzels, J.W.G.H.; Meijer, G.J.; Koole, R.; Adang, E.M.; Merkx, M.A.W.; Speksnijder, C.M. Costs and clinical outcomes of implant placement during ablative surgery and postponed implant placement in curative oral oncology: A five-year retrospective cohort study. *Clin. Oral Implant. Res.* **2017**, *28*, 1433–1442. [CrossRef] [PubMed]
23. In'T Veld, M.; Schulten, E.A.J.M.; Leusink, F.K.J. Immediate dental implant placement and restoration in the edentulous mandible in head and neck cancer patients: A systematic review and meta-analysis. *Curr. Opin. Otolaryngol. Head Neck Surg.* **2021**, *29*, 126–137. [CrossRef]
24. Coppen, C.; Verhoeven, T.; Snoeijink, T.; Weijs, W.; Verhulst, A.; van Rijssel, J.; Maal, T.; Dik, E. Fibula free flap reconstruction: Improving the accuracy of virtual surgical planning using titanium inserts. *Int. J. Oral Maxillofac. Surg.* **2025**, *54*, 1037–1042. [CrossRef] [PubMed]

https://doi.org/10.3390/cmtr19010015

25. Blanc, J.; Fuchsmann, C.; Nistiriuc-Muntean, V.; Jacquenot, P.; Philouze, P.; Ceruse, P. Evaluation of virtual surgical planning systems and customized devices in fibula free flap mandibular reconstruction. *Eur. Arch. Oto-Rhino-Laryngol.* **2019**, *276*, 3477–3486. [CrossRef] [PubMed]
26. Roser, S.M.; Ramachandra, S.; Blair, H.; Grist, W.; Carlson, G.W.; Christensen, A.M.; Weimer, K.A.; Steed, M.B. The accuracy of virtual surgical planning in free fibula mandibular reconstruction: Comparison of planned and final results. *J. Oral Maxillofac. Surg.* **2010**, *68*, 2824–2832. [CrossRef]

Disclaimer/Publisher's Note: The statements, opinions and data contained in all publications are solely those of the individual author(s) and contributor(s) and not of MDPI and/or the editor(s). MDPI and/or the editor(s) disclaim responsibility for any injury to people or property resulting from any ideas, methods, instructions or products referred to in the content.

https://doi.org/10.3390/cmtr19010015

craniomaxillofacial
trauma & reconstruction

MDPI

Technical Note

Expanding Horizons in Craniomaxillofacial Reconstruction: The Role of Exoscopic Microsurgery in Head and Neck Surgery

Khalid Abdel-Galil * and Kemal Mustafa Tekeli *

Sheikh Tahnoon Bin Mohamed Medical City, Al-Ain, Abu Dhabi P.O. Box 15258, United Arab Emirates
* Correspondence: khalidabdelgalil@doctors.org.uk (K.A.-G.); mtekeli@yahoo.com (K.M.T.)

Abstract

Exoscopic systems are increasingly used as an alternative to the operating microscope in microsurgical reconstruction, offering high-definition visualisation, shared operative viewing, and greater flexibility in surgeon positioning. This retrospective case series describes the use of exoscopic visualisation during microsurgical reconstruction in five illustrative head and neck and reconstructive cases. Different commercially available exoscopic platforms were utilised, and feasibility, workflow integration, and surgeon-perceived ergonomic aspects were assessed descriptively. Exoscopic visualisation was feasible for completion of microvascular anastomoses across a range of complex reconstructions. From the surgeons' perspective, exoscopy allowed a more flexible working posture during prolonged microsurgical tasks and may offer advantages in training environments, particularly for junior surgeons. Further studies incorporating objective outcome measures are required to better define the role of exoscopy in microsurgical practice.

Keywords: exoscope; microsurgery; head and neck reconstruction; free flap; robotics; surgical ergonomics

1. Introduction

Microsurgical head and neck reconstruction demands precision, depth perception, and prolonged operating times, necessitating superior visualisation tools. Traditionally, the operating microscope (OM) has been regarded as the gold standard for microvascular reconstruction. However, prolonged use of the operating microscope has been associated with significant ergonomic challenges for surgeons, particularly sustained neck flexion, shoulder elevation, and static postures during lengthy microsurgical procedures. Multiple studies have reported a high prevalence of work-related musculoskeletal disorders among microsurgeons, including chronic neck and lower back pain, which may negatively impact surgeon well-being and career longevity. These ergonomic limitations have driven growing interest in alternative visualisation platforms that allow a more neutral posture and dynamic positioning of the surgical team [1,2]. Exoscopy, particularly advanced 3D 4K systems, has gained increasing interest due to improved ergonomics and high-resolution imaging [3–5]. Initially developed for neurosurgical applications [4], exoscopic systems are now increasingly utilised in craniomaxillofacial (CMF) and reconstructive surgery [6–10].

2. Methodology

This work was conducted as a retrospective case series examining the use of exoscopic visualisation during microsurgical reconstruction in head and neck & free tissuereconstructive surgery. Cases in which an exoscope was used for the microvascular component

of reconstruction were identified from operative records and reviewed. Five cases were included. These cases were selected to illustrate the use of exoscopic systems in a range of complex reconstructive scenarios requiring microsurgical free tissue transfer. The intention was not to create a comparative or consecutive cohort but to demonstrate feasibility and practical application across different anatomical regions and reconstructive demands. All procedures were performed by experienced microsurgeons. Exoscopic systems were employed during microvascular anastomoses. The choice of exoscopic platform varied between cases and reflected availability at the time of surgery and institutional resources. In one case, both an exoscope and a conventional operating microscope were used during reconstruction. All systems provided high-definition three-dimensional visualisation. Clinical data were collected retrospectively from patient medical records and operative notes. Information recorded included patient demographics, diagnosis, type of resection and reconstruction, and the exoscopic platform used. Ergonomic aspects, including surgeon posture, comfort during prolonged microsurgical tasks, and perceived musculoskeletal strain, were assessed descriptively based on the operating surgeons' experience. No objective ergonomic assessment tools or validated scoring systems were used. Ethical approval for the study was obtained from the appropriate institutional review board. All procedures were performed in accordance with the Declaration of Helsinki. Written informed consent was obtained from all patients for inclusion in the study and for the use of anonymised clinical data and clinical images for publication.

3. Case Vignettes

3.1. Case 1

A 66-year-old male underwent subtotal mandibulectomy with bilateral neck dissections for a pT4aN0M0 moderately differentiated squamous cell carcinoma with free fibula osseoseptocutaneous flap reconstruction in February 2023.

The Aesculap Aeos robotic digital exoscope (Aesculap Inc., Lehigh County, PA, USA) was used during microvascular anastomoses providing excellent depth perception and ergonomics as well as allowing simultaneous visualization for assistants, operating room staff and trainees (Figures 1–3). The exoscopic setup also permitted a more neutral working posture during the microsurgical phase.

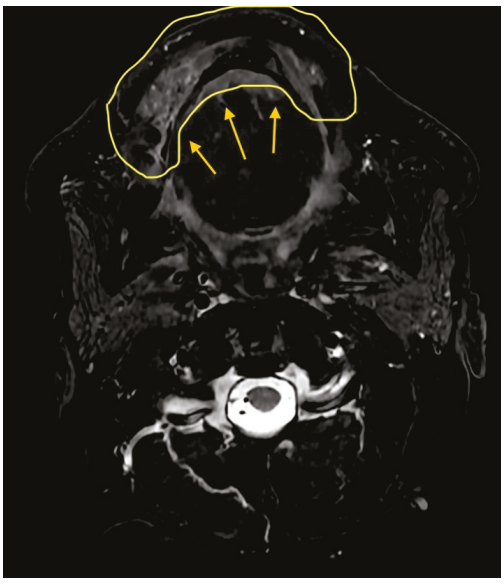

Figure 1. Case 1—Preoperative MRI. Yellow arrows and circle indicate the primary tumor extension.

https://doi.org/10.3390/cmtr19010010

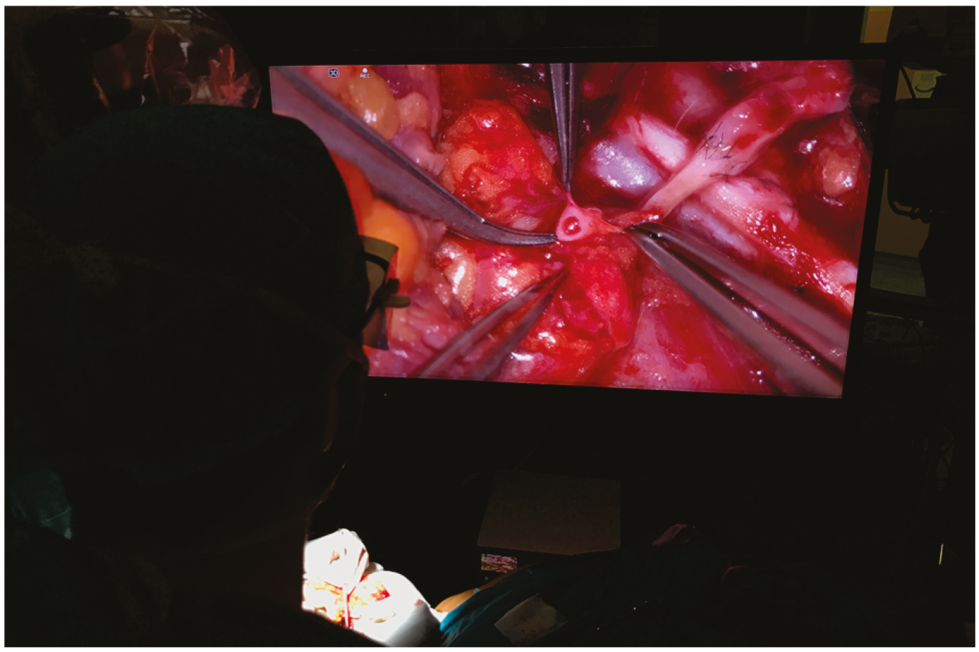

Figure 2. Case 1—Intraoperative exoscopic view.



Figure 3. Case 1—Intraoperative exoscopic setup.

3.2. Case 2

A 37-year-old female underwent extended hemiglossectomy with ipsilateral neck dissection in April 2024 for a pT3N1M0 (DOI 17mm) moderately differentiated squamous cell carcinoma. Immediate reconstruction was undertaken using a modified non-dominant radial forearm fasciocutaneous free flap using the Mitaka Hawksight platform (Mitaka USA Inc., Wheat Ridge, CO, USA) for microsurgery (Figures 4–7).

Adequate illumination and visual clarity facilitated successful microvascular anastomoses without reverting to the OM.

https://doi.org/10.3390/cmtr19010010

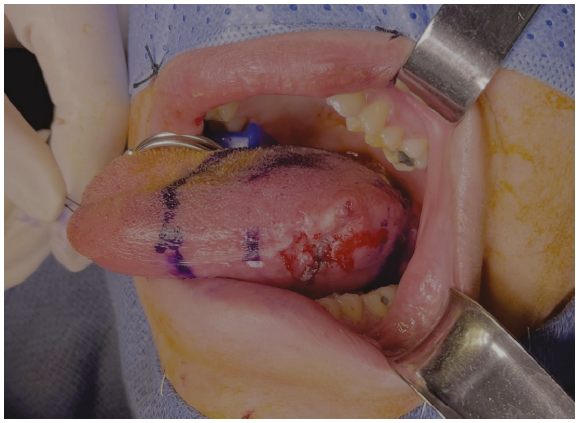

Figure 4. Case 2—Tongue Tumor surgical marking.



Figure 5. Case 2—Completed Forearm flap harvest.



Figure 6. Case 2—Mitaka exoscope in use during microsurgery.

https://doi.org/10.3390/cmtr19010010



Figure 7. Case 2—Postoperative status at 3 months.

3.3. Case 3

A 41-year-old female underwent secondary post-mastectomy bilateral breast reconstruction using deep inferior epigastric perforator (DIEP) flaps in May 2024. Microsurgical anastomoses to the internal mammary vessels were performed using the Aesculap Aeos exoscope following appropriate chest wall access. Although operative time was slightly longer compared with conventional microscope-assisted procedures, image stability was satisfactory, and the operating surgeons noted a more comfortable working posture during the microsurgical phase (Figures 8–10).



Figure 8. Case 3—DIEP flap harvest.

https://doi.org/10.3390/cmtr19010010



Figure 9. Case 3—completed flap harvest showing vascular pedicle.

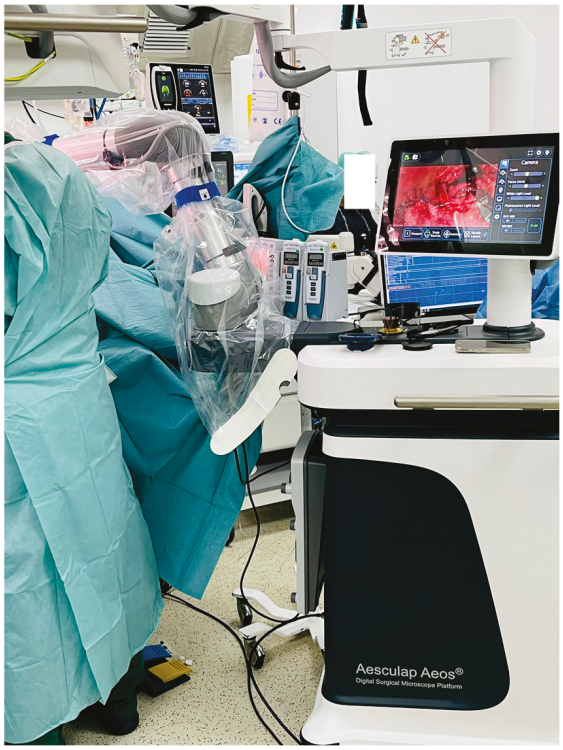

Figure 10. Case 3—Aeos exoscope in use intraoperatively.

3.4. Case 4

A 58-year-old male with pT2N0M0 buccal/commissural squamous cell carcinoma underwent composite resection and radial forearm free flap reconstruction in August 2024. Cervical microvascular anastomoses were completed using the Olympus Orbeye 4K 3D exoscope camera system (Olympus Deutschland GmbH, Hamburg, Germany). Implantable

https://doi.org/10.3390/cmtr19010010

Cook microdoppler dual-channel monitoring system was utilized perioperatively to ensure microvascular patency and flow (Figures 11–14).



Figure 11. Case 4—Ablative defect.

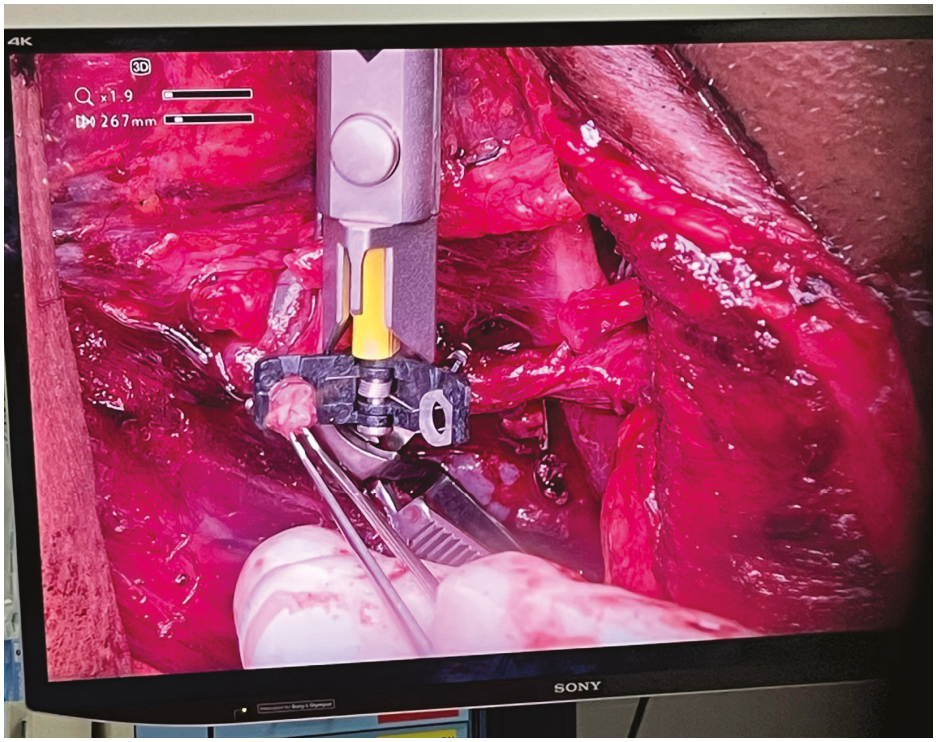

Figure 12. Case 4—Orbeye 4K 3D Camera visual display.

https://doi.org/10.3390/cmtr19010010



Figure 13. Case 4—Intraoperative Orbeye overhead camera position.



Figure 14. Case 4—Immediate postoperative status.

3.5. Case 5

A 36-year-old male with locoregionally advanced pT4aN2cM0 PDL-1 positive bucco-cervical/mandibular well-differentiated keratinizing squamous cell carcinoma underwent composite resection involving mandible, cheek and cervical skin in December 2024. Dual

https://doi.org/10.3390/cmtr19010010

free flap reconstruction was achieved using free fibula osseomyocutaneous as well as anterolateral thigh perforator flaps. Microsurgery was completed using both Mitaka Hawksight exoscope as well as Zeiss Pentero (Carl Zeiss Meditech AG, Oberkochen, Germany) operating microscope (Figures 15–19).

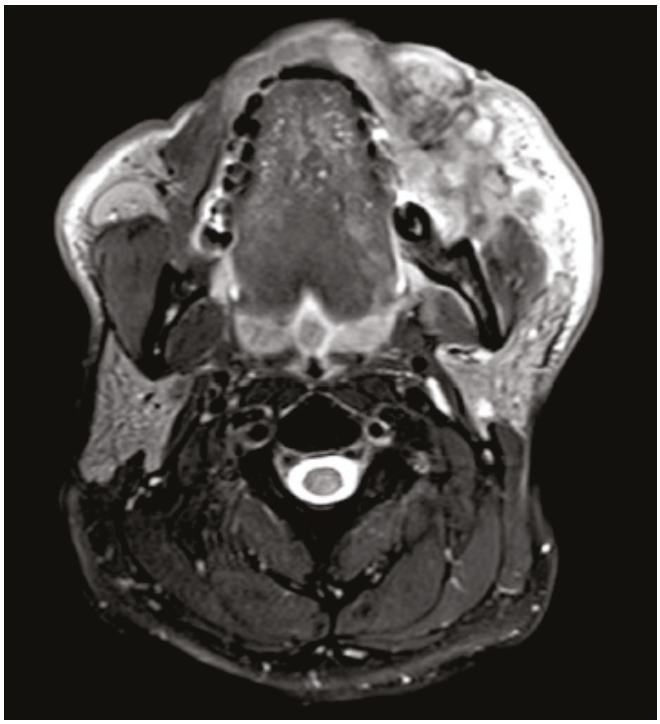

Figure 15. Case 5—Preoperative staging T2W magnetic resonance imaging (axial view).

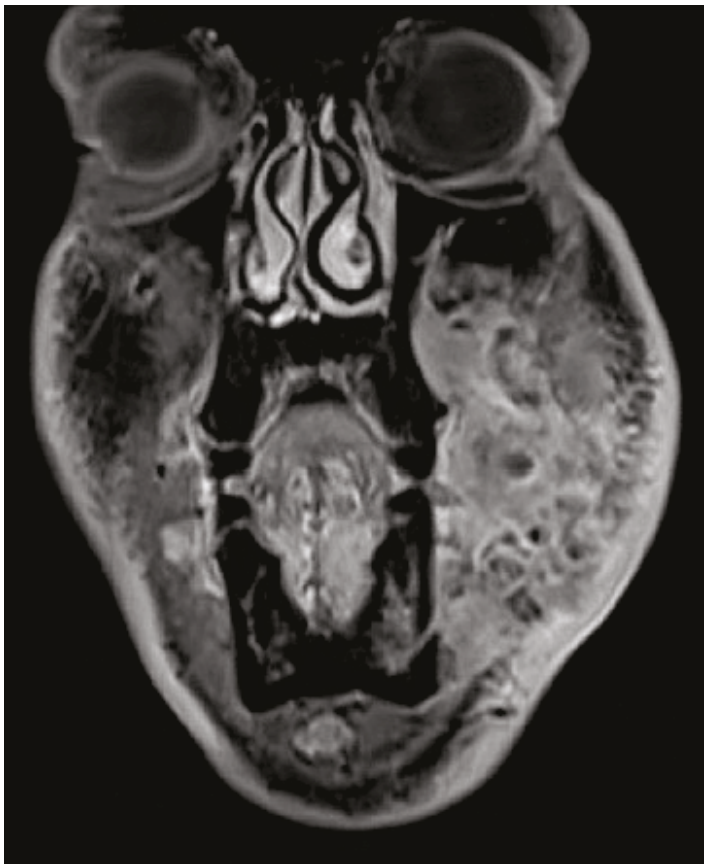

Figure 16. Case 5—Preoperative staging T2W magnetic resonance imaging (coronal view).

https://doi.org/10.3390/cmtr19010010



Figure 17. Case 5—Completed fibula flap harvest.



Figure 18. Case 5—Completed cervicofacial reconstruction.

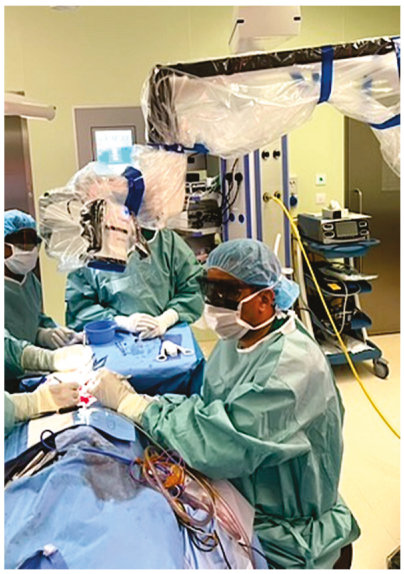

Figure 19. Case 5—Intraoperative exoscope setup during microsurgery.

https://doi.org/10.3390/cmtr19010010

4. Discussion

The term exoscope is derived from the Greek exō ("outside") and skopeîn ("to look"), reflecting its role as an external visualisation device. It functions as a high-definition optical system that provides magnified real-time views of the surgical field on a 3D and/or 4K monitor. Currently available systems, including the VITOM 3D (Karl Storz SE & Co. KH, Tuttlingen, Germany), ORBEYE 4K 3D (Olympus, Germany), and Modus V (Synaptive, Canada), offer high-quality illumination, focus control, and increased flexibility in surgeon positioning [5,11,12].

Although originally developed for neurosurgical procedures [4], exoscopy has gained wider application in craniomaxillofacial and reconstructive surgery. Previous reports have demonstrated comparable outcomes between exoscope-assisted and operating microscope-assisted microvascular reconstruction, with similar rates of vessel patency and flap survival [7–10]. An additional advantage frequently reported is the ability for the wider operating team to share the same operative view, which may improve communication and facilitate teaching during complex procedures [13,14].

Ergonomics has become an increasingly relevant consideration in microsurgical practice. Prolonged use of the operating microscope is known to require sustained non-neutral postures, and this has been associated with a high prevalence of work-related musculoskeletal symptoms among microsurgeons, particularly affecting the neck and lower back [1,2]. Exoscopic systems remove the need for fixed oculars and allow the surgeon to work in a more upright position, which may help address some of these issues. In the present series, no formal ergonomic assessment tools were used; however, from the surgeons' perspective, exoscopy allowed greater flexibility in positioning and was perceived to be more comfortable during prolonged microsurgical tasks.

An additional potential advantage of exoscopic visualisation relates to surgical training and performance, particularly among less experienced surgeons. The shared high-definition operative view allows trainees to observe microsurgical steps in real time and facilitates closer supervision during critical phases of reconstruction. Previous work in microsurgical free flap surgery, including studies involving radial forearm free flap anastomosis, has suggested that exoscopic systems may support performance and help shorten the learning curve for junior surgeons when compared with conventional microscope-based approaches [8]. Assessment of surgeon performance was beyond the scope of the present case series; however, this remains an important area for future study.

There remain recognised limitations to the wider adoption of exoscopic systems, including cost, the need to adapt to digital depth perception, and potential visual fatigue associated with prolonged use of 3D displays [7,9]. Despite these challenges, the combination of shared visualisation, workflow flexibility, and perceived ergonomic benefits makes exoscopy an appealing alternative to the conventional operating microscope for selected reconstructive procedures [12,14]. As with much of the existing literature, the present report is limited by small numbers, and larger multicentre studies will be required to better define long-term outcomes and the role of exoscopy in routine microsurgical practice [7,8,12].

5. Conclusions

Exoscopic microsurgery is increasingly being used in craniomaxillofacial and head and neck reconstruction and offers a practical alternative to the conventional operating microscope in selected cases. In our experience, exoscopic systems provide high-quality visualisation while allowing greater flexibility in surgeon positioning and facilitating shared viewing for the wider operating team. Although cost, adaptation to digital depth perception, and prolonged use of 3D displays remain relevant considerations, exoscopy was

https://doi.org/10.3390/cmtr19010010

found to be feasible for microsurgical reconstruction across a range of complex procedures. The present case series is limited by small numbers and its descriptive nature; however, it supports the growing body of literature suggesting a role for exoscopy in modern microsurgical practice. Exoscopic visualisation may also offer advantages in training environments by facilitating supervision and shared operative viewing, particularly for junior surgeons undertaking microsurgical reconstruction.

Author Contributions: Conceptualization, K.A.-G.; methodology, K.A.-G. and K.M.T.; investigation, K.A.-G. and K.M.T.; writing—original draft preparation, K.A.-G.; writing—review and editing, K.A.-G. and K.M.T.; supervision, K.A.-G. All authors have read and agreed to the published version of the manuscript.

Funding: This research received no external funding.

Institutional Review Board Statement: Ethical approval for conducting this study was obtained from Al Ain Region Human Research Ethics Committee on 16 January 2026 (reference number MF2058-2025-1318).

Informed Consent Statement: All patients involved in this study provided informed consent for participation.

Data Availability Statement: The data presented in this study are available on request from the corresponding author. The data are not publicly available due to ethical and privacy restrictions involving patient information.

Conflicts of Interest: All authors declare no conflicts of interest.

References

1. Albayrak, A.; van Veelen, M.A.; Prins, J.F.; Snijders, C.J.; de Ridder, H. Ergonomic evaluation of the microscope and the exoscope in microsurgery. *Surg. Endosc.* **2007**, *21*, 681–687.
2. Capone, A.C.; Parikh, P.M.; Gatti, M.E.; Davidson, B.J. Work-related musculoskeletal discomfort among otolaryngologists. *Am. J. Otolaryngol.* **2010**, *31*, 333–338.
3. Jacobson, J.H., 2nd; Wallman, L.J.; Schumacher, G.A.; Flanagan, M.; Suarez, E.L.; Donaghy, R.M. Microsurgery as an aid to middle cerebral artery endarterectomy. *J. Neurosurg.* **1962**, *19*, 108–115. [CrossRef] [PubMed]
4. Mamelak, A.N.; Danielpour, M.; Black, K.L.; Hagike, M.; Berci, G. A high-definition exoscope system for neurosurgery and other microsurgical disciplines. *Surg. Innov.* **2008**, *15*, 38–46. [CrossRef] [PubMed]
5. Krishnan, K.G.; Schöller, K.; Uhl, E. Application of a compact high-definition exoscope for illumination and magnification in high-precision surgical procedures. *World Neurosurg.* **2017**, *97*, 652–660. [CrossRef] [PubMed]
6. Oertel, J.M.; Burkhardt, B.W. VITOM-3D for exoscopic neurosurgery. *World Neurosurg.* **2017**, *105*, 153–162. [CrossRef] [PubMed]
7. De Virgilio, A.; Iocca, O.; Di Maio, P.; Mercante, G.; Mondello, T.; Yiu, P.; Malvezzi, L.; Pellini, R.; Ferreli, F.; Spriano, G. Free flap microvascular anastomosis using a 4K 3D exoscope. *Int. J. Oral Maxillofac. Surg.* **2020**, *49*, 1169–1173. [CrossRef] [PubMed]
8. Piatkowski, A.A.; Keuter, X.H.; Schols, R.M.; van der Hulst, R.R. Potential of performing microvascular free flap reconstruction using a 3D exoscope. *J. Plast. Reconstr. Aesthet. Surg.* **2018**, *71*, 1664–1678. [CrossRef] [PubMed]
9. Pafitanis, G.; Hadjiandreou, M.; Alamri, A.; Uff, C.; Walsh, D.; Myers, S. Exoscope versus operating microscope: A non-inferiority trial. *Arch. Plast. Surg.* **2020**, *47*, 242–249. [PubMed]
10. Grammatica, A.; Schreiber, A.; Vural, A.; Deganello, A.; Ferrari, M.; Lancini, D.; Montalto, N.; Nicolai, P. Application of a 3D 4K exoscope to head and neck reconstruction. *Eur. J. Plast. Surg.* **2019**, *42*, 611–614. [CrossRef]
11. Olympus Corporation. Launch of ORBEYE Surgical Microscope with 4K 3D Capabilities Supporting Precision Surgery with High-Resolution Digital Images with Stereoscopic Visual Field. Olympus Global News, Tokyo, Japan, 19 September 2017. Available online: https://www.olympus-global.com/news/2017/nr00611.html (accessed on 19 January 2026).
12. Molteni, G.; Nocini, R.; Ghirelli, M.; Molinari, G.; Fior, A.; Veneri, A.; Nocini, P.F.; Marchioni, D. Free flap head and neck microsurgery with VITOM 3D. *Auris Nasus Larynx* **2021**, *48*, 464–470. [CrossRef] [PubMed]

https://doi.org/10.3390/cmtr19010010

13. Catalfamo, L.; Calvo, A.; Cicchiello, S.; La Fauci, A.; De Ponte, F.S.; Scozzaro, C.; De Rinaldis, D. Can 3D exoscopy-assisted surgery replace traditional endoscopy in septoplasty? *J. Clin. Med.* **2025**, *14*, 5279. [CrossRef] [PubMed]
14. De Rinaldis, D.; Scozzaro, C.; Calvo, A.; Basilicata, M.; De Ponte, F.S.; Catalfamo, L. Exoscope-assisted surgery for benign parotid tumours. *Indian. J. Otolaryngol. Head Neck Surg.* **2024**, *76*, 4506–4515. [CrossRef] [PubMed]

Disclaimer/Publisher's Note: The statements, opinions and data contained in all publications are solely those of the individual author(s) and contributor(s) and not of MDPI and/or the editor(s). MDPI and/or the editor(s) disclaim responsibility for any injury to people or property resulting from any ideas, methods, instructions or products referred to in the content.

https://doi.org/10.3390/cmtr19010010

craniomaxillofacial
trauma & reconstruction

MDPI

Technical Note

Jaw in a Day: How to Perform Your First Case—Our Workflow

Camilo Mosquera * and Hisham Marwan

Head and Neck Oncologic Surgery and Microvascular Reconstruction, Department of Surgery, Division of Oral and Maxillofacial Surgery, University of Texas Medical Branch, Galveston, TX 77555, USA; himarwan@utmb.edu
* Correspondence: camosque@utmb.edu

Abstract: Jaw in a Day (JIAD) reconstruction provides immediate restoration of mandibular form and function through a single-stage procedure that integrates fibula free flap reconstruction, virtual surgical planning (VSP), immediate dental implant placement, and delivery of a prefabricated prosthesis. Although the technique provides significant benefits in reducing rehabilitation time and improving patient outcomes, its adoption has been limited due to perceived technical complexity and unfamiliarity with dental workflow. This manuscript provides a detailed, step-by-step protocol to guide surgeons through their first JIAD case, from patient selection and data acquisition to VSP execution, intraoperative coordination, and implant positioning. Emphasis is placed on accurate osteotomy design, implant placement using guided protocols, fabrication of patient-specific hardware, and precise prosthesis pickup techniques. This guide also addresses essential OR team preparation and sterile handling of non-sterile components. By breaking down the process into actionable stages and highlighting common pitfalls and technical tips, this resource aims to lower the barrier for early adopters and enhance the success of initial JIAD cases.

Keywords: free tissue flaps; fibula free flap; dental implants; head and neck; reconstructive surgery

1. Introduction

The reconstruction of segmental mandibular defects using fibula free flaps has become a cornerstone of modern head and neck surgery, allowing for reconstructive teams to achieve the goals of mandibular reconstruction by restoring jaw continuity, facial support, and alveolar bone for dental rehabilitation [1]. With the integration of virtual surgical planning (VSP), immediate dental implant placement, design of custom reconstruction plates, and 3D-printed dental prosthesis delivery, the concept of "Jaw-in-a-Day" (JIAD) has emerged as a transformative technique [2,3]. This approach enables the simultaneous restoration of mandibular continuity, function, and esthetics in a single operative stage, reducing overall rehabilitation time and improving quality of life.

Despite its benefits, the JIAD protocol remains underutilized, mainly due to its perceived complexity, cost, and the steep learning curve associated with multi-team coordination, digital planning, and intraoperative execution. For many surgeons unfamiliar with the dental aspect of the reconstruction, their first case can be daunting. Without adequate preparation and insight into the process, first-time attempts can be prone to avoidable errors.

The purpose of this article is to provide a comprehensive step-by-step guide for performing a surgeon's first fibula JIAD reconstruction. Our specific aim is to outline the essential elements of preoperative planning, virtual surgical design, intraoperative execution, and postoperative care, while highlighting key technical tips, common pitfalls,

and logistical considerations to help early adopters avoid complications and achieve successful outcomes.

2. Materials and Methods

The authors categorized the steps for the JIAD procedure into three categories: Preoperative planning, Intraoperative execution, and postoperative care.

3. Results

3.1. Preoperative Planning

Preoperative evaluation is crucial in determining whether a patient is a suitable candidate for reconstruction using a free fibula flap following segmental mandibulectomy. Many patients requiring this procedure are older and have multiple comorbidities, making medical optimization before surgery critically important. Additionally, preoperative planning must include an assessment of the anatomical variations in the lower leg, its arterial vascularization, and any arteriosclerosis, as these factors may contraindicate the use of the free fibula flap (FFF). Such conditions can increase the risk of vascular compromise to the foot and distal lower extremity [4].

CT-Angiography (CTA) of the bilateral lower extremities is the gold standard for vascular assessment. It is essential for virtual surgical planning and creating 3D-printed custom cutting guides and custom reconstruction plates [5]. The success of the JIAD reconstruction relies on the accuracy of the osteotomies in the fibula and the resection site, which can only be achieved by using custom-made devices, patient-specific implants, and stereolithographic models during the surgical procedure.

3.1.1. Data Gathering

To obtain high-quality and fidelity in custom-made implants and guides, it is essential to have high-quality imaging and data. Low-quality data will produce low-quality products, leading to inaccurate and unsuccessful JIAD reconstruction.

The necessary data to be collected (Table 1) is a maxillofacial CT-scan with 1 mm thickness cuts and increments, CTA Bilateral lower extremities with 1 mm cuts and increments, and an STL file of the teeth that should be ideally obtained with an intraoral scanner, or by obtaining dental impressions and using a desktop scanner to digitalize the teeth. These files are then sent to the vendor for use during the virtual surgical planning (VSP) meeting.

Table 1. Data required for jaw in a day.

CT-SCAN	• CT maxillofacial or neck with or without contrast. • CTA bilateral lower extremities • Slice thickness < 1.25 mm
DENTAL SCAN	• Recommended: intraoral scan • Impressions and table scan of cast models accepted
PREOPERATIVE PICTURES	• Standard pre-operative pictures (Front, Profile, Smile)

3.1.2. VSP Meeting

During the VSP meeting, the dental data are superimposed with the CT maxillofacial data to increase the accuracy of the fabricated guides [6]. This dental data is also used to 3D print the temporary dental prosthesis that will be placed intraoperatively. In the case of complete edentulous patients, where a full arch reconstruction is planned, the vendor can idealize the dentition and virtually position the occlusion.

The VSP starts with the simulated jaw resection. The surgical team determines the bony margins for the surgical resection; the authors recommend resecting enough to fit fibula segments of at least 2.5 cm. In the posterior mandible, it is recommended to include the coronoid process in patients with cancer or osteoradionecrosis (ORN) to prevent or improve trismus. For mandibular body defects, it is recommended to extend the osteotomy up to the first premolar or canine, if the margin allows, designing the osteotomy through the socket rather than between teeth, to maintain bone on the remaining teeth. For defects crossing the midline, consider including all four incisors to allow enough space for a sufficiently large anterior fibula segment.

The mandibular resection cutting guides can be designed as one bridged guide or as distinct, independent guides. The authors typically design individual guides to facilitate smaller incisions in the neck or, on occasion, intraoral resections of the tumors. It is essential to note that a single bridged piece enhances the accuracy of the resection by reducing the likelihood of mispositioning the cutting guide. In contrast, the independent guides have the potential to slide over the bone and be placed in the incorrect position. To prevent this, it is essential to use anatomical landmarks as registration points to set the guides precisely (Figure 1).

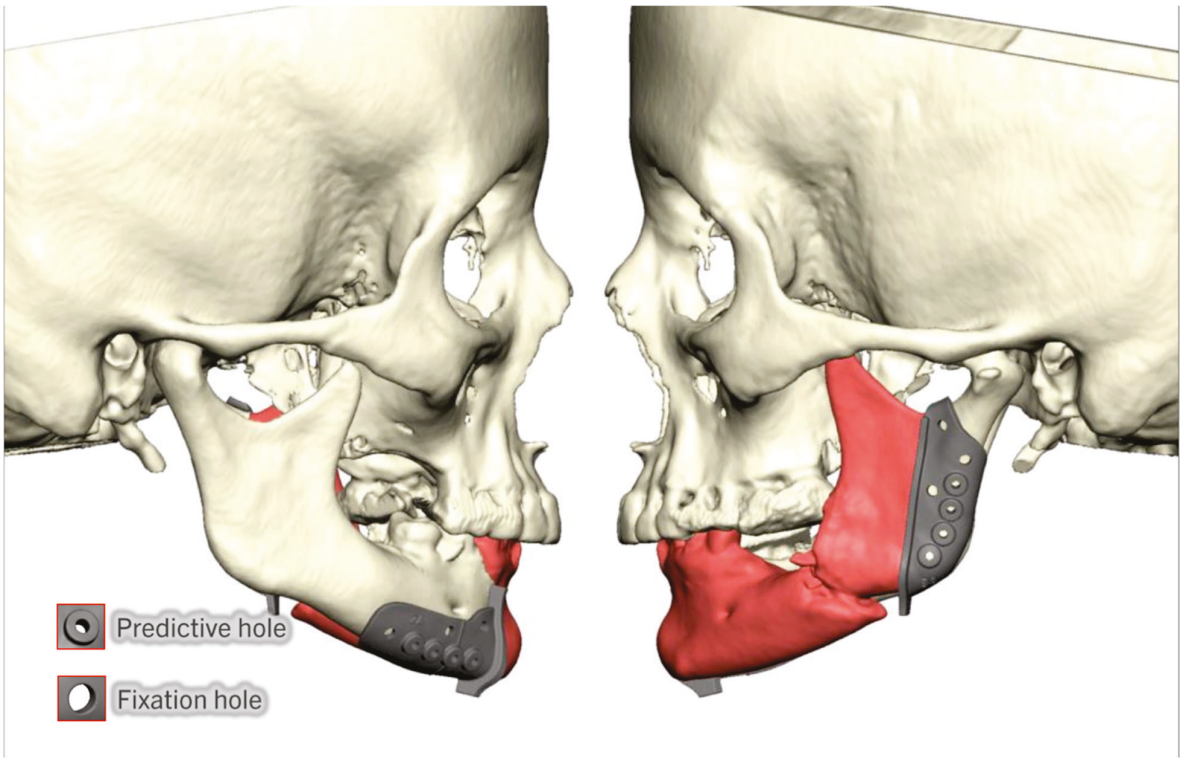

Figure 1. Individual mandibular cutting guides with registration points in the posterior border of the mandibular ramus, sigmoid notch, mental foramen, and inferior border of the mandible. Area highlighted in red corresponds to planned resection.

The resection cutting guides can also be designed to have slots or cutting walls to fit the saw for the osteotomies (Figure 2). The authors believe that using the wall design increases visibility at the osteotomy site, allowing for the surgeon to make sure that the saw is seated passively against the wall. This allows for the accurate reproduction of the osteotomy angle and avoids interferences during the fibula inset.

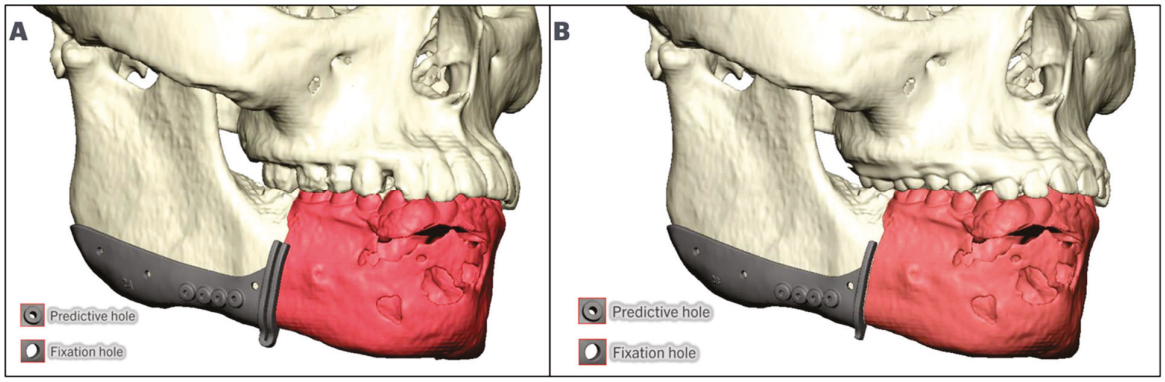

Figure 2. Example of two resection cutting guide designs. (**A**): Cutting guide with slots design. (**B**): Cutting guide with wall design. Area highlighted in red corresponds to planned resection.

The right or left fibula is selected based on vascular supply and the surgeon's preference. The lateral face of the fibula is used as the plating surface, and the anterior surface of the fibula is used to place the dental implants. However, the authors have used the posterior surface of the fibula when the case does not allow otherwise, particularly in bone-only reconstructions. The vascular pedicle can be oriented anteriorly or posteriorly, depending on the surgeon's preference and the availability of receptor vessels. If a skin paddle is to be used, it is recommended to design it to come over the buccal surface, thereby recreating a vestibule.

The fibula position is maintained low and aligned with the inferior border of the posterior mandible. It is raised anteriorly at the symphysis/parasymphysis level to allow for 13–18 mm of restorative space. In some cases where the vertical facial height is decreased, it may be necessary to place the fibula aligned with the inferior border anteriorly or displace the posterior segment lower than the mandibular angle to allow for enough restorative space, while maintaining bone-to-bone contact (Figure 3). Once the position of the fibula has been defined, the dental implants are placed. The authors recommend placing at least two implants at each fibula segment, oriented in such a way that they emerge lingual or at the level of the occlusal surfaces of the teeth, avoiding extreme angulation towards the lingual or buccal plate. The parallelism of the implants is checked to ensure a passive insertion path for the temporary prosthesis. The authors recommend maintaining a distance of at least 5 mm from the osteotomy and 5 mm between implants (Figure 4).

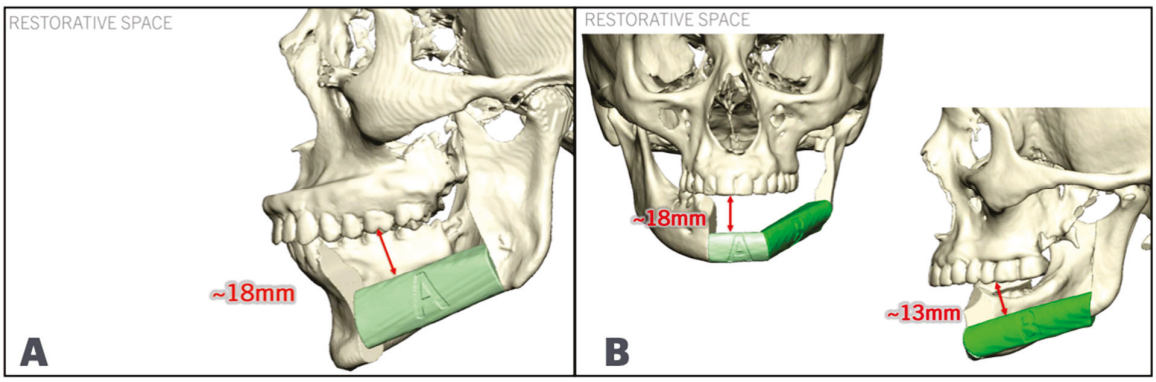

Figure 3. Fibula (In green) positioning for mandibular defects, achieving enough restorative space. (**A**): Fibula segment aligned with the inferior border posteriorly and raised anteriorly. (**B**): Anterior fibula segment aligned with inferior border, and posterior fibula segment lowered to allow for minimal restorative space.

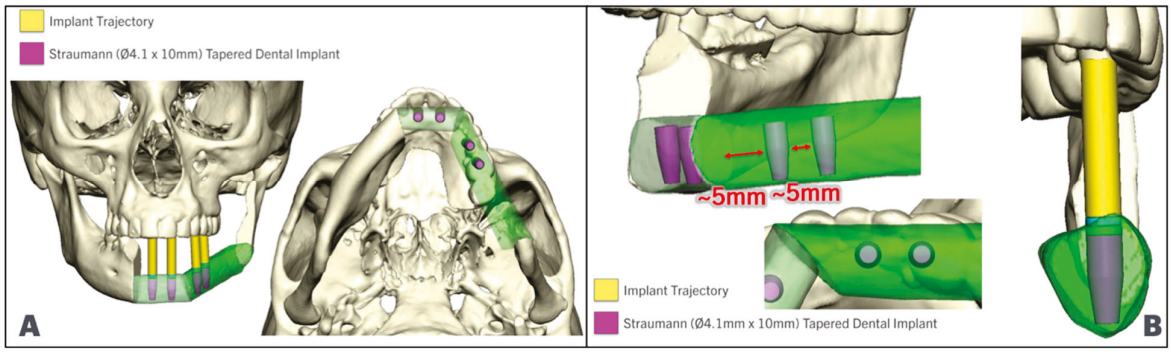

Figure 4. Implant positioning in fibula segments (In green), (**A**): Implant parallelism in anterior and lateral fibula segments. (**B**): Implants are positioned allowing for 5 mm between implant and osteotomy, and 5 mm between implants while maintaining parallelism and implant trajectory aligned with the occlusal surface.

The fibula cutting guides are designed with an implant-restrictive positioning guide incorporated. This implant positioning guide enables the placement of dental implants during the harvesting of the flap, and it is restrictive, meaning that it prevents the surgeon from accidentally modifying the angle of drilling or implant insertion. The implant placement area in the fibula cutting guide must have a diameter that matches the sleeves of the guided implant kit that the surgeon prefers. The authors typically use the Straumann Bone-Level Tapered (BLT) Implant System and have found that most cases are suitable for using 4.1 × 10 mm or 4.1 × 12 mm BLT implants.

Both the mandible and the fibula cutting guides can be designed in polyamide or titanium. The authors recommend using titanium guides for both resection and flap; however, if Polyamide guides are used, metal sleeves are highly recommended for the fibula guide to allow for a more precise cut (Figure 5).

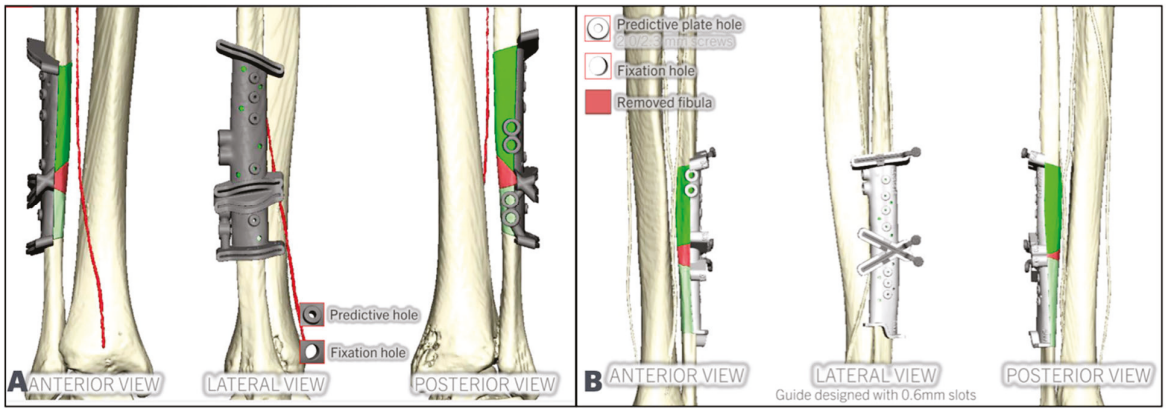

Figure 5. Examples of fibula cutting guides made in titanium. The planned fibula segments are shown in green (**A**), and polyamide with titanium sleeves (**B**). Note how the implant guides are incorporated into both fibula cutting guides.

The patient-specific plate is designed next, located low on the fibula segments, with the fixation holes placed in between or behind the implants. In the native mandible, the number of fixation holes follows the reconstructive plating principles. The reconstruction plate holes are designed to match the predictive holes of the resection cutting guide (Figure 6).

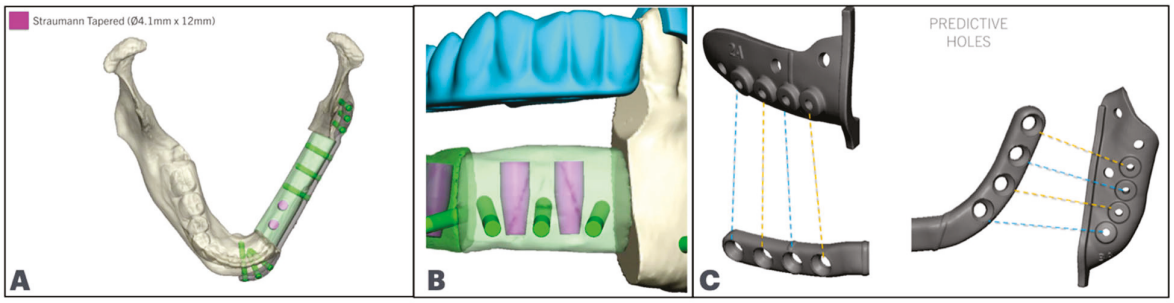

Figure 6. (**A**): Fixation screws posterior to dental implants. The planned fibula segments are shown in green. (**B**): Fixation screws in between implants. (**C**): Cutting guides predictive holes match the fixation screws.

Once the resection and the fibula guides are designed, the dental data is used to create a 3D reconstruction of the dentition. The temporary prosthesis can be designed as a floating device if enough native teeth are still present. This floating denture serves as a splint, enabling the precise positioning of the denture over the fibula and maintaining an adequate vertical position of the denture in relation to the implants. In the case of a total arch reconstruction, where no native dentition remains, the authors use a maxillary Stealth model and an articulated maxillary model, designed by Khatib et al. and referred to as the "Fibiculator [7]." The stealth model is used to hold the temporary prosthesis in place and correctly position the prosthesis vertically. The maxillary articulated model is used to verify occlusion after the prosthesis is picked up. The temporary prosthesis is designed with enough space between the lower surface and the fibula to allow for closure and hygiene after surgery (Figure 7).

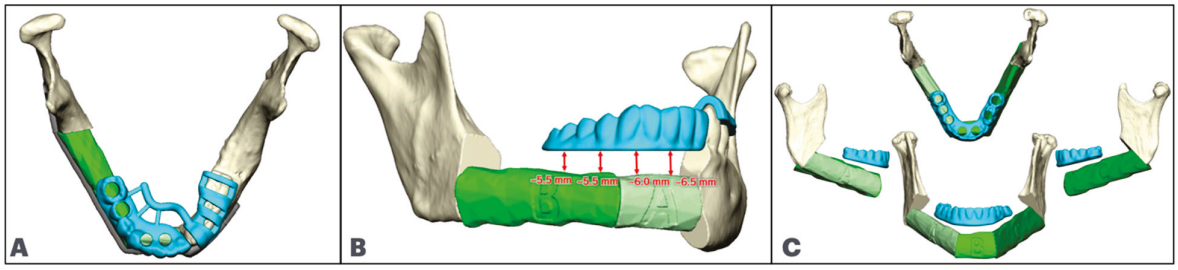

Figure 7. (**A**): Floating temporary prosthesis shown in blue. (**B**): Space between the temporary prosthesis and the fibula segment. (**C**): Floating prosthesis in full arch reconstruction. The planned fibula segments are shown in green.

After the VSP meeting, the surgeon should request the following devices to be available in surgery (Figure 8).

- Patient-specific reconstruction plate;
- Patient-specific resection cutting guides;
- Patient-specific fibula cutting guide with implant guide incorporated;
- Resected model with fixation holes to secure the reconstruction plate;
- Temporary dental prosthesis;
- Stealth maxilla and articulated maxillary model for total arch reconstructions (Figure 9).

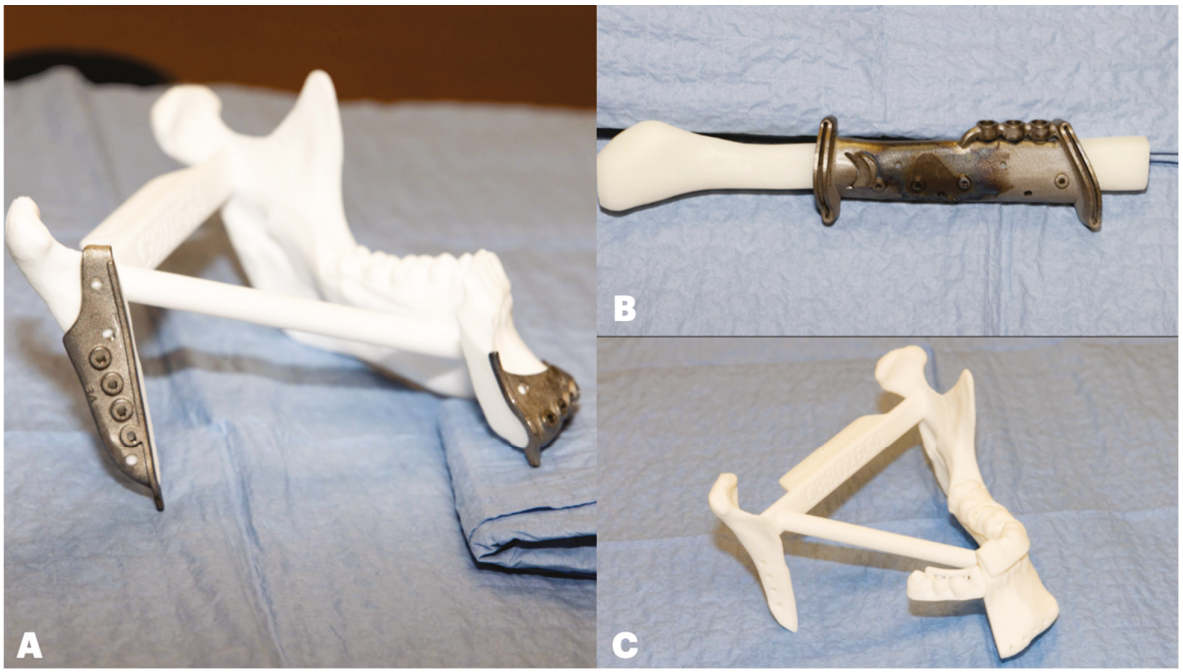

Figure 8. (**A**): Mandibular resected model with cutting guide in position. (**B**): Fibula cutting guide with incorporated dental implant guide. (**C**): Verification model of 3D-printed prosthesis over mandibular resected model.

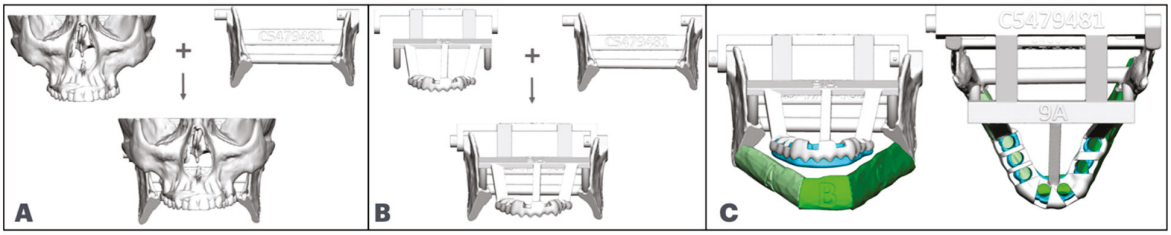

Figure 9. (**A**): Articulated maxillary model. (**B**): Stealth maxillary articulated model. (**C**): Stealth maxillary model holding the temporary prosthesis.

3.2. Intraoperative Execution

3.2.1. Operating Room (OR) Staff Training

Performing a successful first JIAD reconstruction requires not only surgical expertise but also a highly coordinated and knowledgeable OR team. Because this procedure uniquely integrates microvascular free flap techniques with immediate dental implant placement and prosthetic workflows, it presents novel challenges for OR staff who may be unfamiliar with the specialized dental implant components and materials involved.

Many OR nurses, scrub technicians, and circulating staff have limited prior experience with dental implant systems. This encompasses a wide range of components, including implant fixtures, multi-unit abutments, impression copings, and prosthetic parts. Furthermore, materials such as acrylic resin used for prosthesis fabrication, along with the specific handling and sterilization requirements, often fall outside their regular practice. This lack of familiarity can result in delays, an increased risk of contamination, or unintentional damage to costly components.

The JIAD procedure involves introducing non-sterile components into the surgical field, such as 3D-printed prostheses, acrylic tip applicators, and impression coping abutments. This can raise concerns among OR staff unfamiliar with dental workflows, particularly regarding the risk of cross-contamination [8]. To address this, the authors

follow an institutional protocol where these items are submerged in povidone-iodine for 10 min before use. The acrylic tip applicator is enclosed in a sterile plastic bag, allowing intraoperative application while preserving sterility. Clear protocols like this are essential to maintain aseptic technique and reduce anxiety among inexperienced OR teams.

To address these challenges, it is essential to conduct dedicated preoperative training sessions for OR staff. These sessions should include hands-on familiarization with implant kits and their components, detailed instruction on aseptic protocols for handling non-sterile parts, and clear labeling and organization of implant surgical trays. Involving dental implant representatives in these training sessions can boost staff confidence and ensure proper handling of components. Additionally, assigning a dedicated surgical technologist or circulating nurse with specialized training in implant workflows during the first few JIAD cases can enhance efficiency and reduce the likelihood of intraoperative errors.

3.2.2. Surgical Procedure

The authors usually perform the procedure in a two-team approach with the ablative and reconstructive teams working in parallel. Following airway protection, the head and neck team initiates the procedure with neck dissection and tumor ablation, utilizing patient-specific resection cutting guides designed during virtual surgical planning. Care is taken to precisely position the cutting guide using the anatomic landmarks planned as registration points during the virtual surgical meeting. This part of the procedure is essential, as failure to position the guides correctly will result in a larger or smaller defect, where the fibula segments will not fit properly.

The resection cutting guides are fixated, and the predictive holes are drilled. Care is then turned to perform the osteotomies. This is a deceptive, simple step; however, care must be taken to accurately reproduce the same angle with the saw that the cutting guide has. To achieve this, the authors emphasize maintaining the saw blade flush and parallel to the cutting guide wall. Separating the saw blade from the guide wall will result in a different angle that will generate an interference point with the fibula segment.

Once the resection is complete, the authors recommend verifying the accuracy of the resection by using the resected 3D printed model (Figure 10). This allows the ablative team to eliminate any identified interferences before the reconstructive team enters ischemia time.

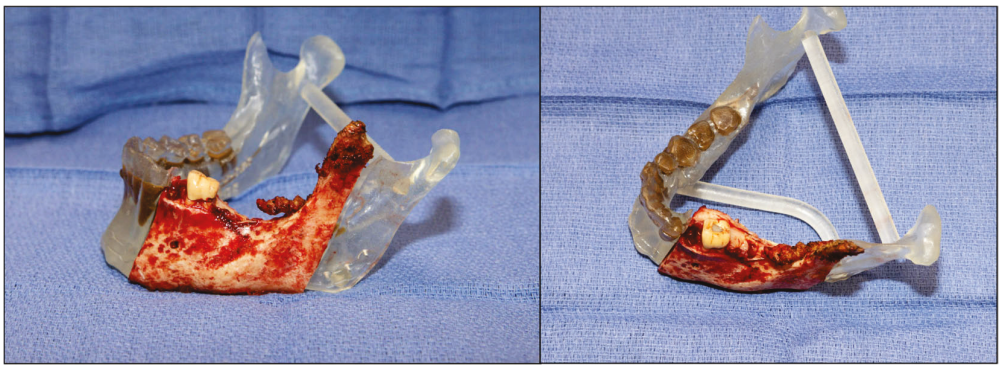

Figure 10. Specimen on the resected model to verify the accuracy of osteotomies.

Simultaneously with the resection, the reconstructive team harvests the FFF in the standard fashion [9]. If a skin paddle is anticipated, it is desirable to position it buccally as it will create a vestibule. A limited skin paddle is advisable in cases with minimal soft tissue defects. The authors typically prefer primary closure and a bone-only flap in cases with limited soft tissue defects. After the proximal and distal fibular osteotomies are completed, the fibula has been mobilized laterally. The pedicle has been traced proximally to the

trifurcation; attention is turned to the osteotomies and placement of the dental implants. The fibula cutting guide is positioned and secured with screws. Care is taken to verify that the dental implant guides are located over the anterior surface with enough available bone. Next, the dental implants are placed. The recommended hard-bone protocol from the implant company must be followed, and the implant drilling sequence is completed in the standard fashion with controlled irrigation, speed, and torque. Due to the hardiness of the fibula bone, the authors recommend bi-cortical drilling.

In addition, the authors recommend using countersinks or increasing the drill size by one, only on the outer cortex, to allow for passive implant placement while preserving immediate retention. The authors usually place Bone-Level implants one millimeter sub-crestal, taking care to avoid bi-cortical implant anchorage. Although not yet supported by definitive clinical evidence, some surgeons intentionally avoid bicortical anchorage when placing dental implants into the fibula, based on the belief that this approach may reduce the risk of fibula segment fracture in the event of peri-implantitis extending to the implant apex. It is important to note that this theoretical concern remains anecdotal and warrants further investigation.

Once the implants are placed and the fibular closing osteotomies are completed, the cutting guide is removed, allowing access to the dental implants. At this point, straight multi-unit abutments are used to raise the prosthetic platform, and then the straight coping abutments are placed. The authors usually use a 4 mm straight multi-unit abutment and a straight temporary coping abutment (Figure 11).

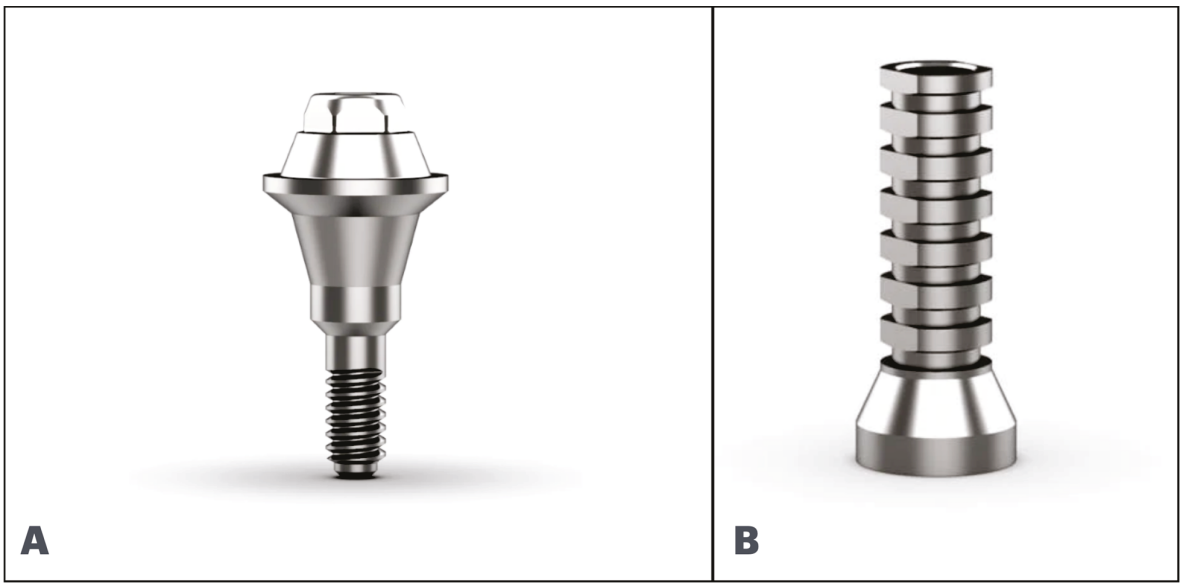

Figure 11. (**A**): Multi-unit abutment. (**B**): Temporary coping abutment.

Once the multi-unit and temporary coping abutments have been placed, the custom-made reconstruction plate is secured to the resected model using the screws removed from the fibula cutting guide. Next, the fibula flap is adapted to the resected model and loosely fixed to the plate, allowing for slight rotational movement of the segments. At this point, the 3D printed floating temporary prosthesis is placed over the resected model dentition, and the temporary abutments are aligned with the occlusal opening prepared for the emergence of the implants' abutments. It is common to see at this step that the abutments are hitting against the lingual or buccal surface of the temporary prosthesis; this is usually due to a "barrel-roll" effect on the fibula segment that can be solved by rotating it buccally or lingually as needed until the abutments are located passively on the

prosthesis openings. Suppose the temporary prosthesis is not passively aligned with the temporary abutments and is forced into position; the patient will have a malocclusion once the flap is transferred to the head. The authors recommend achieving the best and most passive positioning and insertion pathway of the fibula on the model and the prosthesis on the implants' abutments. Once the position of the fibula segments and the emergence of the implants' abutments on the temporary prosthesis have been confirmed, the fibula fixation screws are tightened, taking care to prevent rotation of the bony segment as the screws secure the bone to the plate. Once this is complete, the opening of the temporary coping screw is covered with a small red rubber catheter to prevent acrylic inflow during the prosthesis pickup (Figure 12).

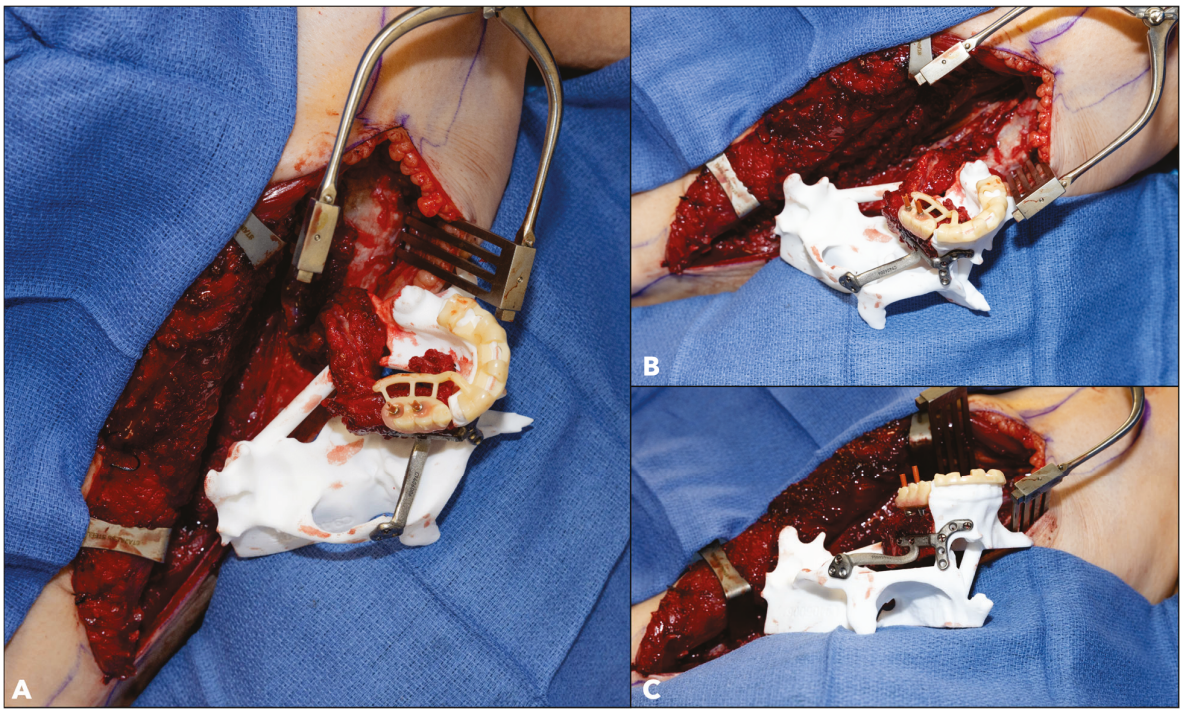

Figure 12. Example of Maxillary Jaw in a Day. (**A**): Emergence of implants' temporary coping abutments aligned with perforations on the occlusal surface of the dental prosthesis. (**B**): Passive position of the fibula segment on the resected model with good fit and no interferences. (**C**): Verification of passive inset of fibula segment and correct vertical position of dental prosthesis.

3.2.3. Temporary Prosthesis Pickup

After confirming the passive position of the temporary prosthesis and the fibula segments, the prosthesis pickup is performed. The authors use Stellar DC Acrylic, a dual-cure Poly Methyl Methacrylate (PMMA) pickup acrylic with a light-curing time of 20 s and a self-curing time of 120 s. The dual-curing feature enables the reconstructive team to use the acrylic without the need for a curing light in the operating room. The acrylic tube is enclosed in a sterile plastic bag, allowing intraoperative application while preserving sterility. The application tips are submerged in povidone-iodine for 10 min before use. Next, the acrylic is applied around the temporary coping abutments, taking care to avoid injecting the acrylic into the opening of the temporary coping abutments. It is then left to self-cure (Figure 13). After 120 s, the red rubber catheter is removed, the temporary coping retaining screws are removed, and the prosthesis is removed from the flap. At this point, the temporary prosthesis is bonded to the temporary coping abutments, thereby maintaining the spatial position of the implants in the fibula.

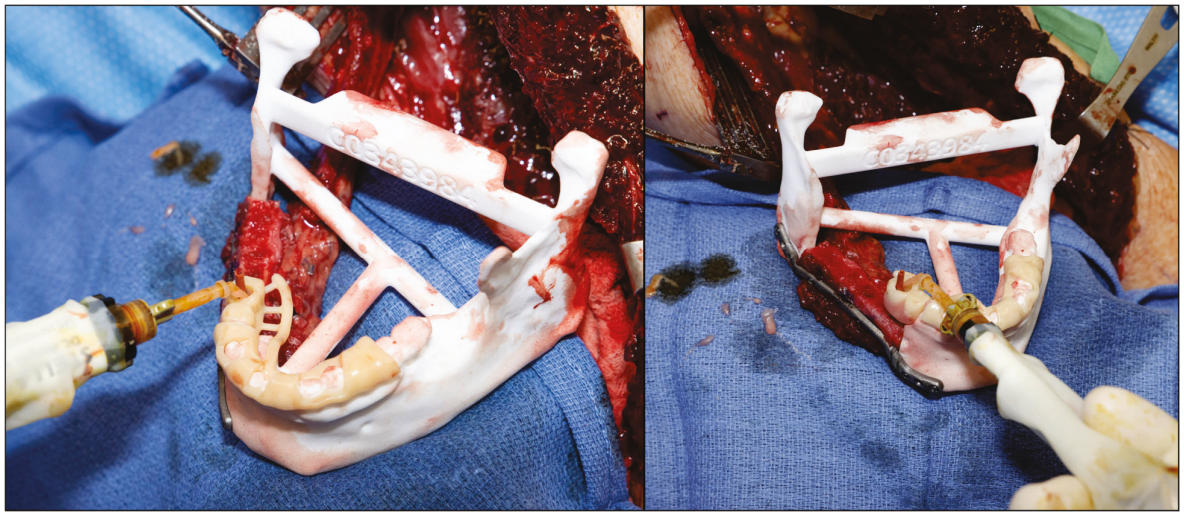

Figure 13. Temporary denture pick-up process. Note the opening of the temporary coping abutment, sealed with a red rubber catheter to prevent inadvertent acrylic flow into it.

Once the stability and complete curing process of the acrylic have been verified, the arms of the floating prosthesis are removed using a pineapple rotating bur, and the sharp edges are trimmed down. Any remaining space between the denture and coping abutment is filled with acrylic and left to cure. Once this is complete, the temporary denture is placed again over the multi-unit abutments, now without the floating part, and the temporary coping abutments are secured to the fibula with the retaining screws. At this point, the position of the implants is verified on the resected model, and the articulated maxilla model is used to check the occlusion (Figure 14).

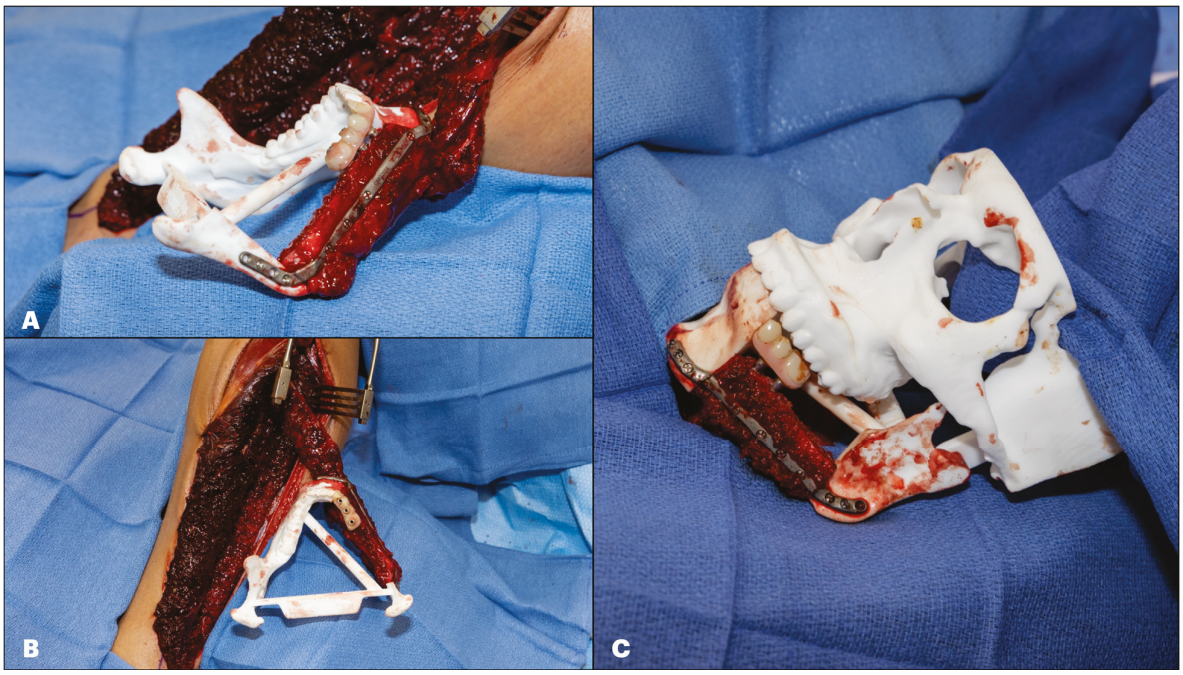

Figure 14. (**A**): Verification of the vertical position of the denture on reconstruction. (**B**): Verification of the transverse position of the denture. (**C**): Verification of occlusion with articulated maxillary model.

After verifying the position of the implants and the reconstruction, the resected model is removed. The construct, comprising the flap, implants, reconstruction plate, and prosthesis, is then ready to be transferred to the neck.

The flap is inset into the defect, the arterial and venous anastomosis is performed in the standard fashion, and the intraoral closure is finalized. Closing the mucosa or skin paddle under the temporary prosthesis is a challenging yet crucial step to prevent salivary leakage. The authors recommend using horizontal mattress sutures to encircle the multi-unit abutments and cinch the tissue to the implants. In some cases, a parachuting technique is employed, where all the sutures are initially placed and then tied at the end to allow for more space during the suturing process. At the end of the case, the occlusion is verified, and any premature contacts are removed to avoid occlusal contacts with the denture. (Figure 15).

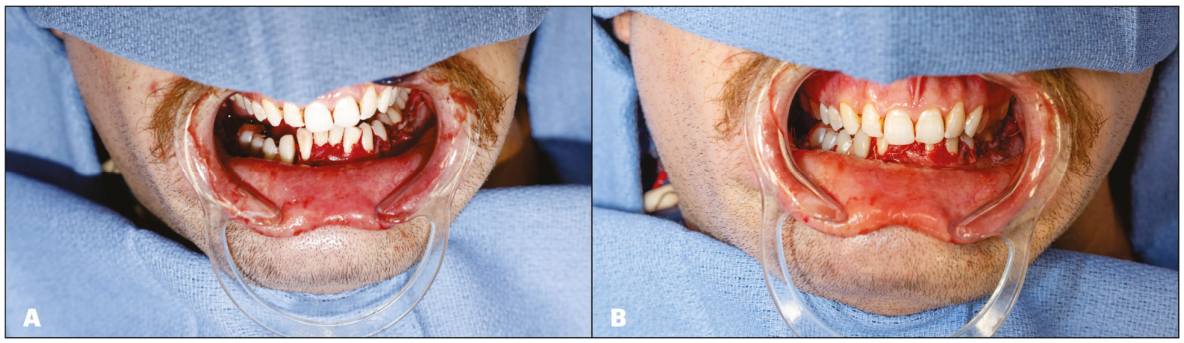

Figure 15. Jaw in a day after flap inset. (**A**): Temporary denture on the right posterior mandible. (**B**): Appreciate the small occlusal gap between the denture and the native maxillary dentition on the Right.

3.3. Post-Operative Care

As with any other microvascular flap, post-operative care following JIAD reconstruction is critical to ensure flap viability, implant integration, and prosthetic hygiene. Flap monitoring adheres to standard microsurgical protocols, which involve daily assessments of perfusion, skin paddle integrity (if present), and intraoral closure [10]. Patients are maintained with a nasogastric feeding tube for one to two weeks, until intraoral soft tissue closure is confirmed. At this point, the patients transition to a full liquid diet, followed by a soft, non-chewing diet for at least 4–6 weeks, to minimize functional loading of the implants. Prosthetic hygiene is reinforced through collaboration with the patient's prosthodontic team, which will oversee the transition to a definitive dental rehabilitation once bone healing and dental integration are complete, approximately 6 months after the initial surgery.

4. Conclusions

JIAD surgery marks a groundbreaking advancement in mandibular reconstruction, delivering immediate functional and esthetic rehabilitation. While the technique may seem complex, it is entirely achievable with thorough preparation and strict adherence to this proven protocol. This guide serves as a crucial resource for early adopters, clearly outlining each step of the process and emphasizing critical technical and logistical considerations. With this roadmap, surgeons can confidently and precisely embark on their first JIAD reconstruction.

Author Contributions: Conceptualization, C.M. and H.M.; methodology, C.M.; data curation, C.M.; writing—original draft preparation, C.M.; writing—review and editing, H.M.; visualization, C.M.; supervision, C.M. and H.M.; project administration, C.M. All authors have read and agreed to the published version of the manuscript.

Funding: This research received no external funding.

Institutional Review Board Statement: UTMB IRB review determined that this submission does not meet the definition of "human subject research", as defined by the regulations at 45 CFR 46.102. This acknowledgement confirms that the project performed does not require IRB approval or oversight.

Informed Consent Statement: Patient consent was waived because this manuscript and the images used in it contain no PHI information, as no patient identifiers are visible.

Data Availability Statement: The original contributions presented in this study are included in the article. Further inquiries can be directed to the corresponding author.

Conflicts of Interest: The authors declare no conflicts of interest.

References

1. Khatib, B.; Cheng, A.; Sim, F.; Bray, B.; Patel, A. Challenges with the Jaw in a Day Technique. *J. Oral Maxillofac. Surg.* **2020**, *78*, 1869.e1–1869.e10. [CrossRef] [PubMed]
2. Sukato, D.C.; Hammer, D.; Wang, W.; Shokri, T.; Williams, F.; Ducic, Y. Experience with "Jaw in a Day" Technique. *J. Craniofac. Surg.* **2020**, *31*, 1212–1217. [CrossRef] [PubMed]
3. Levine, J.P.; Bae, J.S.; Soares, M.; Brecht, L.E.; Saadeh, P.B.; Ceradini, D.J.; Hirsch, D.L. Jaw in a day: Total maxillofacial reconstruction using digital technology. *Plast. Reconstr. Surg.* **2013**, *131*, 1386–1391. [CrossRef] [PubMed]
4. Su, Y.X.; Ganry, L.; Ozturk, C.; Lohman, R.; Al Afif, A.; McSpadden, R.; Frias, V.; Pu, J.J. Fibula Flap Reconstruction for the Mandible: Why It Is Still the Workhorse? *Atlas Oral Maxillofac. Surg. Clin. N. Am.* **2023**, *31*, 121–127. [CrossRef] [PubMed]
5. Wei, F.C.; Santamaria, E.; Chang, Y.M.; Chen, H.C. Mandibular reconstruction with fibular osteoseptocutaneous free flap and simultaneous placement of osseointegrated dental implants. *J. Craniofac. Surg.* **1997**, *8*, 512–521. [CrossRef] [PubMed]
6. Omole, D.; Khatib, B.; Patel, A.A.; Cheng, A.; Salama, A.; Brecht, L.E.; Hirsch, D.L. Reconstructing the Mandible: Jaw-In-A-Day: Where We Were, Where We Are, and the Future. *Atlas Oral Maxillofac. Surg. Clin. N. Am.* **2023**, *31*, 153–164. [CrossRef] [PubMed]
7. Khatib, B. Surgeon Led Intraoperative Prosthetic Conversion In The Jaw In A Day Technique—A Novel Approach Using The Fibiculator And Stacked Bone Guide. *Int. J. Oral Maxillofac. Surg.* **2024**, *52*, 84–85. [CrossRef]
8. Neal, T.W.; Williams, F.C.; Jelmini, J.; Spresser, W.; Schwitzer, D.; Kim, R.Y. Immediate Teeth in Fibulas Versus Standard Fibula Free Flap: A Comparison of Donor Surgical Site Infections. *J. Oral Maxillofac. Surg.* **2024**, *82*, 494–500. [CrossRef] [PubMed]
9. Fernandes, R. Fibula free flap in mandibular reconstruction. *Atlas Oral Maxillofac. Surg. Clin. N. Am.* **2006**, *14*, 143–150. [CrossRef] [PubMed]
10. Yetzer, J.G.; Pirgousis, P.; Li, Z.; Fernandes, R. Clinical Pathway Implementation Improves Efficiency of Care in a Maxillofacial Head and Neck Surgery Unit. *J. Oral Maxillofac. Surg.* **2017**, *75*, 190–196. [CrossRef] [PubMed]

Disclaimer/Publisher's Note: The statements, opinions and data contained in all publications are solely those of the individual author(s) and contributor(s) and not of MDPI and/or the editor(s). MDPI and/or the editor(s) disclaim responsibility for any injury to people or property resulting from any ideas, methods, instructions or products referred to in the content.

MDPI AG
Grosspeteranlage 5
4052 Basel
Switzerland
Tel.: +41 61 683 77 34

Craniomaxillofacial Trauma & Reconstruction Editorial Office
E-mail: cmtr@mdpi.com
www.mdpi.com/journal/cmtr



Disclaimer/Publisher's Note: The title and front matter of this reprint are at the discretion of the Guest Editors. The publisher is not responsible for their content or any associated concerns. The statements, opinions and data contained in all individual articles are solely those of the individual Editors and contributors and not of MDPI. MDPI disclaims responsibility for any injury to people or property resulting from any ideas, methods, instructions or products referred to in the content.





Academic Open
Access Publishing

mdpi.com

ISBN 978-3-7258-9138-2